Ligand-Assisted Catalysis Using Metal SNS Complexes

Atousa Khanzadeh

Thesis Submitted to the University of Ottawa
in Partial Fulfilment of the Requirements for
the Degree of Doctor of Philosophy in Chemistry

Department of Chemistry and Biomolecular Science

Faculty of Science

University of Ottawa

ABSTRACT

In molecular transition metal catalyst architectures, ligand design plays a crucial role in enhancing the efficiency of catalytic reactions. Selected ligands can play a bifunctional role in ligand-assisted catalysis, providing first coordination sphere basic sites and facilitating formation of multinuclear species through monomer bridging, as well as through their electronic and steric effects. This research addresses the underutilization of SNS complexes in various catalytic cycles. Our aim is to expand their activity in different cycles, unlocking untapped reactivity. Specifically, we focus on SNS ligands with soft thiolate and hard amido donors, comparing their catalytic performance in diverse coupling reactions. This comparative study provides insights into the suitability of these ligands with different transition metals, contributing to the understanding of ligand-assisted catalysis. Chapter 1 introduces these concepts and outlines the relevant catalytic reactions studied herein.

To gain a deeper understanding of the chemistry involved, a comparative analysis of the reactivity differences between transition metal complexes with similar coordination structures is conducted. This investigation is crucial as it provides valuable insights into the design of suitable ligands for transition metal catalysts. Specifically, Chapters 2 and 3 of this thesis delve into a comparison of the reactivity of coordination complexes with identical metal centers and similar ligands, or even the same molecular formula, in catalysis.

In the second chapter, we introduce a new cobalt (II) complex bearing an (SNS) amido ligand for the bifunctional hydroboration of carbonyls. Following an unsuccessful attempt to mono-protonate the amido donor in the bis(amido) complex $Co(S^{Me}NS^{Me})_2$ (**2.1**) treatment with 1 equivalent of 1,3-bis(1-adamantyl)imidazolium chloride (IAd•HCl) resulted in the liberation of one protonated ligand, affording $Co^{II}Cl(S^{Me}NS^{Me})$(*a*-IAd) (**2.2**) with an "abnormally" coordinated IAd ligand, i.e., specifically bound through C4 instead of C2 of the imidazole ring. Compound **2.2** exhibited excellent catalytic activity in the hydroboration of aldehydes, displaying high substrate tolerance under mild reaction conditions and short reaction times. Stoichiometric reactions of **2.2** with pinacolborane (HBpin) revealed a bifunctional catalyst activation step, generating free SNS-amine, ClBpin and the active cobalt dihydride catalyst. Generation of an analogous catalyst with a normally coordinated IAd ligand showed poor reactivity in the hydroboration of aldehydes and was unable to effect ketone hydroboration.

In Chapter 3, two tetranuclear copper(I) complexes bearing thiolate $[Cu(SNS^{Me})]_4$ (**3.1**) and amido $[Cu(SNS^{Me})]_4$ (**3.2**) SNS ligands are synthesized and their catalytic activity in a base-free azide-alkyne cycloaddition is compared. Complex **3.1** (1 mol%) demonstrated excellent reactivity for performing this 'click' reaction in water, exhibiting a broad substrate scope and enabling the production of various triazole compounds, including bioactive compound **3.16**, which holds potential as an anti-cancer drug. DFT calculations suggested a proton shuttle role for the thiolate donor in conversion of the Cu-coordinated terminal alkyne to the key Cu-alkynyl intermediate. On the other hand, complex **3.2** exhibited reactivity similar to copper chloride. This observation was attributed to the basic nature of the amido ligand, which undergoes protonation by the coordinated alkyne C-H bond, with subsequent dissociation of the SNS-amine from the copper. Without a ligand to stabilize the copper in the less stable +1 oxidation state, a disproportionation reaction occurs, leading to catalyst deactivation.

Chapter 4 introduces two palladium(II) thiolate complexes: $PdI(\kappa^3\text{-}SNS^{Me})$ (**4.1)** exhibits catalytic activity in promoting the Heck cross-coupling reaction, while $Pd(\kappa^2\text{-}SNS^{Me})_2$ (**4.2)** affords no coupling

product. In concert with triethylamine base, catalyst **4.1** efficiently produces olefin products with excellent yields, even at low catalyst loadings, and exhibits broad substrate tolerance over a 5 h reaction period. In contrast, the limited catalytic activity of **4.2** can be rationalized by proposing the formation of a Pd(N_2S_2) complex through ligand imine coupling at elevated temperatures, a reaction reported previously for Ni and Co analogs. The tetra-coordinated ligand formed through this isomerization occupies critical coordination sites around the metal, thereby preventing oxidative addition of the organohalide substrate, a key step in the Heck reaction mechanism. This work sheds light on the divergent catalytic behaviors of these two intriguing complexes.

Finally, in Chapter 5 we assess what has been learned and identify relevant implications for further work.

ACKNOWLEDGMENT

I want to express my heartfelt gratitude to everyone who has been with me on this challenging yet enlightening journey of completing my PhD thesis. This adventure has been a chapter in my life to deeply understand the beauty of nature's rules and the vastness of the universe—a perspective I've cherished throughout my life.

First and foremost, a big thankyou goes to my mentor, Prof. Baker. Your support, valuable insights, and endless patience have been the foundation of my research and academic growth. Your dedication to my success has always kept me motivated, and I'm truly lucky to have learned from you.

Saeed and Behnaz, my respected colleagues, have been incredibly supportive. They've been there to help, offering valuable advice and constructive feedback. What's made our collaboration even more special is that we share the same mother tongue, which made me feel at home even when far away. Their willingness to share their knowledge and offer support has been priceless.

Loïc, a dear colleague, has been a constant source of support and wisdom. His calming presence and patience, along with his invaluable insights, have greatly enriched my academic journey. I'm grateful for the valuable lessons he has shared with me.

To my family, I owe a huge debt of gratitude. Your unwavering support and encouragement have been my rock throughout this academic journey. Your belief in me has been my biggest motivation, and I'm truly fortunate to have you by my side.

My friends and colleagues have been a constant source of encouragement and friendship. Your presence has made the ups and downs of this journey more enjoyable. I'd like to extend my heartfelt thanks to Alex Sicard, Fernanda Mendonca, and Luana Porto for their unwavering support and camaraderie. Your friendship has been a bright light on this academic path.

Science, which has always fascinated me, has helped me see the world more clearly. It has revealed the intricate web of natural forces and patterns that shape our existence. From science, I've learned the profound lesson of how little I truly know about our world.

Lastly, I want to thank the University, its faculty and staff, and everyone who has contributed to my academic growth. Without their support and resources, this thesis would not have been possible.

This accomplishment is the result of the collective efforts and support of many, and for that, I am truly grateful.

Atousa

Table of Contents

LIST OF SCHEMES

LIST OF FIGURES

LIST OF TABLES

LIST OF ABBREVIATIONS/SYMBOLS

α	alpha position, or angle label (X-ray crystallography)
Å	Ångström
acac	acetylacetonate
Ar	aryl
B	boron
bpy	bipyridine
Br	bromine
β	beta position, or angle label (X-ray crystallography)
br	broad (NMR spectroscopy)
cm^{-1}	wavenumbers
^{13}C	carbon-13
C_6D_6	benzene-d_6
$CDCl_3$	chloroform-d
CuAAC	copper-catalyzed azide-alkyne cycloaddition
Cys	cysteine
δ	chemical shift
Δ	delta (difference between variables) or raise temperature
ΔS	change in entropy
‡	double dagger (transition state)
D	deuterium, ^2H
d	doublet (NMR spectroscopy)
dd	doublet of doublets (NMR spectroscopy)
deg (or °)	degrees

DFT	density functional theory
DMSO-d_6	dimethylsulfoxide-d_6
dtr	doublet of triplet (NMR spectroscopy)
e-	electron
EI-MS	electron impact mass spectroscopy
EPR	electron paramagnetic resonance
ESI-MS	electrospray ionization mass spectroscopy
equiv	equivalents
EtOH	ethanol
F	structure factor (X-ray crystallography)
fac	facial
γ	gamma, angle label (X-ray crystallography)
g	gram
ΔG	Gibbs free energy
$\Delta G^{‡}$	Gibbs free energy of activation
η^n	Hapticity
h	hour(s)
HBpin	pinacolborane
$HNTf_2$	bistriflimide
His	histidine
HMDS	bis(trimethylsilyl)amine
HRMS	high-resolution mass spectroscopy
^1H	proton
$\{^1H\}$	proton-decoupled

Hz	Hertz
ΔH	enthalpy
$\Delta H^{\ddagger}$	enthalpy of activation
IAd	1,3-bis(1-adamantyl)imidazol-2-ylidene
IPr	1,3-bis(2,6-diisopropylphenyl)imidazol-2-ylidene
J	Joules
$^{n}J_{AB}$	n-bond scalar coupling constant between nuclei A and B (NMR spectroscopy)
K	Kelvin
kcal	kilocalorie
kJ	kilojoule
$KO^{t}Bu$	potassium tert-butoxide
λ	wavelength
L	neutral ligand donor
μ	bridging ligand or absorption coefficient (X-ray crystallography)
M	central metal atom (or molar when referring to concentration)
M^{+}	parent ion (mass spectrometry)
m	multiplet
Me	methyl, $–CH_3$
MeCN	acetonitrile
mer	meridional
mg	milligram
MHz	megahertz
min	minutes
mL	milliliter

MLC	metal-ligand cooperation/cooperativity
mmol	millimoles
mol	moles
MW	molecular weight
NaO^tBu	sodium tert-butoxide
NHC	N–heterocyclic carbene
NMR	nuclear magnetic resonance
No.	number
OAc	acetoxy group
OMe	methoxy group, $–OCH_3$
OTf	trifluoromethanesulfonate or triflate
π	pi-bonding or orbital
PCy_3	tricyclohexylphosphine
Ph	phenyl group, $–C_6H_6$
PPh_3	triphenylphosphine
ppm	part per million
^iPr	isopropyl group, $–CH(CH_3)_2$
%	percent
Θ	theta diffraction/Bragg angle (X-ray crystallography)
q	quartet (NMR spectroscopy)
R	alkyl group
R	reliability factor (X-ray crystallography)
Reflns	reflections (X-ray crystallography)
RT	room temperature

σ	estimated standard deviation, type of bonding or orbital
s	singlet (NMR spectroscopy)
SOD	superoxide dismutase
Solv	solvent
^{t}Bu	tert-butyl
tr	triplet (NMR spectroscopy)
trd	triplet of doublet (NMR spectroscopy)
T	temperature in Kelvin or degrees
THF	tetrahydrofuran
TMS	tetramethylsilane
TOF	turnover frequency
TS	transition state
Tyr	tyrosine
UV-Vis	ultraviolet-visible
V	unit cell volume
X	halide substituent (or anionic ligand donor)
XRD	X-ray diffraction
Z	number of formula units per unit cell (X-ray crystallography)

Chapter 1. Introduction

1.1 General Introduction

The aim of this thesis is to delve deeply into the fascinating interplay between ligand design and its impact on catalytic processes, with a specific focus on transition metal complexes bearing SNS ligands.[1] These ligands, characterized by their distinctive sulfur-nitrogen-sulfur arrangement, show promising potential in guiding a diverse array of catalytic reactions. By unraveling the intricate details of their mechanisms and understanding their unique characteristics, we intend not only to enhance our fundamental grasp of molecular-level catalysis but also to shed light on their strategic use in creating vital industrial and pharmaceutical compounds.

Commencing our journey into the world of ligand-assisted catalysis[2] using metal SNS complexes, this opening chapter sets the stage. We begin by emphasizing the pivotal role of catalysis in today's scientific landscape and its vital contribution to sustainability. We then delve into the potential bifunctional role of ligands, highlighting their capabilities and exploring various strategies in metal-ligand cooperation (MLC). In this context, the word "bifunctional" is employed to explain a ligand that does not just have a supporting role in the coordination sphere to stabilize the metal center (monofunctional), but also engages in chemical reactions with the metal (bifunctional) during the catalytic cycle. This approach to reactivity was named "metal-ligand cooperation" by Hansjörg Grützmacher[3] in 2008, and it has been extensively studied over the past decades.[1,4] Next we summarize some previous coordination chemistry and catalysis studies on first row metal amido- and thiolate-SNS complexes by the Baker group. From this groundwork, we finally outline the structural framework for the upcoming chapters, with each chapter embarking on an exploration of unique transition-metal-SNS complexes and their catalytic effectiveness across diverse reactions.

1.2 Catalysis Overview

In today's rapidly evolving world, in which concerns about environmental sustainability and the responsible utilization of Earth's resources take center stage, the imperative to minimize our ecological footprint has become preeminent.[5] At the heart of this endeavor lies the pursuit of novel scientific and technological pathways that can address the challenges posed by our energy needs, resource depletion, and the deleterious effects of waste generation. Among these, catalysis emerges as a pivotal field that offers transformative solutions to usher in a more sustainable future.[6]

Catalysis, a crucial part of modern chemistry, provides a bridge between fundamental scientific principles and their tangible applications in industry, manufacturing, pharmaceuticals, and beyond.[7] It offers a powerful means to harness the potential of abundant and accessible compounds found in nature, while concurrently mitigating the energy requirements and environmental consequences associated with traditional synthetic processes. By adapting reactions through intricately designed catalysts, researchers endeavor to steer chemical transformations along pathways that not only demand reduced energy inputs but also yield fewer unwanted byproducts, aligning with the broader focus on green and sustainable chemistry.

In the quest for efficient catalysis, the distinction between heterogeneous and homogeneous catalysis plays a pivotal role. Heterogeneous catalysis harnesses solid catalysts, often metal surfaces or metal oxides, that interact with reactants in a separate phase.[8] While this approach offers advantages such as facile catalyst separation, reuse, and stability under harsh conditions, it introduces challenges related to diffusion hindrances and compromised selectivity due to limitations in reactant-catalyst interactions.[9] In contrast, homogeneous catalysis stands out for its use of molecular catalysts uniformly dispersed within the reaction mixture.[10] Here, the complexities of ligand design come to the fore, enabling precise tailoring of the catalyst's structure to dictate reactivity and selectivity. This mastery of catalyst architecture speeds up reaction rates and improves selectivity, which is crucial in fields like pharmaceuticals and industry. In pharmaceuticals, homogeneous catalysis reduces byproducts and impurities, simplifying purification steps and expediting the synthesis of vital pharmaceutical agents. Similarly, in industrial settings, homogeneous catalysis fosters cost-effective production of specialty chemicals with elevated yield and purity.[11]

1.3 Moving Through First-Row Transition-Metal Complexes

For a considerable time, homogeneous transition metal catalysis has played a crucial role in enabling complex chemical transformations, resulting in valuable products.[12] Processes like hydrogenation[13], metathesis[14], and hydrocyanation[15], carried out through homogeneous catalysis, make up a significant portion of the global production of bulk chemicals.[16] Historically, precious metals (Pd, Pt, Rh, Ru, Ir) have been at the forefront of this field. Some noteworthy catalyst examples for these reactions are illustrated in **Figure 1.1** (A: Crabtree's hydrogenation catalyst;[17] B: Wilkinson's hydrogenation catalyst;[18] C: hydroformylation catalyst[19] and D: Grubbs' catalyst for olefin metathesis.[20])

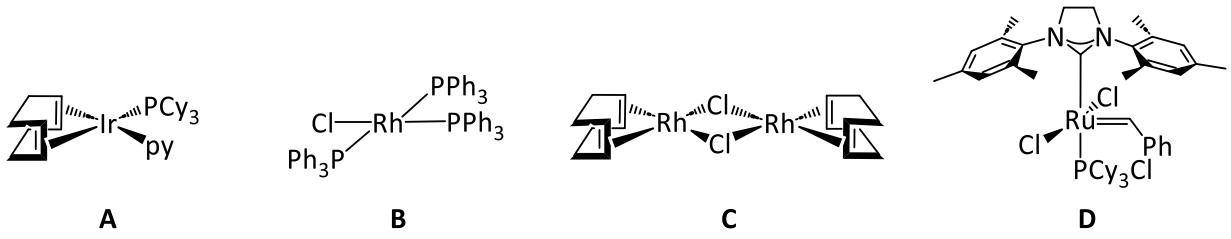

Figure 1.1 Prominent examples of homogeneous catalysts based on precious metals.

While precious metal catalysis has demonstrated remarkable efficiency, there has been a noticeable trend over the past few decades towards employing first-row transition metals in catalysis.[21] These metals are valued for their cost-effectiveness, compatibility with biological systems, and widespread availability, ultimately resulting in a decrease in environmental impact.[22] Nonetheless, navigating the realm of organometallic complexes built upon lighter metals presents significant challenges, such as air sensitivity and the existence of diverse oxidation states with closely related electronic structures, rendering these complexes less predictable. To pave the way for the widespread application of first-row metals in homogeneous catalysis, innovative strategies that capitalize on their distinctive attributes must be conceived and implemented. Within this context, ligand design has proven influential in catalytic activity, with the utilization of bifunctional ligands emerging as a promising avenue to address the challenge of developing stable and efficient catalysts centered around first-row transition metals.

1.4 Metal-ligand Cooperative Catalysis (MLC)

Designing a ligand to enhance the catalytic activity of a complex, while taking into account its assisting capability, is a powerful strategy for achieving effective and selective catalyst reactions.[3,23] Nature has consistently served as a wellspring of inspiration for human innovation, and the concept of metal-ligand cooperative catalysis is no exception. Numerous instances of ligand-assisted catalysis can be found in metal-based enzymes.[24] One notable example is superoxide dismutase (SOD),[25] a metalloenzyme that leverages metal-ligand cooperation to facilitate the conversion of superoxide—an oxygen metabolism byproduct—into oxygen and hydrogen peroxide, thereby averting potentially damaging cellular effects. Although SOD was initially discovered by Fridovich and McCord in 1969,[26] it was the pioneering insights of Henry Taube[27] in electron transfer reactions and coordination chemistry that illuminated the bifunctional role of the ligand in this catalytic system (**Scheme 1.1**). Taube's contributions earned him the Nobel Prize in Chemistry in 1983. Furthermore, Ryoji Noyori's remarkable achievements in the realm of asymmetric hydrogenation earned him the Nobel Prize in Chemistry in 2001 (**Scheme 1.2**).[28] His breakthroughs centered on the utilization of ruthenium complexes bearing bifunctional amide ligand for the enantioselective hydrogenation of ketones and imines. These novel ligands combined a phosphine moiety that directed metal coordination with a

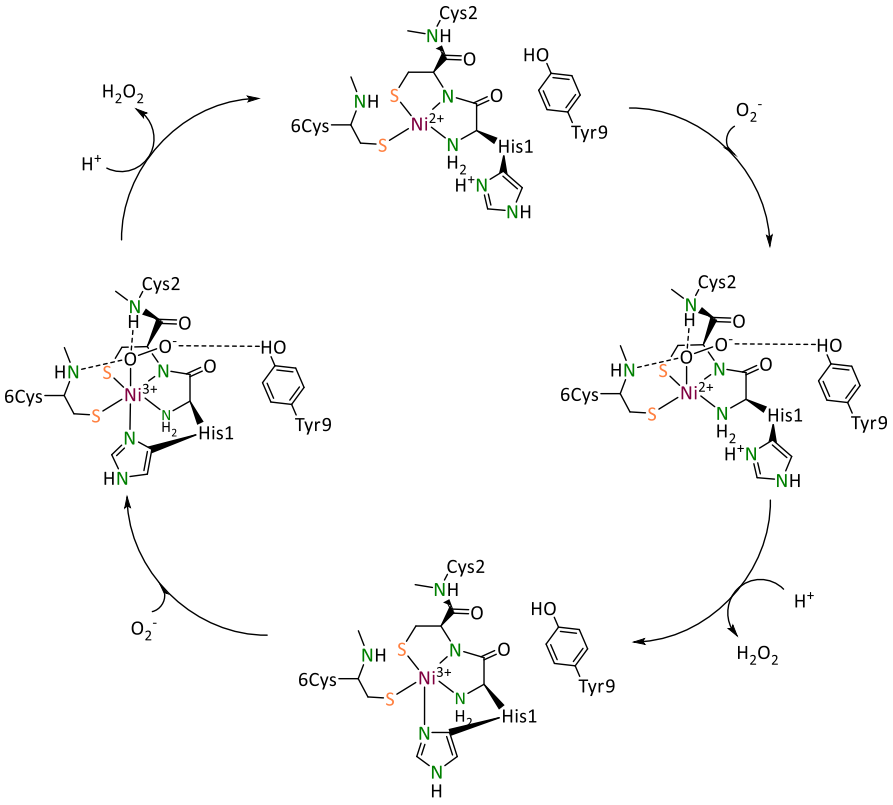

Scheme 1.1 Proposed mechanism for SOD metalloenzyme. * The amino acid structures are omitted for clarity. (His: Histidine, Cys: Cysteine, Tyr: Tyrosine)

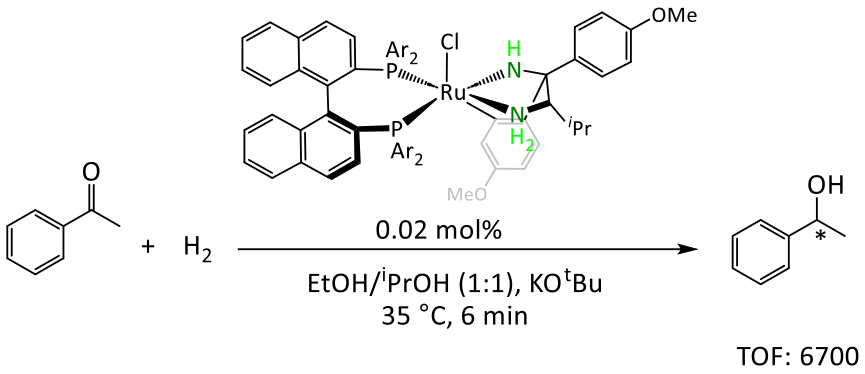

Scheme 1.2 Noyori's catalyst system for asymmetric hydrogenation of ketones.

chiral amine unit that engaged with the substrate, harmonizing a symphony of enantioselectivity in bifunctional hydrogenation reactions. Noyori's discoveries highlighted the intricate workings of these versatile dual-purpose ligands in coordination chemistry and catalysis, emphasizing their many important roles.

1.5 Bifunctional Ligands in MLC

Ever since the discovery of the multifunctional capacity of ligands in catalytic reactions, diverse strategies have been implemented in the realm of MLC catalysis. By offering this assisting role during the catalytic reaction, the chemical structure of the ligand may undergo reversible transformations, including processes like protonation and deprotonation, or may remain intact. In specific cases, the ligand's role might be limited to catalyst activation, as observed in some examples of hydroboration[29] and hydrosilylation.[30] Within this framework, several categories of bifunctional ligands warrant discussion: **1) Ligand acts as Lewis base** - an anionic "X" ligand[31] bearing an additional lone pair of electrons, such as amido, alkoxide or thiolate, can function as a Lewis base in the activation of E-H bonds (E = H, B, Si), *i.e.,* M-X + BHR_2 → MH-BR_2X.[32] These ligands also have the ability to interact with the substrate through H-bonding.[33] Furthermore, some aromatic chelating ligands possess the intriguing ability to undergo dearomatization upon deprotonation, effectively maintaining the metal center's oxidation state throughout the catalytic cycle (**Scheme 1.3**).[34] **2) Ligand acts as Lewis acid**: Alternatively, a ligand with an available empty orbital, such as boryl, aluminyl or phosphenium, can act as a Lewis acid, activating E-H bonds with complementary regioselectivity, *i.e.,* M-X + BHR_2 → MBR_2-XH.[35] These ligands also have the ability to interact with heteroatom-containing substrates through lone-pair coordination.[36] **3) Redox non-innocent ligands**: Ligands with valence orbitals of similar energy to those of the metal d orbitals can serve as reservoirs for electrons, again preserving the oxidation state of the central metal throughout the catalytic cycle.[37] These multifaceted roles collectively contribute to the rich landscape of MLC catalysis.

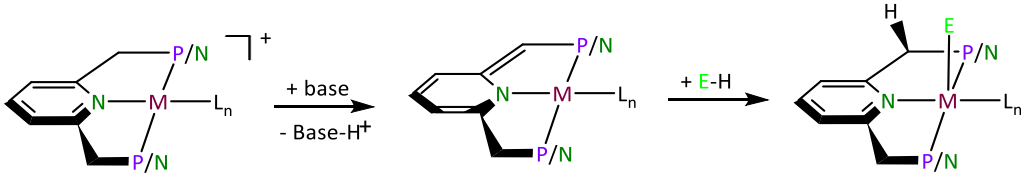

Scheme 1.3 General mechanism for aromatization / dearomatization in MLC.

The central focus of this dissertation revolves around the application of transition-metal catalysts that employ the primary mode of metal-ligand cooperation (MLC), utilizing an amido or thiolate Lewis base X-donor to facilitate collaborative bond activations by the bifunctional arm. Consequently, the majority of attention and emphasis will be directed towards this category, aiming to gain a deeper understanding of the bifunctional activity of these ligands in catalysis. This emphasis is particularly crucial for evaluating their suitability based on their hard or soft basic nature, contributing valuable insights to the field of transition-metal catalysis.

1.6 Ligand Acts as Lewis Base

The main group of cooperative ligands includes those that use an X donor with multiple lone pairs, often in a multidentate structure. In this context, the X donor employs one of its lone pairs to strongly attach to the Lewis acidic metal center. Concurrently, another lone pair plays a crucial part by acting as a Lewis base; this collaborative action enables bifunctional catalysis in cooperation with the metal. Different studies have shown that nitrogen-, sulfur-, and oxygen-donor ligands all have the potential to function in MLC.[1]

The interaction between the Lewis base ligand and the Lewis acidic central metal enables them to cooperate through three distinct mechanisms, as illustrated in **Scheme 1.4**. These mechanisms include 1) **outer-sphere reduction**, 2) **inner-sphere insertion**, and 3) **inner-sphere hydride transfer**.[38] In mechanisms 1 and 3, each cycle relies on the cooperative interplay between the metal and the ligand, whereas in the second mechanism, the bifunctional ligand only plays a role in catalyst activation. In contrast, in monofunctional ligand systems, the ligand remains uninvolved in both catalyst activation and the formation/separation of chemical bonds.

Our research focuses on multidentate amido- and thiolate-SNS ligands, which are prime examples of bifunctional donors displaying Lewis base characteristics. These ligands have consistently been used in hydroboration and hydrosilylation catalytic reactions, mainly due to their significant role as a Lewis base.[2] In the upcoming section, we will shift our attention to bifunctional ligands containing nitrogen and sulfur donors with a bifunctional role as Lewis base. This exploration will expand our understanding of cooperative catalysis, with a stronger emphasis on their Lewis base characteristics.

1.6.1 Nitrogen-based ligands

Due to the pronounced electronegativity of the nitrogen atom, complexes featuring metal-nitrogen bonds demonstrate a remarkable capacity for engaging in metal-ligand cooperative catalysis, with the nitrogen donor fulfilling the role of a Lewis base. Numerous examples of these catalysts have been reported, primarily for two types of reactions:[39] 1) **Hydrogenation and dehydrogenation**, and 2) **E-H bond activation** (where E = B, Si) in the context of hydroboration and hydrosilylation.

1.6.1.1 Hydrogenation and dehydrogenation catalysis

An array of first-row metal complexes excels in catalyzing hydrogenation reactions for both polar and nonpolar unsaturated organic molecules. Many of these ligands are designed on a multidentate [N, P] scaffold, in which the strong-field phosphine donors participate significantly in stabilizing active catalyst species in low-spin states. This field's growth owes much to diligent efforts from various

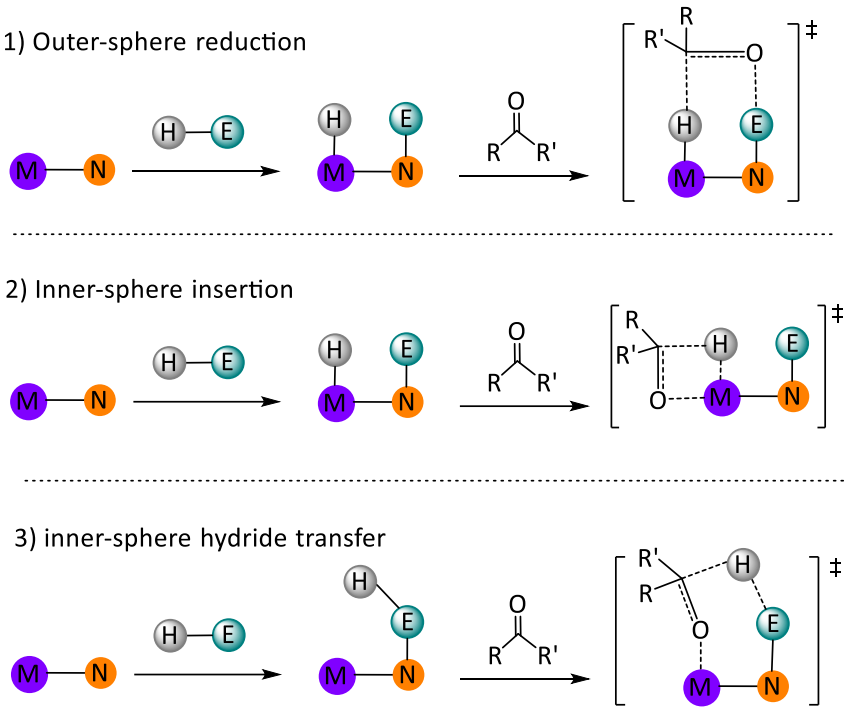

Scheme 1.4 Different types of mechanisms in ligand-assisted catalytic reduction of carbonyls in which the N donor acts as a Lewis base. (R = alkyl, aryl; R' = H, alkyl, aryl; E = H, B, Si).

research groups focused on bifunctional hydrogenation of alkenes, carbonyls, nitriles, and N-heterocycles.[40] For example, in 2012, Hanson and colleagues introduced the active catalyst (PNHP)-Co(II)-alkyl, which performs exceptionally well in hydrogenating a wide range of unsaturated organic compounds.[41] Their 2013 studies on alcohol dehydrogenation identified a cobalt hydride as a key intermediate (**Scheme 1.5**). The N-H moiety displayed no indications of bifunctional activity as confirmed by the similar effectiveness of the N-Me analogue, essentially ruling out a bifunctional outer-sphere mechanism.[42] Further research uncovered detailed mechanistic understanding, elucidating different reaction pathways catalyzed by the initial catalyst across various substrates.[43] Notably, the N-Me analogue encountered challenges with ketone hydrogenation, suggesting an outer-sphere ligand-assisted mechanism for these substrates.

1.6.1.2 E-H bond activation in hydroboration and hydrosilylation

Hydroboration and hydrosilylation reactions stand as catalytic pathways yielding sought-after organoboranes and organosilanes, pivotal starting materials for cross-coupling reactions aimed at generating complex organic molecules.[44] Traditionally, these catalytic processes involved the use of precious metal complexes (Ru, Ir, Rh). However, recent years have witnessed remarkable advances in employing first-row metal complexes.[45] Hydrosilanes and boranes exhibit a resemblance to dihydrogen due to comparable electronegativity values. The heterolytic cleavage of relatively weaker Si–H and B–H bonds (*vs* H-H) can be facilitated by first row metal catalysts employing MLC. Throughout the literature, there are several examples of the utilization of Lewis base bifunctional ligands in these contexts.[46,32]

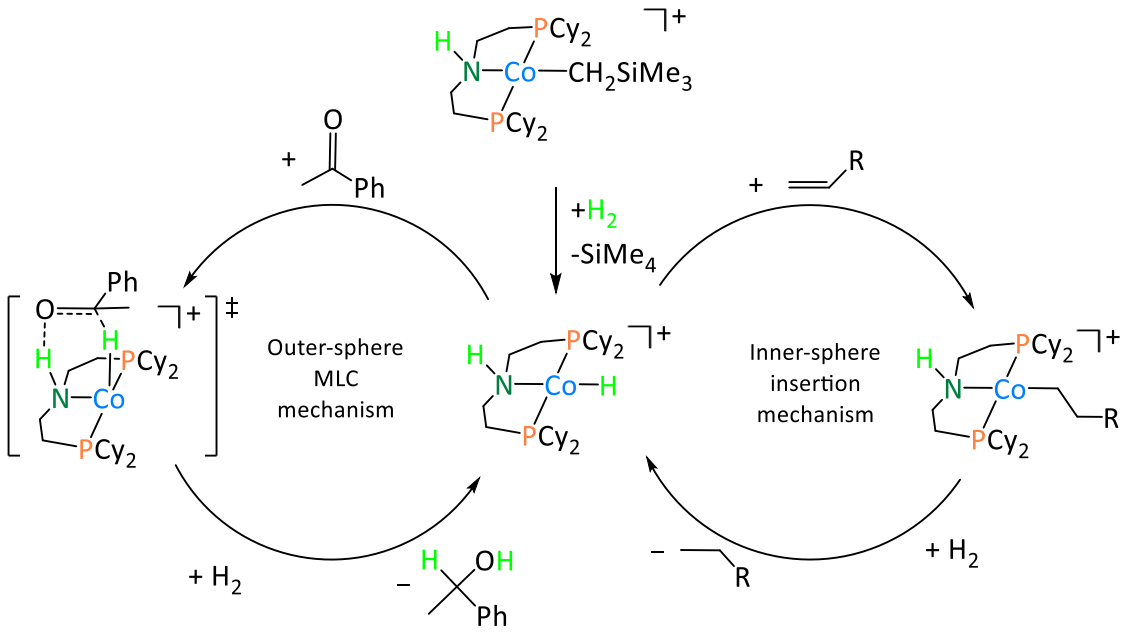

Scheme 1.5 Proposed mechanisms for Co(CH_2SiMe_3)(PN^HP)-catalyzed hydrogenation of ketones (left) and alkenes (right).

The theoretical pathways through which Si–H or B–H bonds can be activated by bifunctional amido ligands are similar to the process for H_2, resulting in the electrophilic Si/B fragment being located at the Lewis basic ligand site and the hydrogen on the Lewis acidic metal center.

In 2018, Leitner and colleagues reported a manganese complex featuring a PNP pincer ligand with the capability to catalyze the hydroboration of carbon dioxide and other challenging carbonyl groups (**Scheme 1.6**).[47] In their mechanistic inquiries, they successfully isolated and characterized a reaction intermediate using X-ray crystallography. This intermediate formed in the presence of stoichiometric amounts of base and HBPin. The crystallographic data revealed the existence of a four-membered ring (Mn-H-B-N), indicative of B-H bond cleavage across the Mn-N bond, thus emphasizing the Lewis basic bifunctional role of the amido donor. Mild heating of this intermediate then afforded the Mn-H complex. These intermediates both served as competent catalyst precursors for CO_2 hydroboration, confirming their role in the catalytic cycle.

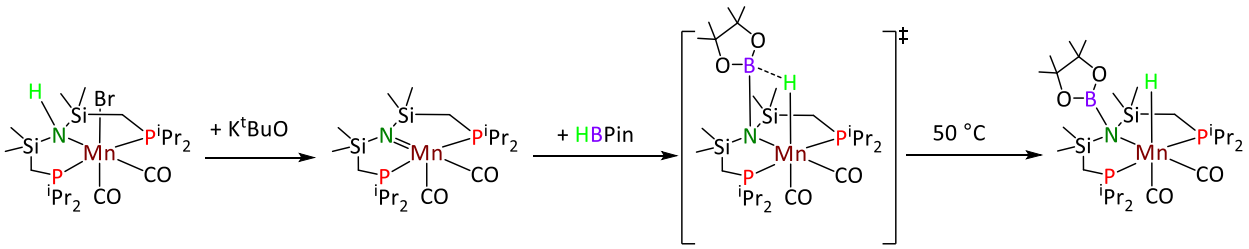

Scheme 1.6 Isolation of Mn–H intermediates from bifunctional B–H bond activation.

1.6.2 Sulfur-based ligands

The concept of harnessing the cooperative dynamics between a Lewis acidic metal and a coordinated Lewis base has proven to be a strong approach in homogeneous catalysis. While focus has mostly centered on metal amido complexes in the landscape of metal-ligand cooperation, it is important to see the potential of alternative donors like sulfur in analogous catalysis reactions. This avenue of exploration is still in its early stages, given the few examples of cooperative S donor ligands in the literature (Figure 1.2).

The metal-sulfur interaction plays a fundamental role within biological systems, often displaying key functions in metalloenzyme reactions. A prime example is [FeFe]-hydrogenase, an enzyme comprised of a dinuclear Fe complex featuring bridging thiolates.[48] This enzyme effectively catalyzes the reversible conversion of protons and electrons into dihydrogen (**Scheme 1.7**). Unraveling the details of the roles played by the sulfur donors in this metalloenzyme is challenging, with several research groups involved.[49] Consequently, further exploring the bifunctional activity of sulfur donors within MLC not only reveals insights into these biological pathways but also drives us toward more environmentally sustainable and biocompatible realms of homogeneous catalysis. This shift is vital for advancing green and eco-friendly approaches to catalysis, aligning with the growing demand for environmentally conscious and biocompatible chemical methodologies in contemporary research.

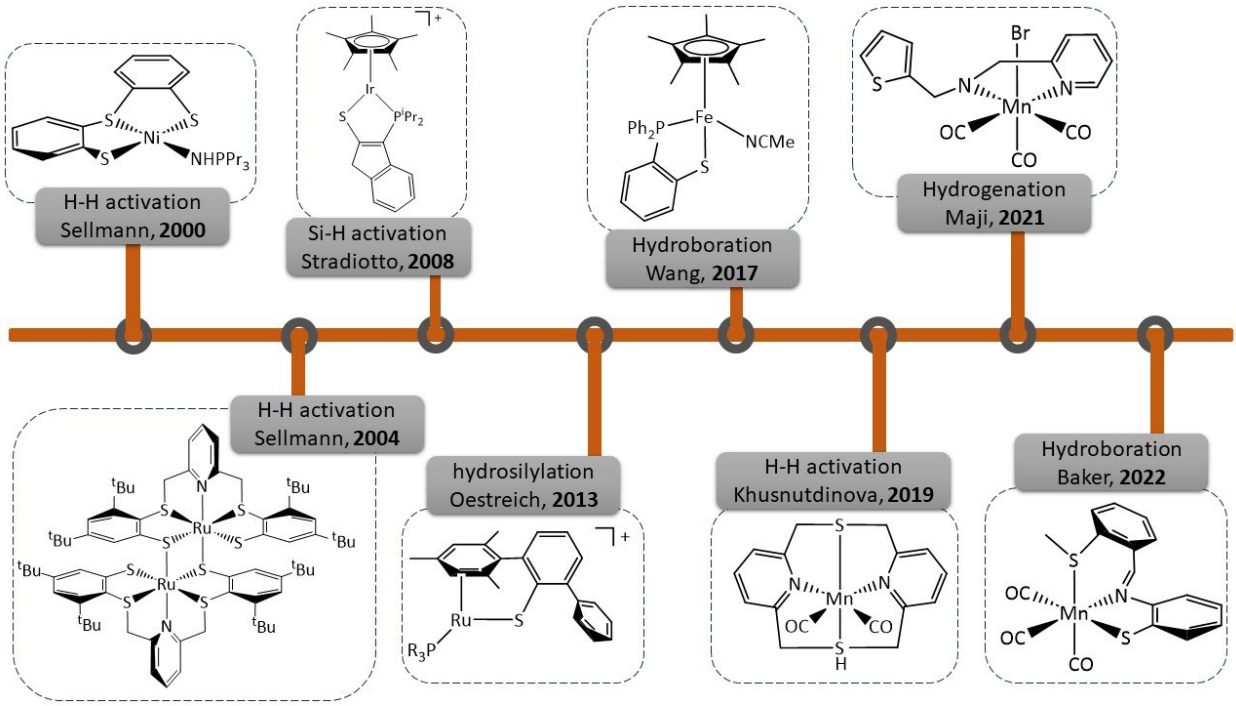

Figure 1.2 Timeline of bifunctional sulfur-based ligands for stoichiometric or catalytic E-H bond activation in cooperation with a metal.

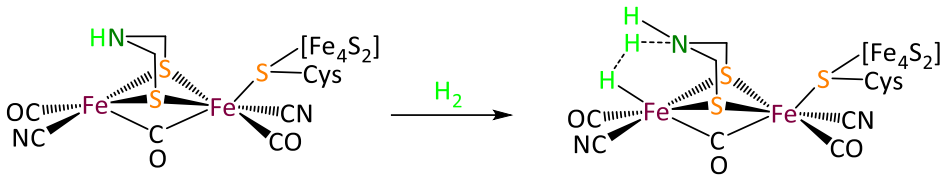

Scheme 1.7 Proposed activation of H_2 by [FeFe]-hydrogenase.

Thiolate donors emerge as strong candidates to showcase their Lewis basic nature, thanks to their natural tendency due to their electronic structure to share their electron pair through bridging interactions.[50] Noteworthy studies have harnessed the ligand-assisted activity of thiolate donors within metal complexes to perform catalytic reactions of significance. Key milestones include pioneering work by Sellmann on a Ni(II) thiodibenzenethiolate complex for cooperative H_2 cleavage, and subsequent studies on Ru and Ir complexes for H_2 activation.[51] More recent research includes the exploration of sulfur-modified [PNP] ligands and the development of Ru-thiolate hydrosilylation catalysts.[52] In another study, Stradiotto demonstrated the reversible activation of organosilane Si–H bonds. This was achieved using a coordinatively unsaturated cationic Ir complex containing a bidentate [SP] ligand. However, despite its effectiveness in this activation, it did not exhibit catalytic activity.[53] More recently, the Khusnutdinova group reported a Mn complex that featured a macrocyclic [N_2S_2] pyridinophane ligand. This complex underwent double dearomatization at the methylene linkers, leading to H_2 activation. However, it did not exhibit catalytic activity similar to the previous case.[54] The most significant advancements in bifunctional catalysis using sulfur-based ligands originated from the Oestreich research team. They formulated a series of Ru-thiolate hydrosilylation catalysts with bifunctional capabilities over the past decade.[55]

In recent years, the Wang group expanded the application range of thiolate complexes involving first row transition metals in metal-ligand cooperative catalysis. In 2017, they reported an iron thiolate complex **1.1A**, which exhibits regiocontrol over the hydroboration of aryl epoxides (**Scheme 1.8**).[56] Notably, an intriguing departure from the typical initiation process was observed. Instead of the conventional B–H bond activation, the pivotal initial stage involved the direct insertion of the epoxide into the Fe–S bond. In a different investigation, the Wang research group expanded the concept of metal-thiolate collaboration to include the hydroboration of N-heteroarenes using 1 mol% of the N_2-bridged diiron complex **1.2A**.[57] Hydride transfer from HBpin to C_2 (proceeding through **1.2C**) gives rise to **1.2D**. Following this step, the Bpin group migrates from sulfur to the reduced heterocycle, ultimately yielding the hydroborated product and regenerating **1.2E**. Lastly, the Maji group recently introduced a Mn(I) catalyst for the transfer hydrogenation of nitriles. In this case, the sulfur donor in the ligand doesn't serve as the bifunctional donor; however, the thioether acts as a hemilabile donor, providing stability to coordinatively unsaturated intermediates during the catalytic cycle.[58]

1.7 Toward Sustainable S-Donor Bifunctional Ligands

A commonly-used ligand motif for metal-ligand cooperation (MLC) catalysis with first-row metals involves phosphine-based multidentate ligands with actor amine/amido functional groups. This ligand design has significantly advanced protocols for (de)hydrogenation catalysis.[59] Some of the most

effective metalloenzymes in nature, such as [FeFe]- and [FeNi]-hydrogenases, incorporate sulfur-based ligands in their active sites for heterolytic H_2 activation.[48,60] However, outside of these biological systems, the utilization of first-row metal-sulfur complexes for cooperative activation of small molecules has been limited, with precious metals being predominant.

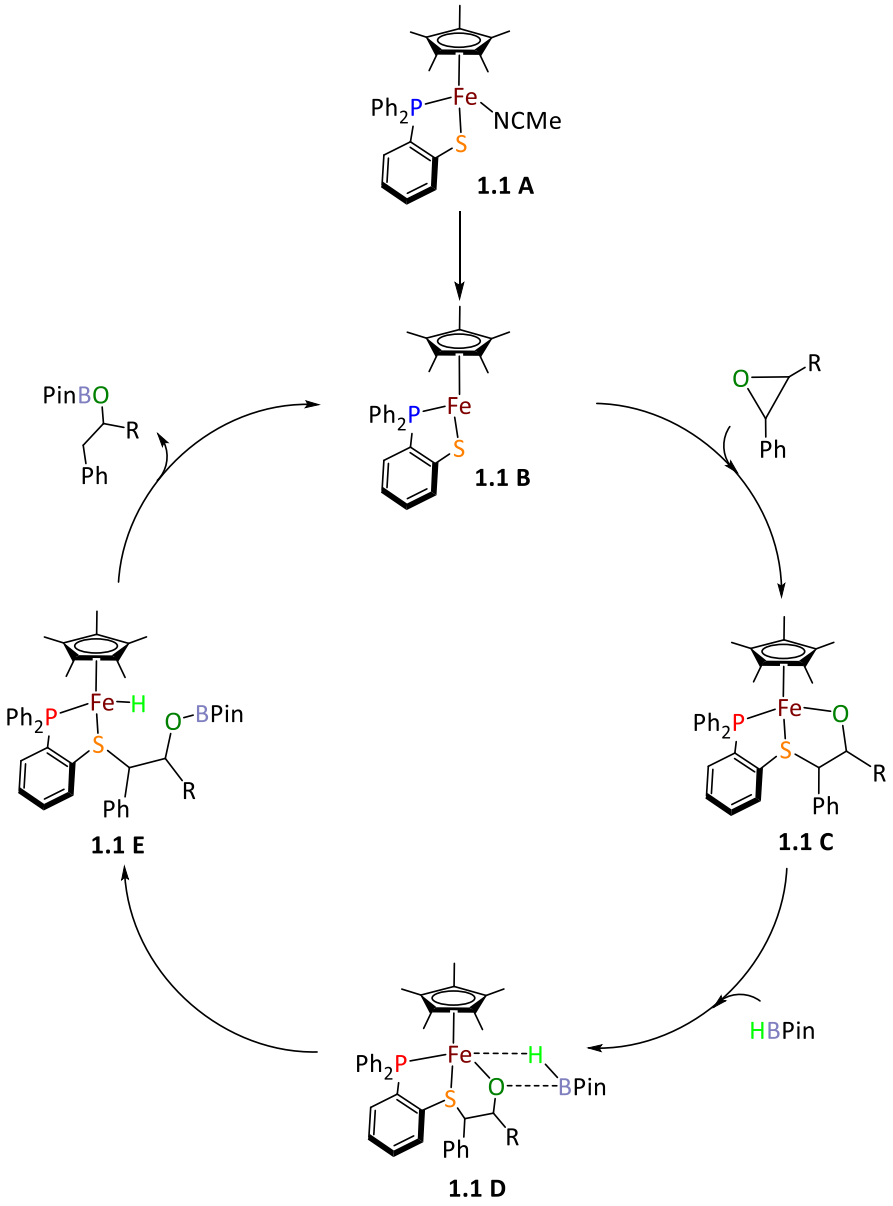

Scheme 1.8 Proposed mechanism for Fe thiolate complex-catalyzed hydroboration of aryl epoxides.

Attempting to grow this field, the Wang research group has expanded the application range of thiolate complexes involving first row transition metals in metal-ligand cooperation catalysis. In 2017, they reported their findings on a thiolate complex involving iron, which exhibited regioselective control over the hydroboration of aryl epoxides (**Scheme 1.8**).[61.a] In a different investigation, the Wang

research group expanded the concept of metal-thiolate collaboration to involve the hydroboration of heteroarenes (**Scheme 1.9**).[61.b] Despite these advances, progress with first-row metals has been comparatively slower. A critical aspect often overlooked is the sustainability of ligands used in these reactions. While sulfur-based bifunctional ligands show promise as highly active catalysts, variants free of phosphines remain underexplored. Moreover, the use of Lewis-base S-donors is rare compared to the widespread use of Lewis-base N-donors. Exploring the role of sulfur in bifunctional pincer

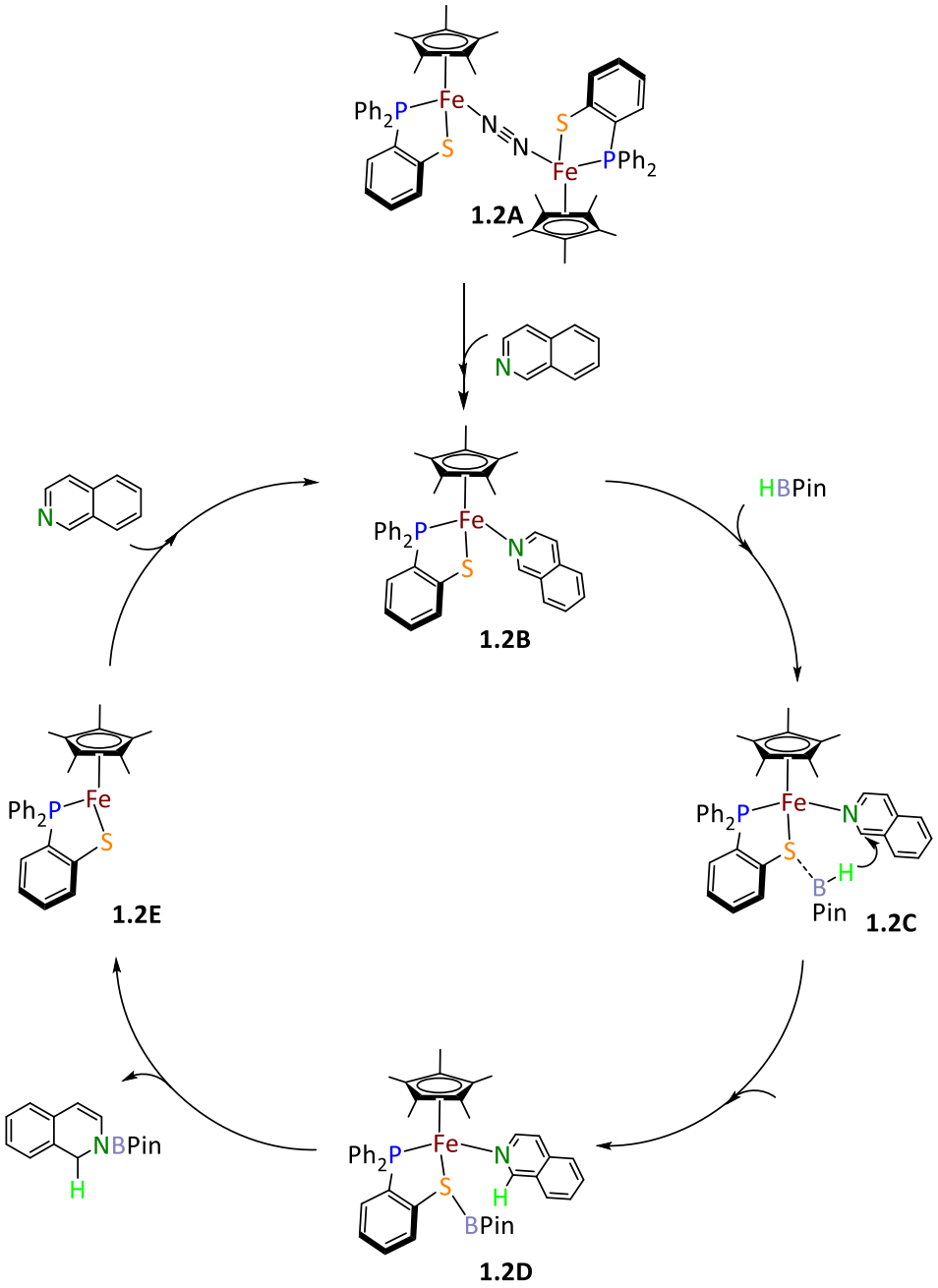

Scheme 1.9 Proposed mechanism for Fe thiolate-catalyzed hydroboration of N-heteroarenes.

ligands is intriguing due to its oxidation state flexibility and 'soft' donor properties. Thiolate ligands have demonstrated involvement in redox events, generating thiyl radicals and facilitating addition reactions.[62] Thus, understanding the reactivity of [N,S]-donor ligands could promote more widespread adoption of sustainable ligand designs.

Over the past 8 years, the Baker research group has revealed the diverse reactivity of two simple amido- and thiolate-[SNS] pincer ligands and identified their mechanistic roles in MLC catalysis (**Scheme 1.9**).[2]

1.8 Amido and Thiolate SNS Ligands

The Baker research group has recently undertaken a comparative study involving 'soft' thiolate (**L1**) and 'hard' amido ligands (**L2**) within the realm of ligand-assisted catalysis.[2] Their investigation spanned base metals ranging from Mn to Zn, revealing diverse bifunctional mechanisms for catalyzing hydroboration[63.a-d] and hydrosilylation[63.e] reactions involving carbonyls, nitriles,[64] and N-heterocycles.[65] This section provides a concise introduction to this chemistry.

1.8.1 Thiolate-SNS ligand (L1)

Synthesis of the benzothiazolidine **HL1** is achieved with a high 90% yield using a straightforward condensation reaction between 2-(methylthio)benzaldehyde and 2-aminothiophenol (**Scheme 1.10**).[66] Quantitative deprotonation then gives the thioether-imine-thiolate SNS ligand **L1**. Reaction

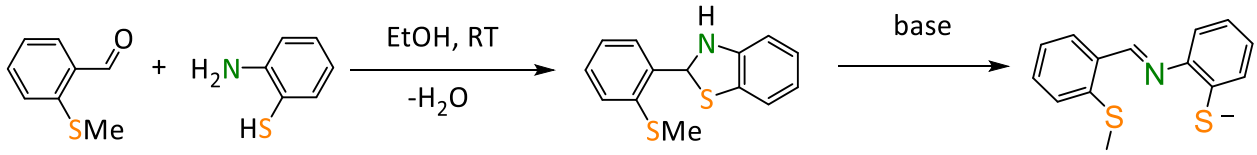

Scheme 1.10 Synthesis of benzothiazolidine (**HL1**) and thiolate-SNS ligand (**L1**).

of $Fe(OTf)_2$ with 1 equiv. of both **HL1** and NaOtBu afforded a trinuclear complex $\{Fe[\mu_2\text{-}Fe(\kappa^3\text{-}SNS^{Me})_2]_2\}(OTf)_2$ (**1.1**) featuring a central iron center coordinated to two bidentate pseudo-octahedral $Fe[\kappa^3\text{-}SNS^{Me}]_2$ units in a distorted tetrahedral fashion (**Scheme 1.11**). Formation of multinuclear complexes confirms the capacity of thiolate ligands for bridging.[66] Note that the imine and thiolate donors form a 5-membered ring with the Fe center, whereas the coordinated thioether and imine donors form a 6-membered ring. Addition of ancillary phosphorus ligands then afforded both dinuclear and mononuclear analogs such as $Fe(\kappa^3\text{-}SNS^{Me})[P(OMe)_3]_3$. Although an iron bis(thiolate) complex $Fe(\kappa^3\text{-}SNS^{Me})(\kappa^2\text{-}SNS^{Me})(CO)$, was obtained from reaction with CO,[67] $Ni(acac)_2$ reacts with **L1** to afford *cis*-$Ni(\kappa^2\text{-}SNS^{Me})_2$ (**1.2**), demonstrating the hemilability of the thioether donor (**Scheme 1.12**).[68] Thermolysis of **1.2** afforded the $Ni(N_2S_2)$ complex (**1.3**) via imine C-C bond formation, as reported previously by Kawamoto for $Ni(NS)_2$ complexes.[69] Note that the $(N_2S_2)^{2-}$ ligand in **1.3** is redox active, affording a diamagnetic Ni complex.[70]

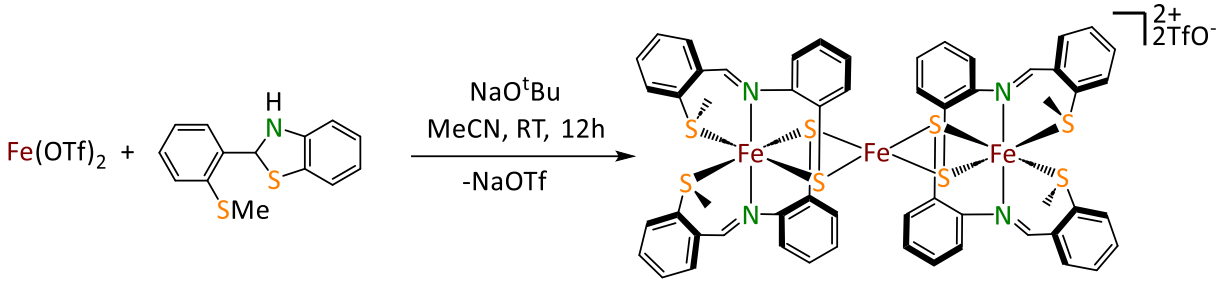

1.1

Scheme 1.11 Synthesis of the trinuclear $[Fe_3(SNS^{Me})_4]^{2+}$ cationic complex (**1.1**).

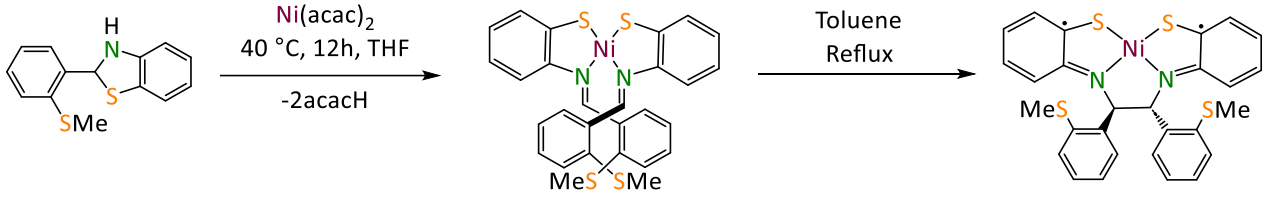

1.2 **1.3**

Scheme 1.12 Synthesis of Ni bis(thiolate) (**1.2**) and $Ni(N_2S_2)$ (**1.3**) complexes.

1.8.2 Amido-SNS ligand (L2)

The bis(thioether)-amine ligand (**HL2**) can be synthesized with yields exceeding 90% by condensing 2-(methylthio)benzaldehyde and 2-(methylthio)aniline, followed by imine reduction using 4 equiv of ammonia-borane (**Scheme 1.13**).[71] Upon deprotonation, **L2** presents a "hard" amido group as the bifunctional donor, flanked by two thioether groups—one forming a 5-membered ring and the other a 6-membered ring. The latter was conceptualized to possess potential hemilabile properties.[72] The weaker acidity of the N-H bond in **HL2** (vs **HL1**) necessitates the use of stronger bases for deprotonation. Thus, metal precursors incorporating strongly basic X groups such as hexamethyldisilazanide (HMDS) were selected for the salt-free synthesis of the bis(amido) complexes, *trans*-$M(\kappa^3\text{-}S^{Me}NS^{Me})_2$ with M = Mn (**1.4**), Fe (**1.5**), and Co (**1.6**) (**Scheme 1.14**).[62(b),71,73] A notable observation for these complexes is the longer $M\text{-}S^{Me}$ distance within the 6-membered ring compared to the 5-membered ring. This potential hemilability was realized in reactions with the bipyridine ligand which cleaved both thioether donors from the 6-membered rings, yielding $M(\kappa^2\text{-}S^{Me}NS^{Me})_2(bpy)$ [M = Mn, Fe] complexes. (**Scheme 1.15**).

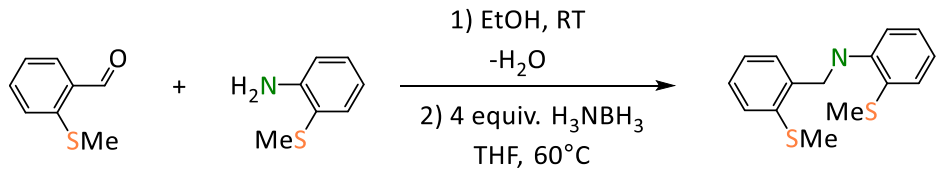

Scheme 1.13 Synthesis of protonated SNS amido ligand (**HL2**).

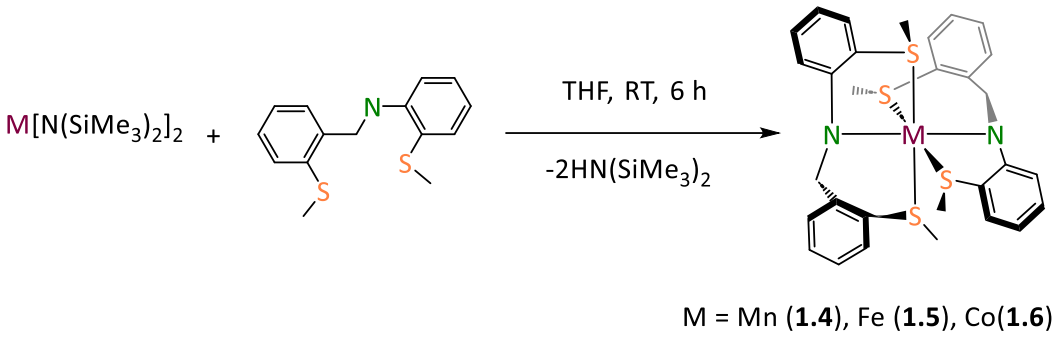

Scheme 1.14 Synthesis of first row metal bis(amido) complexes **1.4-1.6.**

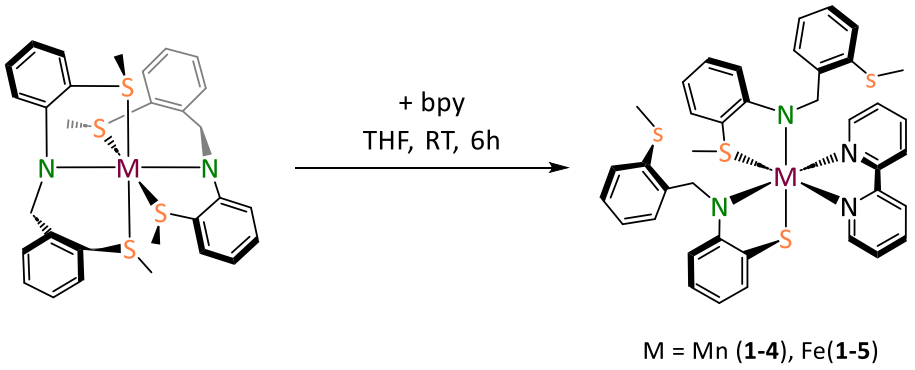

Scheme 1.15 Demonstrating the hemilability of the thioether donors in the 6-membered rings of **1.4** and **1.5**.

Protonation of complex **1.5** with $NHTf_2$ gave the cationic amido-amine complex (**1.7**) that then serves as a precursor for monoamido complexes with ancillary ligands such as triphos (**1.8**; **Scheme 1.16**), which proved to be a selective catalyst for ammonia-borane dehydrogenation.[71]

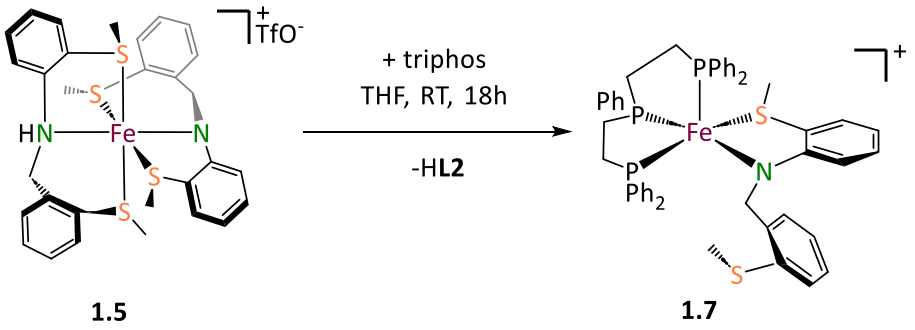

Scheme 1.16 Protonation of iron bis(amido) complex (**1.5**) gives cationic monoamido complex (**1.7)** with triphos.

1.9 Catalysis Using First-row Metal Complexes Bearing Amido- and Thiolate-SNS Ligands

Despite the existing literature on bifunctional hydroboration catalysts, the Baker research group took a novel approach by using this reaction as a foundation to explore the Lewis base MLC potential of the newly introduced SNS ligands. The various complexes shown in **Figure 1.3**, showcased remarkable efficacy in catalyzing carbonyl hydroboration. Impressively, these complexes accomplished the

conversion of both aldehydes and ketones to full completion at room temperature, with catalyst loadings of less than 1 mol%. Notably, the catalytic process exhibited versatility in accommodating a diverse range of substrates, encompassing electron-withdrawing and electron-donating groups on both aryl and alkyl carbonyls. Furthermore, a comprehensive examination into the mechanistic intricacies unveiled distinct pathways governing the MLC $M(SNS)_n$-catalyzed hydroboration. As discussed earlier, two distinct mechanisms come to the fore in bifunctional E-H bond activation. In one scenario, E-H bond

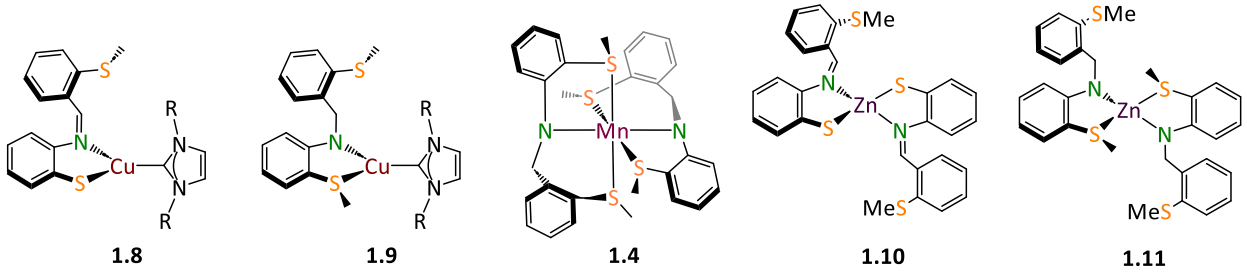

Figure 1.3 Active hydroboration catalysts containing SNS ligands.

cleavage across the M-L bond initiates an outer-sphere six-membered transition state, in which direct interaction between the substrate and the metal center is absent. In an alternate scenario, an inner-sphere mechanism take place, involving the coordination of the substrate to the metal followed by insertion into the M-H bond. Several mechanistic investigations utilizing the complexes featured in **Figure 1.3**, not only revealed contrasting coordination chemistry linked to the amido- and thiolate-SNS ligands but also illuminated their distinct modes of facilitating the reaction across diverse metals.

In one example, the mechanistic exploration of hydroboration utilizing the zinc bis-thiolate precatalyst Zn(**L1**)$_2$ (**1.10**) disclosed a rare example of borylated ligand dissociation to yield an active hydroboration catalyst.[74] This intriguing phenomenon was achieved by initiating the activation of the B-H bonds via reduction of the imine group. Subsequently, the activation pathway involved the interaction of a Zn[**L1**-HBpin] unit with benzaldehyde, leading to a series of reactions that encompassed deoxygenation and the creation of a benzothiazoline heterocycle. This process likely gave rise to the formation of $Zn[OBpin]_2$, which, in the presence of both HBpin and benzaldehyde, generated $O(Bpin)_2$ and the catalytically active Zn species (**Figure 1.4**). This intriguing reaction pathway involving the deployment of a sacrificial ligand underscores the diversity of options presented by these SNS ligands.

To draw a comparative analysis between the two SNS ligands, an investigation into the catalytic performance of two copper complexes (**1.8** and **1.9**) was undertaken (**Figure 1.3**). While the (IPr)Cu(**L2**) complex exhibited catalytic activity in both hydroboration and hydrosilylation of carbonyls, its thiolate analogue, (IPr)Cu(**L1**), exclusively demonstrated catalysis in the hydroboration reaction.[63]

In another investigation, the Baker research team reported a catalyst system demonstrating exceptional efficacy in effecting the dihydroboration of nitriles, thereby affording access to valuable N,N-diborylamine precursors.[75] The Mn-based thiolate-SNS complex $Mn(CO)_3$(**L1**) exhibited the remarkable capability to reduce nitriles, utilizing a mere 1 mol% catalyst loading with a good

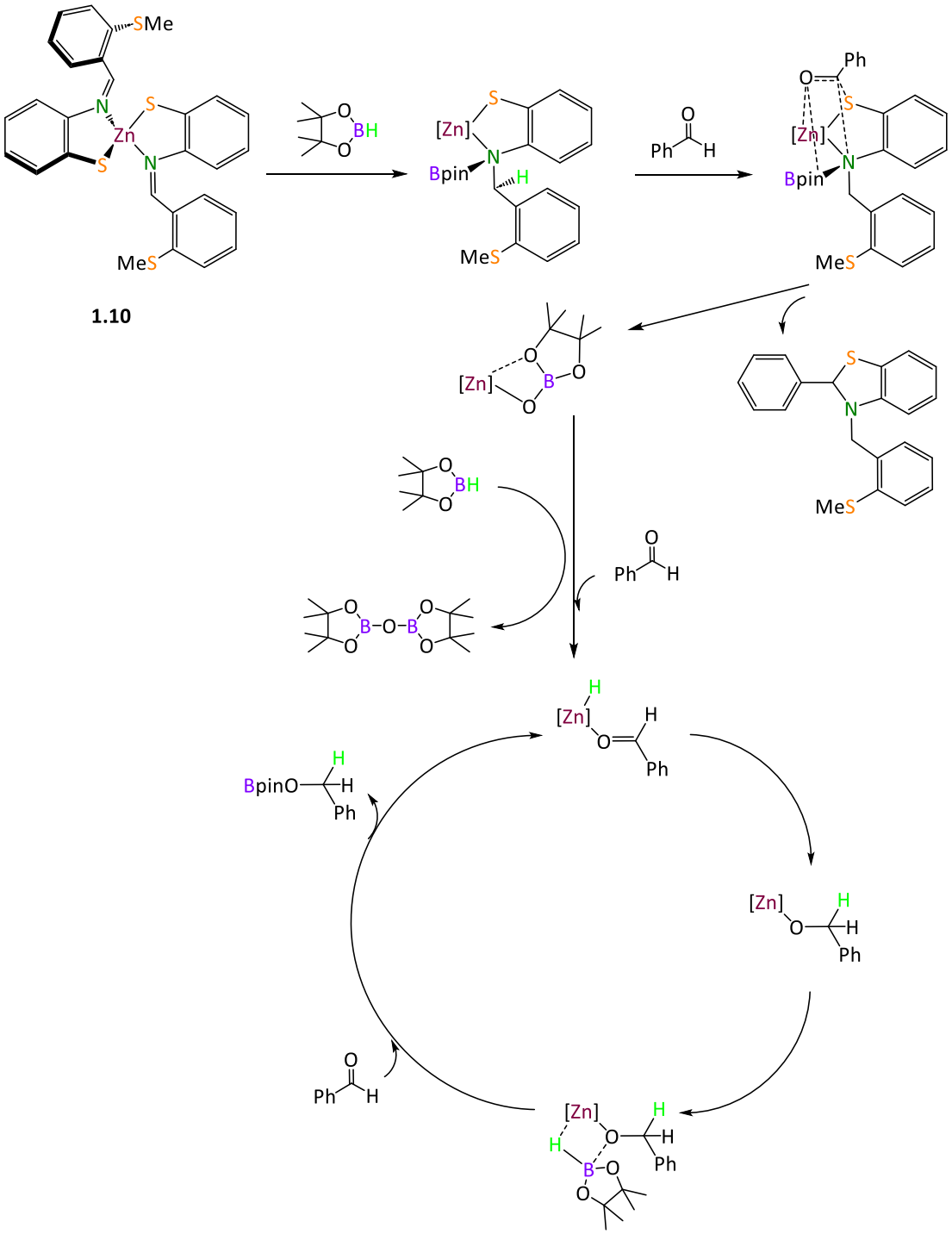

Scheme 1.17 Proposed reaction pathway for benzaldehyde hydroboration using HBPin and Zn(**L1**)$_2$ bis(thiolate) precatalyst. On the right, one of the **L1** ligands is omitted for clarity.

substrate scope tolerance, all at room temperature (**Scheme 1.18**). This accomplishment necessitated only ongoing photolysis to introduce an additional coordination site on the metal center.

Central to the objectives of this thesis is the aspiration to extend the catalytic capabilities of this family of bifunctional ligands beyond E-H bond activation reaction. The aim is to enable diverse

and valuable bond-forming reactions, thereby contributing to the advancement of synthetic methodologies and enhancing the repertoire of tools available to synthetic chemists.

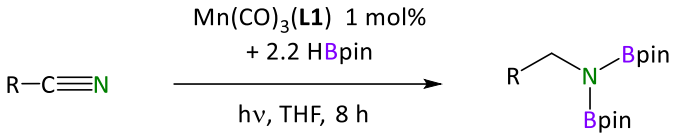

Scheme 1.18 Photolytic dihydroboration of nitriles utilizing the $Mn(CO)_3$(**L1**) complex.

In the ensuing chapters, we delve into the exploration of arrays comprising SNS-transition metal complexes, elucidating their applications in the realm of metal-ligand cooperation catalysis. Additionally, a comprehensive analysis unfolds as we examine the distinctive attributes of soft thiolate and hard amido donors, particularly in the context of their involvement in a click reaction within the thiolate and amido complexes. This comparative investigation serves to deepen our understanding of the unique catalytic properties inherent in these diverse ligand frameworks.

1.10 References

1. Elsby, M. R.; Baker, R. T., Through the looking glass: Using the lens of [SNS]-pincer ligands to examine first-row metal bifunctional catalysts, *Acc. Chem. Res.*, 2023, **56**, 798-809.
2. Elsby, M. R.; Baker, R. T., Strategies and mechanisms of metal-ligand cooperativity in first-row transition metal complex catalysts, *Chem. Soc. Rev.,* 2020, **49**, 8933-8987.
3. Grützmacher, H. Cooperating Ligands in Catalysis. *Angew. Chem,. Int. Ed.,* 2008, **47**, 1814-1818.
4. Khusnutdinova, J. R.; Milstein, D., Metal-ligand cooperativity, *Angew*. *Chem,. Int. Ed.,* 2015, **54**, 12236-12273.
5. Sankar, M.; Dimitratos, N.; Miedziak, P. J.; Wells, P. P.; Kiely, C. J.; Hutchings, G. J., Designing bimetallic catalysts for a green and sustainable future, *Chem. Soc. Rev.,* 2012, **42**, 8099-8139.
6. Rodriguez-Padron, D.; Puente-Santiago, A. R.; Balu, A. M.; Munoz-Batista, M. J.; Luque, R., Environmental catalysis: Present and future, *ChemCatChem,.* 2019, **11**, 18-38.
7. Chorkendorff, I.; Niemantsverdriet, J. W. *Concepts of Modern Catalysis and Kinetics*; John Wiley & Sons, 2017.
8. Fechete, I., Wang, Y., & Védrine, J. C., The past, present and future of heterogeneous catalysis, *Catalysis Today*, 2012, **189**(1), 2-27.
9. van Leeuwen, P. W. M. *Homogeneous catalysis: Understanding the art*; Springer Science & Business Media, 2006.
10. Cornils, B.; Herrmann, W. A., Concepts in homogeneous catalysis: The industrial view, *J. Catal.,* 2003, **216**, 23-31.
11. Cornils, B.; Herrmann, W. A. *Applied homogeneous catalysis with organometallic compounds*, Wiley VCH, 2002.
12. Chiusoli, G. P; Maitlis, P. M, Eds., *Metal-catalysis in industrial organic processes*; *Royal Society of Chemistry*, 2019.
13. Chaloner, P. A.; Esteruelas, M. A.; Joó, F.; Oro, L. A. *Homogeneous hydrogenation*, Springer Science & Business Media, 2013.
14. Fürstner, A. Olefin Metathesis and Beyond. *Angew. Chem,. Int. Ed.* 2000, **39**, 3012-3043.
15. Bini, L.; Müller, C.; Vogt, D. Mechanistic Studies on Hydrocyanation Reactions, *ChemCatChem,.* 2010, **2**, 590-608.
16. De Vries, J. G.; Jackson, S. D. Homogeneous and heterogeneous catalysis in industry. *Catal. Sci.,* 2012, **2**, 2009-2009.
17. Loch, J. A.; Crabtree, R. H., Rapid screening and combinatorial methods in homogeneous organometallic catalysis, *Pure Appl. Chem.,* 2009, **73**, 119-128.
18. Osborn, J. A.; Wilkinson, G.; Mrowca, J. J.; Tris(triphenylphosphine)halorhodium(I), *Inorg. Synth.* 1967, **10**.
19. Slaugh, L. H.; Mullineaux, R. D., Novel hydroformylation catalysts, *J. Organomet. Chem.,* 1968, **13**, 469-477.
20. (a) Schwab, P.; France, M.; Ziller, J. W.; Grubbs, R. H., A series of well-defined metathesis catalysts-synthesis of $[RuCl_2(=CHR')(PR_3)_2]$ and its reactions, *Angew. Chem., Int. Ed.,* 1995, **34**,

2039-2041. (b) Schwab, P.; Grubbs, R. H.; Ziller, J. W., Synthesis and application of $RuCl_2(=CHR')(PR_3)_2$: The influence of the alkylidene moiety on metathesis activity, *J. Am. Chem. Soc.,* 1996, **118**, 100-110.

21. (a) Loup, J.; Dhawa, U.; Pesciaioli, F.; Wencel-Delord, J.; Ackermann, L., Enantioselective C−H activation with earth-abundant 3d transition metals. *Angew. Chem., Int. Ed.,* 2019, **58**, 12803-12818. (b) Tamang, S. R.; Findlater, M., Emergence and applications of base metals (Fe, Co, and Ni) in hydroboration and hydrosilylation, *Molecules,* 2019, **24**, 3194.
22. (a) Wedepohl, K. H. The composition of the continental crust, *Geochim. Cosmochim. Acta* 1995, **59**, 1217-1232. (b) Egorova, K. S.; Ananikov, V. P. Which metals are green for catalysis? Comparison of the toxicities of Ni, Cu, Fe, Pd, Pt, Rh, and Au salts, *Angew. Chem., Int. Ed.,* 2016, **55**, 12150-12162.
23. (a) Buchwald, S. L.; Milstein, D., *Ligand design in metal chemistry: Reactivity and catalysis*; *John Wiley & Sons*, 2016. (b) Stradiotto, M.; Lundgren, R. J., Ligand Design in Metal Chemistry; *Wiley Online Library*, 2016.
24. (a) Bullock, R. M.; Chen, J. G.; Gagliardi, L.; Chirik, P. J.; Farha, O. K.; Hendon, C. H.; Jones, C. W.; Keith, J. A.; Klosin, J.; Misteer, S. D., Using nature's blueprint to expand catalysis with earth-abundant metals, *Science*, 2020, **369**. (b) Fontecilla-Camps, J. C.; Volbeda, A.; Cavazza, C.; Nicolet, Y., Structure/function relationships of [NiFe]-and [FeFe]-hydrogenases, *Chem. Rev.,* 2007, **107**, 4273-4303.
25. Barondeau, D. P.; Kassmann, C. J.; Bruns, C. K.; Tainer, J. A.; Getzoff, E. D., Nickel superoxide dismutase structure and mechanism, *Biochem.*, 2004, **43**, 8038-8047.
26. McCord, J. M.; Fridovich, I., Superoxide dismutase: An enzymic function for erythrocuprein, *J. Biol. Chem.,* 1969, **244**, 6049-6055.
27. Richardson, D. E.; Taube, H., Electronic interactions in mixed-valence molecules as mediated by organic bridging groups, *J. Am. Chem. Soc.,* 1983, **105**, 40-51.
28. Ohkuma, T.; Ooka, H.; Hashiguchi, S.; Ikariya, T.; Noyori, R. Practical enantioselective hydrogenation of aromatic ketones, *J. Am. Chem. Soc.,* 1995, **117**, 2675–2676.
29. Wan, X.; Li. M.; Liao, R., Ligand-assisted hydride transfer: A pivotal step for CO_2 hydroboration catalyzed by a mononuclear Mn(I) PNP complex, *Chem. Asian J.,* 2021, **16**, 2529-2537.
30. Mathew, J.; Nakajima, Y.; Choe. Y. K.; Urabe, Y.; Ando, W.; Sato, K.; Shimada, S., Olefin hydrosilylation catalyzed by cationic nickel(II) allyl complexes: A non-innocent allyl ligand-assisted mechanism, *Chem. Commun.,* 2016, **52**, 6723-6726.
31. Ikariya, T.; Blacker, A. J., Asymmetric transfer hydrogenation of ketones with bifunctional transition metal-based molecular catalysts, *Acc. Chem. Res.,* 2007, **40**, 1300-1308.
32. Hatzis, G. P.; Thomas, C. M., Metal-ligand cooperativity across two sites of a square planar iron (II) complex ligated by a tetradentate PNNP ligand, *Chem. Commun.,* 2020, **56**, 8611-8614.
33. Fryzuk, M. D.; MacNeil, P. A.; Rettig, S. J., Stereoselective formation of rhodium and iridium hydrides via intramolecular hydrogen bonding, *J. Am. Chem. Soc.,* 1987, **109**, 2803-2812.
34. (a) Zhang, J.; Leitus, G.; Ben-David, Y.; Milstein, D., Facile conversion of alcohols into esters and dihydrogen catalyzed by new ruthenium complexes, *J. Am. Chem. Soc.,* 2005, **127**, 10840-10841. (b) Langer, R.; Iron, M. A.; Konstantinovski, L.; Diskin-Posner, Y.; Leitus, G.; Ben-David, Y.; Milstein, D., Iron borohydride pincer complexes for the efficient hydrogenation of ketones

under mild, base-free conditions: Synthesis and mechanistic insight, *Chem. Eur. J.,* 2012, **18**, 7196-7209.

35. (a) Mihalcik, D. J.; White, J. L.; Tanski, J. M.; Zakharov, L. N.; Yap, G. P.; Incarvito, C. D.; Rheingold, A. L.; Rabinovich, D., Cobalt tris(mercaptoimidazolyl)borate complexes: Synthetic studies and the structure of the first cobaltaboratrane, *Dalton Trans.,* 2004, 1626-1634. (b) Figueroa, J. S.; Melnick, J. G.; Parkin, G., Reactivity of the metal→BX_3 dative σ-bond: 1,2-addition reactions of the Fe→BX_3 moiety of the ferraboratrane complex [k^4-B(mimBut)$_3$]Fe(CO)$_2$, *Inorg. Chem.,* 2006, **45**, 7056-7058.
36. Leitl, J.; Marquardt, M.; Coburger, P.; Scott, D. J.; Streitferdt, V.; Gschwind, R. M.; Müller, C.; Wolf, R., Facile C=O bond splitting of carbon dioxide induced by metal–ligand cooperativity in a phosphinine iron (0) complex, *Angew. Chem., Int. Ed.,* 2019, **58**, 15407-15411.
37. (a) Lyaskovskyy, V.; de Bruin, B. Redox non-innocent ligands: Versatile new tools to control catalytic reactions, *ACS Catal.,* 2012, **2**, 270-279. (b) Kaim, W., The shrinking world of innocent ligands: Conventional and non-conventional redox-active ligands, *Eur. J. Inor. Chem.,* 2012, **2012**, 343-348. (c) Praneeth, V. K.; Ringenberg, M. R.; Ward, T. R., Redox-active ligands in catalysis, *Angew. Chem., Int. Ed.,* 2012, **51**, 10228-10234.
38. Elsby, M. R.; Son, M.; Oh, C.; Martin, J.; Baik, M.–H.; Baker, R. T., Mechanistic study of metal–ligand cooperativity in Mn(II)-catalyzed hydroborations: Hemilabile SNS ligand enables metal hydride-free reaction pathway, *ACS Catal.,* 2021, **11**, 9043–9051.
39. (a) Forster, F.; Oestreich, M., *Organosilicon chemistry: Novel approaches and reactions*, Wiley VCH, 2020, 115-130. (b) Palacios, A. A.; Alemany, P.; Alvarez, S., Electronic structure and bonding in tricoordinate amido complexes of transition metals, *Inorg. Chem.,* 1999, **38**, 707-715.
40. (a) Dong, K.; Elangovan, S.; Sang, R.; Spannenberg, A.; Jackstell, R.; Junge, K.; Li, Y.; Beller, M., Selective catalytic two-step process for ethylene glycol from carbon monoxide, *Nat. Commun.,* 2016, **7**, 1-7. (b) Schneck, F.; Assmann, M.; Balmer, M.; Harms, K.; Langer, R., Selective hydrogenation of amides to amines and alcohols catalyzed by improved iron pincer complexes, *Organometallics,* 2016, **35**, 1931-1943. (c) Bornschein, C.; Werkmeister, S.; Wendt, B.; Jiao, H.; Alberico, E.; Baumann, W.; Junge, H.; Junge, K.; Beller, M., Mild and selective hydrogenation of aromatic and aliphatic (di)nitriles with a well-defined iron pincer complex, *Nat. Commun.,* 2014, **5**, 1-11. (d) Lange, S.; Elangovan, S.; Cordes, C.; Spannenberg, A.; Jiao, H.; Junge, H.; Bachmann, S.; Scalone, M.; Topf, C.; Junge, K., Selective catalytic hydrogenation of nitriles to primary amines using iron pincer complexes, *Catal. Sci.,* 2016, **6**, 4768-4772. (e) Werkmeister, S.; Junge, K.; Wendt, B.; Alberico, E.; Jiao, H.; Baumann, W.; Junge, H.; Gallou, F.; Beller, M., Hydrogenation of esters to alcohols with a well-defined iron complex, *Angew. Chem., Int. Ed.,* 2014, **53**, 8722-8726.
41. Zhang, G.; Scott, B. L.; Hanson, S. K., Mild and homogeneous cobalt-catalyzed hydrogenation of C–C, C–O, and C–N bonds, *Angew. Chem., Int. Ed.,* 2012, **51**, 12102-12106.
42. Zhang, G.; Hanson, S. K., Cobalt-catalyzed acceptorless alcohol dehydrogenation: Synthesis of imines from alcohols and amines, *Org. Lett.,* 2013, **15**, 650-653.

43. Zhang, G.; Vasudevan, K. V.; Scott, B. L.; Hanson, S. K., Understanding the mechanisms of cobalt-aatalyzed hydrogenation and dehydrogenation reactions, *J. Am. Chem. Soc.,* 2013, **135**, 8668-8681.
44. (a) Suzuki, A., Cross-coupling reactions of organoboranes: An easy way to construct C–C bonds (Nobel Lecture), *Angew. Chem., Int. Ed.,* 2011, **50**, 6722-6737. (b) Hiyama, T., How I came across the silicon-based cross-coupling reaction, *J. Organomet. Chem.,* 2002, **653**, 58-61.
45. Obligacion, J. V.; Chirik, P. J., Earth-abundant transition metal catalysts for alkene hydrosilylation and hydroboration, *Nat. Rev. Chem.,* 2018, **2**, 15.
46. (a) Pang, M.; Wu, C.; Zhuang, X.; Zhang, F.; Su, M.; Tong, Q.; Tung, C.-H.; Wang, W., Addition of a B–H bond across an amido–cobalt bond: Co^{II}–H-catalyzed hydroboration of olefins, *Organometallics,* 2018, **37**, 1462-1467. (b) Ghosh, C.; Kim, S.; Mena, M. R.; Kim, J.-H.; Pal, R.; Rock, C. L.; Groy, T. L.; Baik, M.-H.; Trovitch, R. J., Efficient cobalt catalyst for ambient-temperature nitrile dihydroboration, the elucidation of a chelate-assisted borylation mechanism, and a new synthetic route to amides, *J. Am. Chem. Soc.,* 2019, **141**, 15327-15337.
47. Erken, C.; Kaithal, A.; Sen, S.; Weyhermüller, T.; Hölscher, M.; Werlé, C.; Leitner, W., Manganese-catalyzed hydroboration of carbon dioxide and other challenging carbonyl groups, *Nat. Commun.,* 2018, **9**, 1-9.
48. Kubas, G. J., Fundamentals of H_2 binding and reactivity on transition metals underlying hydrogenase function and H_2 production and storage, *Chem. Rev.,* 2007, **107**, 4152–4205.
49. (a) Sellmann, D.; Sutter, J., In quest of competitive catalysts for nitrogenases and other metal sulfur enzymes, *Acc. Chem. Res.,* 1997, **30**, 460. (b) Gennari, M.; Duboc, C., Bio-inspired, multifunctional metal-thiolate motif: From electron transfer to sulfur reactivity and small-molecule activation, *Acc. Chem. Res.,* 2020, **53**, 2753-2761.
50. Denny, J. A.; Darensbourg, M. Y., Metallodithiolates as ligands in coordination, bioinorganic, and organometallic chemistry, *Chem. Rev.,* 2015, **115**(11), 5248-5273.
51. Sellmann, D.; Geipel, F.; Moll, M., (Ni(NHPnPr_3)(S_3'))], the first nickel thiolate complex modeling the nickel cysteinate site and reactivity of [NiFe] hydrogenase, *Angew. Chem., Int. Ed.,* 2000, **39**, 561-563.
52. Sellmann, D.; Prakash, R.; Heinemann, F. W.; Moll, M.; Klimowicz, M., Heterolytic Cleavage of H_2 at a Sulfur-Bridged Dinuclear Ruthenium Center, *Angew. Chem., Int. Ed*., 2004, **43** (14), 1877−1880.
53. Hesp, K. D.; McDonald, R.; Ferguson, M. J.; Stradiotto, M., New cationic and zwitterionic Cp*M(k^2-P,S) complexes (M= -Rh, -Ir): Divergent reactivity pathways arising from alternative modes of ancillary ligand participation in substrate activation, *J. Am. Chem. Soc.,* 2008, **130**, 16395-16404.
54. Sarbajna, A.; Patil, P. H.; Dinh, M. H.; Gladkovskaya, O.; Fayzullin, R. R.; Lapointe, S.; Khaskin, E.; Khusnutdinova, J. R. Facile and reversible double dearomatization of pyridines in non-phosphine Mn(I) complexes with N,S-donor pyridinophane ligand, *Chem. Commun*., 2019, **55**, 3282−3285.

55. Omann, L.; Königs, C. D. F.; Klare, H. F.; Oestreich, M., Cooperative catalysis at metal−sulfur bonds*, Acc. Chem. Res*., 2017, **50**, 1258−1269.
56. Song, H.; Ye, K.; Geng, P.; Han, X.; Liao, R.; Tung, C.-H.; Wang, W., Activation of epoxides by a cooperative iron–thiolate catalyst: Intermediacy of ferrous alkoxides in catalytic hydroboration, *ACS Catal.,* 2017, **7**, 7709-7717.
57. Zhang, F.; Song, H.; Zhuang, X.; Tung, C. H.; Wang, W., Iron-catalysed 1,2 selective hydroboration of N-heteroarenes, *J. Am. Chem. Soc.,* 2017, **139**, 17775-17778.
58. Sarkar, K.; Das, K.; Kundu, A.; Adhikari, D.; Maji, B., Phosphine-free manganese catalyst enables selective transfer hydrogenation of nitriles to primary and secondary amines using ammonia−borane, *ACS Catal.,* 2021, **11**, 2786−2794.
59. Alig, L.; Fritz, M.; Schneider, S. First-row transition metal (de)hydrogenation catalysis based on functional pincer ligands, *Chem. Rev.,* 2019, **119**, 2681−2751.
60. Newton, W. E., Sulfide and other sulfur containing ligands in metalloproteins and enzymes, *Inorg. Chem.,* 1984, **5**, 409-477.
61. (a) Song, H.; Ye, K.; Geng, P.; Han, X.; Liao, R.; Tung, C. H..; Wang, W. Activation of epoxides by a cooperative iron-thiolate catalyst: intermediacy of ferrous alkoxides in catalytic hydroboration, *ACS. Catal*., 2017, **7**, 7709-7717. (b) Zhang, F.; Song. H.; Zhuang, X.; Tung, C. H.; Wang, W., Iron-catalyzed 1, 2-selective hydroboration of N-heteroarenes, *J. Am. Chem. Soc*. 2017, **139**, 17775-17778.
62. (a) Ray, K.; Bill, E.; Weyhermüller, T.; Wieghardt, K. Redox- noninnocence of the S,S '-coordinated ligands in bis (benzene-1,2-dithiolato) iron complexes, *J. Am. Chem. Soc*., 2005, **127**, 5641− 5654. (b) Kaim, W. Manifestations of noninnocent ligand behavior, *Inorg. Chem.,* 2011, **50**, 9752−9765.
63. (a) Ataie, S.; Lohoar, M. I.; Mangin, L. P.; Baker, R. T. Ligand exchange through preprotonation in iron(II)- and cobalt(II)-SNS bis-amido complexes, *Chem. Commun.,* 2023, **59**, 4044. (b) Ataie, S.; Dudra, S. L.; Johnson, E. R.; Baker, R. T., Selective cobalt(II)-SNS dithiolate complex-catalyzed bifunctional hydroboration of aldehydes: Kinetics and mechanistic studies, *ACS Catal.*, 2023, **13**, 10076. (c) Elsby, M. R.; Baker, R. T., Cu(I)-SNS complexes for outer-sphere hydroboration and hydrosilylation of carbonyls, *Chem. Commun.*, 2019, **55**, 13574.
64. (a) Ataie, S.; Ovens, J. S.: Baker, R. T., Solvent-free Zn(NSNO) complex-catalysed dihydroboration of nitriles, *Chem. Commun.,* 2022, **58***,* 8266. (b) Ataie, S.; Baker, R. T., Comparing B-H bond activation in $Ni^{II}X$(NNN)-catalyzed nitrile dihydroboration (X = anionic N-, C-, O-, S-, or P-donor), *Inorg. Chem.,* 2022, **61**, 19998.
65. Ataie, S.; Baker, R. T., Bifunctional activation of NHC-zinc pre-catalyst for effective hydroboration of quinolines and nitriles, *ChemCatChem*, 2023, e2023006.
66. Das, U. K.; Daifuku, S. L.; Gorelsky, S. I.; Korobkov, I.; Neidig, M. L.; Le Roy, J. J.; Murugesu, M.; Baker, R. T., Mononuclear, dinuclear and trinuclear iron complexes featuring a new monoanionic SNS thiolate ligand, *Inorg. Chem.,* 2016, **55**, 987-997.
67. Das, U. K.; Higman, C. S.; Gabidullin, B.; Hein, J. E.; Baker, R. T., Efficient and selective iron complex-catalyzed hydroboration of aldehydes, *ACS. Catal*., 2018, **8**, 1076.

68. Albkuri, Y. M.; Ovens, J. S.; Martin. J.; Baker, R. T., Nickel(II)-SNS thiolate complexes: Reactivity and solution dynamics, *Inorg. Chem*., 2021, **60**, 10934-10942.
69. Tatsuya, K.; Hiro, K.; Yoshihiko, K., Valence isomerization, synthesis and characterization of cobalt and nickel complexes with non-innocent N_2S_2 ligand, *Bull. Chem. Soc. Jpn.,* 1997, **70**, 1599-1606.
70. Albkuri, Y. M. Nickel catalysis chemistry: Synthesis, reactivity and ligand dynamics of Ni SNS thiolate complexes, University of Ottawa PhD thesis, 2021.
71. Das, U. K.; Daifuku, S. L.; Iannuzzi, T. E.; Gorelsky, S. I.; Korobkov, I.; Gabidullin, B.; Neidig, M. L.; Baker, R. T., Iron (II) complexes of a hemilabile SNS amido ligand: Synthesis, characterization, and reactivity, *Inorg. Chem*., 2017, **56**, 13766−13776.
72. Blacquiere, J. M. Structurally-responsive ligands for high performance catalysts, *ACS Catal*., 2021, **11**, 5416−5437.
73. Elsby, M. R.; Kim, S. Y.; Steinmann, S. N.; Baker, R. T., Same ligand, three first-row metals: Comparing M-amido bifunctional reactivity (Mn, Fe, Co), *Dalton Trans.*, 2021, **50**, 14542-14546.
74. Ataie, S.; Hogeterp, S.; Ovens, J. S.; Baker, R. T., SNS ligand-assisted catalyst activation in Zn-catalysed carbonyl hydroboration, *Chem. Commun.,* 2022, **58**, 3795.
75. Elsby, M. R.; Oh, C.; Son, M.; Kim, S. Y. H.; Baik, M.-H.; Baker, R. T., Spin-state crossover in photo-catalyzed nitrile dihydroboration via Mn-thiolate cooperation, *Chem. Sci.,* 2022, **13**, 12550.

Chapter Two: Cobalt Amido Complexes Bearing N-Heterocyclic Carbenes as Pre-catalysts for Carbonyl Hydroboration

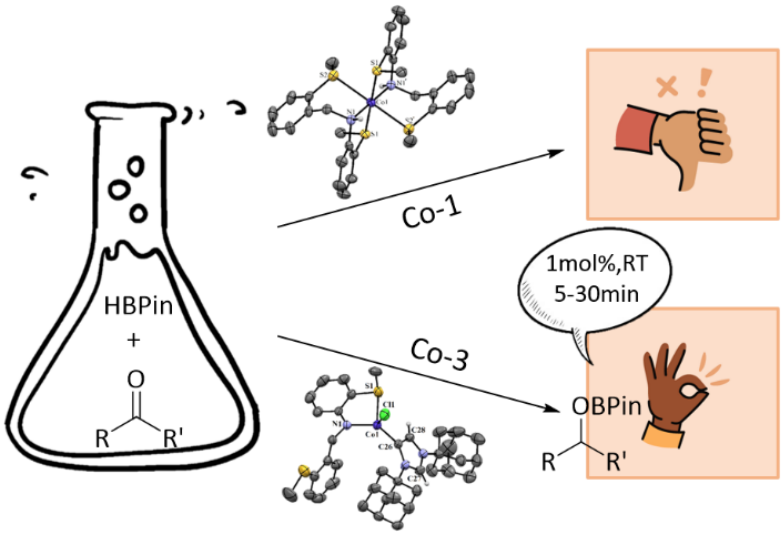

2.1 Contribution to Knowledge

Bifunctional Hydroboration Catalyst Activation Using an Abnormal-NHC Co SNS Amido Complex. Atousa Khanzadeh, Saeed Ataie, Loïc P. Mangin, Maxwell I. Lohoar, Brandon Fitchett and R. Tom Baker, *Organometallics* **2023**, in press.

Author Contributions

Atousa conducted the catalytic reactions, prepared the complexes, recorded and analyzed the EPR spectra under the expert guidance and supervision of Prof. Baker. Saeed took charge of growing the crystals and conducted in-depth analysis of the X-ray and mass spectra. Loïc was responsible for the DFT calculations studies and Max recorded the Evan's NMR spectra. Atousa, Saeed and Prof. Baker wrote the manuscript. Each author played a crucial role in advancing our understanding of the subject matter and contributed significantly to the completion of this research project.

Abstract: In previous work, supporting ligands were incorporated in Fe(II) SNS pincer catalysts by monoprotonation of the bis(amido) complex, *mer*-[Fe(κ^3-$S^{Me}NS^{Me}$)$_2$], affording the isolable Fe amido-amine cation with an easily displaced SNS amine ligand. Herein we show that protonation of the Co analogue (**2.1**) proceeds directly to the bis(amine) dication, *fac*-[Co(κ^3-$S^{Me}NHS^{Me}$)$_2$]$^{2+}$. DFT studies clearly corroborate the *mer*- to fac-isomerization upon diprotonation of both Fe and Co complexes. To access an ancillary ligated hydroboration precatalyst, treatment of **2.1** with 1,3-bis(1-adamantyl)imidazolium chloride (IAd·HCl) effects both amido ligand protonation and chloride addition, yielding the abnormally-coordinated IAd complex, $Co^{II}Cl(\kappa^2$-$S^{Me}NS^{Me})$(a-IAd) (**2.3**). DFT calculations showed that **2.3** is only slightly more stable than the complex containing the normal IAd isomer, suggesting a role for kinetic control due to steric factors. Stoichiometric treatment of both **2.1** and **2.3** with pinacolborane (HBpin) afforded free N-borylamine but only **2.3** served as an effective carbonyl hydroboration catalyst, showing the important role of a-IAd in stabilizing cobalt throughout the catalytic cycle.

2.2 Introduction

In Chapter one I discussed the role of amido ligands in cooperative metal-ligand catalysis either in the catalytic cycle [Mn bis(amido) photo-catalyzed nitrile hydroboration][1] or in an initial pre-catalyst activation step [Zn bis(amido)-catalyzed carbonyl hydroboration].[2] In this chapter I demonstrate a similar ligand-assisted pre-catalyst activation step using a Co amido complex bearing an abnormally-coordinated N-heterocyclic carbene (NHC) ligand.

B-H bond activation is a fundamental step in metal complex-catalyzed hydroboration reactions,[3-5] in which the ligand can play multiple roles.[6] Although anionic ligands possessing an additional lone pair as potential Lewis-base donor have shown remarkable potential to participate in cooperative B-H bond activation,[4,10-20] borylation of these ligands often decreases their donor power, leading to facile dissociation.[10-17] For some ligands in precatalysts, this dissociation may result in irreversible catalyst deactivation. To address this problem, two methods have been reported: first, using a multidentate XL_n ligand that retains strong donors in its borylated form,[4,19-25] and second, employing a supporting ligand to stabilize the metal center after dissociation of the borylated ligand.[26-29] In previous work the Baker group employed amido- and thiolate-SNS complexes of first row metals (Mn, Fe, Co, Cu, Zn) as bifunctional hydroboration catalysts. While reactions of HBpin with Cu and Zn κ^2-amido complexes led to dissociation of the N-borylamine (and generation of M-H), protonation of the bis(amido) Fe complex afforded the Fe amido-amine cation in which the latter retained its κ^3-coordination (**Scheme 2.1**-top). Nonetheless, facile dissociation of the tridentate bis(thioether)amine ligand allowed for the isolation of a series of precatalysts Fe(κ^3-$S^{Me}NS^{Me}$)L_n containing a variety of supporting ligands i.e., $P(OMe)_3$, triphos.[30]

Cobalt complexes have demonstrated promising activity in hydroboration of various unsaturated organic groups such as carbonyls,[31-36] N-heterocycles,[37] nitriles,[38] alkenes,[39] and alkynes.[40,41] Among cobalt complexes studied in catalytic carbonyl hydroboration, two different mechanistic pathways have been reported (**Scheme 2.2**). First is Fout's Co(I) bis(NHC) complex,[35] which adds a B-H bond to form a CoH(Bpin) core much like previously reported Rh catalysts.[42] Second, the Baker group's recent Co(II) complex[36] benefits from two Lewis-basic thiolate donors to bifunctionally activate the B-H bond through metal-ligand cooperation. In this cooperation the thiolate donor activates HBpin and the Co center activates the carbonyl through O-coordination, thus directing the reaction through an inner-sphere hydride transfer mechanism not involving a Co-H intermediate. Herein, we examine the catalytic potential of our previously reported cobalt(II) bis(amido) SNS complex (**2.1**; **Scheme 2.1**-bottom)[43] with and without supporting NHC ligands in hydroboration reactions.

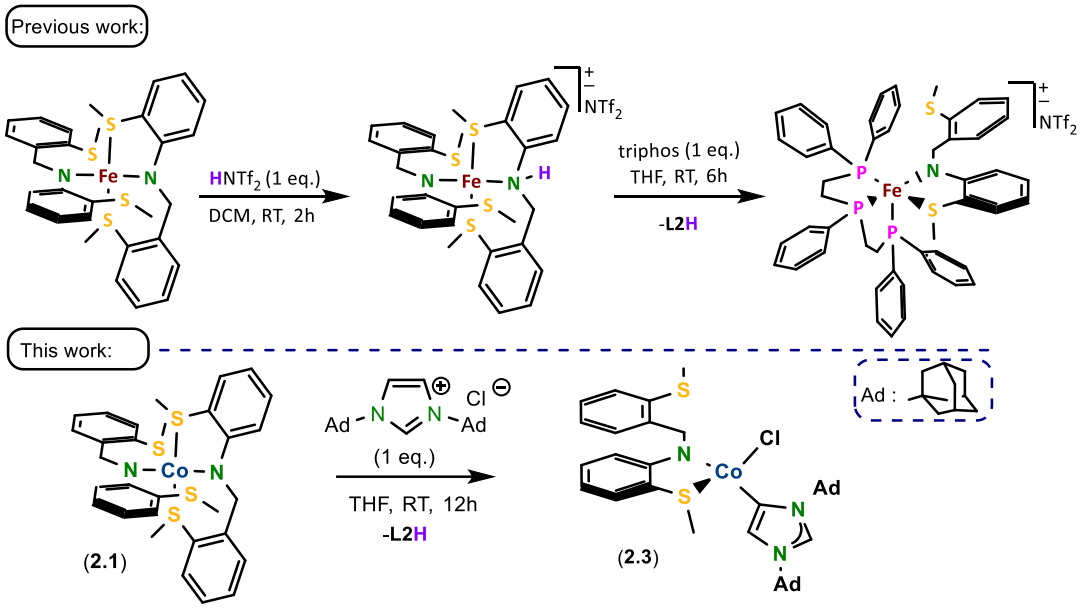

Scheme 2.1 Supporting ligand addition following protonation of amido-SNS ligand in Fe- and Co- complexes.

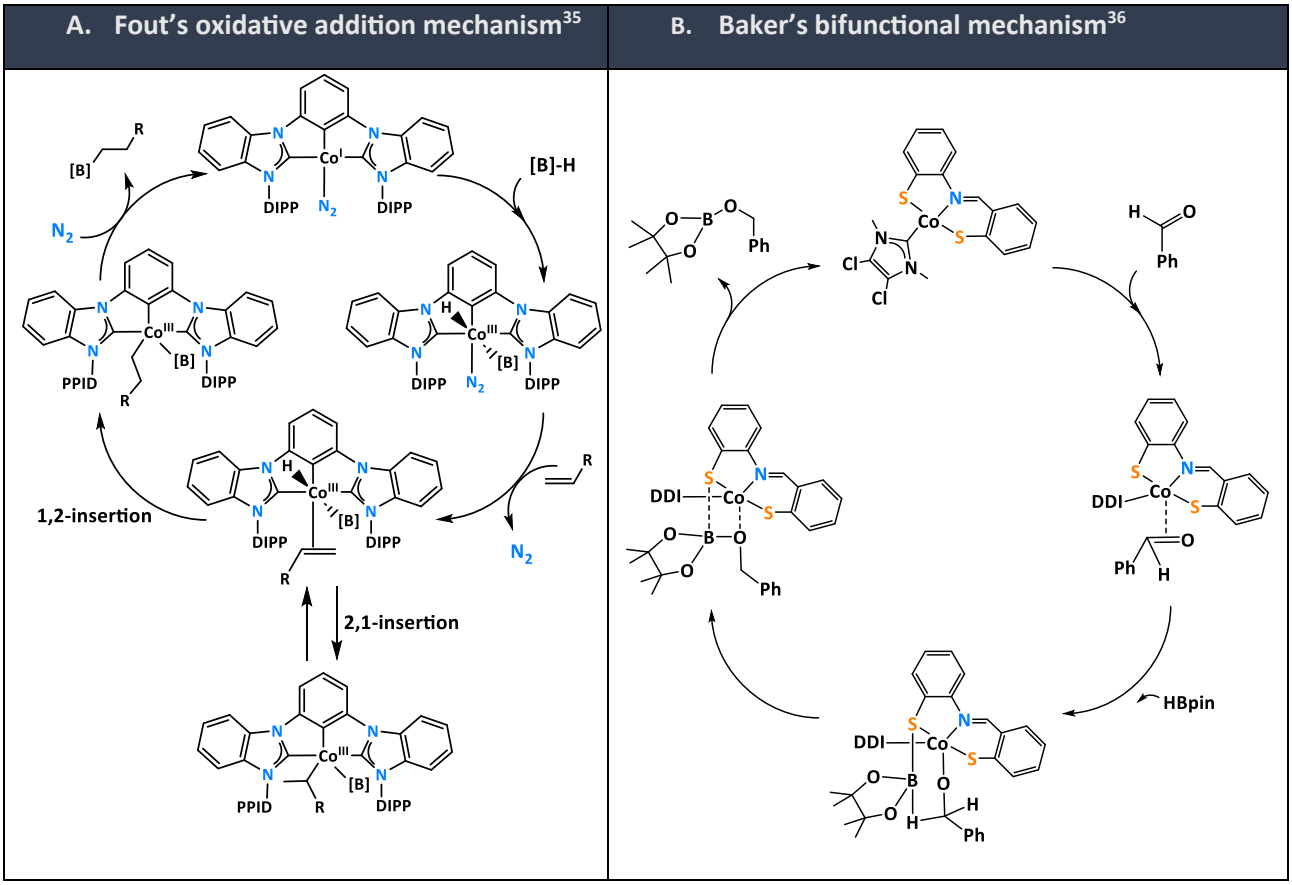

Scheme 2.2 Diverse reaction pathways for Co-catalyzed hydroboration.

2.3 Results and Discussion

2.3.1 Protonation of $Co^{II}(S^{Me}NS^{Me})_2$ (2.1)

Treatment of a green benzene solution of bis(amido) complex $Co^{II}(\kappa^3\text{-}S^{Me}NS^{Me})_2$ (**2.1**) with 1 equiv of $HNTf_2$ gave a brown-yellow solution and dark yellow precipitate of $[Co(\kappa^3\text{-}S^{Me}N^{H}S^{Me})_2](NTf_2)_2$ (**2.2**). All efforts to synthesize and isolate the mono-protonated complex, such as using 0.9 equiv of $HNTf_2$ in THF at -110 °C, were unsuccessful, as the green solution quickly converted to brown-yellow, containing both **2.2** and unreacted **2.1**. Hence **2.1** was treated with 2 equiv of $HNTf_2$, affording **2.2** in 87% yield (**Scheme 2.3**). Paramagnetic ^1H NMR of **2.2** showed two singlets at δ 0.74 and 0.95, each due to two SMe groups (**Figure 2.2**). The two NCH_2- moieties gave a singlet at δ 2.72 and 16 hydrogens were observed between δ 4.85-5.8, in agreement with the expected number of aromatic hydrogens.

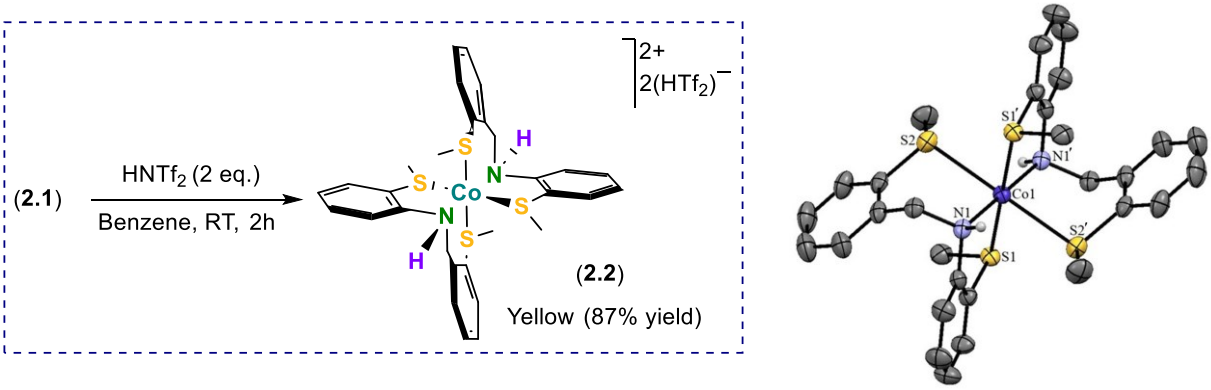

Scheme 2.3 Synthesis and molecular structure of **2.2** with 50% probability. Thermal ellipsoids, hydrogen atoms refined via the riding model and counter NTf_2^- anions are omitted for clarity. Selected bond distances (Å) and angles (°): Co-S1 = Co-S1' 2.2785, Co-S2 =Co-S2' 2.6522, Co-N1 = Co-N1' 1.993, S1-Co-S2= S1'-Co-S2' 100.04, S1-Co-S2' = S1'-Co-S2 79.96, S1-Co-N1=S1'-Co-N1' 87.74, S1-Co-N1'=S1'-Co-N1 92.26, S1-Co-S1' 180.00, S2-Co-N = S2'-Co-N1' 89.68, S2-Co-N1'=S2'-Co-N1 90.32, S2-Co-S2' 180.00.

The solution magnetic moment of **2.2** determined by Evans' NMR method[42] was 4.64 BM in accord with other octahedral high-spin cobalt(II) complexes.[43,44] The molecular structure of **2.2** (**Scheme 2.3**) shows that protonation of mer-Co(**L2**)$_2$ gives rise to the facial isomer of $[Co(\mathbf{L2}H)_2]^{2+}$. The Co-S bonds in 5-membered rings of **2.2** (2.2785 Å) are shorter than those of **2.1** (2.4723(7) and, as observed for the Fe amine-SNS ligand,[30] the difference in Co-S bond distances between the 5- and 6-membered rings is small (0.004 Å), in contrast to that in **2.1** (0.230 Å). As expected, the Co-N bond distance is significantly longer in **2.2** (by 0.023 Å vs **2.1**) due to protonation.

2.3.2 DFT investigation of 2.1 isomerization upon protonation

To shed some light on the isomerism change upon protonation, we undertook DFT calculations (see section **2.6.4** for detailed discussion) at the PBE0-D3(BJ)/6-311(+)g**/ def2TZVP(D) level of theory in implicit THF. The results demonstrate that the two protonations of M(**L2**)$_2$ complexes (M = Co or Fe) by $HNTf_2$ are strongly exothermic and exergonic, the second one releasing slightly less energy (**Table 2.1**). The thermodynamics of the Co and Fe complexes are relatively similar, and the meridional isomer is clearly favoured over the facial one in the neutral complexes. The first and easiest protonation reduces the energy

gap between the isomers and the second protonation then induces a conformational change leading to the [*fac*-M(**L2**H)$_2$]$^{2+}$ cation that is strongly stabilized by ionic pairing to the $(NTf_2)^-$ counter-anions (ca. 10 kcal/mol per anion), as observed for both [Fe(**L2**)(**L2**H)][NTf_2] and [Co(**L2**H)$_2$][NTf_2]$_2$ in the solid state. Protonation is also accompanied by a lengthening of both the N-C_{Ar} and Co-N bonds, allowing for a greater flexibility of the SNS ligand without compromising its binding ability.

Table 2.1 Gibbs free energies (in kcal/mol) for sequential stepwise protonation of the mer/fac-[M(**L2**)$_2$]$^{n+}$ complexes (n = 0,1,2).

	M = Co		M = Fe	
	mer	*fac*	*mer*	*fac*
M(**L^1**)$_2$	**0**	+5.3	**0**	+11.2
↓ HNTf$_2$				
[M(**L^1**H)(**L^1**)][NTf_2]	**-24.6**	-22.4	**-25.3**	-21.2
↓ HNTf$_2$				
[M(**L^1**H)$_2$][NTf_2]$_2$	-41.4	**-45.1**	-44.0	**-44.8**

2.3.3 Adding a NHC supporting ligand to the coordination sphere

In light of the protonation reactivity of **2.1**, we sought an alternate strategy to install a supporting ligand for catalysis studies. Taking a page from our earlier work with Co(**L1**)$_2$,[34] we treated **2.1** with 1 equiv. of IAd•HCl, affording **2.3** as a dark green powder in 81% yield (**Scheme 2.4**). In this method, protonation of **L2** by the imidazolium salt adds both IAd and Cl ligands to Co with expulsion of **L2**H. The paramagnetic ^{1}H NMR of **2.3** showed 19 resonances between δ -51.71 and 106.95 ppm, in agreement with the number of

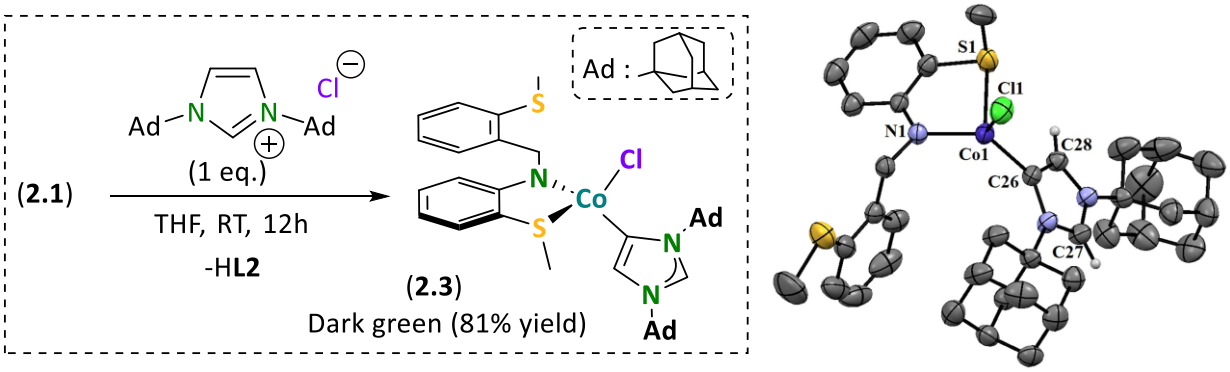

Scheme 2.4 Synthesis and molecular structure of **2.3** with 50% probability thermal ellipsoids. Backbone hydrogen atoms omitted for clarity. Selected bond distances (Å) and angles (deg): Co1-S1 2.411(1), Co1-C26 2.034(3), Co1-N1 1.919(3), Co1-Cl1 2.269(1), S1-Co1-N1 85.7(1), S1-Co1-Cl1 103.18(4), S1-Co1-C26 103.1(1), N1-Co1-Cl1 113.0(1), N1-Co1-C26 122.7(1), Cl1-Co1-C26 119.3(1).

inequivalent protons in **2.3** (**Figure A2.3**). The solution magnetic moment of **2.3** determined by Evans' NMR method was 3.80 BM.

Although **2.1**, **2.2** and **2.3** are high spin complexes with S = 3/2, **2.2** has a larger magnetic moment due to its cationic nature causing a larger energy difference between the e_g and t_2g orbital sets in octahedral geometry.[47.a] The molecular structure of **2.3** showed a slightly distorted tetrahedral geometry ($\tau'_4 = 0.98$)[47.b] in which IAd is coordinated abnormally (i.e., through C26 instead of C27). The Co-S bond in **2.3** is 0.133 Å longer than its peer in **2.2**, and very close to that of **2.1**. The Co-C26 bond length of 2.034(3) Å is in agreement with those previously reported in other pseudotetrahedral abnormal-NHC cobalt(II) complexes.[47.c] The average bond lengths of Co-C_{NHC} in normal cobalt(II) carbene complexes are in the same range.[48,49]

2.3.4 DFT investigation of abnormal coordination of IAd

Although the majority of abnormal NHC metal complexes have been prepared using 2-substituted imidazolium precursors,[51] examples of selective C4-H activation in conventional NHCs with bulky N-substituents have been reported previously.[52] To better understand why IAd is coordinated abnormally in **2.3**, we turned to DFT to compare the binding modes of IAd to our Co(SNS) core (**Figure 2.1**). The optimized geometry of **2.3** agrees well with the experimental SC-XRD structure with a Co-C bond distance of 2.032 Å (vs. 2.034(4) Å in the solid state at 200 K). Structure optimization of the isomer with a normally coordinated IAd showed a significantly longer Co-C bond (2.101 Å) and a clear lengthening of all bonds around the metal center. Moreover, an increased deviation from the ideal tetrahedral geometry ($\tau'_4 = 0.73$)[47.b] was observed, caused by a significant increase of the Ĉ-Co-S angle (from 103 ° (XRD) / 106 ° (DFT) to 127 °) and a reduction of the Ĉ-Co-Cl angle (from 119 ° (XRD) / 122 (DFT) to 106 °). This most likely results from the large steric hindrance of the adamantyl substituents. Although the free *α*-IAd zwitterion is significatively less stable (by ΔG = 12 kcal/mol) than the normal free carbene, the calculations predict that the abnormal coordination mode is only slightly favoured over the normal isomer by ΔG = 0.6 kcal. This thermodynamic preference is attributed mostly to the entropic factor (normal → abnormal; ΔH^r = +1.9 kcal/mol and ΔS^r = +8 cal/mol·K) and highlights once more the steric effects of the bulky adamantly substituents. Thus, we believe that the selectivity leading to **2.3** arises from kinetic control, and that the approach of the imidazolium $IAdH^+$ towards the amido-cobalt bond is easier from the less hindered C4 of the imidazolium, and that further abnormal→normal rearrangement is kinetically inaccessible at room temperature.

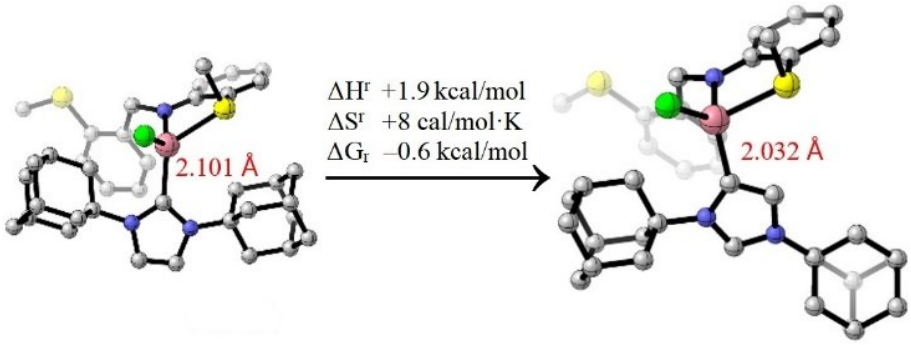

Figure 2.1 Calculated geometries and energy differences (at 298 K) of **2.3** (right) and its normal IAd isomer (left).

While the abnormal IAd coordination did not provide significant stabilization for **2.3** *vs*. the unobserved normally-coordinated IAd isomer, thermolysis of $Co[N(SiMe_3)_2]_2(IPr)$ at 80 °C has been shown to afford the more stable *a*-IPr isomer.[53] The strong donor power of these so-called "mesoionic" carbenes[54] has proven useful in a number of catalytic processes although most involve precious metal complexes.[51c]

2.3.5 Synthesis and characterization of $[CoCl_2(n\text{-}IAd)]_2$ (2.4)

In an effort to prepare the normal-IAd version of **2.3**, we prepared $[CoCl(\mu\text{-}Cl)(IAd)])_2$ (**2.4**; **Scheme 2.5**). In **2.4** two $CoCl_2(IAd)$ units form a symmetrical chloro-bridged dimer with two strained pseudotetrahedral Co centers [C1-Co-Cl1' = 130.85(8) and Cl1-Co1-Cl1' = 88.32(3) °]. Interestingly, the normally coordinated form of IAd in **2.4** makes the Co-C bond slightly longer compared to that of **2.3** (2.057(3) Å *vs.* 2.034(3) Å). **2.4** is structurally similar to previously reported dichlorocobalt dimers ligated by a bulky carbene ligand such as IMes,[55] IPr[50] and 4-butylamino-IPr.[56] The Co1-C1 bond in **2.4** is slightly longer than that of previously reported analogs (2.057(3) Å vs. 2.0298(13)[50] Å, vs. 2.031(2)[55] Å and vs. 2.045(5)[56] Å) which is expected due to the steric bulk of IAd in **2.4**. The angle between Co and the two Cl bridges is smaller in **2.4** (88.32(3) compared to 95.24(1)[50], 94.86(2)[55] and 92.89(5)[56], which is in agreement with Co-Cl bridges being relatively longer in **2.4** (2.3562(8) and 2.3725(7) Å compared to 2.3272(16) and 2.3525(16) Å as the longest bridges[56] among the previously reported cases). Theoretically, treatment of **2.4** with Na**L2** could afford an analogue of **2.3** with IAd being normally coordinated, but in practice all efforts to isolate and characterize the target complex were unsuccessful (see SI). However, comparing **2.4** and **2.3** in hydroboration reactions helped us to assess the importance of **L2** in the latter precatalyst (*vide supra*).

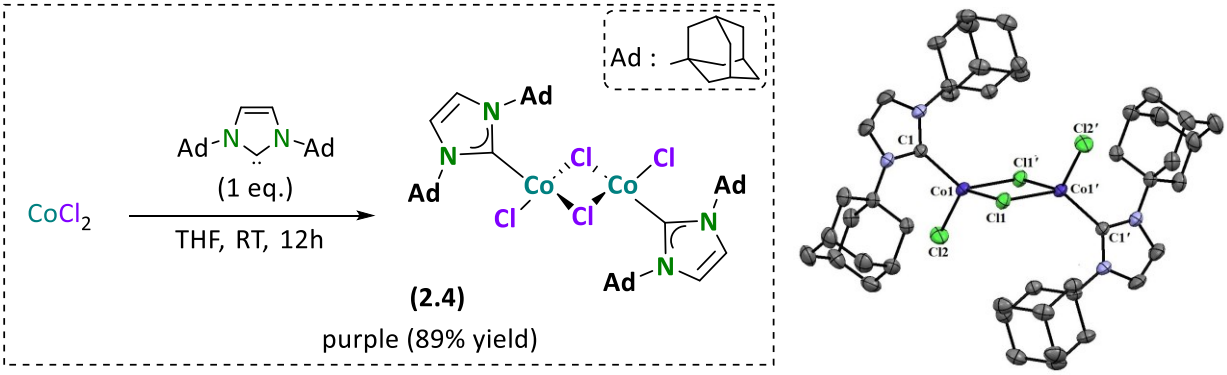

Scheme 2.5 Synthesis and molecular structure of **2.4** with 50% probability thermal ellipsoids and hydrogen atoms omitted for clarity. Selected bond distances (Å) and angles (deg): Co1-Cl1=Co1'-Cl1' 2.3562(8), Co1-Cl1'=Co1'-Cl1 2.3725(7), Co1-Cl2=Co1'-Cl2' 2.2551(9), Co1-C1=Co1'-C1' 2.057(3), C1-Co1-Cl2=C1'-Co1'-Cl2' 113.20(8), C1-Co1-Cl1=C1'-Co1'-Cl1' 105.95(8), C1-Co1-Cl1'=C1'-Co1'-Cl1 130.85(8), Cl2-Co1-Cl1=Cl2'-Co1'-Cl1' 124.56(3), Cl2-Co1-Cl1'=Cl2'-Co1'-Cl1 94.08(3) Cl1-Co1-Cl1' 88.32(3) Co1-Cl1-Co1'=Co1'-Cl1'-Co1 91.68(3).

To compare the protonation of **L2** in **2.3** with that in **2.1**, the former was treated with 1 equiv of $HNTf_2$. In addition to dissociation of H**L2**, however, a ligand redistribution afforded the dinuclear dication $\{[Co(\mu\text{-}Cl)(a\text{-}IAd)_2]_2\}^{2+}(NTf_2)_2$ (**2.5**, **Scheme 2.6**). The inorganic byproduct(s) were not characterized. The Co1-C bond distances in **2.5** (2.013(3) and (2.020(4) Å) are somewhat shorter than that in **2.3** (2.034(3) Å) and the Cl-Co-Cl bridge angle in **2.5** (93.60(4)°) is larger than that in **2.4** (88.32(3)°).

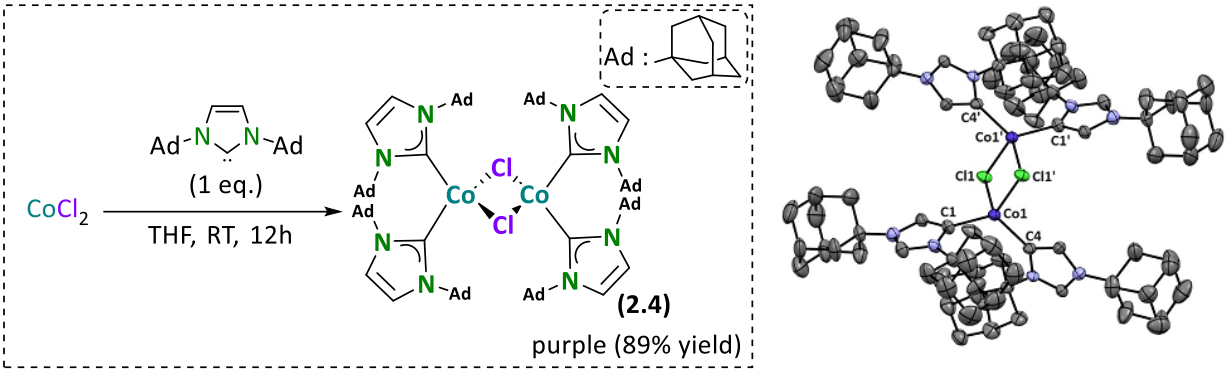

Scheme 2.6 Synthesis and molecular structure of **2.5** with 50% probability thermal ellipsoids and hydrogen atoms, NTf_2 moieties and THF solvent molecules omitted for clarity. Selected bond distances (Å) and angles (deg): Co1-Cl1=Co1'-Cl1' 2.367(1), Co1-Cl1'=Co1'-Cl1 2.376(1), C1-Co1=C1'-Co1' 2.013(3), C4-Co1=C4'-Co1' 2.020(4), Cl1-Co1-Cl1'=Cl1'-Co1'-Cl1 93.60(4), Co1-Cl1-Co1'=Co1-Cl1'-Co1 86.40(4), C1-Co1-C4=C1'-Co1'-C4' 124.0(2), C1-Co1-Cl1=C1'-Co1'-Cl1' 115.6(1), C1-Co1-Cl1'=C1'-Co1'-Cl1 102.4(1), C4-Co1-Cl1=C4'-Co1'-Cl1' 103.1(1), C4-Co1-Cl1'=C4'-Co1'-Cl1 114.3(1).

2.3.6 Carbonyl hydroboration catalysis

Using 1 mol% of complexes **2.1**, **2.2** and **2.3** as catalysts for the hydroboration of benzaldehyde using HBpin in benzene showed that only **2.3** was effective (**Table 2.2**, entries 1-3). **2.3** also proved to be efficient in hydroboration of acetophenone both in benzene (entry 4) and THF (entry 5), with the former giving quantitative yield after 30 min. To shed some light on this observation, one equiv of **2.1** was treated with 2 equiv of HBpin, resulting in a black precipitate (presumably Co metal). The precipitate was filtered off, the filtrate was evaporated under vacuum, and the remaining residue was confirmed as **L2**-Bpin by ESI-

Table 2. 2 Hydroboration of carbonyls in presence of cobalt complexes.

Entry	**[Co]**[a]	Sub.	Solv.	Time	Yield
1	**2.1**	Benz.	C_6D_6	1 h	n.p.
2	**2.2**	Benz.	C_6D_6	1 h	n.p.
3	**2.3**	Benz.	C_6D_6	5 m	>99 %
4	**2.3**	Acet.	C_6D_6	30 m	>99 %
5	**2.3**	Acet.	THF	30 m	91 %
6	**2.4**	Benz.	C_6D_6	15 m	84 %
7	**2.4**	Acet.	C_6D_6	45 m	<5 %
8	$CoCl_2$	Benz.	C_6D_6	30 m	84 %
9	$CoCl_2$	Acet.	C_6D_6	30 m	n.p.

*Reaction conditions: **2.1**, **2.2**, **2.3**, $CoCl_2$ (1 mol%), and **2.4** (0.5 mol%), carbonyl substrate (0.53 mmol), pinacolborane (0.53 mmol), C_6D_6 (0.5 mL) and THF (0.5 mL). Yields were determined by ^1H NMR and ^{11}B NMR analyses based on substrates and HBpin. Selectivity in all cases was 100%. [a] (1 mol%). n.p. = no product. Benz = Benzaldehyde and Acet = Acetophenone. m= minutes. Sub = substrate.

Table 2.3 Hydroboration of carbonyls using **2.3** precatalyst.

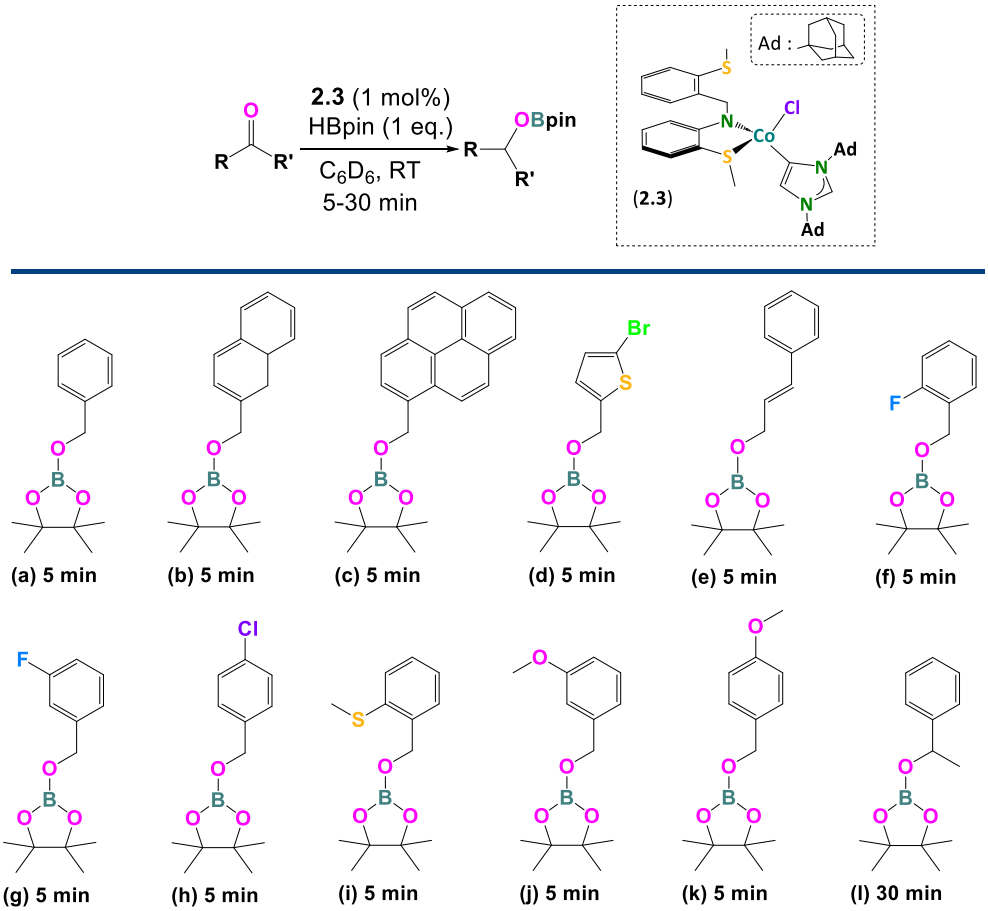

*Reaction conditions: **2.3** (1 mol%), carbonyl substrate (0.53 mmol), pinacolborane (0.53 mmol) and C_6D_6 (0.5 mL). Yields were determined by ^{1}H NMR and ^{11}B NMR analyses based on substrates and HBpin. Selectivity in all cases was 100% for the reported products. Quantitative yields were obtained for all substrates in 5 min, except for acetophenone.

MS (**Figure 2.7**). In contrast, treating **2.3** with a stoichiometric amount of HBpin resulted in a color change from dark green to brown and no precipitate formed. Evaporation of the solvent followed by hexane extraction and evaporation again confirmed formation of **L1**-Bpin. No evidence was found in the EI mass spectrum for free IAd or IAd-Bpin, confirming that a-IAd plays an important role in stabilizing the cobalt catalyst. The ^{11}B NMR spectrum of this reaction also showed two resonances at 24.6 (**L2**-Bpin)[14] and 21.6 ppm (Cl-Bpin),[48] showing that both chloride and **L2** are taking part in the B-H bond activation.

To find out which plays the more effective role, **2.4** was employed in hydroboration of benzaldehyde and acetophenone (entries 6 and 7), showing that **2.4** can only catalyze benzaldehyde hydroboration of benzaldehyde (84% yield in 15 min) while it failed to convert acetophenone. Removing IAd as a supporting ligand from the catalytic system by switching **2.4** to $CoCl_2$, benzaldehyde hydroboration gave 84% yield after 30 min (entry 8) while acetophenone did not undergo hydroboration at all (entry 9). These observations clearly show the important role of both IAd and **L2**-Bpin in stabilizing the Co center.

Precatalyst **2.3** was then tested as a hydroboration catalyst for a range of aldehydes and ketones (**Table 2.3**). Aldehyde reactions were quantitative in 5 min even for bulky substrates (entries b and c) and those having an electron-donating group on different positions (entries i-k). Switching aldehyde to ketone (acetophenone) resulted in a longer reaction time (30 min) for quantitative hydroboration (entry l). The paramagnetism of the used catalyst was confirmed by EPR spectroscopy, suggesting that the catalyst resting state is likely the substrate-derived bis(aryloxide) Co(II)-NHC complex as recently proposed for a similar Zn(II) system.[16]

2.4 Experimental Section

2.4.1 General considerations

All experiments were carried out under nitrogen, using a Schlenk line or an MBraun glovebox unless otherwise stated. Hexane, diethyl ether, acetonitrile and THF were dried on columns of activated alumina using a J. C. Meyer (formerly Glass Contour) solvent purification system. Anhydrous benzene (Aldrich), CD_3OD and C_6D_6 were dried with activated alumina (ca. 10 wt %) overnight, followed by filtration. Dichloromethane (DCM) and $CDCl_3$ were refluxed over calcium hydride under nitrogen, collected by distillation, dried further by passing through activated alumina (ca.10 wt%), and stored over activated 4 Å molecular sieves (heated at 250 °C for 3 d under vacuum). Ligand precursor 2-(methylthio)-benzaldehyde,[53] 1,3-bis(1-adamantyl)imidazolium chloride (IAd·HCl),[48] $S^{Me}N^{H}S^{Me}$ (H**L2**)[28] ligand, and as well as $Co^{II}(\kappa^3\text{-}S^{Me}NS^{Me})_2$ (**2.1**)[41] were prepared according to literature procedures. Other chemicals were used as obtained commercially: 2-(methylthio)-aniline (Alfa Aesar, 98%), $CoCl_2$ (Alfa Aesar, 97%), trifluoromethane sulfonimide ($NHTf_2$, Aldrich >95%), and sodium bis(trimethylsilyl)amide (Alfa Aesar, 98%). ^1H and ^{11}B NMR spectra were recorded on a 300 MHz Bruker Avance or Avance II instrument at room temperature (21−25 °C). ^1H NMR spectra were referenced respectively to residual solvent proton signals (C_6D_6, δ 7.15; $CDCl_3$, δ 7.26; CD_3OD, δ 1.75 and 3.31 ppm) and ^{11}B NMR spectra to external BF_3 etherate at 0.0 ppm. EPR spectra were recorded on a Bruker Elexsys E580 X-band spectrometer equipped with nitrogen gas temperature control system. Mass spectra were recorded on an AB Sciex Q1MS mass spectrometer with electrospray ionization (ESI-MS) in positive mode (ion spray voltage: 5000.0 V, TEM: 400 °C, declustering potential: 11.00 V and focusing potential: 300.0 V) with samples prepared to *ca.* 0.05 mg/mL in acetonitrile. For electron impact (EI), solid samples were prepared by drying products under vacuum, and spectra obtained using a Kratos Concept S1 instrument (Hres 7000−10000). X-ray diffraction data were collected on a Bruker Smart or Kappa diffractometer equipped with an ApexII CCD detector and a sealed-tube Mo K source (λ = 0.71073 Å).

2.4.2 Synthesis of 2.2

A 20 mL scintillation vial was charged with **2.1** (100 mg, 0.164 mmol) and 4 mL of benzene. To this solution, was added a solution containing 92 mg of bis(trifluoromethane)sulfonimide (0.328 mmol) in 8 mL of benzene, dropwise. The resulting yellowish solution was stirred for 2 h at room temperature, resulting in a pale yellow precipitate which was filtered, washed with hexane (3 × 10 mL) and then dried in vacuum affording 168 mg of **2.2** (87 %). Crystals of **2.2** suitable for X-ray crystallography were obtained by hexane layering of a concentrated DCM solution at room temperature. Selected ^1H NMR resonances (300 MHz,

methanol-d_4): δ 0.73 (s, 6H), 0.94 (s, 6H), 2.86 (s, 4H), 4.93 (br, d, 2H), 5.00 (br, t, 2H), 5.51 (br, ov mult, 4H), 5.76 (br, ov mult, 8H). MS: [M^+] 609.0667, Calcd. 609.093 (**Figure 2.3**). μ_{eff} (for **2.1** is 3.75 and for **2.2** is 4.64).

2.4.3 Synthesis of 2.3

A 42 mL scintillation vial was charged with **2.1** (200 mg, 0.328 mmol) and 15 mL of THF. To this solution, IAd·HCl (122 mg, 0.328 mmol) in 10 mL THF was added dropwise. The solution turned dark green after 3-4 h and was then stirred overnight at room temperature. The solvent was removed under vacuum and the residue was washed with diethyl ether (3 × 3 mL) and dried under vacuum, affording 187 mg of **2.3** (81%). Crystals of **2.3** suitable for X-ray crystallography were obtained by hexane layering of a concentrated DCM solution at room temperature; MS: [M^+] 704.2270, Calcd. 704.230 (**Figure 2.5**). μ_{eff} = 3.80.

2.4.4 Synthesis of 2.4

A 42 mL scintillation vial was charged with $CoCl_2$ (200 mg, 1.54 mmol) in 10 mL of THF. To this solution, IAd.HCl (518 mg, 1.54 mmol) in 10 mL THF was added dropwise at room temperature. The solution turned purple blue from the starting blue and then stirred overnight at room temperature. Then, the solvent was removed, and the residue was washed with diethyl ether (3 × 3 mL) and dried under vacuum affording 640 mg **2.4** (89%) as purple powder. Crystals suitable for X-ray diffraction were grown by hexane layering of a concentrated DCM solution at room temperature. EI-MS: Calcd for $C_{46}H_{66}Cl_4Cl_4Co_2N_4$ m/z 932.27 ([M^+]). Found m/z 932.24 (**Figure 2.10**).

2.4.5 Stochiometric reaction of 2.1 and 2.3 with HBpin

To a purple solution of **2.1** (0.010 g, 0.016 mmol, in 2 mL of THF) was added pinacolborane (4.6 µL, 0.032 mmol, 2 equiv) and the mixture immediately turned black, and a black precipitate formed. Then, the black precipitate was filtered, and the solvent of the filtrate was evaporated and the residue was analyzed by EI-MS, showing N-borylated **L2** (**L2**-Bpin, Figure S7-top). In a separate reaction, **2.3** (0.010 g, 0.014 mmol) and pinacolborane (2 µL, 0.014 mmol, 1 equiv), were treated in 2 mL of THF affording a quick color change from deep green to dark brown. Then, the solvent was evaporated, and the residue was analyzed by EI-MS, showing N-borylated **L2** (**Figure 2.7**).

2.4.6 General procedure for hydroboration of carbonyls

A vial was charged by **2.3** (3 mg, 0.005mmol, 1 mol%), the carbonyl substrate (0.53 mmol) and C_6D_6 (0.5 mL). Then the solution was transferred to an NMR tube. Subsequently, pinacolborane (77 µL, 0.53 mmol) was added and the NMR tube was capped and well shaken. Every 5 min, an ^{1}H NMR was recorded. Reaction times varied from 5-30 min at room temperature. The yield was determined by ^{1}H NMR in reference to characteristic aldehyde peak of starting substrates for aldehyde substrates, and ^{11}B NMR in reference to

peak of starting HBpin for acetophenone. The reaction mixture was filtered through a short silica plug, rinsed with ethyl acetate (2 mL), and concentrated under vacuum to yield the isolated product.

2.5 Conclusions

In this work we employed a bis(amido-SNS) cobalt complex (**2.1**) to generate an active catalyst for hydroboration of carbonyls. Although **2.1** was an ineffective precatalyst due to its decomposition in the presence of HBpin, replacement of one amido ligand by Cl and IAd ligands afforded **2.3**, with IAd being abnormally coordinated (*a*-IAd). DFT studies showed that the *a*-IAd ligand did not stabilize **2.3** *vs*. the unobserved normally-coordinated IAd analog, suggesting that the sterically crowded Co coordination sphere in **2.1** was responsible for coordination of IAd at C4 instead of C2.

At 1 mol% loading, **2.3** catalyzed acetophenone hydroboration quantitatively in 30 min under ambient conditions in benzene. Stoichiometric studies indicated that **2.3** undergoes a bifunctional catalyst activation, forming the N-borylamine and chloroborane to generate the active Co-(*a*-IAd) dihydride catalyst. In contrast, **2.4** is unable to catalyze acetophenone hydroboration, suggesting a key role for the increased donor power of the *a*-IAd ligand vs C2-coordinated IAd. As reported previously for a related Zn catalyst,[2] further work will be required to determine whether reversible coordination of **L2**-Bpin to Co could also be contributing to the catalytic activity of **2.3** by preventing oligomerization of reaction intermediates via aryloxide bridges. Overall, the results reported herein build on previous examples in which a stable precursor can undergo bifunctional B-H bond activation to generate reactive first row metal hydride catalysts.

2.6 Appendix

2.6.1 Spectroscopic data

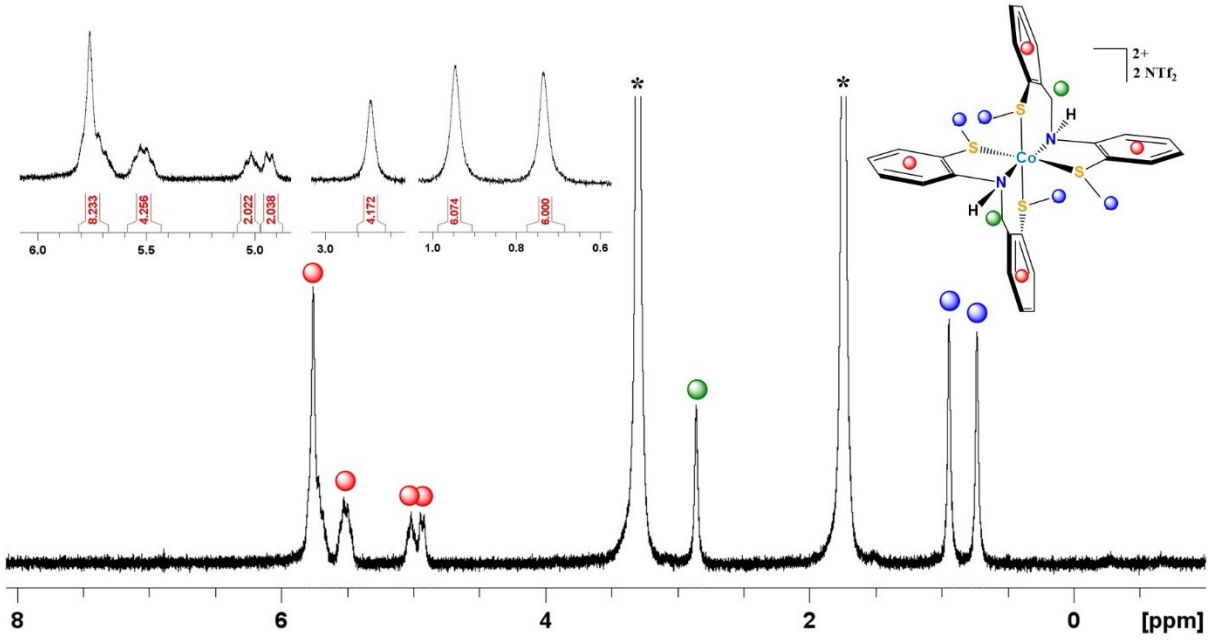

Figure A2.1 ^{1}H NMR spectrum (300 MHz, CD_3OD) of **2.2**. * Indicates protic impurity in CD_3OD.

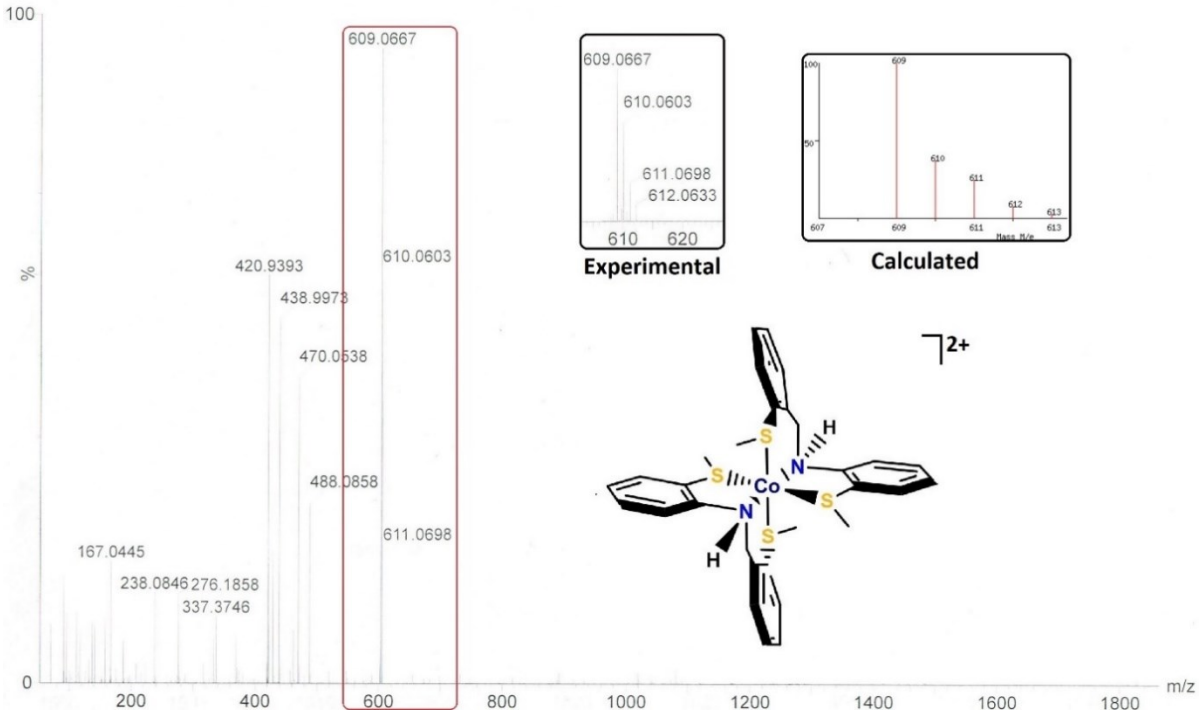

Figure A2.2 ESI-mass spectrum of **2.2** $[M]^+$.

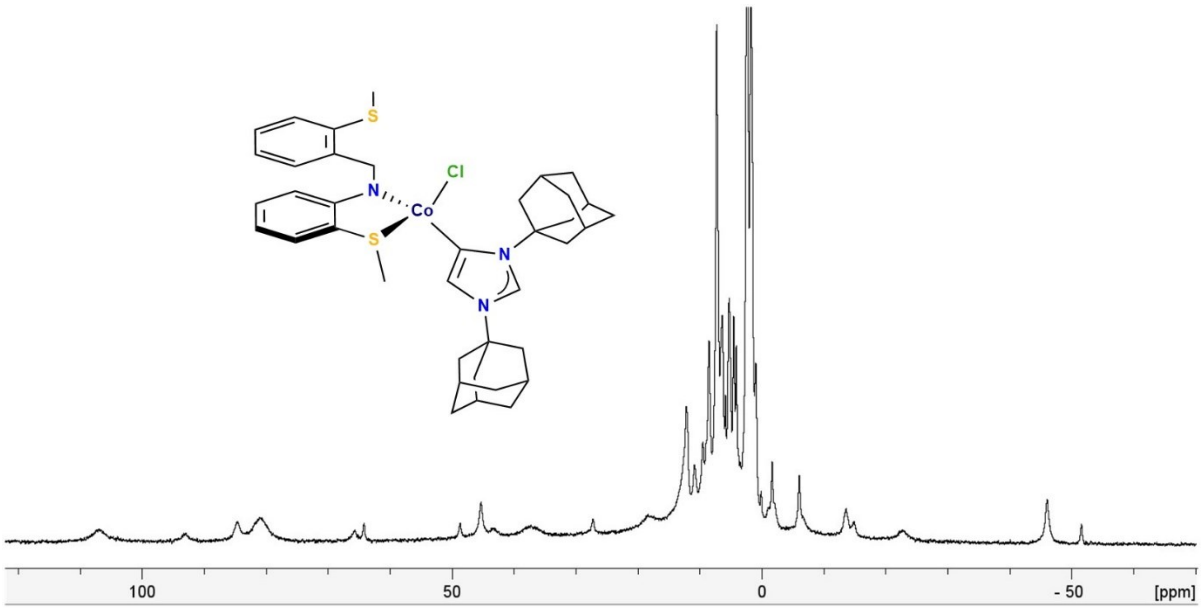

Figure A2.3 ^{1}H NMR spectrum (300 MHz, $CDCl_3$) of **2.3**. ^{1}H NMR: δ -51.71, -46.03, -22.71, -14.88, -13.50, -6.14, -1.69, 18.41, 27.16, 37.29, 43.27, 45.42, 48.64, 64.14, 65.67, 80.87, 84.55, 93.29, 106.95.

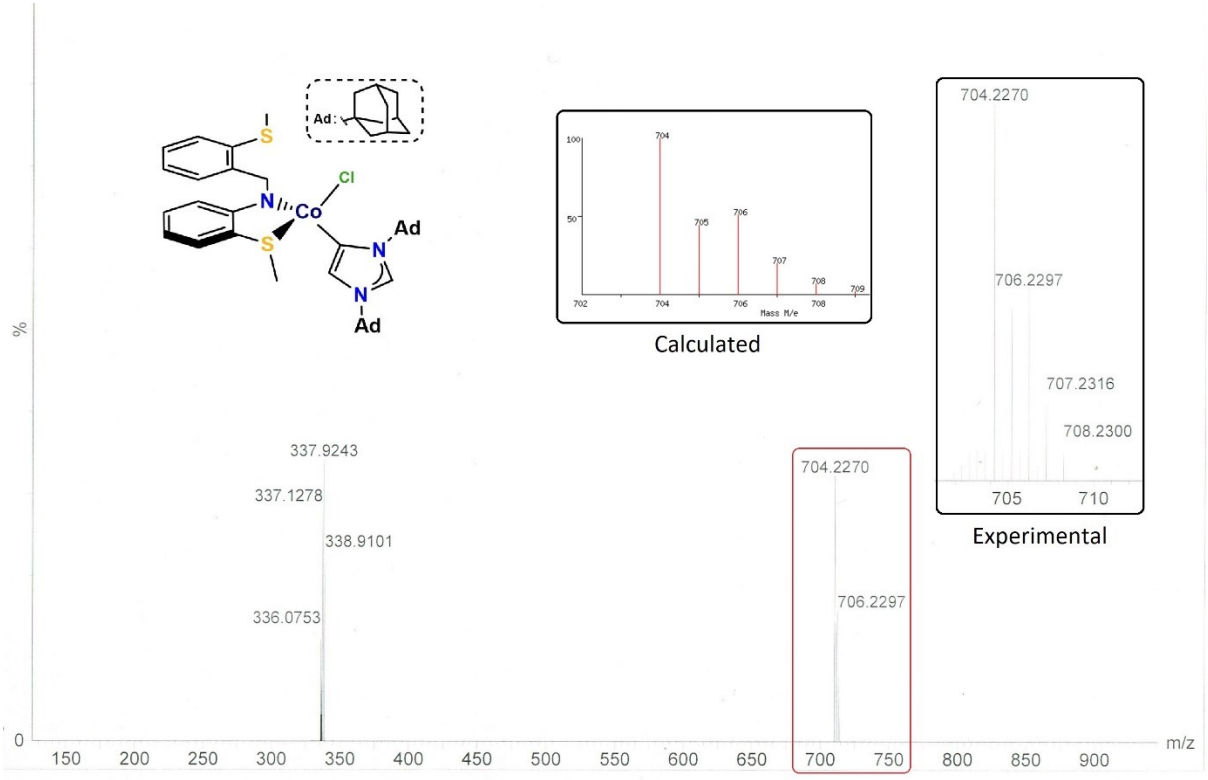

Figure A2.4 ESI-mass spectrum of **2.3** $[M]^{+}$.

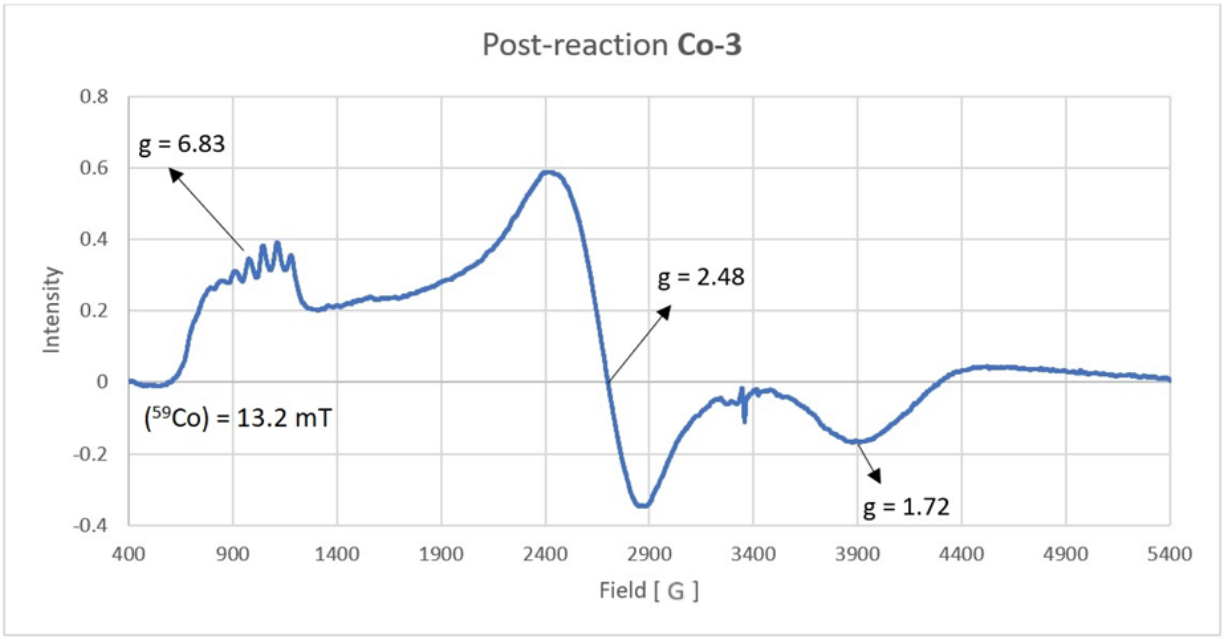

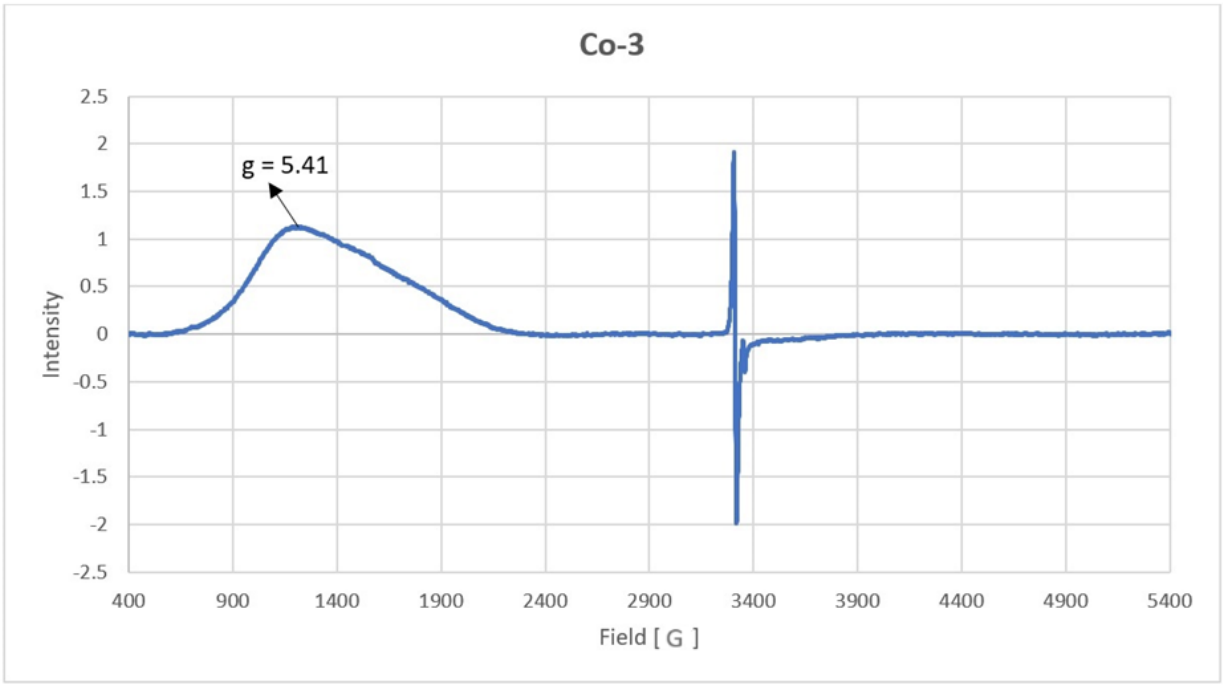

Figure A2.5 EPR spectrum (toluene, 19K) of **2.3** (bottom), and reaction mixture after **2.3** catalyzed benzaldehyde hydroboration (top).

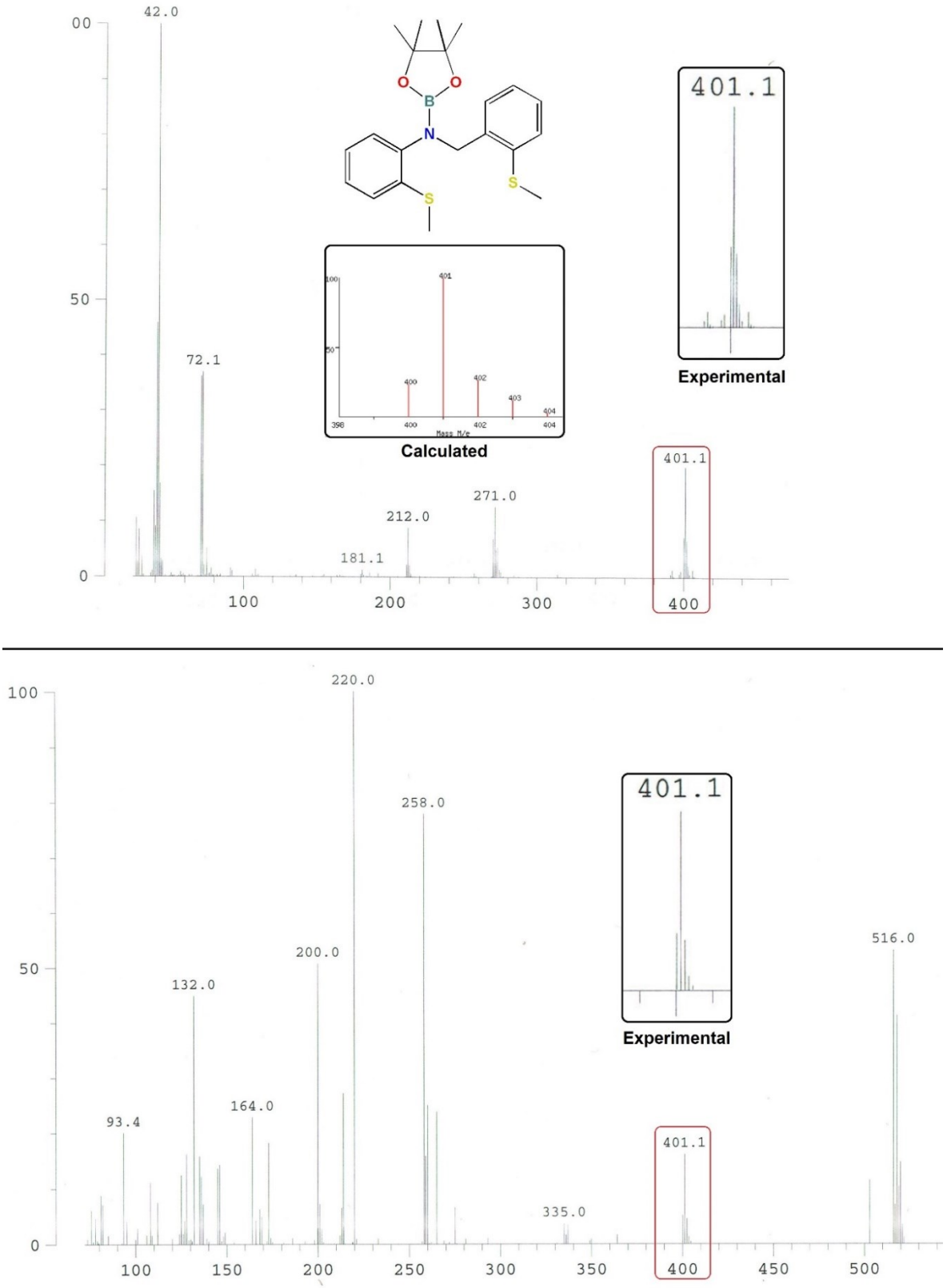

Figure A2.6 EI-mass spectrum of solid reaction residue from **2.1** and HBpin (top), and from **2.3** and HBpin (bottom).

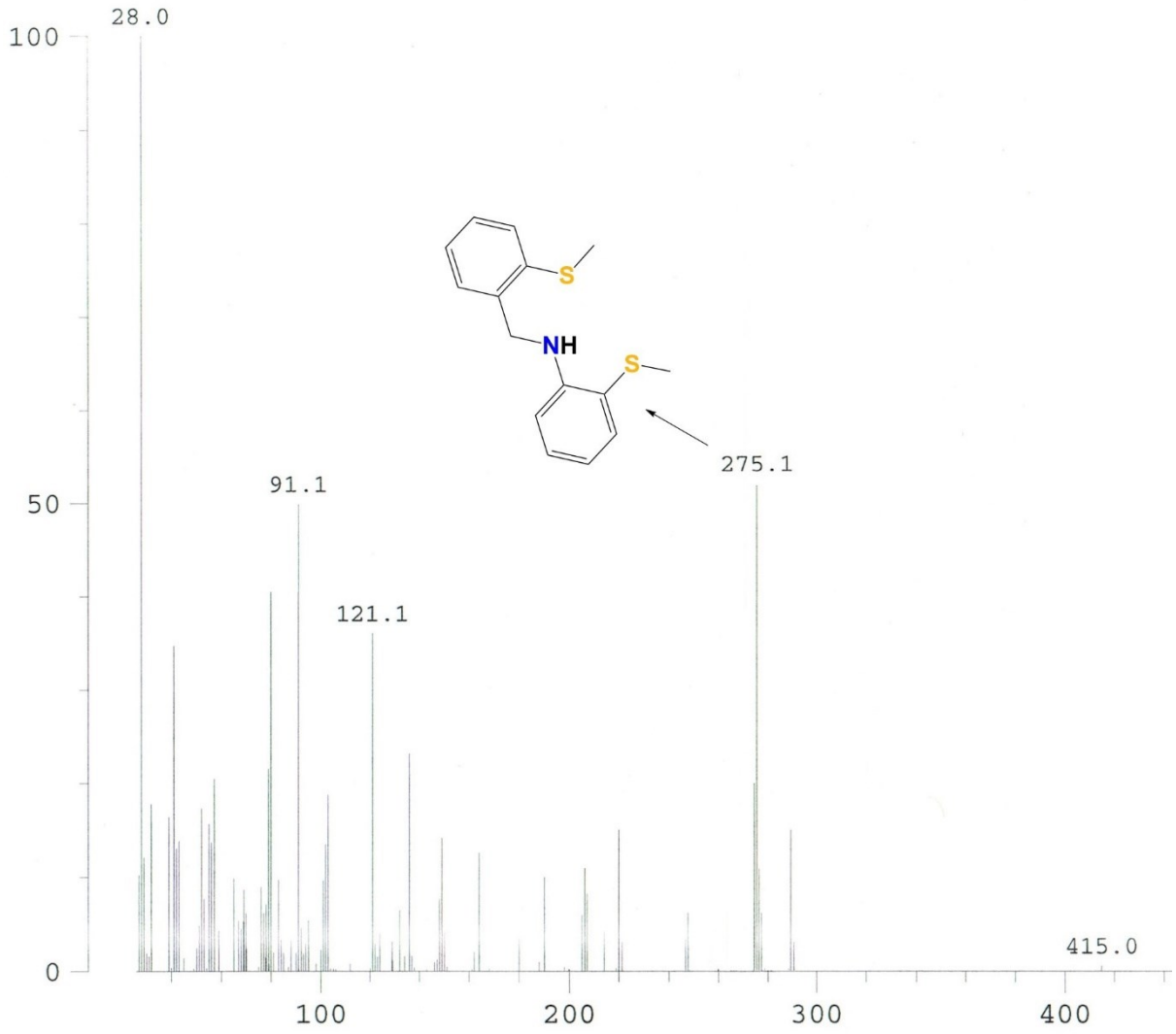

Figure A2.7 EI-mass spectrum of the filtrate portion of the workup process of synthetic reaction of **2.3**.

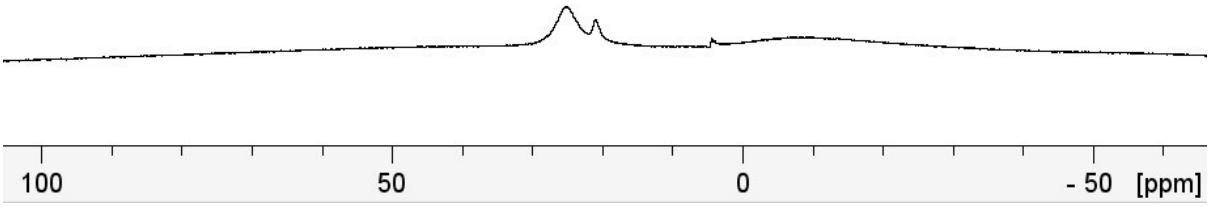

Figure A2.8 ^{11}B NMR (96 MHz) spectra of reaction mixture of **2.3** and HBpin. ^{11}B NMR: 24.6 and 21.2 ppm.

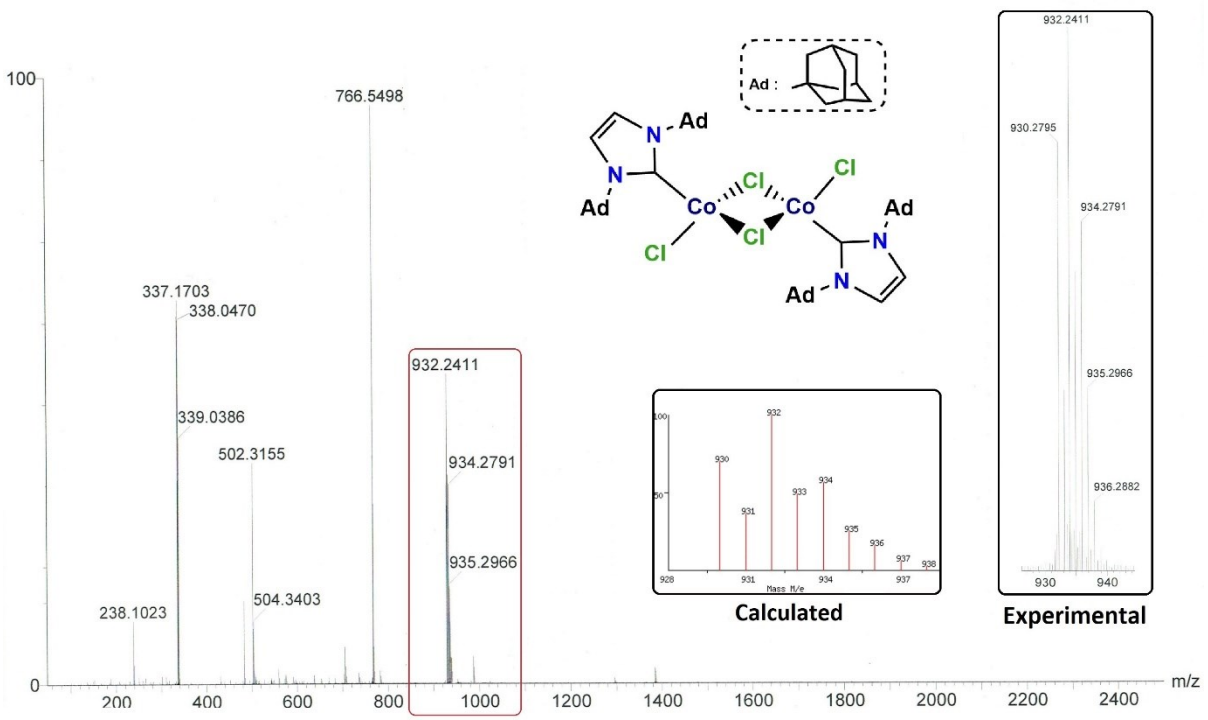

Figure A2.9 EI-mass spectrum of **2.4** $[M]^+$.

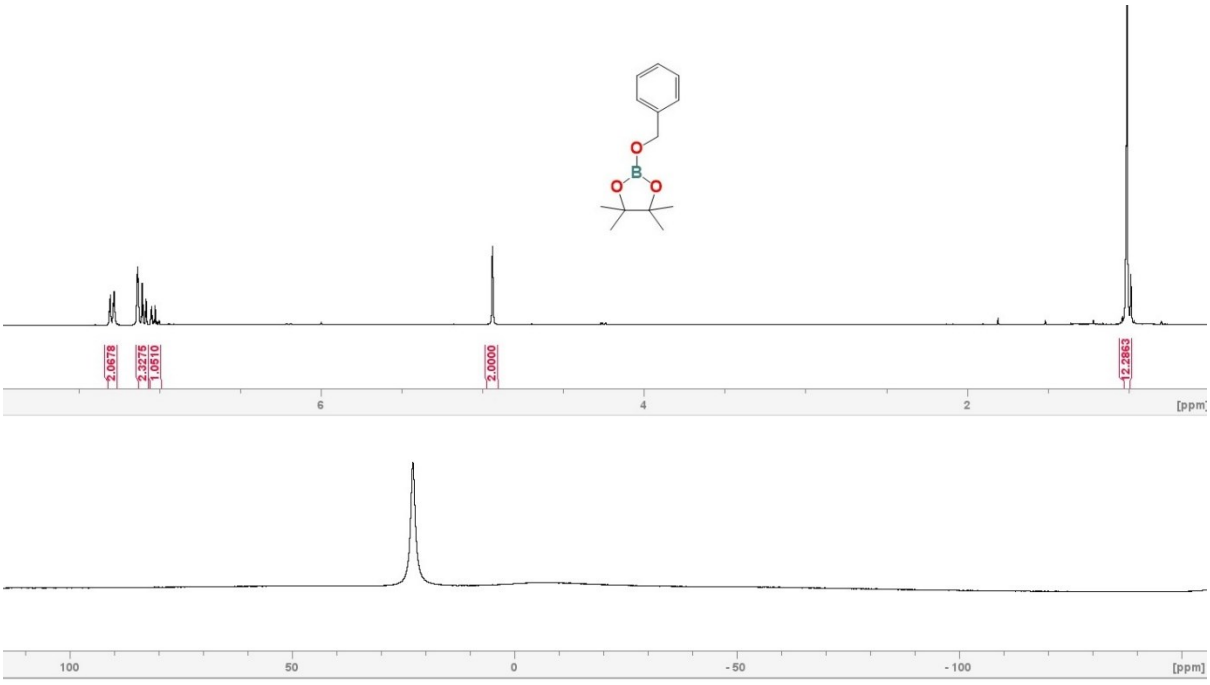

Figure A2.20 ^{1}H (300 MHz, C_6D_6) and ^{11}B (96 MHz) NMR spectra of hydroborated benzaldehyde. Chemical shifts matched with literature values.[36] (

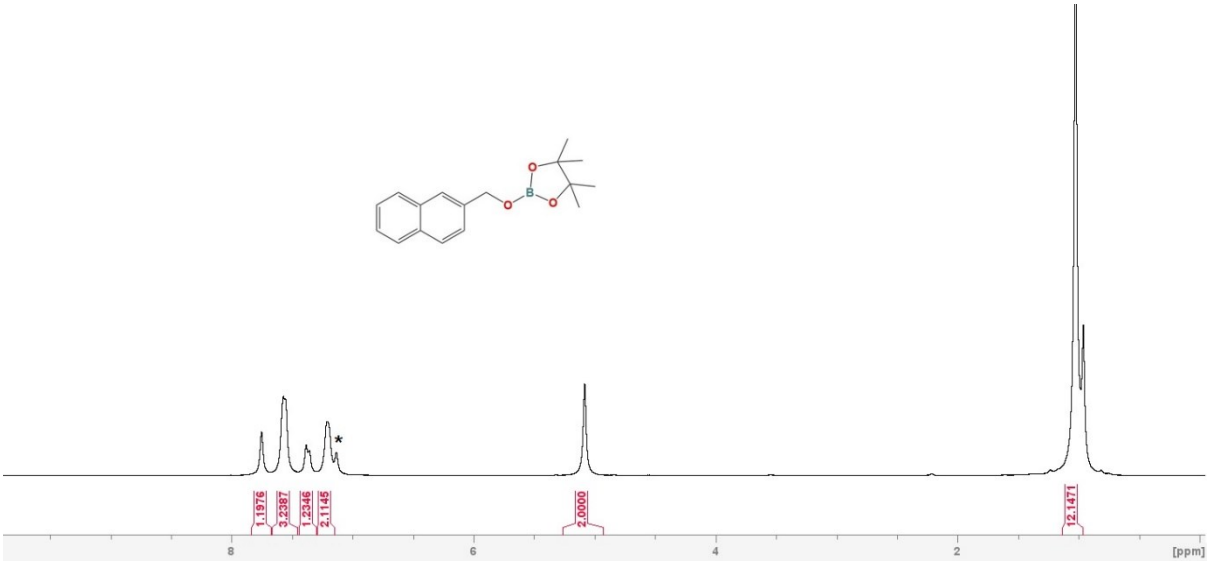

Figure A2.11 ^{1}H (300 MHz, C_6D_6) and ^{11}B (96 MHz) NMR spectra of hydroborated 2-naphthaldehyde. * indicates protic impurity in C_6D_6. Chemical shifts matched with literature values.[36]

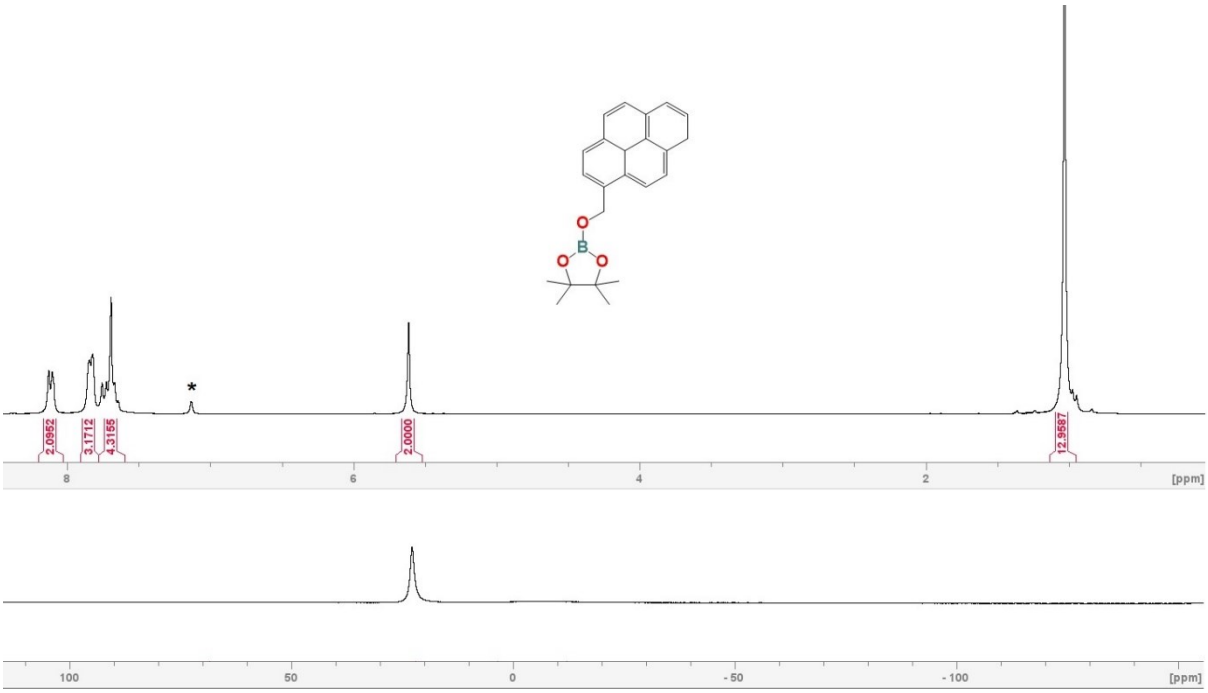

Figure A2.12 ^{1}H (300 MHz, C_6D_6) and ^{11}B (96 MHz) NMR spectra of hydroborated 1-pyrenecarboxaldehyde. * indicates protic impurity in C_6D_6. Chemical shifts matched with literature values.[36]

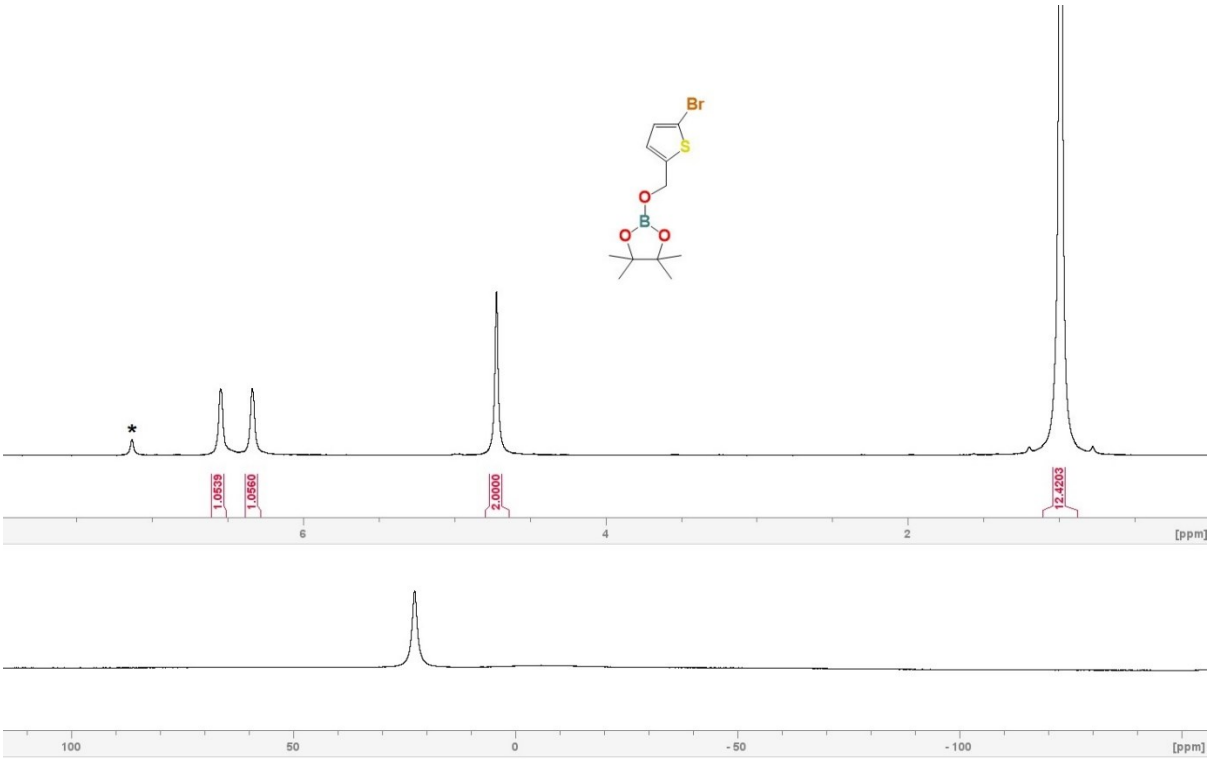

Figure A2.13 ^{1}H (300 MHz, C_6D_6) and ^{11}B (96 MHz) NMR spectra of hydroborated 5-bromo-2 thiophenecarboxaldehyde. * indicates protic impurity in C_6D_6. Chemical shifts matched with literature values.[36]

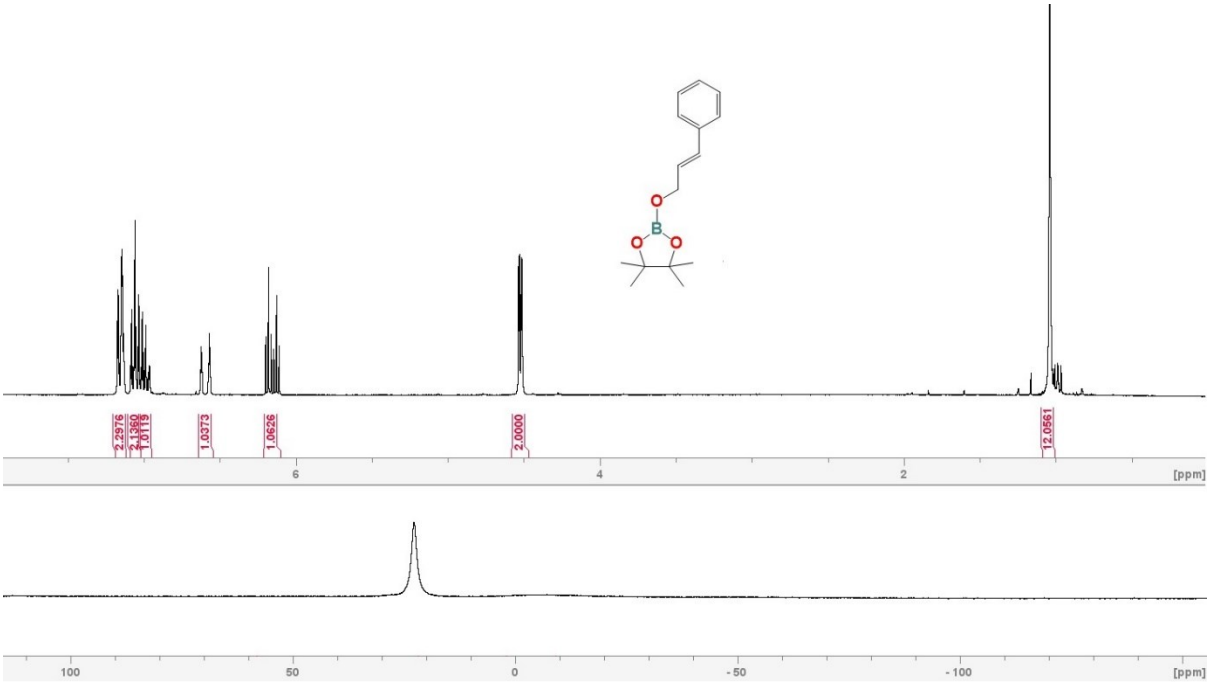

Figure A2.14 ^{1}H (300 MHz, C_6D_6) and ^{11}B (96 MHz) NMR spectra of hydroborated cinnamaldehyde. Chemical shifts matched with literature values.[36]

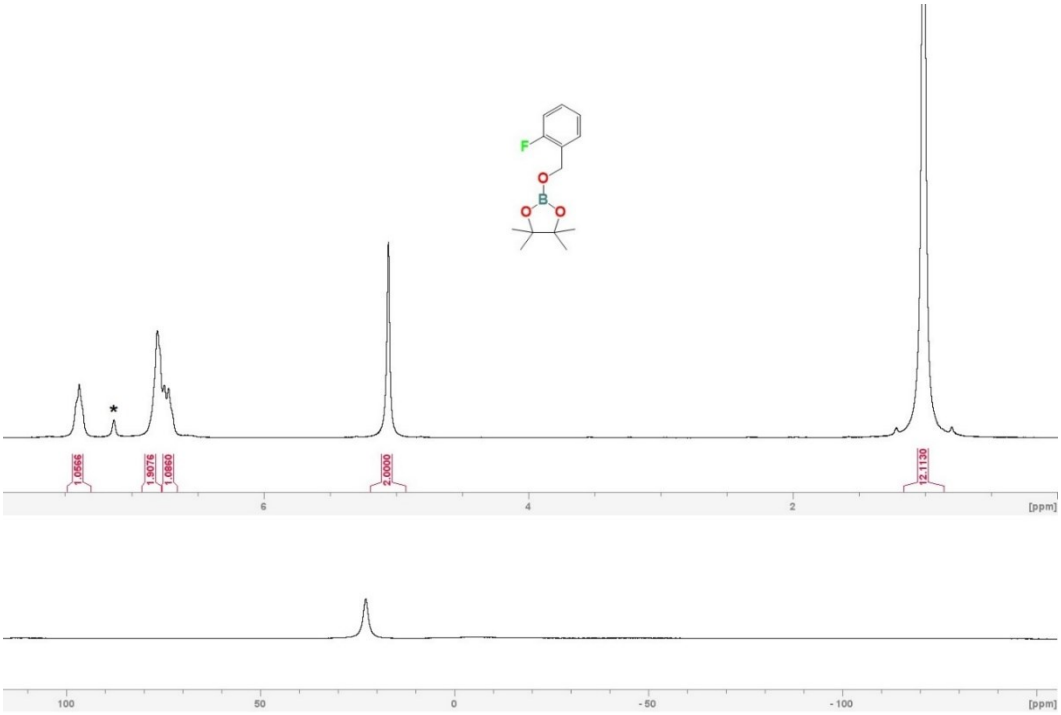

Figure A2.15 ^{1}H (300 MHz, C_6D_6) and ^{11}B (96 MHz) NMR spectra of hydroborated 2-fluorobenzaldehyde. * indicates protic impurity in C_6D_6. Chemical shifts matched with literature values.[36]

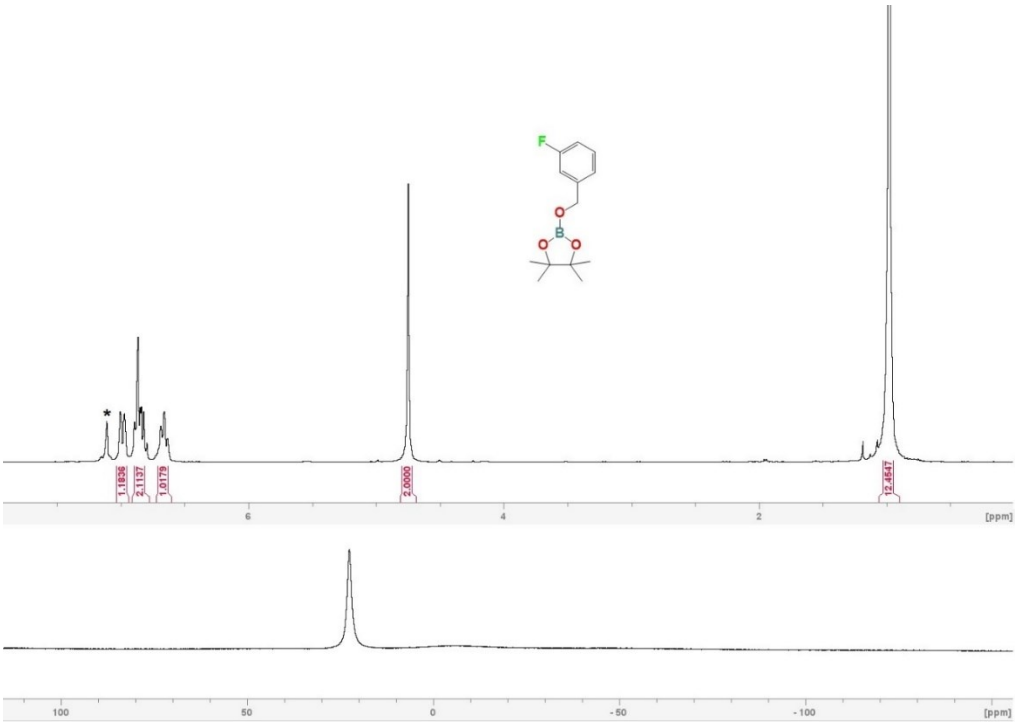

Figure A2.16 ^{1}H (300 MHz, C_6D_6) and ^{11}B (96 MHz) NMR spectra of hydroborated 3-fluorobenzaldehyde. * indicates protic impurity in C_6D_6. Chemical shifts matched with literature values.[36]

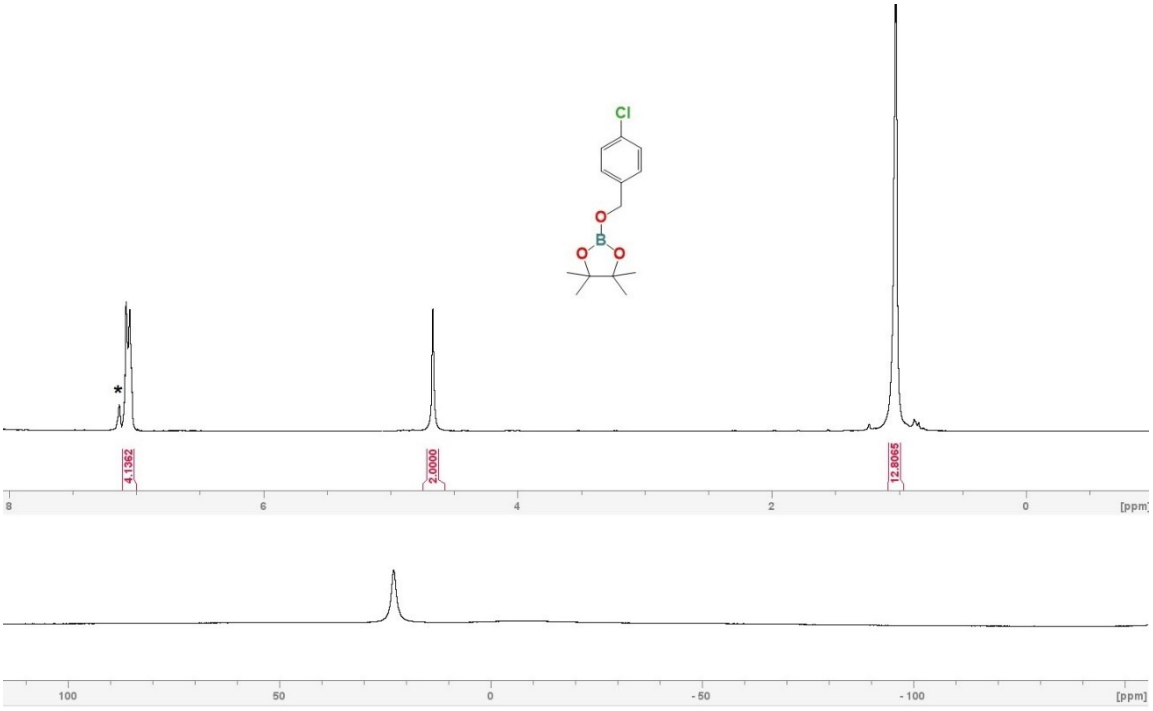

Figure A2.17 ^{1}H (300 MHz, C_6D_6) and ^{11}B (96 MHz) NMR spectra of hydroborated 4-chlorobenzaldehyde. * indicates protic impurity in C_6D_6. Chemical shifts matched with literature values.[36]

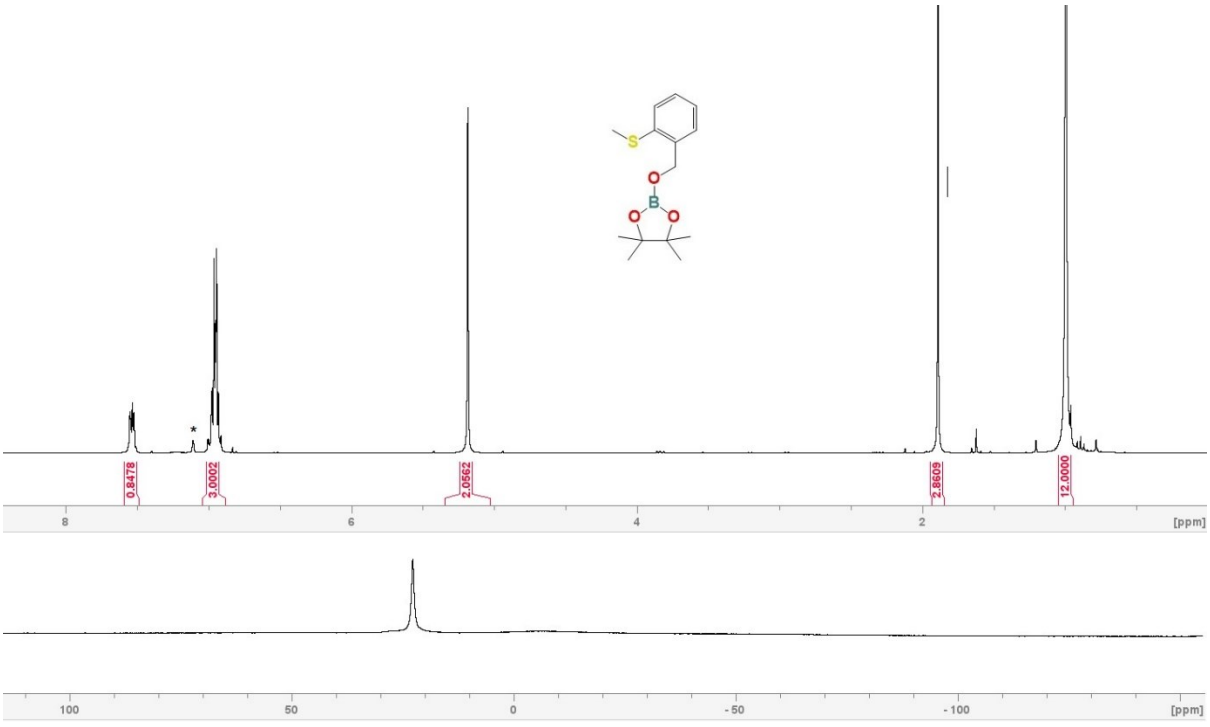

Figure A2.18 ^{1}H (300 MHz, C_6D_6) and ^{11}B (96 MHz) NMR spectra of hydroborated 2-(methylthio)-benzaldehyde. * indicates protic impurity in C_6D_6. Chemical shifts matched with literature values.[36]

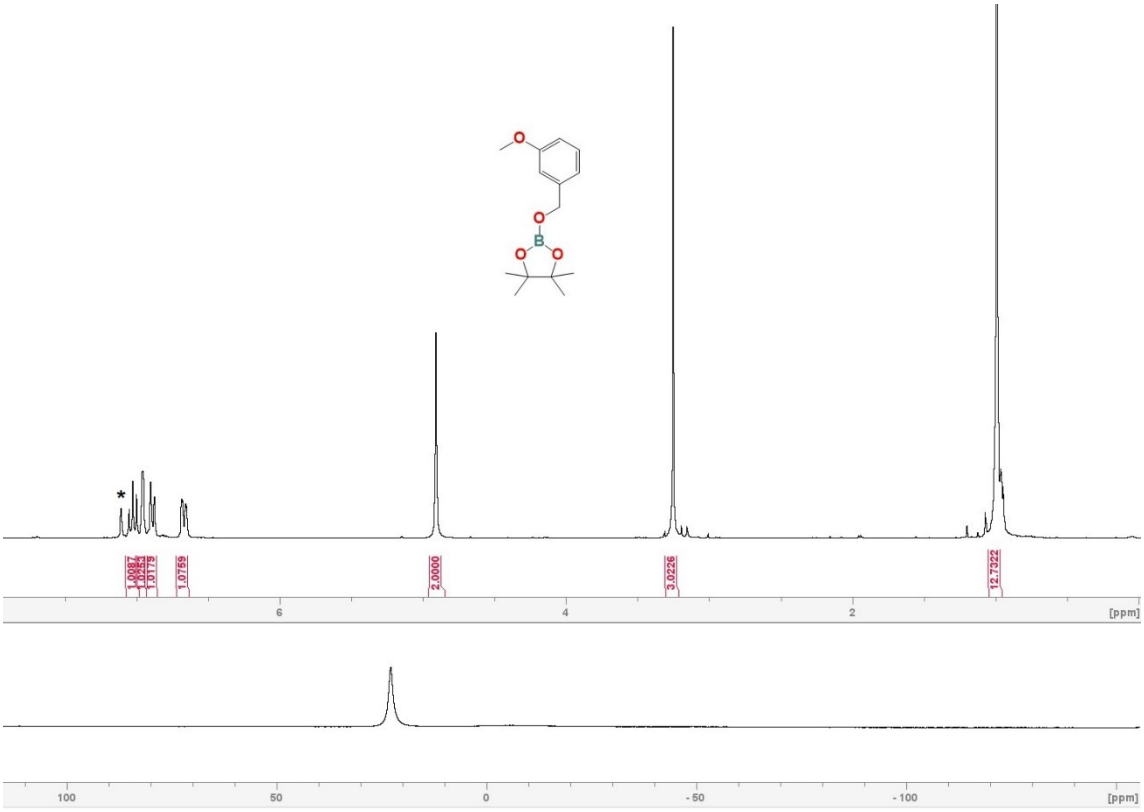

Figure A2.19 ^{1}H (300 MHz, C_6D_6) and ^{11}B (96 MHz) NMR spectra of hydroborated 3-methoxybenzaldehyde. * indicates protic impurity in C_6D_6. Chemical shifts matched with literature values.[36]

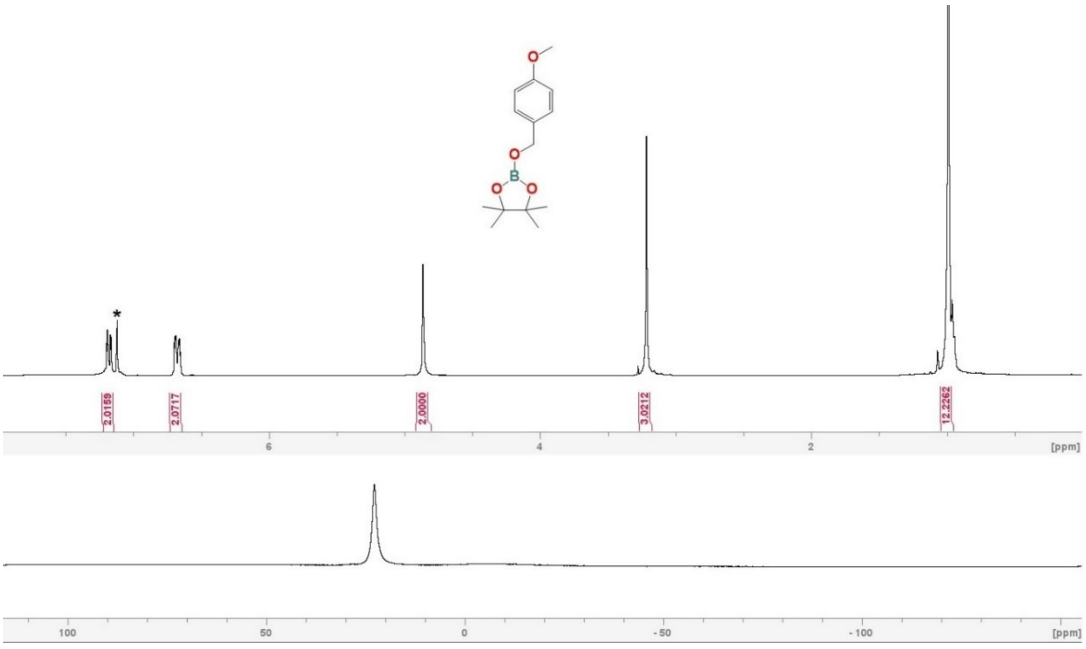

Figure A2.20 ^{1}H (300 MHz, C_6D_6) and ^{11}B (96 MHz) NMR spectra of hydroborated 4-methoxybenzaldehyde. * indicates protic impurity in C_6D_6. Chemical shifts matched with literature values.[36]

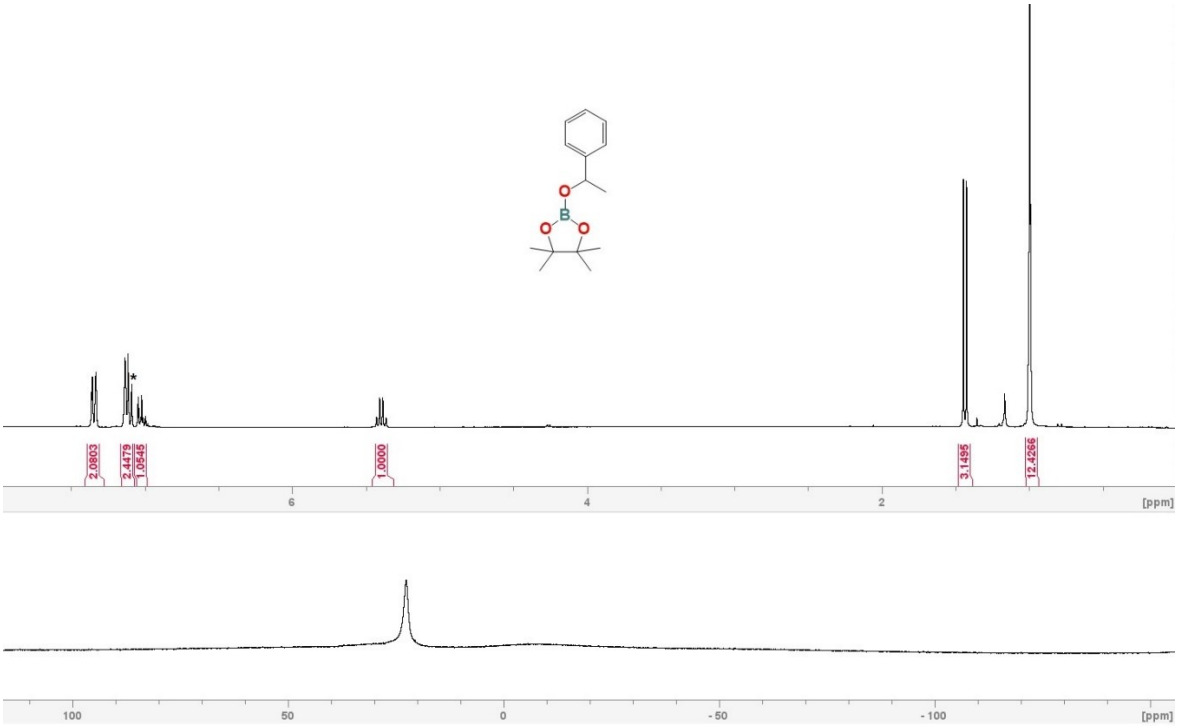

Figure A2.21 ^{1}H (300 MHz, C_6D_6) and ^{11}B (96 MHz) NMR spectra of hydroborated acetophenone. * indicates free HBpin in C_6D_6. Chemical shifts matched with literature values.[16]

2.6.2 Crystallographic Details

Crystallographic data were collected from single crystals mounted on MiTeGen dual thickness MicroMounts using Parabar oil. Data were collected on a Bruker Kappa Evans II single crystal diffractometer equipped with a graphite monochromator. The instrument was equipped with a sealed tube Mo Kα source ($\lambda = 0.71073$ Å), an ApexII CCD detector and a dry compressed air-cooling system. All samples were cooled to 203(2) K during data collection. Raw data collection and processing were performed with the Apex3 software package from Bruker.[56] Initial unit cell parameters were determined from 36 data frames from select ω scans. Semi-empirical absorption corrections based on equivalent reflections were applied.[57] Systematic absences in the diffraction dataset and unit-cell parameters were consistent with the assigned space group. The initial structural solutions were determined using ShelXT (direct methods),[58] and refined with full-matrix least-squares procedures based on F^2 using ShelXL or ShelXle.[59] Hydrogen atoms were placed geometrically and refined using a riding model. Deposition Numbers: 2183655-2183657.

Table A2.1 Data collection and refinement metrics for **2.2** and **2.3**.

	2.2 (K0475)	**2.3** (K0676)	**2.4** (K0842)
empirical formula	$C_{34}H_{34}CoF_{12}N_4O_8S_8$	$C_{38}H_{48}ClCoN_3S_2$	$C_{25}H_{36}Cl_6CoN_2$
formula weight (g·mol^{-1})	1170.06	705.29	636.19
crystal system	Triclinic	Monoclinic	Monoclinic
space group	$P\,\bar{1}$	$P\,2_1/c$	$P\,2_1/c$
***a* (A)**	8.7564(11)	14.349(3)	14.0357(4)
***b* (A)**	13.0048(17)	11.711(2)	9.1640(2)
***c* (A)**	20.590(3)	21.383(4)	22.4666(6)
α (deg)	91.159(4)	90	90
β (deg)	93.835(4)	101.770(3)	101.231(1)
γ (deg)	102.856(3)	90	90
***V* (A^3)**	2279.3(5)	3517.9(11)	2834.39(13)
Z	2	4	4
***T* (K)**	203(2)	203(2)	203(2)
ρ_{calcd} (g·cm^{-3})	1.705	1.332	1.491
μ (mm^{-1})	0.845	0.714	1.189
$2\theta_{max}$ (deg)	52.876	51.356	51.906
total/unique reflections	41619/9384	40358/6687	19997/5470
Reflections [$I_o \geq 2\sigma(I_o)$]	5691	4079	4431
R_1, wR_2 [$I_o \geq 2\sigma(I_o)$]	0.0449, 0.0770	0.0545, 0.1267	0.0424, 0.1166
goodness of fit	0.993	1.011	1.035
CCDC number	2183656	2183657	2183655

Table A2.2 Bond lengths (Å) for **2.2**

Atom1	**Atom2**	**Length**
Co1	S1	2.2785
Co1	S2	2.6522
Co1	N1	1.993
Co1	S1	2.2785
Co1	S2	2.6522
Co1	N1	1.993
S1	C1	1.810(3)
S1	C2	1.775(3)
S2	C8	1.799(4)
S2	C9	1.772(4)
N1	H1	0.99
N1	C7	1.469(4)
N1	C15	1.515(5)
C1	H1A	0.97
C1	H1B	0.97
C1	H1C	0.97

C2	C3	1.382(5)
C2	C7	1.386(4)
C3	H3A	0.94
C3	C4	1.380(5)
C4	H4	0.94
C4	C5	1.390(6)
C5	H5	0.94
C5	C6	1.376(5)
C6	H6	0.94
C6	C7	1.390(5)
C8	H8A	0.97
C8	H8B	0.97
C8	H8C	0.97
C9	C10	1.392(5)
C9	C14	1.398(5)
C10	H10	0.94
C10	C11	1.382(6)
C11	H11	0.941
C11	C12	1.365(7)
C12	H12	0.941
C12	C13	1.375(6)
C13	H13	0.94
C13	C14	1.393(5)
C14	C15	1.492(5)
C15	H15A	0.98
C15	H15B	0.98
S1	C1	1.810(3)
S1	C2	1.775(3)
S2	C8	1.799(4)
S2	C9	1.772(4)
N1	H1	0.99
N1	C7	1.469(4)
N1	C15	1.515(5)
C1	H1A	0.97
C1	H1B	0.97
C1	H1C	0.97
C2	C3	1.382(5)
C2	C7	1.386(4)
C3	H3A	0.94
C3	C4	1.380(5)
C4	H4	0.94
C4	C5	1.390(6)
C5	H5	0.94

C5	C6	1.376(5)
C6	H6	0.94
C6	C7	1.390(5)
C8	H8A	0.97
C8	H8B	0.97
C8	H8C	0.97
C9	C10	1.392(5)
C9	C14	1.398(5)
C10	H10	0.94
C10	C11	1.382(6)
C11	H11	0.941
C11	C12	1.365(7)
C12	H12	0.941
C12	C13	1.375(6)
C13	H13	0.94
C13	C14	1.393(5)
C14	C15	1.492(5)
C15	H15A	0.98
C15	H15B	0.98
Co2	S5	2.462
Co2	S6	2.6107
Co2	N3	2.111
Co2	S5	2.462
Co2	S6	2.6107
Co2	N3	2.111
S5	C21	1.805(4)
S5	C22	1.774(3)
S6	C28	1.802(4)
S6	C29	1.771(3)
N3	H3	0.99
N3	C27	1.460(4)
N3	C35	1.510(4)
C21	H21A	0.97
C21	H21B	0.97
C21	H21C	0.97
C22	C23	1.385(5)
C22	C27	1.396(4)
C23	H23	0.94
C23	C24	1.379(5)
C24	H24	0.94
C24	C25	1.367(6)
C25	H25	0.94
C25	C26	1.376(5)

C26	H26	0.94
C26	C27	1.384(4)
C28	H28A	0.97
C28	H28B	0.97
C28	H28C	0.97
C29	C30	1.382(5)
C29	C34	1.404(5)
C30	H30	0.94
C30	C31	1.378(6)
C31	H31	0.94
C31	C32	1.372(6)
C32	H32	0.94
C32	C33	1.393(6)
C33	H33	0.94
C33	C34	1.385(5)
C34	C35	1.491(4)
C35	H35A	0.98
C35	H35B	0.98
S5	C21	1.805(4)
S5	C22	1.774(3)
S6	C28	1.802(4)
S6	C29	1.771(3)
N3	H3	0.99
N3	C27	1.460(4)
N3	C35	1.510(4)
C21	H21A	0.97
C21	H21B	0.97
C21	H21C	0.97
C22	C23	1.385(5)
C22	C27	1.396(4)
C23	H23	0.94
C23	C24	1.379(5)
C24	H24	0.94
C24	C25	1.367(6)
C25	H25	0.94
C25	C26	1.376(5)
C26	H26	0.94
C26	C27	1.384(4)
C28	H28A	0.97
C28	H28B	0.97
C28	H28C	0.97
C29	C30	1.382(5)
C29	C34	1.404(5)

C30	H30	0.94
C30	C31	1.378(6)
C31	H31	0.94
C31	C32	1.372(6)
C32	H32	0.94
C32	C33	1.393(6)
C33	H33	0.94
C33	C34	1.385(5)
C34	C35	1.491(4)
C35	H35A	0.98
C35	H35B	0.98
S3	O1	1.417(3)
S3	O2	1.435(3)
S3	N2	1.566(3)
S3	C16	1.817(5)
S4	O3	1.427(3)
S4	O4	1.426(3)
S4	N2	1.573(3)
S4	C17	1.823(4)
F1	C16	1.319(5)
F2	C16	1.318(6)
F3	C16	1.321(6)
F4	C17	1.316(5)
F5	C17	1.308(5)
F6	C17	1.318(4)
S7	O5	1.415(3)
S7	O6	1.425(3)
S7	N4	1.558(3)
S7	C36	1.822(4)
S8	O7	1.427(3)
S8	O8	1.419(3)
S8	N4	1.575(3)
S8	C37	1.812(4)
F10	C37	1.321(4)
F11	C37	1.322(5)
F12	C37	1.315(5)
C36	F7	1.38(1)
C36	F8	1.30(1)
C36	F9	1.29(1)

Table A2.3 All angles (°) for **2.2**

Atom1	Atom2	Atom3	Angle (Å)
S1	Co1	S2	100.04
S1	Co1	N1	87.74
S1	Co1	S1	180
S1	Co1	S2	79.96
S1	Co1	N1	92.26
S2	Co1	N1	89.68
S2	Co1	S1	79.96
S2	Co1	S2	180
S2	Co1	N1	90.32
N1	Co1	S1	92.26
N1	Co1	S2	90.32
N1	Co1	N1	180
S1	Co1	S2	100.04
S1	Co1	N1	87.74
S2	Co1	N1	89.68
Co1	S1	C1	118.9
Co1	S1	C2	96.9
C1	S1	C2	101.9(2)
Co1	S2	C8	117.5
Co1	S2	C9	102.7
C8	S2	C9	105.0(2)
Co1	N1	H1	104.8
Co1	N1	C7	113.5
Co1	N1	C15	116.8
H1	N1	C7	104.8
H1	N1	C15	104.8
C7	N1	C15	110.8(2)
S1	C1	H1A	109.5
S1	C1	H1B	109.5
S1	C1	H1C	109.5
H1A	C1	H1B	109.5
H1A	C1	H1C	109.4
H1B	C1	H1C	109.5
S1	C2	C3	121.0(3)
S1	C2	C7	118.2(2)
C3	C2	C7	120.7(3)
C2	C3	H3A	120.2
C2	C3	C4	119.5(3)
H3A	C3	C4	120.2
C3	C4	H4	120.2
C3	C4	C5	119.8(3)

H4	C4	C5	120.1
C4	C5	H5	119.6
C4	C5	C6	120.9(3)
H5	C5	C6	119.5
C5	C6	H6	120.4
C5	C6	C7	119.3(3)
H6	C6	C7	120.4
N1	C7	C2	119.6(3)
N1	C7	C6	120.6(3)
C2	C7	C6	119.8(3)
S2	C8	H8A	109.4
S2	C8	H8B	109.5
S2	C8	H8C	109.4
H8A	C8	H8B	109.5
H8A	C8	H8C	109.5
H8B	C8	H8C	109.5
S2	C9	C10	122.9(3)
S2	C9	C14	116.4(3)
C10	C9	C14	120.6(3)
C9	C10	H10	120.2
C9	C10	C11	119.6(4)
H10	C10	C11	120.2
C10	C11	H11	119.9
C10	C11	C12	120.3(4)
H11	C11	C12	119.8
C11	C12	H12	119.8
C11	C12	C13	120.4(4)
H12	C12	C13	119.8
C12	C13	H13	119.4
C12	C13	C14	121.1(4)
H13	C13	C14	119.4
C9	C14	C13	117.9(3)
C9	C14	C15	121.6(3)
C13	C14	C15	120.5(3)
N1	C15	C14	114.2(3)
N1	C15	H15A	108.7
N1	C15	H15B	108.7
C14	C15	H15A	108.7
C14	C15	H15B	108.7
H15A	C15	H15B	107.6
Co1	S1	C1	118.9
Co1	S1	C2	96.9
C1	S1	C2	101.9(2)

Co1	S2	C8	117.5
Co1	S2	C9	102.7
C8	S2	C9	105.0(2)
Co1	N1	H1	104.8
Co1	N1	C7	113.5
Co1	N1	C15	116.8
H1	N1	C7	104.8
H1	N1	C15	104.8
C7	N1	C15	110.8(2)
S1	C1	H1A	109.5
S1	C1	H1B	109.5
S1	C1	H1C	109.5
H1A	C1	H1B	109.5
H1A	C1	H1C	109.4
H1B	C1	H1C	109.5
S1	C2	C3	121.0(3)
S1	C2	C7	118.2(2)
C3	C2	C7	120.7(3)
C2	C3	H3A	120.2
C2	C3	C4	119.5(3)
H3A	C3	C4	120.2
C3	C4	H4	120.2
C3	C4	C5	119.8(3)
H4	C4	C5	120.1
C4	C5	H5	119.6
C4	C5	C6	120.9(3)
H5	C5	C6	119.5
C5	C6	H6	120.4
C5	C6	C7	119.3(3)
H6	C6	C7	120.4
N1	C7	C2	119.6(3)
N1	C7	C6	120.6(3)
C2	C7	C6	119.8(3)
S2	C8	H8A	109.4
S2	C8	H8B	109.5
S2	C8	H8C	109.4
H8A	C8	H8B	109.5
H8A	C8	H8C	109.5
H8B	C8	H8C	109.5
S2	C9	C10	122.9(3)
S2	C9	C14	116.4(3)
C10	C9	C14	120.6(3)
C9	C10	H10	120.2

C9	C10	C11	119.6(4)
H10	C10	C11	120.2
C10	C11	H11	119.9
C10	C11	C12	120.3(4)
H11	C11	C12	119.8
C11	C12	H12	119.8
C11	C12	C13	120.4(4)
H12	C12	C13	119.8
C12	C13	H13	119.4
C12	C13	C14	121.1(4)
H13	C13	C14	119.4
C9	C14	C13	117.9(3)
C9	C14	C15	121.6(3)
C13	C14	C15	120.5(3)
N1	C15	C14	114.2(3)
N1	C15	H15A	108.7
N1	C15	H15B	108.7
C14	C15	H15A	108.7
C14	C15	H15B	108.7
H15A	C15	H15B	107.6
S5	Co2	S6	92.27
S5	Co2	N3	80.76
S5	Co2	S5	180
S5	Co2	S6	87.73
S5	Co2	N3	99.24
S6	Co2	N3	86.67
S6	Co2	S5	87.73
S6	Co2	S6	180
S6	Co2	N3	93.33
N3	Co2	S5	99.24
N3	Co2	S6	93.33
N3	Co2	N3	180
S5	Co2	S6	92.27
S5	Co2	N3	80.76
S6	Co2	N3	86.67
Co2	S5	C21	113
Co2	S5	C22	93.6
C21	S5	C22	101.0(2)
Co2	S6	C28	121.1
Co2	S6	C29	97.8
C28	S6	C29	105.4(2)
Co2	N3	H3	105.3
Co2	N3	C27	111.4

Co2	N3	C35	117.9
H3	N3	C27	105.3
H3	N3	C35	105.3
C27	N3	C35	110.5(2)
S5	C21	H21A	109.5
S5	C21	H21B	109.5
S5	C21	H21C	109.5
H21A	C21	H21B	109.5
H21A	C21	H21C	109.5
H21B	C21	H21C	109.5
S5	C22	C23	122.4(2)
S5	C22	C27	118.5(2)
C23	C22	C27	119.1(3)
C22	C23	H23	119.8
C22	C23	C24	120.3(3)
H23	C23	C24	119.8
C23	C24	H24	119.8
C23	C24	C25	120.2(3)
H24	C24	C25	119.9
C24	C25	H25	119.8
C24	C25	C26	120.5(3)
H25	C25	C26	119.8
C25	C26	H26	120.1
C25	C26	C27	119.9(3)
H26	C26	C27	120
N3	C27	C22	119.5(2)
N3	C27	C26	120.7(3)
C22	C27	C26	119.9(3)
S6	C28	H28A	109.5
S6	C28	H28B	109.5
S6	C28	H28C	109.5
H28A	C28	H28B	109.4
H28A	C28	H28C	109.4
H28B	C28	H28C	109.5
S6	C29	C30	123.2(3)
S6	C29	C34	115.8(3)
C30	C29	C34	120.9(3)
C29	C30	H30	120.2
C29	C30	C31	119.7(3)
H30	C30	C31	120.2
C30	C31	H31	119.7
C30	C31	C32	120.7(4)
H31	C31	C32	119.6

C31	C32	H32	120.1
C31	C32	C33	119.7(4)
H32	C32	C33	120.2
C32	C33	H33	119.5
C32	C33	C34	121.0(4)
H33	C33	C34	119.5
C29	C34	C33	118.1(3)
C29	C34	C35	120.7(3)
C33	C34	C35	121.1(3)
N3	C35	C34	111.4(3)
N3	C35	H35A	109.4
N3	C35	H35B	109.4
C34	C35	H35A	109.4
C34	C35	H35B	109.3
H35A	C35	H35B	108
Co2	S5	C21	113
Co2	S5	C22	93.6
C21	S5	C22	101.0(2)
Co2	S6	C28	121.1
Co2	S6	C29	97.8
C28	S6	C29	105.4(2)
Co2	N3	H3	105.3
Co2	N3	C27	111.4
Co2	N3	C35	117.9
H3	N3	C27	105.3
H3	N3	C35	105.3
C27	N3	C35	110.5(2)
S5	C21	H21A	109.5
S5	C21	H21B	109.5
S5	C21	H21C	109.5
H21A	C21	H21B	109.5
H21A	C21	H21C	109.5
H21B	C21	H21C	109.5
S5	C22	C23	122.4(2)
S5	C22	C27	118.5(2)
C23	C22	C27	119.1(3)
C22	C23	H23	119.8
C22	C23	C24	120.3(3)
H23	C23	C24	119.8
C23	C24	H24	119.8
C23	C24	C25	120.2(3)
H24	C24	C25	119.9
C24	C25	H25	119.8

C24	C25	C26	120.5(3)
H25	C25	C26	119.8
C25	C26	H26	120.1
C25	C26	C27	119.9(3)
H26	C26	C27	120
N3	C27	C22	119.5(2)
N3	C27	C26	120.7(3)
C22	C27	C26	119.9(3)
S6	C28	H28A	109.5
S6	C28	H28B	109.5
S6	C28	H28C	109.5
H28A	C28	H28B	109.4
H28A	C28	H28C	109.4
H28B	C28	H28C	109.5
S6	C29	C30	123.2(3)
S6	C29	C34	115.8(3)
C30	C29	C34	120.9(3)
C29	C30	H30	120.2
C29	C30	C31	119.7(3)
H30	C30	C31	120.2
C30	C31	H31	119.7
C30	C31	C32	120.7(4)
H31	C31	C32	119.6
C31	C32	H32	120.1
C31	C32	C33	119.7(4)
H32	C32	C33	120.2
C32	C33	H33	119.5
C32	C33	C34	121.0(4)
H33	C33	C34	119.5
C29	C34	C33	118.1(3)
C29	C34	C35	120.7(3)
C33	C34	C35	121.1(3)
N3	C35	C34	111.4(3)
N3	C35	H35A	109.4
N3	C35	H35B	109.4
C34	C35	H35A	109.4
C34	C35	H35B	109.3
H35A	C35	H35B	108
O1	S3	O2	118.7(2)
O1	S3	N2	109.3(2)
O1	S3	C16	104.2(2)
O2	S3	N2	116.2(2)
O2	S3	C16	103.6(2)

N2	S3	C16	102.6(2)
O3	S4	O4	118.8(2)
O3	S4	N2	108.6(2)
O3	S4	C17	103.8(2)
O4	S4	N2	115.9(2)
O4	S4	C17	103.7(2)
N2	S4	C17	103.9(2)
S3	N2	S4	123.7(2)
S3	C16	F1	109.9(3)
S3	C16	F2	111.7(3)
S3	C16	F3	112.1(3)
F1	C16	F2	108.7(4)
F1	C16	F3	106.8(4)
F2	C16	F3	107.4(4)
S4	C17	F4	111.5(3)
S4	C17	F5	109.2(3)
S4	C17	F6	110.7(3)
F4	C17	F5	108.8(3)
F4	C17	F6	107.5(3)
F5	C17	F6	109.0(3)
O5	S7	O6	116.8(2)
O5	S7	N4	118.0(2)
O5	S7	C36	105.0(2)
O6	S7	N4	108.9(2)
O6	S7	C36	102.4(2)
N4	S7	C36	103.5(2)
O7	S8	O8	119.5(2)
O7	S8	N4	116.2(2)
O7	S8	C37	105.1(2)
O8	S8	N4	108.7(2)
O8	S8	C37	103.3(2)
N4	S8	C37	101.5(2)
S7	N4	S8	126.4(2)
S7	C36	F7	107.5(4)
S7	C36	F8	111.5(6)
S7	C36	F9	118.2(5)
F7	C36	F8	104.9(7)
F7	C36	F9	103.5(6)
F8	C36	F9	110.0(8)
S8	C37	F10	110.2(3)
S8	C37	F11	111.2(3)
S8	C37	F12	112.3(3)
F10	C37	F11	107.4(3)

F10	C37	F12	107.9(3)
F11	C37	F12	107.7(3)

Table A2.4 Bond lengths (Å) for **2.3**

Atom1	**Atom2**	**Length**
Co1	Cl1	2.269(1)
Co1	S1	2.411(1)
Co1	N1	1.919(3)
Co1	C26	2.034(3)
S1	C1	1.802(5)
S1	C2	1.776(4)
S2	C14	1.758(5)
S2	C15	1.787(7)
N1	C7	1.374(5)
N1	C8	1.451(5)
N2	C16	1.493(5)
N2	C26	1.408(4)
N2	C27	1.333(5)
N3	C27	1.334(5)
N3	C28	1.386(5)
N3	C29	1.491(5)
C1	H1A	0.97
C1	H1B	0.97
C1	H1C	0.97
C2	C3	1.396(5)
C2	C7	1.402(6)
C3	H3	0.939
C3	C4	1.373(6)
C4	H4	0.94
C4	C5	1.377(7)
C5	H5	0.94
C5	C6	1.362(6)
C6	H6	0.94
C6	C7	1.404(5)
C8	H8A	0.98
C8	H8AB	0.98
C8	C9	1.527(5)
C9	C10	1.392(6)
C9	C14	1.401(6)
C10	H10	0.94
C10	C11	1.400(7)
C11	H11	0.941

C11	C12	1.364(8)
C12	H12	0.941
C12	C13	1.375(8)
C13	H13	0.94
C13	C14	1.387(7)
C15	H15A	0.97
C15	H15B	0.97
C15	H15C	0.97
C16	C17	1.534(5)
C16	C21	1.519(6)
C16	C24	1.528(5)
C17	H17A	0.979
C17	H17B	0.98
C17	C18	1.550(6)
C18	H18	0.99
C18	C19	1.517(7)
C18	C25	1.498(7)
C19	H19A	0.979
C19	H19B	0.981
C19	C20	1.515(6)
C20	H20	0.99
C20	C21	1.537(6)
C20	C22	1.522(7)
C21	H21A	0.98
C21	H21B	0.979
C22	H22A	0.979
C22	H22B	0.981
C22	C23	1.512(6)
C23	H23	0.989
C23	C24	1.536(6)
C23	C25	1.523(5)
C24	H24A	0.98
C24	H24B	0.98
C25	H25A	0.98
C25	H25B	0.98
C26	C28	1.357(6)
C27	H27	0.94
C28	H28	0.94
C29	C30	1.529(5)
C29	C34	1.514(6)
C29	C35	1.499(6)
C30	H30A	0.98
C30	H30B	0.98

C30	C31	1.535(7)
C31	H31	0.99
C31	C32	1.472(9)
C31	C38	1.493(8)
C32	H32A	0.98
C32	H32B	0.98
C32	C33	1.508(8)
C33	H33	0.989
C33	C34	1.559(9)
C33	C37	1.51(1)
C34	H34A	0.98
C34	H34B	0.98
C35	H35A	0.98
C35	H35B	0.98
C35	C36	1.558(8)
C36	H36	0.99
C36	C37	1.550(9)
C36	C38	1.491(7)
C37	H37A	0.979
C37	H37B	0.98
C38	H38A	0.981
C38	H38B	0.98

Table A2.5 All angles (°) for **2.3**

Atom1	**Atom2**	**Atom3**	**Angle (Å)**
Cl1	Co1	S1	103.18(4)
Cl1	Co1	N1	113.0(1)
Cl1	Co1	C26	119.3(1)
S1	Co1	N1	85.7(1)
S1	Co1	C26	103.1(1)
N1	Co1	C26	122.7(1)
Co1	S1	C1	104.3(2)
Co1	S1	C2	93.7(1)
C1	S1	C2	101.2(2)
C14	S2	C15	104.7(3)
Co1	N1	C7	120.2(2)
Co1	N1	C8	121.9(2)
C7	N1	C8	117.9(3)
C16	N2	C26	129.3(3)
C16	N2	C27	120.4(3)
C26	N2	C27	110.2(3)
C27	N3	C28	106.7(3)

C27	N3	C29	123.3(3)
C28	N3	C29	130.0(3)
S1	C1	H1A	109.5
S1	C1	H1B	109.5
S1	C1	H1C	109.5
H1A	C1	H1B	109.4
H1A	C1	H1C	109.4
H1B	C1	H1C	109.5
S1	C2	C3	118.7(3)
S1	C2	C7	118.7(3)
C3	C2	C7	122.6(4)
C2	C3	H3	120.1
C2	C3	C4	119.8(4)
H3	C3	C4	120.1
C3	C4	H4	120.7
C3	C4	C5	118.5(4)
H4	C4	C5	120.8
C4	C5	H5	119
C4	C5	C6	121.8(4)
H5	C5	C6	119.1
C5	C6	H6	119
C5	C6	C7	122.1(4)
H6	C6	C7	119
N1	C7	C2	120.2(3)
N1	C7	C6	124.7(3)
C2	C7	C6	115.1(3)
N1	C8	H8A	108.2
N1	C8	H8AB	108.2
N1	C8	C9	116.4(3)
H8A	C8	H8AB	107.3
H8A	C8	C9	108.3
H8AB	C8	C9	108.2
C8	C9	C10	120.7(4)
C8	C9	C14	119.8(4)
C10	C9	C14	119.4(4)
C9	C10	H10	120.1
C9	C10	C11	119.6(4)
H10	C10	C11	120.2
C10	C11	H11	119.6
C10	C11	C12	120.8(5)
H11	C11	C12	119.6
C11	C12	H12	120.3
C11	C12	C13	119.5(5)

H12	C12	C13	120.1
C12	C13	H13	119.3
C12	C13	C14	121.5(5)
H13	C13	C14	119.2
S2	C14	C9	117.0(3)
S2	C14	C13	123.9(4)
C9	C14	C13	119.1(4)
S2	C15	H15A	109.4
S2	C15	H15B	109.5
S2	C15	H15C	109.5
H15A	C15	H15B	109.5
H15A	C15	H15C	109.5
H15B	C15	H15C	109.5
N2	C16	C17	109.4(3)
N2	C16	C21	110.5(3)
N2	C16	C24	108.1(3)
C17	C16	C21	109.7(3)
C17	C16	C24	109.5(3)
C21	C16	C24	109.6(3)
C16	C17	H17A	109.9
C16	C17	H17B	109.9
C16	C17	C18	108.7(3)
H17A	C17	H17B	108.4
H17A	C17	C18	109.9
H17B	C17	C18	109.9
C17	C18	H18	109.6
C17	C18	C19	108.3(4)
C17	C18	C25	109.6(4)
H18	C18	C19	109.7
H18	C18	C25	109.6
C19	C18	C25	110.0(4)
C18	C19	H19A	109.6
C18	C19	H19B	109.5
C18	C19	C20	110.4(4)
H19A	C19	H19B	108.1
H19A	C19	C20	109.6
H19B	C19	C20	109.6
C19	C20	H20	109.7
C19	C20	C21	109.7(4)
C19	C20	C22	109.3(4)
H20	C20	C21	109.5
H20	C20	C22	109.6
C21	C20	C22	109.0(4)

C16	C21	C20	109.3(3)
C16	C21	H21A	109.8
C16	C21	H21B	109.8
C20	C21	H21A	109.8
C20	C21	H21B	109.8
H21A	C21	H21B	108.3
C20	C22	H22A	109.8
C20	C22	H22B	109.8
C20	C22	C23	109.3(4)
H22A	C22	H22B	108.3
H22A	C22	C23	109.8
H22B	C22	C23	109.8
C22	C23	H23	109.3
C22	C23	C24	110.1(3)
C22	C23	C25	110.3(4)
H23	C23	C24	109.3
H23	C23	C25	109.3
C24	C23	C25	108.5(3)
C16	C24	C23	108.9(3)
C16	C24	H24A	109.9
C16	C24	H24B	109.9
C23	C24	H24A	109.9
C23	C24	H24B	109.9
H24A	C24	H24B	108.3
C18	C25	C23	110.1(4)
C18	C25	H25A	109.6
C18	C25	H25B	109.7
C23	C25	H25A	109.6
C23	C25	H25B	109.6
H25A	C25	H25B	108.1
Co1	C26	N2	132.6(2)
Co1	C26	C28	124.1(3)
N2	C26	C28	103.3(3)
N2	C27	N3	109.1(3)
N2	C27	H27	125.4
N3	C27	H27	125.4
N3	C28	C26	110.7(3)
N3	C28	H28	124.6
C26	C28	H28	124.7
N3	C29	C30	108.9(3)
N3	C29	C34	109.0(3)
N3	C29	C35	109.0(3)
C30	C29	C34	110.3(4)

C30	C29	C35	108.8(3)
C34	C29	C35	110.9(4)
C29	C30	H30A	110
C29	C30	H30B	110
C29	C30	C31	108.4(4)
H30A	C30	H30B	108.4
H30A	C30	C31	110
H30B	C30	C31	110
C30	C31	H31	109
C30	C31	C32	108.9(4)
C30	C31	C38	109.1(4)
H31	C31	C32	109
H31	C31	C38	109.1
C32	C31	C38	111.7(5)
C31	C32	H32A	109.5
C31	C32	H32B	109.5
C31	C32	C33	111.1(5)
H32A	C32	H32B	108
H32A	C32	C33	109.4
H32B	C32	C33	109.4
C32	C33	H33	110.1
C32	C33	C34	108.8(5)
C32	C33	C37	111.0(5)
H33	C33	C34	110
H33	C33	C37	110
C34	C33	C37	106.9(5)
C29	C34	C33	108.6(4)
C29	C34	H34A	110
C29	C34	H34B	110
C33	C34	H34A	109.9
C33	C34	H34B	109.9
H34A	C34	H34B	108.4
C29	C35	H35A	109.8
C29	C35	H35B	109.8
C29	C35	C36	109.2(4)
H35A	C35	H35B	108.3
H35A	C35	C36	109.9
H35B	C35	C36	109.9
C35	C36	H36	110.1
C35	C36	C37	107.0(4)
C35	C36	C38	108.7(4)
H36	C36	C37	110
H36	C36	C38	110.1

C37	C36	C38	110.8(5)
C33	C37	C36	109.8(5)
C33	C37	H37A	109.7
C33	C37	H37B	109.7
C36	C37	H37A	109.7
C36	C37	H37B	109.7
H37A	C37	H37B	108.3
C31	C38	C36	110.2(5)
C31	C38	H38A	109.6
C31	C38	H38B	109.6
C36	C38	H38A	109.6
C36	C38	H38B	109.7
H38A	C38	H38B	108.1

Table A2.6 Bond lengths (Å) for **2.4**

Atom1	**Atom2**	**Length**
Co1	Cl1	2.3562(8)
Co1	Cl2	2.2551(9)
Co1	C1	2.057(3)
Co1	Cl1	2.3725(7)
Cl1	Co1	2.3725(7)
N1	C1	1.360(3)
N1	C2	1.377(4)
N1	C4	1.505(3)
N2	C1	1.368(3)
N2	C3	1.369(4)
N2	C15	1.500(3)
C2	H2	0.94
C2	C3	1.324(5)
C3	H3	0.94
C4	C5	1.530(4)
C4	C6	1.538(4)
C4	C7	1.532(4)
C5	H5A	0.98
C5	H5B	0.98
C5	C8	1.529(4)
C6	H6A	0.98
C6	H6B	0.98
C6	C10	1.525(4)
C7	H7A	0.98
C7	H7B	0.98
C7	C12	1.532(4)

C8	H8	0.99
C8	C9	1.530(5)
C8	C13	1.526(4)
C9	H9A	0.98
C9	H9B	0.98
C9	C10	1.524(5)
C10	H10	0.99
C10	C11	1.526(4)
C11	H11A	0.98
C11	H11B	0.98
C11	C12	1.532(5)
C12	H12	0.99
C12	C13	1.537(4)
C13	H13A	0.98
C13	H13B	0.98
C14	H14A	0.98
C14	H14B	0.98
C14	C15	1.525(4)
C14	C20	1.536(4)
C15	C16	1.529(4)
C15	C17	1.539(4)
C16	H16A	0.98
C16	H16B	0.98
C16	C22	1.543(4)
C17	H17A	0.98
C17	H17B	0.98
C17	C18	1.533(4)
C18	H18	0.99
C18	C19	1.516(5)
C18	C23	1.527(5)
C19	H19A	0.98
C19	H19B	0.98
C19	C20	1.532(5)
C20	H20	0.99
C20	C21	1.522(5)
C21	H21A	0.98
C21	H21B	0.98
C21	C22	1.520(5)
C22	H22	0.99
C22	C23	1.529(5)
C23	H23A	0.98
C23	H23B	0.98
Co1	Cl1	2.3562(8)

Co1	Cl2	2.2551(9)
Co1	C1	2.057(3)
N1	C1	1.360(3)
N1	C2	1.377(4)
N1	C4	1.505(3)
N2	C1	1.368(3)
N2	C3	1.369(4)
N2	C15	1.500(3)
C2	H2	0.94
C2	C3	1.324(5)
C3	H3	0.94
C4	C5	1.530(4)
C4	C6	1.538(4)
C4	C7	1.532(4)
C5	H5A	0.98
C5	H5B	0.98
C5	C8	1.529(4)
C6	H6A	0.98
C6	H6B	0.98
C6	C10	1.525(4)
C7	H7A	0.98
C7	H7B	0.98
C7	C12	1.532(4)
C8	H8	0.99
C8	C9	1.530(5)
C8	C13	1.526(4)
C9	H9A	0.98
C9	H9B	0.98
C9	C10	1.524(5)
C10	H10	0.99
C10	C11	1.526(4)
C11	H11A	0.98
C11	H11B	0.98
C11	C12	1.532(5)
C12	H12	0.99
C12	C13	1.537(4)
C13	H13A	0.98
C13	H13B	0.98
C14	H14A	0.98
C14	H14B	0.98
C14	C15	1.525(4)
C14	C20	1.536(4)
C15	C16	1.529(4)

C15	C17	1.539(4)
C16	H16A	0.98
C16	H16B	0.98
C16	C22	1.543(4)
C17	H17A	0.98
C17	H17B	0.98
C17	C18	1.533(4)
C18	H18	0.99
C18	C19	1.516(5)
C18	C23	1.527(5)
C19	H19A	0.98
C19	H19B	0.98
C19	C20	1.532(5)
C20	H20	0.99
C20	C21	1.522(5)
C21	H21A	0.98
C21	H21B	0.98
C21	C22	1.520(5)
C22	H22	0.99
C22	C23	1.529(5)
C23	H23A	0.98
C23	H23B	0.98
C24	H24A	0.98
C24	H24B	0.98
C24	Cl5A	1.70(1)
C24	Cl6A	1.79(1)
C25	H25A	0.98
C25	H25B	0.979
C25	Cl3A	1.721(8)
C25	Cl4A	1.58(1)

Table A2.7 All angles (°) for **2.4**

Atom1	**Atom2**	**Atom3**	**Angle (Å)**
Cl1	Co1	Cl2	124.56(3)
Cl1	Co1	C1	105.95(8)
Cl1	Co1	Cl1	88.32(3)
Cl2	Co1	C1	113.20(8)
Cl2	Co1	Cl1	94.08(3)
C1	Co1	Cl1	130.85(8)
Co1	Cl1	Co1	91.68(3)
C1	N1	C2	110.0(2)
C1	N1	C4	127.2(2)

C2	N1	C4	122.8(2)
C1	N2	C3	109.9(2)
C1	N2	C15	128.0(2)
C3	N2	C15	122.0(2)
Co1	C1	N1	129.4(2)
Co1	C1	N2	126.0(2)
N1	C1	N2	104.6(2)
N1	C2	H2	126.2
N1	C2	C3	107.5(3)
H2	C2	C3	126.3
N2	C3	C2	107.9(3)
N2	C3	H3	126
C2	C3	H3	126.1
N1	C4	C5	109.9(2)
N1	C4	C6	109.2(2)
N1	C4	C7	110.3(2)
C5	C4	C6	108.5(2)
C5	C4	C7	110.4(2)
C6	C4	C7	108.4(2)
C4	C5	H5A	109.7
C4	C5	H5B	109.7
C4	C5	C8	109.6(2)
H5A	C5	H5B	108.2
H5A	C5	C8	109.8
H5B	C5	C8	109.7
C4	C6	H6A	109.6
C4	C6	H6B	109.6
C4	C6	C10	110.1(2)
H6A	C6	H6B	108.2
H6A	C6	C10	109.7
H6B	C6	C10	109.6
C4	C7	H7A	109.7
C4	C7	H7B	109.7
C4	C7	C12	109.6(2)
H7A	C7	H7B	108.2
H7A	C7	C12	109.8
H7B	C7	C12	109.8
C5	C8	H8	109.4
C5	C8	C9	110.0(3)
C5	C8	C13	109.6(2)
H8	C8	C9	109.3
H8	C8	C13	109.3
C9	C8	C13	109.1(3)

C8	C9	H9A	109.9
C8	C9	H9B	109.9
C8	C9	C10	109.0(3)
H9A	C9	H9B	108.3
H9A	C9	C10	109.9
H9B	C9	C10	109.9
C6	C10	C9	109.7(3)
C6	C10	H10	109.2
C6	C10	C11	109.2(2)
C9	C10	H10	109.2
C9	C10	C11	110.3(3)
H10	C10	C11	109.3
C10	C11	H11A	109.8
C10	C11	H11B	109.8
C10	C11	C12	109.2(3)
H11A	C11	H11B	108.3
H11A	C11	C12	109.8
H11B	C11	C12	109.8
C7	C12	C11	109.0(2)
C7	C12	H12	109.6
C7	C12	C13	109.8(2)
C11	C12	H12	109.6
C11	C12	C13	109.3(2)
H12	C12	C13	109.6
C8	C13	C12	109.7(2)
C8	C13	H13A	109.7
C8	C13	H13B	109.7
C12	C13	H13A	109.7
C12	C13	H13B	109.7
H13A	C13	H13B	108.2
H14A	C14	H14B	108.2
H14A	C14	C15	109.6
H14A	C14	C20	109.7
H14B	C14	C15	109.7
H14B	C14	C20	109.6
C15	C14	C20	110.1(2)
N2	C15	C14	110.2(2)
N2	C15	C16	109.8(2)
N2	C15	C17	109.8(2)
C14	C15	C16	110.6(2)
C14	C15	C17	108.3(2)
C16	C15	C17	108.0(2)
C15	C16	H16A	109.8

C15	C16	H16B	109.7
C15	C16	C22	109.5(3)
H16A	C16	H16B	108.2
H16A	C16	C22	109.8
H16B	C16	C22	109.8
C15	C17	H17A	109.7
C15	C17	H17B	109.7
C15	C17	C18	109.8(2)
H17A	C17	H17B	108.2
H17A	C17	C18	109.7
H17B	C17	C18	109.7
C17	C18	H18	109.1
C17	C18	C19	109.6(3)
C17	C18	C23	109.3(3)
H18	C18	C19	109.1
H18	C18	C23	109
C19	C18	C23	110.7(3)
C18	C19	H19A	109.9
C18	C19	H19B	109.9
C18	C19	C20	109.0(3)
H19A	C19	H19B	108.3
H19A	C19	C20	109.9
H19B	C19	C20	109.9
C14	C20	C19	108.4(2)
C14	C20	H20	109.5
C14	C20	C21	109.5(3)
C19	C20	H20	109.5
C19	C20	C21	110.4(3)
H20	C20	C21	109.5
C20	C21	H21A	109.7
C20	C21	H21B	109.7
C20	C21	C22	109.8(3)
H21A	C21	H21B	108.2
H21A	C21	C22	109.7
H21B	C21	C22	109.7
C16	C22	C21	109.6(3)
C16	C22	H22	109.4
C16	C22	C23	109.2(3)
C21	C22	H22	109.4
C21	C22	C23	109.9(3)
H22	C22	C23	109.4
C18	C23	C22	108.8(3)
C18	C23	H23A	109.9

C18	C23	H23B	109.9
C22	C23	H23A	109.9
C22	C23	H23B	109.9
H23A	C23	H23B	108.3
Cl1	Co1	Cl1	88.32(3)
Cl1	Co1	Cl2	94.08(3)
Cl1	Co1	C1	130.85(8)
Cl1	Co1	Cl2	124.56(3)
Cl1	Co1	C1	105.95(8)
Cl2	Co1	C1	113.20(8)
Co1	Cl1	Co1	91.68(3)
C1	N1	C2	110.0(2)
C1	N1	C4	127.2(2)
C2	N1	C4	122.8(2)
C1	N2	C3	109.9(2)
C1	N2	C15	128.0(2)
C3	N2	C15	122.0(2)
Co1	C1	N1	129.4(2)
Co1	C1	N2	126.0(2)
N1	C1	N2	104.6(2)
N1	C2	H2	126.2
N1	C2	C3	107.5(3)
H2	C2	C3	126.3
N2	C3	C2	107.9(3)
N2	C3	H3	126
C2	C3	H3	126.1
N1	C4	C5	109.9(2)
N1	C4	C6	109.2(2)
N1	C4	C7	110.3(2)
C5	C4	C6	108.5(2)
C5	C4	C7	110.4(2)
C6	C4	C7	108.4(2)
C4	C5	H5A	109.7
C4	C5	H5B	109.7
C4	C5	C8	109.6(2)
H5A	C5	H5B	108.2
H5A	C5	C8	109.8
H5B	C5	C8	109.7
C4	C6	H6A	109.6
C4	C6	H6B	109.6
C4	C6	C10	110.1(2)
H6A	C6	H6B	108.2
H6A	C6	C10	109.7

H6B	C6	C10	109.6
C4	C7	H7A	109.7
C4	C7	H7B	109.7
C4	C7	C12	109.6(2)
H7A	C7	H7B	108.2
H7A	C7	C12	109.8
H7B	C7	C12	109.8
C5	C8	H8	109.4
C5	C8	C9	110.0(3)
C5	C8	C13	109.6(2)
H8	C8	C9	109.3
H8	C8	C13	109.3
C9	C8	C13	109.1(3)
C8	C9	H9A	109.9
C8	C9	H9B	109.9
C8	C9	C10	109.0(3)
H9A	C9	H9B	108.3
H9A	C9	C10	109.9
H9B	C9	C10	109.9
C6	C10	C9	109.7(3)
C6	C10	H10	109.2
C6	C10	C11	109.2(2)
C9	C10	H10	109.2
C9	C10	C11	110.3(3)
H10	C10	C11	109.3
C10	C11	H11A	109.8
C10	C11	H11B	109.8
C10	C11	C12	109.2(3)
H11A	C11	H11B	108.3
H11A	C11	C12	109.8
H11B	C11	C12	109.8
C7	C12	C11	109.0(2)
C7	C12	H12	109.6
C7	C12	C13	109.8(2)
C11	C12	H12	109.6
C11	C12	C13	109.3(2)
H12	C12	C13	109.6
C8	C13	C12	109.7(2)
C8	C13	H13A	109.7
C8	C13	H13B	109.7
C12	C13	H13A	109.7
C12	C13	H13B	109.7
H13A	C13	H13B	108.2

H14A	C14	H14B	108.2
H14A	C14	C15	109.6
H14A	C14	C20	109.7
H14B	C14	C15	109.7
H14B	C14	C20	109.6
C15	C14	C20	110.1(2)
N2	C15	C14	110.2(2)
N2	C15	C16	109.8(2)
N2	C15	C17	109.8(2)
C14	C15	C16	110.6(2)
C14	C15	C17	108.3(2)
C16	C15	C17	108.0(2)
C15	C16	H16A	109.8
C15	C16	H16B	109.7
C15	C16	C22	109.5(3)
H16A	C16	H16B	108.2
H16A	C16	C22	109.8
H16B	C16	C22	109.8
C15	C17	H17A	109.7
C15	C17	H17B	109.7
C15	C17	C18	109.8(2)
H17A	C17	H17B	108.2
H17A	C17	C18	109.7
H17B	C17	C18	109.7
C17	C18	H18	109.1
C17	C18	C19	109.6(3)
C17	C18	C23	109.3(3)
H18	C18	C19	109.1
H18	C18	C23	109
C19	C18	C23	110.7(3)
C18	C19	H19A	109.9
C18	C19	H19B	109.9
C18	C19	C20	109.0(3)
H19A	C19	H19B	108.3
H19A	C19	C20	109.9
H19B	C19	C20	109.9
C14	C20	C19	108.4(2)
C14	C20	H20	109.5
C14	C20	C21	109.5(3)
C19	C20	H20	109.5
C19	C20	C21	110.4(3)
H20	C20	C21	109.5
C20	C21	H21A	109.7

C20	C21	H21B	109.7
C20	C21	C22	109.8(3)
H21A	C21	H21B	108.2
H21A	C21	C22	109.7
H21B	C21	C22	109.7
C16	C22	C21	109.6(3)
C16	C22	H22	109.4
C16	C22	C23	109.2(3)
C21	C22	H22	109.4
C21	C22	C23	109.9(3)
H22	C22	C23	109.4
C18	C23	C22	108.8(3)
C18	C23	H23A	109.9
C18	C23	H23B	109.9
C22	C23	H23A	109.9
C22	C23	H23B	109.9
H23A	C23	H23B	108.3
H24A	C24	H24B	109
H24A	C24	Cl5A	111
H24A	C24	Cl6A	111.1
H24B	C24	Cl5A	111
H24B	C24	Cl6A	111
Cl5A	C24	Cl6A	103.7(5)
H25A	C25	H25B	107.3
H25A	C25	Cl3A	108
H25A	C25	Cl4A	107.9
H25B	C25	Cl3A	108
H25B	C25	Cl4A	108
Cl3A	C25	Cl4A	117.4(5)

2.6.3 Evans method NMR spectra

The Evans method[44] was implemented to determine the magnetic moments of **2.1**, **2.2** and **2.3**. For the experiment, **2.1** (7mg) was dissolved in 1mL of $CDCl_3$, and 30 µL of tert-butanol was added as an internal standard. 100 µL of this solution was added to a capillary tube. A reference solution of 1 mL $CDCl_3$ and 30 µL tert-butanol was added to an NMR tube in a quantity of 0.6 mL. The capillary tube was gently placed in the NMR tube and an ^1H NMR experiment was recorded at room temperature. The presence of paramagnetic **2.1** deshields the tert-butanol ^1H NMR peak in the capillary, while the signal in the reference solution remains unaffected. The difference in frequencies was 42.99Hz. Using Evans Method, the data showed a crystal field of 3 unpaired electrons. The same result was found for **2.2** and **2.3**. While for **2.2** (7 mg), 20 µL of regular chloroform was used as the internal standard in 1 mL of $CDCl_3$, and for **2.3** (5 mg), 30 µL of tert-butanol was used as the internal standard in 1 mL of $CDCl_3$, the calculations and experiments are otherwise similar. The change in frequency was 34.14Hz for **2.2**, and 43.01 Hz for **2.3**

μ_{eff} (**2.1**) = 3.75, μ_{eff} (**2.2**) = 4.67, μ_{eff} (**2.3**) = 3.80.

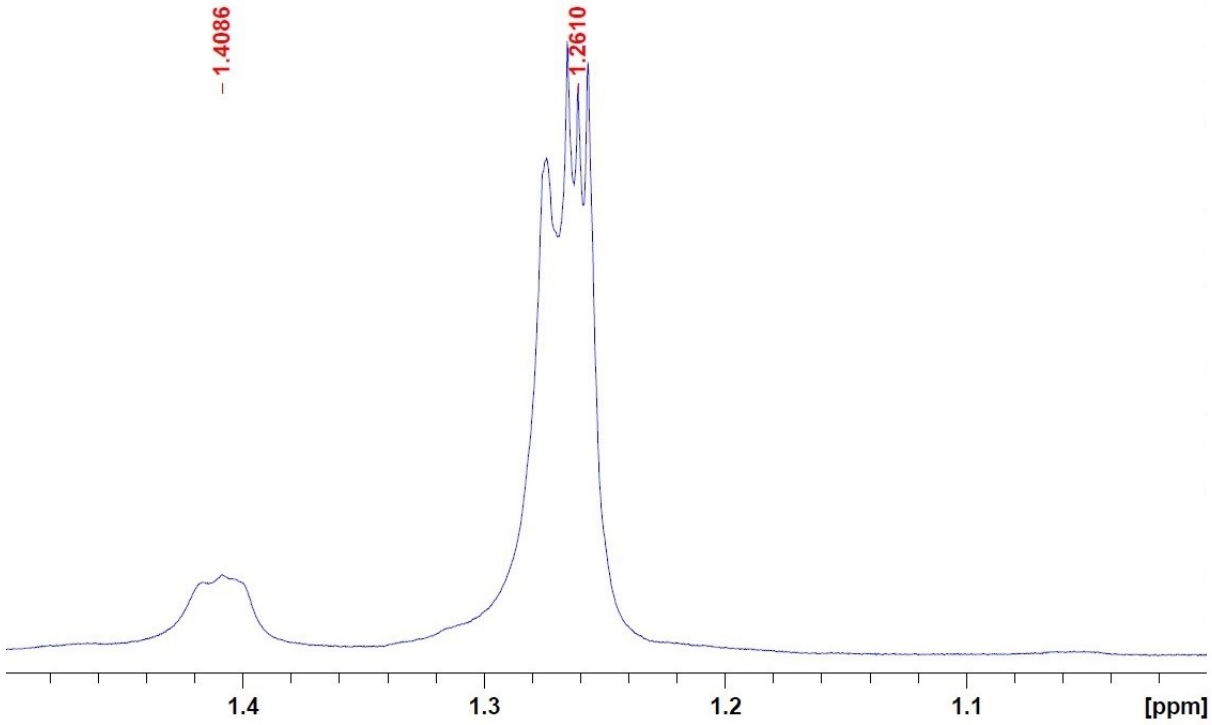

Figure A2.22 ^{1}H NMR (300 MHz, $CDCl_3$) spectrum of **2.1** using the Evans method.

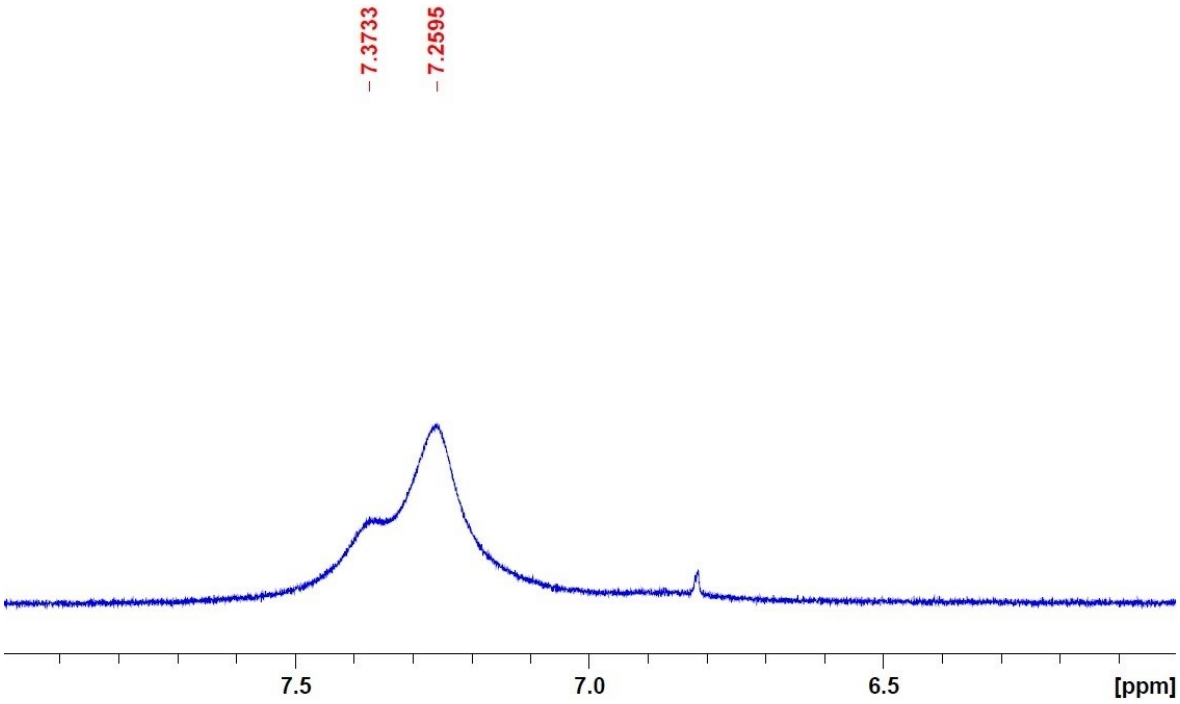

Figure A2.23 ^{1}H NMR (300 MHz, $CDCl_3$) spectrum of **2.2** using the Evans method.

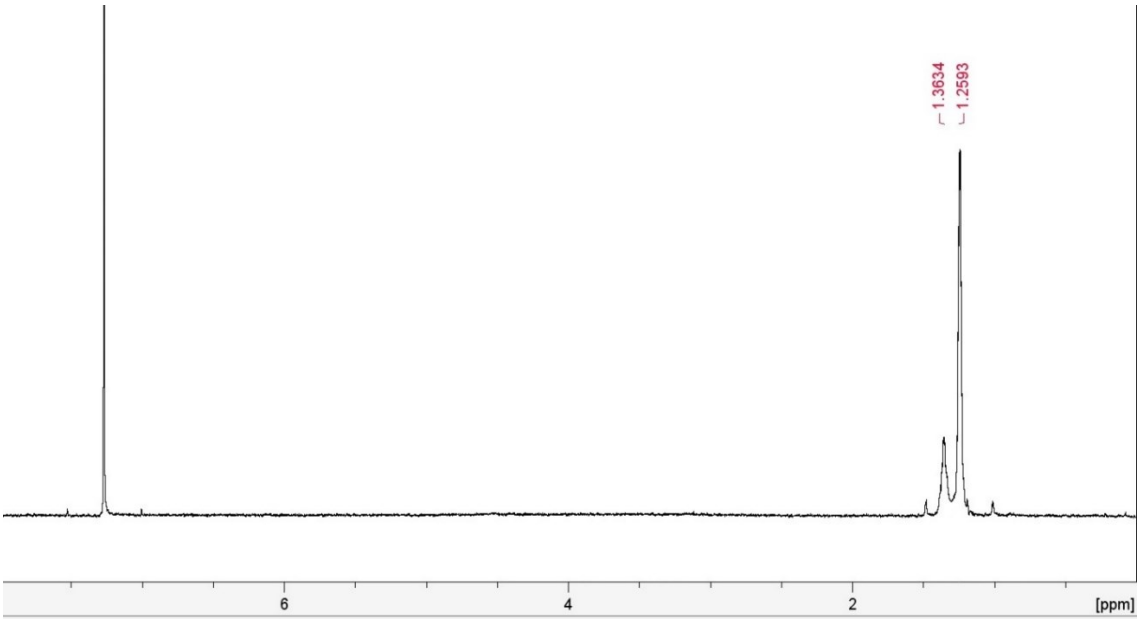

Figure A2.24 ^{1}H NMR (400 MHz, $CDCl_3$) spectrum of **2.4** using the Evans method.

2.6.4 Computational details

2.6.4.1 Experimental

All DFT calculations were performed using Gaussian 16[60] on Graham cluster, with access provided by Compute Canada/Calcul Canada. Several methods (M06,[61] M06-L,[62] PBE0-D3(BJ),[63] B3LYP-D3(BJ),[64] TPSSh-D3(BJ)[65] and TPSS0-D3(BJ)[66]) were benchmarked against the solid-state geometries of the neutral $(SNS)_2Co$ and $(SNS)_2Fe$ complexes (characterized by SC-XRD),[30, 43.b] and the PBE0-D3(BJ) method was found to give the smaller deviations in terms of bond distances and angles around the metal center.

Table A2.8 Comparison of the experimental (found by SC-XRD at 200K) and DFT-computed bonds and angles in cobalt and iron bis-amido complexes.

		M = Co			**M = Fe**	
Bond /Angle		**XRD**	**PBE0-D3(BJ)**		**XRD**	**PBE0-D3(BJ)**
S1-**M**		2.6481(7) 2.7027(7)	2.6636		2.7156(7) 2.7014(8)	2.6726 2.6722
S2-**M**		2.4723(7) 2.4780(7)	2.4940		2.5389(7) 2.5431(7)	2.5322 2.5511
N-**M**		1.967(2) 1.974(2)	1.9927		2.015(2) 2.031(2)	2.0456 2.0516
trans S1-**M**-S2		165.41(3) 167.06(3)	167.62		166.63(2) 160.67(3)	166.68 160.39
trans N-**M**-N'		176.46(8)	175.66		177.60(8)	178.06
cis S1-**M**-N		85.36(6) 85.84(6)	86.62		86.80(6) 83.08(6)	86.54 83.50
cis S2-**M**-N		82.48(6) 83.03(6)	82.27		80.72(6) 78.48(6)	80.33 78.00

Geometry optimization of all complexes were carried out using mixed basis sets:[67] 6-311g** for C and H atoms,[68] 6-311+g** for N, O, F, S and Cl,[69] and def2TZVP for Co or Fe,[70] in implicit THF using the CPCM model.[71] The PBE0 hybrid functional was exploited in conjunction with the D3 version Grimme's empirical dispersion[66] with Becke-Johnson damping.[72] Local minima were assessed by convergence and the absence of imaginary frequencies in the frequency calculation. The electronic energy was further computed using the def2TZVP basis set for all atoms, with an added diffuse function for N, O, F, S and Cl atoms.[73] The thermal energies presented herein correspond to the sum of the electronic energy found with the larger basis set and the thermal corrections outputted from the frequency calculation after the optimization procedure.

2.6.4.2 Results

For all octahedral Co and Fe complexes, the lowest energy wavefunctions were found to be high spin states, *i.e.*, S = 3/2 for cobalt and S = 2 for iron complexes, in accordance with experimentally measured values of the parent (κ^3-SNS)$_2$M complexes, and **2.2**. For the neutral bis-amido complexes and their mono- and di-protonated complexes (either free cations or ion-paired to Tf_2N^- anions (X^-) via O---H hydrogen bonding), a variety of geometries were studied, namely: several conformations for the meridional trans complexes (***trans***), the facial trans complexes (***fac***), and the facial-cis complexes (***cis***). The energies discussed below relate to the lower energy solution found for each of these coordination modes, and are expressed in kcal/mol.

For the neutral complexes, the meridional isomers were found to be lower in energy as found in the solid state. In the free mono-protonated complexes, [M(**L2**)(**L2**H)]$^+$, the meridional isomers are still more favoured, although the difference of energy with the facial coordination mode decreases, and the *cis* isomer is almost isoenergetic in the Co system. In the free di-protonated complexes, [M(**L2**H)$_2$]$^{2+}$, all three isomers are within 1 kcal/mol difference in terms of Gibbs free energy.

When ion-pairing to the TfN_2^- anion is considered, as observed in the solid state structure of of [*fac*-(κ^3-SN^{H}S)(κ^3-SNS)Fe][NTf_2], the mono-protonated complexes [*mer*-M(**L2**H)(**L2**)]X still show the same trend with the *mer* complexes being the most favoured and the *cis* complexes being the less favoured. On the other hand, for the ion-paired di-protonated complexes, the facial coordination is clearly favoured, as observed in the solid state of [*fac*-(κ^3-SN^{H}S)$_2$Co][NTf_2]$_2$, although the difference is small for the iron dication.

Table A2.9 1 DFT computed relative enthalpies and Gibbs free energies of three isomers for the neutral complexes, expressed in kcal/mol.

	M = Co		M = Fe	
Isomer	**ΔH**	**ΔG**	**ΔH**	**ΔG**
mer-M(**L^1**)$_2$	0	0	0	0
fac-M(**L^1**)$_2$	7.6	5.3	13.8	11.2
cis-M(**L^1**)$_2$	6.9	3.9	8.5	5.8

Table A2.10 DFT computed relative enthalpies and Gibbs free energies of three isomers for the free mono- or di-protonated complexes, expressed in kcal/mol.

	M = Co		M = Fe	
Isomer	**ΔH**	**ΔG**	**ΔH**	**ΔG**
[*mer*-M(**L^1**H)(**L^1**)]$^+$	0	0	0	0
[*fac*-M(**L^1**H)(**L^1**)]$^+$	5.6	3.4	2.7	0.1
[*cis*-M(**L^1**H)(**L^1**)]$^+$	–0.1	1.6	3.5	1.3
[*mer*-M(**L^1**H)$_2$]$^{2+}$	–1.8	0	0	0
[*fac*-M(**L^1**H)$_2$]$^{2+}$	0.8	1.0	2.6	1.0
[*cis*-M(**L^1**H)$_2$]$^{2+}$	0	0	2.4	0.7

Table A2.11 2 DFT computed relative enthalpies and Gibbs free energies of three isomers for the NTf_2-bound mono- or di-protonated complexes, expressed in kcal/mol.

	M = Co		M = Fe	
Isomer	**ΔH**	**ΔG**	**ΔH**	**ΔG**
[*mer*-M(**L^1**H)(**L^1**)]X	0	0	0	0
[*fac*-M(**L^1**H)(**L^1**)]X	3.2	2.2	5.0	4.1
[*cis*-M(**L^1**H)(**L^1**)]X	7.4	5.1	8.1	6.0
[*mer*-M(**L^1**H)$_2$]X$_2$	1.3	3.7	–0.6	0.8
[*fac*-M(**L^1**H)$_2$]X$_2$	0	0	0	0
[*cis*-M(**L^1**H)$_2$]X$_2$	5.5	6.7	6.0	6.9

The protonation of *mer*-M(**L2**)$_2$ complexes by one equiv of $HNTf_2$ leading to fully dissociated ions is strongly exergonic, by ca. 20 kcal/mol for cobalt and by ca. 16 kcal/mol for iron, and is even more favoured when tight ion-pairing (ranging 3–6 and 3–9 kcal/mol, respectively for all Co and Fe conformers/isomers) is added, giving a ΔG of ca. –25 kcal/mol for both metals.

On the other hand, the protonation of [*mer*-M(**L2**H)(**L2**)]$^+$ by one additional equiv of $HNTf_2$ leading to free dications is only –1.9 and –4.4 kcal/mol, respectively, for Co and Fe. Again, the ion pairing energy with two NTf_2^- anions (ranging 18–26 kcal/mol for both Co and Fe) allows for a strongly exergonic second protonation of ca. –20.5 and –19.6 kcal/mol for Co and Fe, respectively.

The difference between the two metals is thus very subtle and thus, at the level of theory used, we were not able to rationalize the proton redistribution when *mer*-Co(**L2**)$_2$, is treated with one equiv. $HNTf_2$, where the reaction was calculated to be disfavoured by 2.0 kcal/mol with cobalt, and 2.8 kcal/mol with iron. Analysis of Hirshfeld charges did not allow us to explain the proton redistribution observed with Co through kinetic considerations.

Table A2.12 3 DFT computed enthalpies and Gibbs free energies for each sequential protonation step.

		mer-M(L2)$_2$	Tf_2NH →	[*mer*-M(L2H)(L2)][NTf_2]	Tf_2NH →	[*fac*-M(L2H)$_2$][NTf_2]$_2$
Co	ΔH	0		–37.1		–32.3
	ΔG	0		–24.6		–20.5
Fe	ΔH	0		–37.8		–31.9
	ΔG	0		–25.3		–19.6

Another aspect of this study is the formation of the abnormally coordinated NHC complex derived from $IAdH^+$ (1,3-bisadamantyl-imidazolium) upon deprotonation by one amido-ligand of $(SNS)_2Co$. DFT optimization of the resulting (SNS)Co(aIAd)Cl led to a geometry fairly close to that observed in the solid state (SC-XRD at 200 K) in terms of bond lengths and angles around the Co center, except for the Ĉ-Co-N angle which was found significantly wider in the solid state.

Although the free abnormal carbene (1,3-bisadamantylimidazol-4-ylidene) is found to much less stabilized than the normal IAd (by a ΔG of ca. 12 kcal/mol), coordination to the Co center leads to two complexes of very similar energies. The aIAd coordination mode is favoured in terms of Gibbs free energy by only 0.6 kcal/mol, while it is predicted to be disfavoured enthalpically. We believe that it arises from the high steric hindrance of the adamantly groups, that translates into significantly elongated bonds around the metal, especially with a Co-Ĉ that theory envisages to increase from 2.032 to 2.101 Å in the event of a normally coordinated carbene. It suggests that the isolation of complex **2.3** exclusively relies on a kinetic control, where the deprotonation at C4 of the imidazolium is much more accessible.

Table A2.13 Comparison of the experimental (found by SC-XRD at 200K) and DFT-computed bonds and angles in the abnormally and normally bound IAd complexes, and their thermal energies.

Bond / Angle	**(aIAd)Co(κ^2-SNS)Cl**		**(IAd)Co(κ^2-SNS)Cl**
	XRD	**PBE0-D3(BJ)**	**PBE0-D3(BJ)**
Co-Ĉ	2.034(4)	2.032	2.101
Co-S	2.4112(12)	2.433	2.482
Co-N	1.919(3)	1.951	1.970
Co-Cl	2.2691(12)	2.311	2.341
Ĉ-Co-Cl	119.28(11)	121.93	105.71
Ĉ-Co-N	122.66(14)	112.34	118.78
Ĉ-Co-S	103.09(11)	105.55	127.07
S-Co-Cl	103.18(5)	104.50	92.14
S-Co-N	85.75(9)	85.17	81.94
N-Co-Cl	113.02(10)	118.69	128.15
Energy	**ΔH**	0	+1.8
	ΔG	0	–0.6

Table A2.14 4 Comparison of the experimental (found by SC-XRD at 200K) and DFT-computed bonds for abnormally bound IAd complexes in quartet and doublet spin states, and their thermal energies.

Bond / Angle		(aIAd)Co(κ^2-SNS)Cl	
	XRD	PBE0-D3(BJ) quartet	PBE0-D3(BJ) doublet
Co-Ĉ	2.034(4)	2.032	1.970
Co-S	2.4112(12)	2.433	2.342
Co-N	1.919(3)	1.951	1.911
Co-Cl	2.2691(12)	2.311	2.360
Ĉ-Co-Cl	119.28(11)	121.93	98.09
Ĉ-Co-N	122.66(14)	112.34	154.58
Ĉ-Co-S	103.09(11)	105.55	97.39
S-Co-Cl	103.18(5)	104.50	110.37
S-Co-N	85.75(9)	85.17	85.49
N-Co-Cl	113.02(10)	118.69	104.58
Energy	ΔH	0	24.2
	ΔG	0	21.6

2.7 References

1. Elsby, M. R.; Oh, C.; Son, M.; Kim, S. Y. H.; Baik, M. H.; Baker, R. T., Spin-state crossover in photo-catalyzed nitrile dihydroboration via Mn-thiolate cooperation, *Chem. Sci*., 2022, **13**, 12550-12559.
2. Ataie, S.; Hogeterp, S.; Oven, J. S.; Baker, R. t., SNS ligand-assisted catalyst activation in Zn-catalysed carbonyl hydroboration, *Chem. Commun*., 2022, **58**, 3795-3798.
3. Marder, T. B.; Lin, Z. Contemporary metal boron chemistry I: Borylenes, boryls, borane σ-complexes and borohydrides, *Struct. Bond.*, 2008, **130**.
4. Pang, M.; Wu, C.; Zhuang, X.; Zhang, F.; Su, M.; Tong, Q.; Tung, C.-H.; Wang, W. Addition of a B−H bond across an amido−cobalt bond: Co^{II}−H-catalyzed hydroboration of olefins, *Organometallics* 2018, **37**, 1462−1467.
5. Cao, K.; Xu, T-T.; Wu, J.; Zhang, C-Y.; Wen, X-Y.; Yang, J. The in situ NHC-palladium-catalyzed selective activation of B(3)−H or B(6)−H bonds of o-carboranes for hydroboration of alkynes: An efficient approach to alkenyl-o-carboranes, *Inorg. Chem.,* 2021, **60**, 1080−1085.
6. Ataie, S.; Baker, R. T. Comparing B−H bond activation in $Ni^{II}X$(NNN)-catalyzed nitrile dihydroboration (X = anionic N-, C-, O-, S-, or P-donor), *Inorg. Chem.,* 2022, **61**, 19998–20007.
7. Elsby, M. R.; Baker, R. T. Strategies and mechanisms of metal–ligand cooperativity in first-row transition metal complex catalysts, *Chem. Soc. Rev.,* 2020, **49**, 8933-8987.
8. Khusnutdinova, J. R.; Milstein, D. Metal–ligand cooperation, *Angew. Chem., Int. Ed.*, 2015, **54**, 12236–12273.
9. Fritz, M.; Schneider, S. The renaissance of base metal catalysis enabled by functional ligands in *The periodic table II: Catalytic, materials, biological and medical applications*, Mingos, D. M. P. Ed. Springer, 2019.
10. Saha, S.; Eisen, M. S. Catalytic recycling of a Th−H bond via single or double hydroboration of Iinactivated imines or nitriles, *ACS Catal.* 2019, **9**, 5947−5956.
11. Ding, Y.; Ma, X.; Liu, Y.; Liu, W.; Yang, Z.; Roesky, H. W. Alkylaluminum complexes as precatalysts in hydroboration of nitriles and carbodiimides, *Organometallics,* 2019, **38**, 3092−3097.
12. Harinath, A.; Bhattacharjee, J.; Panda, T. K. Catalytic hydroboration of organic nitriles promoted by aluminum complex, *Adv. Synth. Catal.* 2019, **361**, 850–857.
13. Das, S.; Bhattacharjee, J.; Panda, T. K. An imidazolin-2-iminato ligand organozinc complex as a catalyst for hydroboration of organic nitriles, *New J. Chem.* 2019, **43**, 16812–16818.
14. Wang, X.; Zhang, Y.; Yuan, D.; Yao, Y. Regioselective hydroboration and hydrosilylation of n-heteroarenes catalyzed by a zinc alkyl complex, *Org. Lett.* 2020, **22**, 5695−5700.
15. Procter, J. R.; Uzelac, M.; Cid, J.; Rushworth, P. J.; Ingleson, M. J. Low-coordinate NHC−zinc hydride complexes catalyze alkyne C−H borylation and hydroboration using pinacolborane, *ACS Catal.,* 2019, **9**, 5760−5771.
16. Ataie, S.; Hogeterp, S.; Ovens, S. O.; Baker, R. T. SNS ligand-assisted catalyst activation in Zn-catalysed carbonyl hydroboration, *Chem. Commun.,* 2022, **58**, 3795-3798.
17. Ataie, S.; Ovens, S. O.; Baker, R. T. Solvent-free Zn (NSNO) complex-catalysed dihydroboration of nitriles, *Chem. Commun.,* 2022, **58**, 8266-3269.
18. Ataie, S.; Lohoar, M. I.; Mangin, L. P.; Baker, R. T. Coinage metal amido and thiolate SNS complexes: Consequences of catalyst speciation in Cu(I)-catalysed carbonyl hydroboration, Chem. Commun., 2023, **59**, 4044-4046.
19. Liu, J.; Chen, J-Y.; Jia, M.; Ming, B.; Jia, J.; Liao, R-Z.; Tung, C-H.; Wang, W. Ni−O cooperation versus nickel(II) hydride in catalytic hydroboration of N-heteroarenes, *ACS Catal.,* 2019, **9**, 3849−3857.
20. Elsby, M. R.; Baker, R. T. Cu(I)–SNS complexes for outer-sphere hydroboration and hydrosilylation of carbonyls, *Chem. Commun.,* 2019, **55**, 13574–13577.

21. Geri, J. B.; Szymczak, N. K. A proton-switchable bifunctional ruthenium complex that catalyzes nitrile hydroboration, *J. Am. Chem. Soc.,* 2015, **137**, 12808−12814.
22. Tseng, K.-N. T.; Kampf, J. W.; Szymczak, N. K. Modular attachment of appended boron Lewis acids to a ruthenium pincer catalyst: Metal-ligand cooperativity enables selective alkyne hydrogenation, *J. Am. Chem. Soc.,* 2016, **138**, 10378−10381.
23. Stahl, T.; Müther, K.; Ohki, Y.; Tatsumi, K.; Oestreich, M. Catalytic generation of borenium ions by cooperative B−H bond activation: The elusive direct electrophilic borylation of nitrogen heterocycles with pinacolborane, *J. Am. Chem. Soc.,* 2013, **135**, 10978−10981.
24. Drover, M. W.; Schafer, L. L.; Love, J. A. Capturing $HBCy_2$ using N,O-chelated complexes of rhodium(I) and iridium(I) for chemoselective hydroboration, *Angew. Chem., Int. Ed.,* 2016, **55**, 3181−3186.
25. Chu, W. Y.; Zhou, X.; Rauchfuss, T. B. Cooperative metal− ligand reactivity and catalysis in low-spin ferrous alkoxides, *Organometallics,* 2015, **34**, 1619−1626.
26. Kaithal, A.; Chatterjee, B.; Gunanathan, C. Ruthenium catalyzed selective hydroboration of nitriles and imines, *J. Org. Chem.,* 2016, **81**, 11153–11161.
27. Ding, Y.; Ma, X.; Liu, Y.; Liu, W.; Yang, Z.; Roesky, H. W. Alkylaluminum complexes as precatalysts in hydroboration of nitriles and carbodiimides, *Organometallics,* 2019, **38**, 3092–3097.
28. Ataie, S.; Baker, R. T. Bifunctional activation of NHC-zinc pre-aatalyst for effective hydroboration of quinolines and nitriles, *ChemCatChem*, 2023, e202300649.
29. Weetman, C.; Anker, M. D.; Arrowsmith, M.; Hill, M. S.; Kociok-Kohn, G.; Liptrot, D. J.; Mahon, M. F. Magnesium-catalysed nitrile hydroboration, *Chem. Sci,.* 2016, **7**, 628–641.
30. Das, U. K.; Daifuku, S. L.; Iannuzzi, T. E.; Gorelsky, S. I.; Korobkov, I.; Gabidullin, B.; Neidig, M. L.; Baker, R. T. Iron(II) complexes of a hemilabile SNS Amido Ligand: Synthesis, characterization, and reactivity, *Inorg. Chem.,* 2017, **56**, 13766−13776.
31. Guo, J.; Chen, J.; Lu, Z. Cobalt-catalyzed asymmetric hydroboration of aryl ketones with pinacolborane, *Chem. Commun.,* 2015, **51**, 5725−5727.
32. Zhang, T.; Manna, K.; Lin, W. Metal organic frameworks stabilize solution-inaccessible cobalt catalysts for highly efficient broad-scope organic transformations, *J. Am. Chem. Soc.,* 2016, **138**, 3241−3249.
33. Wu, J.; Zeng, H.; Cheng, J.; Zheng, S.; Golen, J. A.; Manke, D. R.; Zhang, G. Cobalt(II) coordination polymer as a precatalyst for selective hydroboration of aldehydes, ketones, and imines, *J. Org. Chem.,* 2018, **83**, 9442−9448.
34. Tamang, S. R.; Bedi, D.; Shafiei-Haghighi, S.; Smith, C. R.; Crawford, C.; Findlater, M. Cobalt-catalyzed hydroboration of alkenes, aldehydes, and ketones, *Org. Lett.,* 2018, **20**, 6695−6700.
35. Ibrahim, A. D.; Entsminger, S. W.; Fout, A. R., Insight into a chemoselective cobalt catalyst for the hydroboration of alkenes and nitriles, *ACS Catal*, 2017, **7**, 3730-3734.
36. Ataie, S.; Dudra, S. L.; Johnson, E. R.; Baker, R. T. Selective cobalt(II)-SNS dithiolate complex-catalyzed bifunctional hydroboration of aldehydes: Kinetics and mechanistic studies, *ACS Catal.,* 2023, **13**, 10076–10084.
37. Meher, N. K.; Verma, P. K.; Geetharani, K. Cobalt-catalyzed regioselective 1,2-hydroboration of N-hetroarenes, *Org. Lett.,* 2023, **25**, 87-92.
38. Ghosh, C.; Kim, S.; Mena, M. R.; Kim, J.; Pal, R.; Rock, C. L.; Groy, T. L.; Baik, M.; Trovitch, R. J. Efficient cobalt catalyst for ambient-temperature nitrile dihydroboration, the elucidation of a chelate-assisted borylation mechanism and a new synthetic route to amides, *J. Am. Chem. Soc.,* 2019, **141**, 15327-15337.

39. Gutierrez, L.; Martin-Diaconescu, V. Casadevall, C.; Oropeza, F. de la Pena Oshea, V. A.; Meng, J.; Ortuno, M. A.; Lloret-Fillol, J. Low oxidation state cobalt center stabilized by a covalent organic framework to promote hydroboration of olefins, *ACS Catal.,* 2023, **13**, 3044-3054.
40. Yang. X.; Ge. S. Cobalt-catalysed 1,1,3-triborylation of terminal alkynes, *Organometallics*, 2022, **41**, 1823-1828.
41. Zhang, Y.; Li, X.; Mo, Q.; She. W.; Zhao, J.; Zhu. S. Highly regioselective cobalt-catalysed hydroboration of internal alkynes, *Angew. Chem., Int. Ed.,* 2022, **61**, e202208473.
42. Geier, S. J.; Vogels, C. M.; Melanson, J. A.; Westcott, S. A. The transition metal-catalysed hydroboration reaction, *Chem. Soc. Rev.,* 2022, **51**, 8877-8922.
43. (a) Fitchett, B. University of Ottawa MSc thesis, 2018. (b) Elsby, M. R.; Kim, S. Y. H.; Steinmann, S. N.; Baker, R. T. Same ligand, three first-row metals: Comparing M-amido bifunctional reactivity (Mn, Fe, Co), *Dalton Trans.,* 2021, **50**, 14542-14546.
44. (a) Evans, D.F. The determination of the paramagnetic susceptibility of substances in solution by nuclear magnetic resonance, *J. Chem. Soc.,* 1959, 2003-2005. (b) Deutsch, J. L.; Poling, S. M. The determination of paramagnetic susceptibility by nmr: A physical chemistry experiment, *J. Chem. Ed.,* 1969, **46**, 167. (c) Johnson, A. R. The Evans method: Measuring magnetic susceptibility by NMR-application, 2016.
45. Özçelik, B.; Yazıcı, D.; Ekicibil, A. Structural and magnetic properties of cobalt(II) complexes of triphenylphosphine, *J. Supercond. Nov. Magn*., 2013, **26**, 1599–1605.
46. Dojer, B.; Pevec, A.; Belaj, F.; Jagličić, Z.; Kristl, M.; Drofenik, M. Structural and magnetic properties of cobalt(II) complexes with pyridinecarboxamide ligands, *J. Mol. Struct.,* 2014, **1076**, 713-718.
47. (a) Fischer, P. J.; Miessler, L. G.; Tarr, D. A. *Inorganic Chemistry*, Addison Wesley Longman Limited, 2013. (b) Okuniewski, A.; Rosiak. D.; Chojnacki, J.; Becker, B. *Polyhedron*, 2015, **90** , 47-57. (c) Ghadwal, R. S.; Lamm, J. H.; Rottschäfer, D.; Schürmann, C. J.; Demeshko, S. Facile routes to abnormal-NHC-cobalt (II) complexes, *Dalton Trans.,* 2017, **46**, 7664–7667.
48. Danopoulos, A. A.; Braunstein, P. Mono-N-heterocyclic carbene amido and alkyl complexes. Cobalt-mediated C-H activation and C-C coupling reactions involving benzyl ligands on a putative 3-coordinate intermediate, *Dalton Trans.,* 2013, **42**, 7276–7280.
49. Matsubara, K.; Sueyasu, T.; Esaki, M.; Kumamoto, A.; Nagao, S.; Yamamoto, H.; Koga, Y.; Kawata, S.; Matsumoto, T., Cobalt(II) complexes bearing a bulky N-heterocyclic carbene for catalysis of Kumada–Tamao–Corriu cross-coupling reactions of aryl halides, *Eur. J. Inorg. Chem.,* 2012, **2012**, 3079–3086.
50. Herberich, G. E.; Fischer, A. Borylcyclopentadienides, *Organometallics,* 1996, **15**, 58-67.
51. (a) Schuster, O.; Yang, L.; Raubenheimer, H. G.; Albrecht, M. Beyond conventional N-heterocyclic carbenes: Abnormal, remote, and other classes of NHC ligands with reduced heteroatom stabilization, *Chem. Rev.,* 2009*,* **109**, 3445-3478. (b) Krüger, A.; Albrecht, M. Abnormal N-heterocyclic carbenes: More than just exceptionally strong donor ligands, *Aust. J. Chem.,* 2011, **62**, 1113-1117. (c) Vivancos, A.; Segarra, C.; Albrecht, M. Mesoionic and related less heteroatom-stabilized N-heterocyclic carbene complexes: Synthesis, catalysis and other applications, *Chem. Rev.,* 2018, **118***,* 9493-9586.
52. Lebel, H.; Janes, M. K.; Charette, A. B.; Nolan, S. P. Structure and reactivity of "unusual" N-heterocyclic carbene (NHC) palladium complexes synthesized from imidazolium salts, *J. Am. Chem. Soc.,* 2004, **126***,* 5046-5047.

53. Day, B. M.; Pal, K.; Pugh, T.; Tuck, J.; Layfield, R. A. Carbene rearrangements in three-coordinate N-heterocyclic carbene complexes of cobalt(II) bis(trimethylsilyl)amide, *Inorg. Chem.,* 2014**, 53**, 10578−10584.
54. Crabtree, R. H. Abnormal, mesoionic and remote N-heterocyclic carbene complexes, *Coord. Chem. Rev.,* 2013, **257***,* 755-766.
55. Kawamoto, T.; Takeda, K.; Nishiwaki, M.; Aridomi, T.; Konno, T. Square-planar $N_2S_2Ni^{II}$ complexes with an extended π-conjugated system, *Inorg. Chem.,* 2007, **46**, 4239-4247.
56. APEX software suite v 2010 Bruker AXS *Inc. Madison Wisconsin USA*, 2010.
57. Blessing, R. H.; An empirical correction for absorption anisotropy**,** *Acta Crystallogr.,* 1995, **A51**, 33–38.
58. Sheldrick, G. M., A short history of SHELX, *Acta Crystallogr.,* 2008, **A64**, 112–122.
59. Hubschle, C. B.; Sheldrick, G. M.; Dittrich, B., SHeLXLe: A Qt graphical user interface for SHELXL, *J. Appl. Crystallogr.,* 2011, **44**, 1281–1284.
60. Gaussian 16, Revision C.01 Frisch, M. J.; Trucks, G. W.; Schlegel, H. B.; Scuseria, G. E.; Robb, M. A.; Cheeseman, J. R.; Scalmani, G.; Barone, V.; Petersson, G. A.; Nakatsuji, H.; Li, X.; Caricato, M.; Marenich, A. V.; Blonio, J.; Janesko, B. G.; Gomperts, R.; Mennucci, B.; Hratchian, H. P.; Ortiz, J. V.; Izmaylov, A. F.; Sonnenberg, J. L.; WilliamsYoung, D.; Ding, F.; Lipparini, F.; Egidi, F.; Giongs, J.; Peng, B.; Petrona, A.; Henderson, T.; Ranasinghe, D.; Zakrzewski, V. G.; Gao, J.; Rega, N.; Zheng, G.; Liang, W.; Hada, M.; Ehara, M.; Toyota, K.; Fukuda, R.; , Hasegawa, J.; Ishida, M.; Nakajima, T.; Honda, Y.; Kitao, O.; Nakai, H.; Vreven, T.; Throssell, K.; Montgomery, J. A.; Peralta, Jr. J. E.; Ogliaro, F.; Bearpark, M. J.; Heyd, J. J.; Brothers, E. N.; Kudin, K. N.; Staroverov, V. N.; Keith, T. A.; Kobayashi, R.; Normand, J.; Raghavachari, K.; Rendell, A. P.; Burant, J. C.; Iyengar, S. S.; Tomasi, J.; Cossi, M.; Millam, J. M.; Klene, M.; Adamo, C.; Cammi, R.; Ochterski, J. W.; Martin, R. L.; Morokuma, K.; Farkas, O.; Foresman, J. B.; Fox, D. J., Gaussian*, Inc., Wallingford CT*, 2019.
61. Zhao, Y.; Truhlar, D. G., The M06 suite of density functionals for main group thermochemistry, thermochemical kinetics, noncovalent interactions, excited states, and transition elements: Two new functionals and systematic testing of four M06-class functionals and 12 other functionals. *Theor. Chem. Acc.,* 2008, **120**, 215–241.
62. Zhao, Y.; Truhler, D. G., A new local density functional for main-group thermochemistry, transition metal bonding, thermochemical kinetics, and noncovalent interactions*, J. Chem. Phys.,* 2006, **125**, 194101.
63. (a) Perdew, J. P.; Ernzerhof, M.; Bruke, K., Rationale for mixing exact exchange with density functional approximations, *J. Chem. Phys*., 1996, **105**, 9982-9985. (b) Adamo, C.; Barone, V. Toward reliable density functional methods without adjustable parameters: The PBE0 model, *J. Chem. Phys.,* 1999, **110**, 6158-6170.
64. (a) Becke, A. D., Density-functional thermochemistry. III. The role of exact exchange, *J. Chem. Phys.,* 1993, **98**, 5648–5652; (b) Lee, C.; Yang, W.; Parr, R. G., Development of the Colle-Salvetti correlation-energy formula into a functional of the electron density, *Phys. Rev.,* 1988, **37**, 785–789; (c) Vosko, S. H.; Wilk, L.; Nusair, M., Accurate spin-dependent electron liquid correlation energies for local spin density calculations: A critical analysis, *Can. J. Phys.,* 1980, **58**, 1200-1211. (d) Stephens, P. J.; Devlin, F. J.; Chabalowski, C. F.; Frisch, M. J., *Ab initio* calculation of vibrational absorption and circular dichroism spectra using density functional force fields, *J. Phys. Chem.,* 1994, **98**, 11623–11627.

65. (a) Tao, J.; Perdew, J. P.; Staroverov, V. N.; Scuseria, G. E., Climbing the density functional ladder: Nonempirical meta–generalized gradient approximation designed for molecules and solids, *Phys. Rev. Lett.,* 2003, **91**, 146401. (b) Staroverov, V. N.; Scuseria, G. E.; Tao, J.; Perdew, J. P., Comparative assessment of a new nonempirical density functional: Molecules and hydrogen-bonded complexes. *J. Chem. Phys.,* 2003, **119**, 12129-12137.
66. Grimme, S., Accurate calculation of the heats of formation for large main group compounds with spin-component scaled MP2 methods, *J. Phys. Chem.,* 2005, **109**, 3067-3077.
67. Explicit basis sets and references were found on https://www.basissetexchange.org/; (a) Pritchard, B. P.; Altarawy, D.; Didier, B.; Gibson, T. D.; Windus, T. L., New basis set exchange: An open, up-to-date resource for the molecular sciences community, *J. Chem. Inf. Model,* 2019, **59**, 4814-4820. (b) Feller, D., The role of databases in support of computational chemistry calculations, *J. Comput. Chem.,* 1996, **17**, 1571-1586. (c) Schuchardt, K. L.; Didier, B. T.; Elsethagen, T.; Sun, L.; Gurumoorthi, V.; Chase, J.; Li, J.; Windus, T. L., Basis set exchange: A community database for computational sciences, *J. Chem. Inf. Model,* 2007, **47**, 1045-1052.
68. Krishnan, R.; Binkley, J. S.; Seeger, R.; Pople, J. A., Self-consistent molecular orbital methods. XX. A basis set for correlated wave functions, *J. Chem. Phys.,* 1980, **72**, 650-654.
69. (a) McLean, A. D.; Chandler, G. S., Contracted Gaussian basis sets for molecular calculations. I. Second row atoms, *J. Chem. Phys.,* 1980, **72**, 5639-5648. (b) Francl, M. M.; Pietro, W. J.; Hehre, W. J.; Binkley, J. S.; Gordon, M. S.; DeFrees, D. J.; Pople, J. A. Self-consistent molecular orbital methods. XXIII. A polarization-type basis set for second-row elements, *J. Chem. Phys.,* 1982, **77**, 3654-3665. (c) Clark, T.; Chandrasekhar, J.; Spitznagel, G. W.; Schleyer, P. V. R., Efficient diffuse function-augmented basis sets for anion calculations. III. The 3-21+G basis set for first-row elements, Li–F, *J. Comput. Chem.,* 1983, **4**, 294-301. (d) Spitznagel, G. W.; Clark, T.; von Ragué Schleyer, P.; Hehre, W. J., An evaluation of the performance of diffuse function-augmented basis sets for second row elements, Na-Cl, *J. Comput. Chem.,* 1987, **8***,* 1109-1116.
70. Weigend, F.; Ahlrichs, R., Balanced basis sets of split valence, triple zeta valence and quadruple zeta valence quality for H to Rn: Design and assessment of accuracy. *Phys. Chem. Chem. Phys.,* 2005, **7**, 3297-3305.
71. Barone, V.; Cossi, M., Quantum calculation of molecular energies and energy gradients in solution by a conductor solvent model, *J. Phys. Chem.,* 1998, **102**, 1995-2001.
72. Grimme, S.; Ehrlich, S.; Goerigk, L., Effect of the damping function in dispersion corrected density functional theory, *J. Comput. Chem.,* 2011, **32**, 1456-1465.
73. Rappoport, D.; Furche, F., Property-optimized Gaussian basis sets for molecular response calculations, *J. Chem. Phys.,* 2010, **133**, 134105.

Chapter Three: Tetracopper(I) Thiolate- and Amido-(SNS) Complexes as Catalysts for Base-Free, Aqueous Azide-Alkyne Cycloaddition

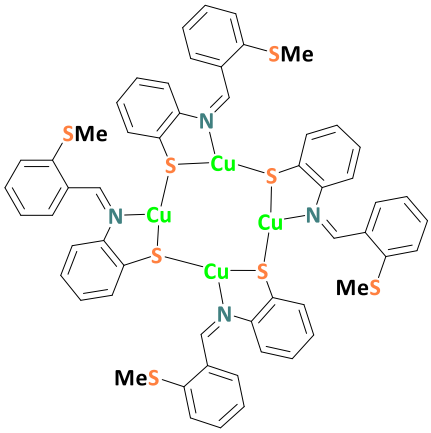

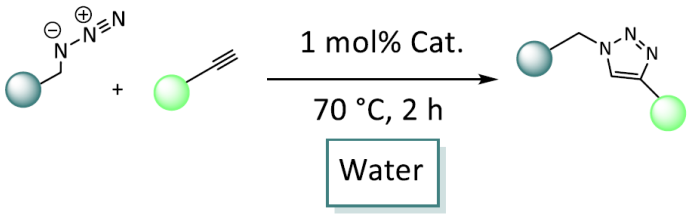

3.1 Contribution to Knowledge

Tetracopper(I) Thiolate- and Amido-(SNS) Complexes and Copper-Catalyzed Azide-Alkyne Cycloaddition in Water. Atousa Khanzadeh, Saeed Ataie, R. Tom Baker, *Dalton Trans*. 2023, **52**, 11768-11772.

Author contributions

Atousa performed all the catalysis experiments and DFT studies, collected the NMR spectra and analyzed the data with Prof. Baker's supervision. Saeed was responsible for some synthesis, crystal growth and X-ray diffraction studies. Atousa and Prof. Baker wrote the manuscript.

Abstract: Two tetranuclear Cu(I) complexes bearing thiolate- and amido-SNS ligands were characterized by X-ray diffraction and mass spectrometry. Although the amido ligand undergoes irreversible N-protonation by the copper-bound alkyne, the thiolate complex demonstrates good activity in the copper-catalyzed azide−alkyne cycloaddition reaction with a variety of substrates. The base-free reactions are performed in water and afford excellent yields over 2 h at 70 °C. DFT calculations suggest a proton-shuttle role for the thiolate donor in formation of the initial dicopper σ,π-alkynyl intermediate.

3.2 Introduction

In the preceding two chapters, we delved into the bifunctional properties of amido- and thiolate-SNS ligands, highlighting their pivotal role in cooperative metal-ligand catalysis. Specifically, we explored their efficacy in activating E-H bonds, a phenomenon evident in reactions like hydroboration[1-5] and hydrosilylation,[6] which enable the transformation of a diverse range of unsaturated bonds (carbonyls,[1,3-5] nitriles[7,8] and N-heterocycles[9]). In these investigations the Baker group has been comparing 'soft' thiolate- (**L1**) and 'hard' amido- (**L2**) SNS ligands in ligand-assisted catalysis.[10,11] These endeavors have illuminated pathways to access a rich array of organic compounds. Nevertheless, the potential of these ligands in catalysis extends beyond their role in these transformations, remaining largely unexplored in other catalytic domains. In the ensuing chapter, we embark on a journey to broaden the horizons of these ligands. Our aim is to extend their applications by investigating the catalytic capabilities of multinuclear copper(I) complexes incorporating thiolate- and amido-SNS ligands in the context of copper-catalyzed azide-alkyne cycloaddition click reactions.

Over the past two decades, click chemistry,[12] as a simple molecular attachment strategy and atom economic route, has attracted the attention of researchers in chemistry,[13] biology[14] and materials science.[15] The copper(I)-catalysed reaction of terminal alkynes and organic azides to give 1,4 disubstituted 1,2,3-triazoles is among the best Click reactions known to date.[16-18] The triazole products of this reaction have various applications in different area such as pharmaceuticals and other bioactive molecules,[13,14] nanomaterials[19] and numerous useful compounds. As a result, copper-catalysed azide-alkyne cycloaddition (CuAAC) has become a powerful tool in synthetic chemistry. Previous mechanistic studies have identified Cu(I) species as the active CuAAC catalyst. The unique catalytic function of Cu(I) can be explained by its ability to engage terminal alkynes in π- interactions and promote the deprotonation to Cu-alkynyl, accompanied by ancillary ligand exchange, especially in aqueous solution.[20] Therefore, introducing a stabilizing ligand to support copper in the required oxidation state should enhance its catalyst performance. CuAAC reports include the use of different sources of copper catalyst ranging from elemental copper[21] to *in situ* formation of Cu(I) species from a combination of readily available, air-stable copper(II) sulfate or acetate with ascorbate as a mild reductant,[16] to Cu(I) halides with heteroatom-based donor ligands,[22] and even metal-organic complexes.[23]

Several experimental and computational studies have investigated the mechanism of CuAAC.[24,25] In kinetic studies, Fokin and co-workers found a second order rate dependence on the catalyst concentration.[24] Subsequent DFT calculations identified low energy pathways involving active participation of two copper atoms as depicted in **Scheme 3.1**.[25] Further support for this mechanism was provided by the isolation and characterization of dicopper σ,π- alkynyl intermediates.[25,26]

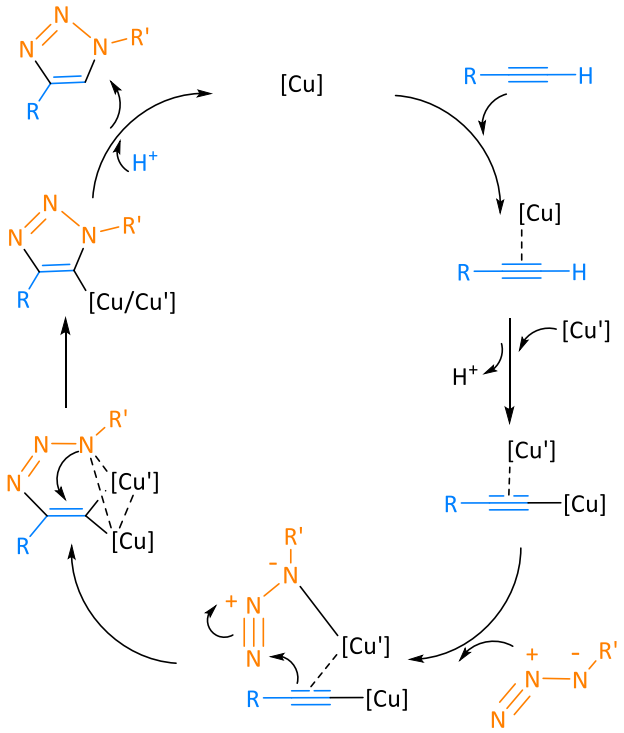

Scheme 3.1 Proposed mechanism for CuAAC reaction

In this chapter we compare the catalyst reactivity of copper(I) thiolate- and amido-SNS complexes in CuAAC click reaction in order to expand the catalytic application of these coordination complexes.

3.3 Results and Discussion

Herein we introduce two new tetranuclear complexes in which copper is coordinated to a thiolate- (**3.1**) or amido-SNS ligand (**3.2**) (**Schemes 3.2** and **3.3**). Moreover, we show that **3.1** is an effective catalyst for CuAAC in water without added base. We used DFT calculations to examine the possibility of a bifunctional role for the thiolate donor in forming the dicopper σ,π-alkynyl intermediate, the first step of the catalytic cycle.[20] Both complexes were synthesized by reaction of the deprotonated proligand and CuCl in a 1:1 ratio in dry THF under nitrogen (**Schemes 3.2** and **3.3**). The copper-thiolate complex (**3.2**) has a very low solubility and was simply filtered from the reaction mixture, washed with THF to remove the salt, dried under vacuum, and collected as a black powder in 97% yield. The copper-amido complex (**3.2**) is soluble in THF so the solvent was removed, the residue extracted with dichloromethane, filtered to remove the salt, evaporated in vacuum, and the solid washed with hexane and dried under vacuum (83% yield). Both complexes were characterized using ESI-MS (**Figures 3.7, 3.8**) and single-crystal X-ray crystallography. Complex **3.2** was also characterized by solution NMR (**Figure 3.8**) and insoluble **3.1** by solid-state $^{13}C\{^{1}H\}$ NMR (**Figure 3.7**). Complex **3.1** consists of a tetrahedral array of four pyramidal three-coordinate Cu centers (Cu is 0.19 Å out of the NS_2 plane) each with a κ^2-SNS^{Me} ligand in which the thiolate donor bridges to a second Cu. The

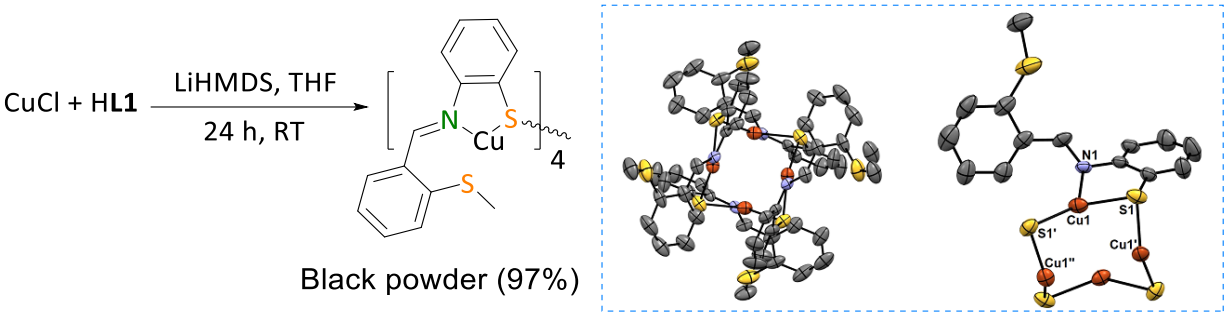

Scheme 3.2 Synthesis and molecular structure of Cu thiolate complex **3.1**. In the molecular structure at right only one SNS ligand is shown in full with the rest omitted to highlight the Cu_4S_4 core. Selected bond distances (Å) and angles (deg): Cu1-N1 2.08(1), Cu1-S1 2.247(5), Cu1-S13 2.181(5), S1-Cu1-N1 88.3(3), S1-Cu1-S13 140.1(2), S13-Cu1-N1 128.9(4), Cu1-S1-Cu12 = Cu1-S13-Cu13 82.6(2).

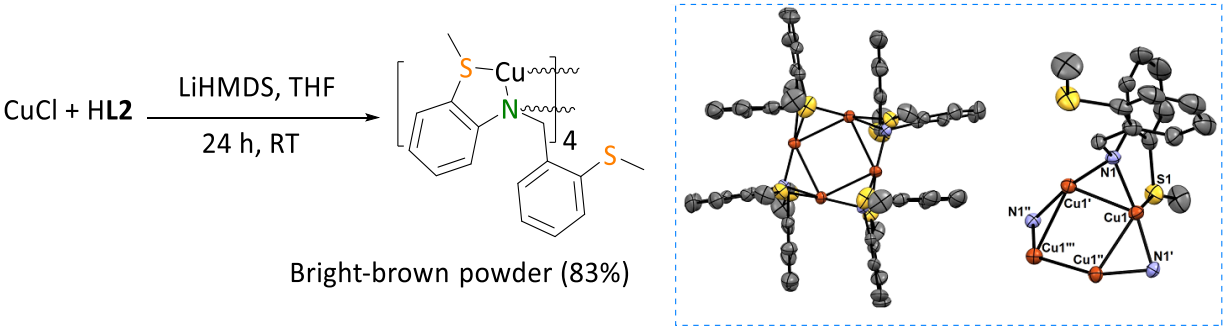

Scheme 3.3 Synthesis and molecular structure of Cu amido complex **3.2**. In the molecular structure at right only one SNS ligand is shown in full with the rest omitted to highlight the Cu_4N_4 core. Selected bond distances (Å) and angles (deg): Cu1-N1 1.934(3), Cu1-S1 2.535(1), Cu1-N12 1.953(3), Cu1-Cu11 2.5666(6), Cu1-N1-Cu11 82.7(1), S1-Cu1-N1 79.58(9), S1-Cu1-N12 110.71(9), N1-Cu1-N12 169.3(1).

thiolate bridges are unsymmetrical [cf. Cu1-S1 = 2.247(5) and Cu1-S1[2] = 2.181(5) Å]. In contrast, **3.2** consists of a planar array of four T-shaped three-coordinate Cu(I) centers [N-Cu-N = 169.3(1) °] each with a κ^2-$S^{Me}NS^{Me}$ ligand in which the amido donor bridges to the adjacent Cu. In this case the amido bridges are more symmetrical [cf. Cu1-N1 = 1.934(3) and Cu1-N-1' = 1.953(3) Å]. For **3.1** the ESI-MS displayed both dimer and monomer cations, whereas only the monomer was observed for **3.2**. The two copper tetramers were then assessed as catalysts for the azide-alkyne cycloaddition reaction.

Conditions were optimized using the model reaction of phenylacetylene and benzyl azide (formed *in-situ* from reaction of benzyl chloride and NaN_3) in a 1:1 ratio at 70°C over 24 h (**Table 3.1**). The reaction yielded no triazole product in the absence of catalyst (entry 1) and 21% yield using unligated CuCl in water (entry 2). A similar yield (23%; entry 4) was obtained using complex **3.2** in water while dry DMF gave an even poorer result (7.5%; entry 3). The poor catalyst activity of **3.2** was not surprising as the basic amido nitrogen will be protonated in water and previous results showed the resulting SNS amine (**HL2**) to be a poor ligand for Cu.[10] Monitoring the reaction in dry DMF also showed formation of **HL2** (**Figure 3.1**), suggesting the acidity of the Cu-coordinated terminal alkyne is sufficient to irreversibly protonate the amido nitrogen. On the other hand, complex **3.1** provided the triazole product (**3.3**) in excellent yields. Of the seven solvents tested, DMF and water gave the

best yields (99%) so the latter was chosen for further optimization due to being a green solvent. Reducing the catalyst loading to 1 mol% still gave a high yield (90%) but reducing the temperature to 60 °C had a negative impact (80%). The time course experiment also confirmed that the reaction proceeds to completion within a span of 2 h. With optimized conditions in hand, we next examined the scope of both azide and alkyne coupling partners (**Table 3.2**). The catalytic reaction was effective for aliphatic alkynes (entries 8,9) or aromatic analogues with electron-donating (entries 4,7,10) and electron-withdrawing (entries 5,6) groups in different positions (ortho and para). The reaction also afforded the 1,4-disubstituted triazole product with reasonable yield when using organoazides with electron-donating (entries 12-15) and electron-withdrawing (entry 15) substrates. Changing the halide from chloride to bromide (entry 11) reduced the yield from 99% to 59%.

Table 3.1 Optimization table for CuAAC reaction using **3.1** and **3.2**.

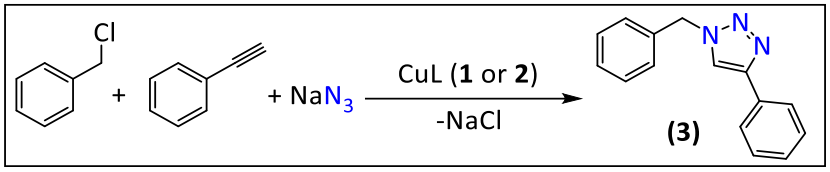

Entry	Complex	Cat. (mol%)	Solvent	Time (h)	Temp. (°C)	Yield (%)*
1	-	-	H_2O	24	70	-
2	CuCl		H_2O	24	70	21
3	**3.2**	5	dry-DMF	24	70	26
4	**3.2**	5	H_2O	48	70	23
5	**3.1**	5	THF	24	70	29
6	**3.1**	5	DMF	24	70	99
7	**3.1**	5	DMSO	24	70	87
8	**3.1**	5	EtOH	24	70	84
9	**3.1**	5	DCE	24	70	31
10	**3.1**	5	C_6D_6	24	70	16
11	**3.1**	5	H_2O	24	70	99
12	**3.1**	4	H_2O	24	70	94
13	**3.1**	3	H_2O	24	70	92
14	**3.1**	1	H_2O	24	70	90
15	**3.1**	3	H_2O	24	60	83
16	**3.1**	3	H_2O	24	50	75
17	**3.1**	3	H_2O	24	40	71
18	**3.1**	3	H_2O	24	RT	69
19	**3.1**	3	H_2O	15	70	97
20	**3.1**	3	H_2O	4	70	99
21	**3.1**	3	H_2O	2	70	99
22	**3.1**	3	H_2O	1	70	91

*Reaction conditions: phenylacetylene (0.5 mmol), benzyl chloride (0.5 mmol), sodium azide (0.5 mmol), and 4 mL of H_2O. Isolated yields.

The reaction also worked well for synthesis of anti-cancer triazole drug **3.16**.[27] This product was isolated in 99% and 87% yield after 2 h at 70 °C using 1.0 and 0.5 mol% catalyst loading, respectively, as characterized by ^{1}H and ^{13}C NMR spectroscopy (**Figure 3.22 and 3.23**). Finally, product

3.3 was scaled up to 23 mmol using 1 mol% **3.1** under the same conditions (90% yield). The used catalyst was then isolated and further characterized.

Catalyst **3.1** is poorly soluble in most solvents, but its dark colour evolves during catalysis to a light green solid (see UV/Vis in **Figure 3.3**) that dissolves to a limited extend in dimethyl sulfoxide. The ^{1}H NMR spectrum shows that the thiolate **L1** ligand is retained (imine C-H at d 8.59 and SMe at d 1.19; **Figure 3.4**). The ESI-mass spectrum, however, also indicated formation of the copper(II) bis(thiolate) complex (**Figure 3.5**) as confirmed by EPR spectroscopy (**Figure 3.6**). Nonetheless, the catalyst could be reused to give **3** in 90% yield under the same conditions as **Table 3.2**. While the

Table 3.2 Substrate scope table for CuAAC reaction under optimized conditions.

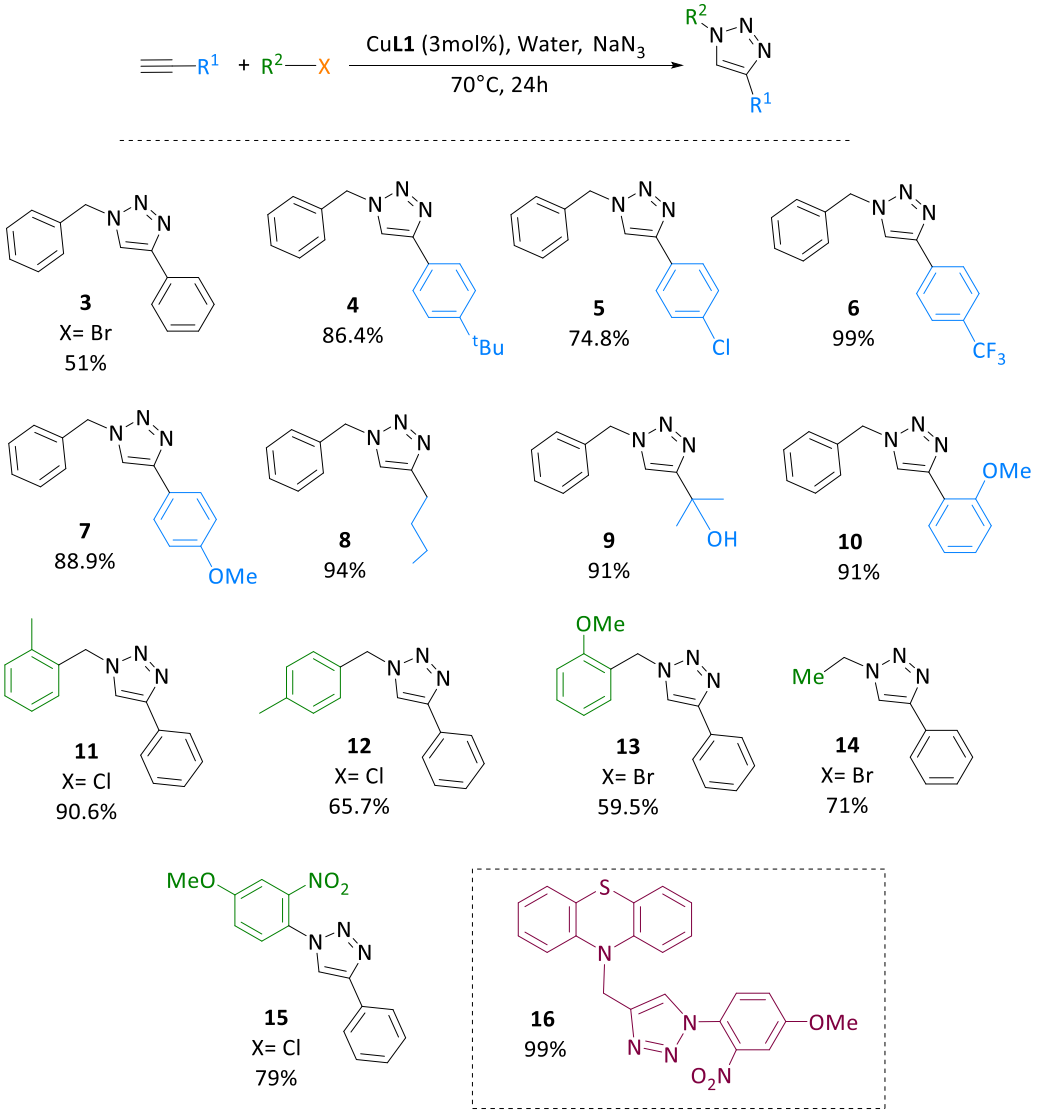

presence of Cu(II) species may explain the reduced activity of the catalyst, it is important to note that the product yield remains reasonably high. The high activity of the used catalyst suggests the rate of

conversion to Cu(II) is relatively low, and that Cu(I) serves as the primary active catalyst. Although there is not universal agreement as to whether metallacycle formation or alkyne deprotonation is the turnover-limiting step in CuAAC,[28-31] formation of the copper-alkynyl intermediate plays a crucial role in the mechanism.

As mentioned above, the thiolate SNS ligand has demonstrated ligand-assistance in several catalyzed reactions.[18-21] Although other base-free azide-alkyne cycloadditions in water have been reported,[32] we speculated that the thiolate donor may play a proton-shuttle role in converting the π-coordinated alkyne to the Cu alkynyl intermediate. To assess this possibility, we used DFT calculations[33] to probe potential low-energy intermediates. Evaluation of the stability (ΔG) of several different potential intermediates in copper alkynyl formation identified one low-energy dinuclear intermediate in which the proton of the π-bound alkyne is transferred to the thiolate (vs. water to form H_3O^+); (see section **3.9** for details; **Scheme 3.4**).

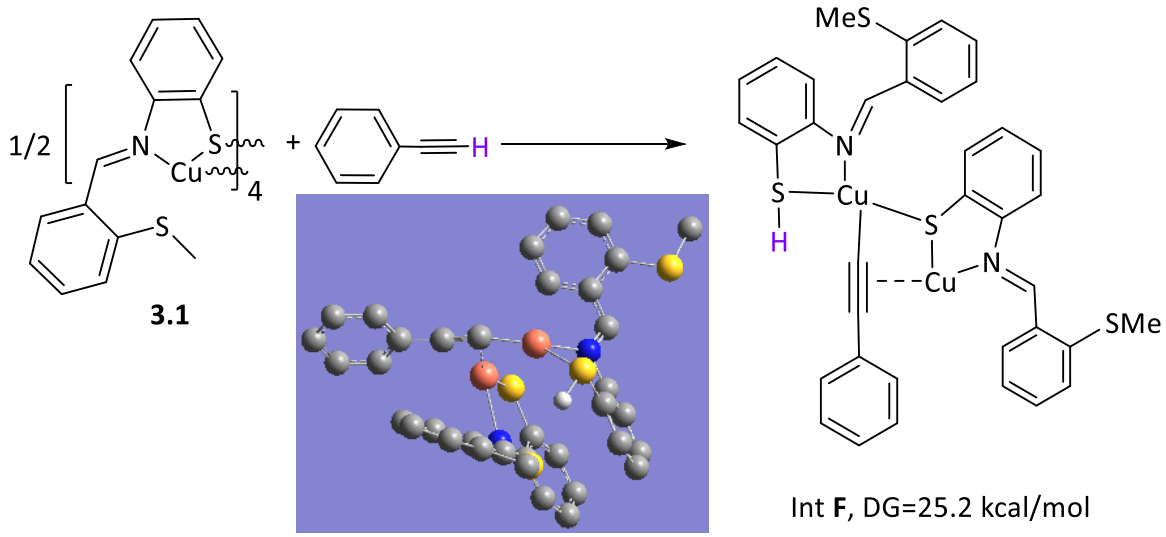

Scheme 3.4 Most thermodynamically favorable intermediate for the first step of the catalytic cycle.

3.4 Experimental Section

3.4.1 General considerations

Synthesis of the complexes (**3.1** and **3.2**) were carried out under dinitrogen, using an MBraun glovebox and stored in the glovebox. THF, DCM and hexane were dried on columns of activated alumina using a J. C. Meyer (formerly Glass Contour) solvent purification system. Anhydrous C_6D_6 were dried with activated alumina (ca. 10 wt %) overnight, followed by filtration. SNS ligands synthesized in the lab based on previous publications in our group.[10,11] All substrates were purchased from commercial suppliers. ^1H and ^{13}C NMR spectra were recorded on a 300 MHz Bruker Avance or Avance II instrument. Solid state ^{13}C NMR spectra recorded as the low solubility of the **3.1** on the Bruker 200 Avance III. For characterization of compound **3.15** the DEPT 135, HSQC and HMBC NMR spectra

recorded on the 300 MHz Bruker Avance II instrument. ^{1}H NMR spectra were referenced respectively to solvent residual protons (C_6D_6, δ 7.15; $CDCl_3$, δ 7.26) and all the NMR spectra recorded at room temperature (21−25 °C). Mass spectra were recorded on an AB Sciex Q1MS mass spectrometer with electrospray ionization (ESIMS) in positive mode (ion spray voltage, 5000.0 V; TEM, 400 °C; declustering potential, 11.00 V; focusing potential, 300.0 V) with samples prepared to ca. 0.05 mg/mL in acetonitrile or dichloromethane. For electron impact (EI), solid samples were prepared by drying products under vacuum, and spectra obtained using a Kratos Concept S1 instrument (Hres 7000−10000). X-ray diffraction data were collected on a Bruker Smart or Kappa diffractometer equipped with an ApexII CCD detector and a sealed-tube Mo K source (λ= 0.71073 Å). EPR spectra recorded on a Bruker EMX plus 10/12 X-band spectrometer at room temperature.

3.4.2 Synthesis of $(CuL1)_4$

A vial was charged with 200 mg H**L1** (0.77 mmol) and 129 mg of LiHMDS (0.77 mmol) in 5 mL of THF and the mixture was stirred for 15 min. In a second vial 76 mg of CuCl (0.77 mmol) was dissolved in 5 mL of THF and the mixture from the first vial was added dropwise with stirring. After stirring the resulting mixture for 24 h at room temperature, complex **3.1** was collected by filtration, washed two times with 5 mL of THF and dried under vacuum to give a dark powder (240 mg, 97% yield). $^{13}C\{^{1}H\}$ MAS NMR (50 MHz): 115-163 (aromatic) 15.5-19.5 ppm (S-Me), ESI-MS: $[(Cu\mathbf{L1})_2H^+]$ 642.9457, Calcd. 642.9492 and $[(Cu\mathbf{L1})H]^+$ 321.9736 Calcd 321.98 (**Figure 3.5**).

3.4.3 Synthesis of $(CuL2)_4$

A vial was charged with 200 mg H**L2** (0.727 mmol) and 121 mg of LiHMDS (0.727 mmol) in 5 mL of THF and the mixture was stirred for 30 min. In a second vial 71 mg of CuCl (0.727 mmol) was dissolved in 5 mL of THF and the mixture from the first vial was added dropwise with stirring. After stirring the resulting mixture for 24 h the solvent was removed in vacuo. The residue was extracted with 5 mL of DCM, filtered and evaporated under vacuum to give a light brown powder (203 mg, 83% yield). ^{1}H NMR (300 MHz, C_6D_6): δ 7.45 (d, 1H, aromatic), 7.20 (d, 1H, aromatic), 6.96 (t, 3H, aromatic), 6.87 (t, 1H, aromatic), 6.56 (t, 1H, aromatic), 6.49 (d, 1H, aromatic), 4.26 (d, 2H, N-CH2), 1.97 (s, 3H, S-CH3) 1.93 (s, 3H, S-CH3). ESI-MS: $[(Cu\mathbf{L2})H]^+$ 338.0061, Calcd. 338.0098 (**Figure 3.6**).

3.4.4 Catalysis protocol, general procedure for CuAAC reaction catalyzed by complex 3.1

A 15 mL vial was charged with 1-5 mol% **3.1** or **3.2** in the glovebox. The vial was then taken out and the organohalide substrate (0.5 mmol), NaN_3 (0.5 mmol), terminal alkyne substrate (0.5 mmol) and 4 ml of distilled water were added to the vial along with a small stir bar. The vial was then left to stir at the desired temperature from 1-24 h. The resulting product was then isolated by extracting three times with 4 mL of ethyl acetate. The extract was evaporated under vacuum and the collected triazole product was dried and weighed to calculate the yield. ^{1}H NMR spectra were then recorded to characterize the known triazole products.

3.4.5 Mechanistic studies

3.4.5.1 Catalysis using copper amido complex $(CuL2)_4$

After the catalytic run using complex **3.2** in dry DMF, the solvent was removed, the residue dissolved in 0.5 mL of $CDCl_3$ and the ^1H NMR spectrum recorded (**Figure 3.1**).
In another experiment, 4 equiv. of water were added to a solution of complex **3.2** in C_6D_6. The ^1H NMR spectrum is compared with that of **3.2** in **Figure 3.2**.

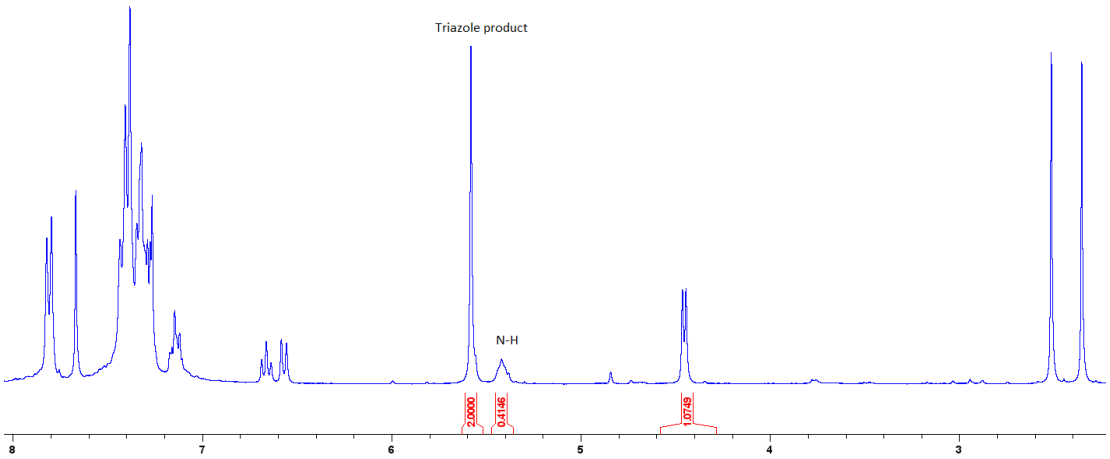

Figure 3.1 ^1H NMR spectrum (300 MZ, D_2O) of CuAAC reaction using complex **3.2** resulting in 7.5% yield of the triazole product and formation of protonated amido-SNS ligand (**L2**).

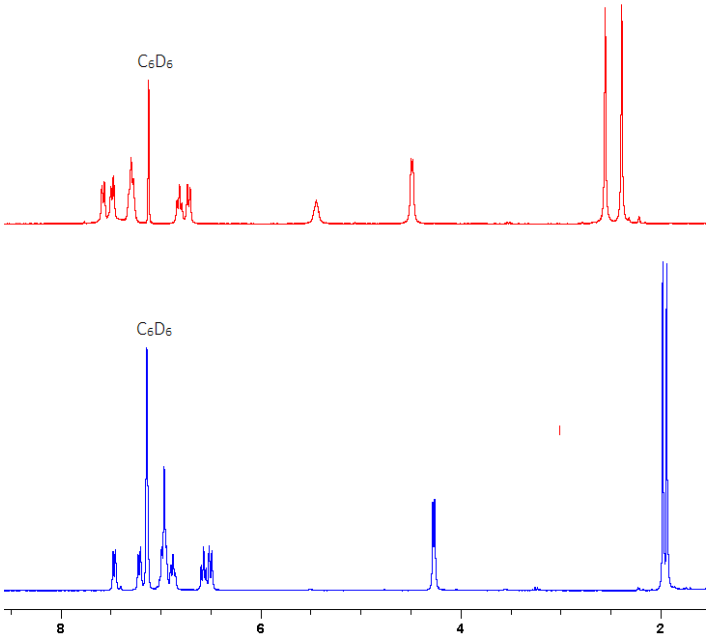

Figure 3.2 ^1H NMR spectrum of **3.2** before (bottom) and after (top) adding water.

3.4.5.2 Catalysis using copper thiolate complex $(CuL1)_4$

Using the above catalysis protocol, one reaction on a higher scale (23 mmol benzyl chloride, 23 mmol sodium azide and 21.9 mmol of phenylacetylene) with 1 mol% of complex **3.1** was conducted. After extraction of the product, the insoluble used catalyst was dried and characterized by UV/Vis (**Figure 3.3**), ^{1}H NMR (**Figure 3.4),** ESI-MS (**Figure 3.5**), and EPR spectroscopy (**Figure 3.6**). In another experiment, the used catalyst was filtered off, dried and then reused in the same protocol to give the triazole product **3.16** in 90% yield.

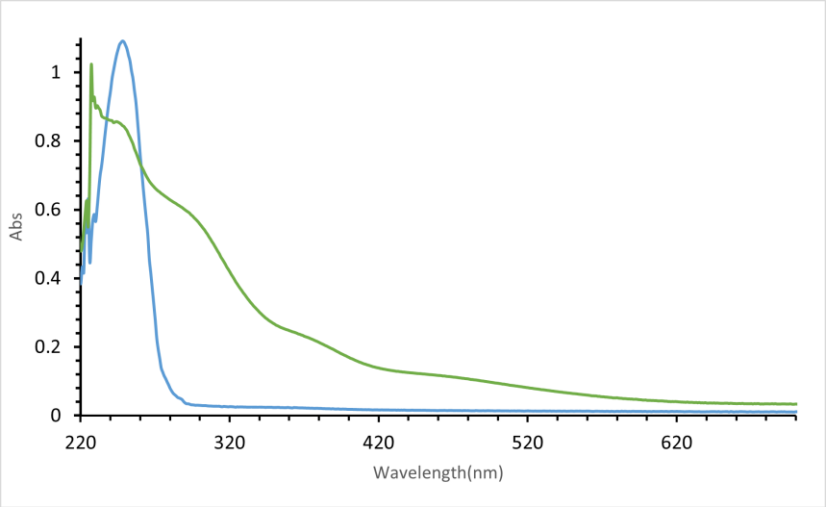

Figure 3.3 UV-Vis spectra comparison of the initial catalyst **3.1** (blue) and the used catalyst (green).

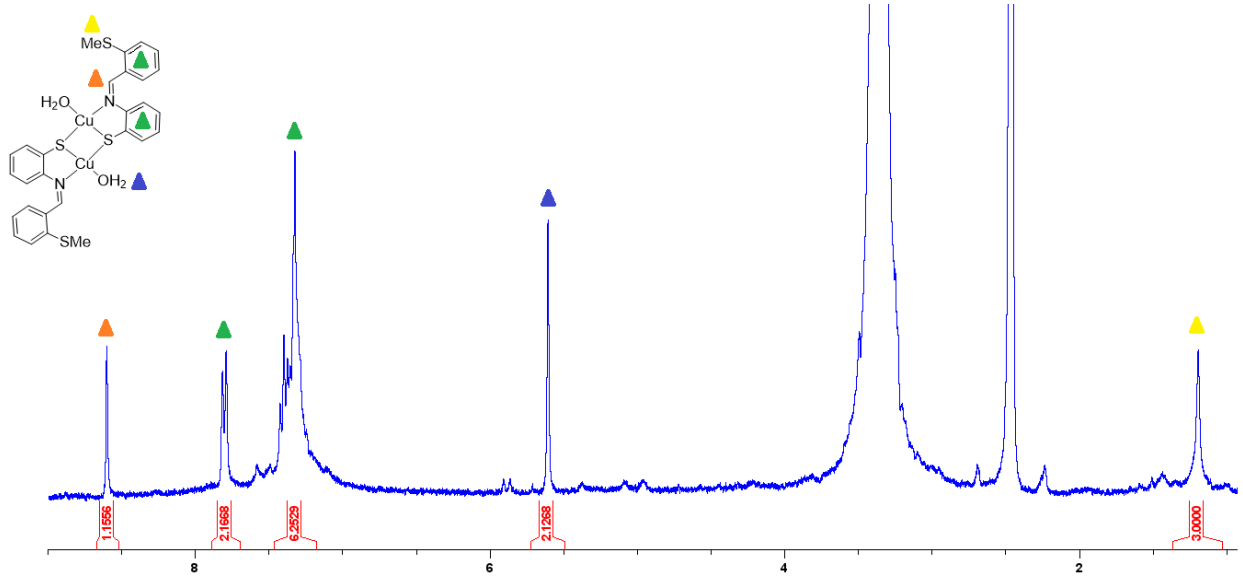

Figure 3.4 ^{1}H NMR spectrum of the used catalyst from **3.1**-catalysed CuAAC. The singlet peak at δ 8.59 is due to the ligand imine hydrogen which shows that the ligand is still coordinated to a copper(I) center.

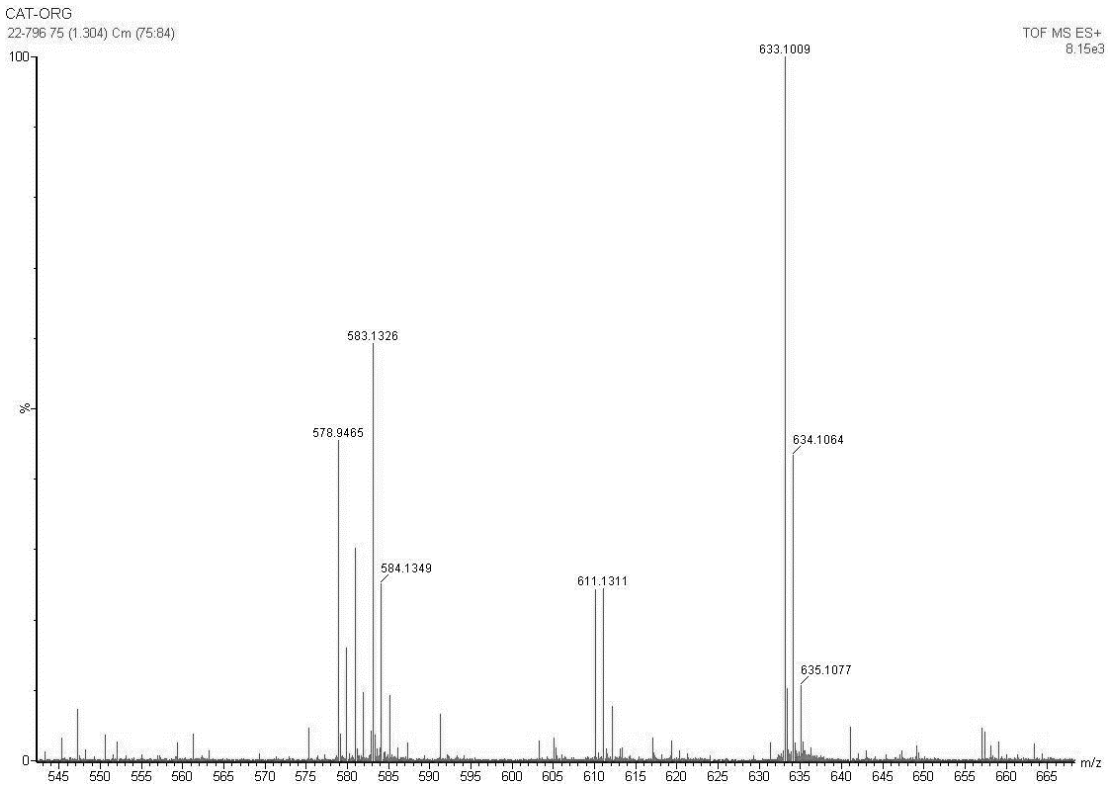

Figure 3.5 ESI-mass spectrum of recovered catalyst from **3.1**-catalysed CuAAC showing $[Cu(\mathbf{L1})_2H]^+$ (Calcd 579.01, found 578.9465) and accumulation of the thiolate ligand (peaks at 583.1 and 633.1).

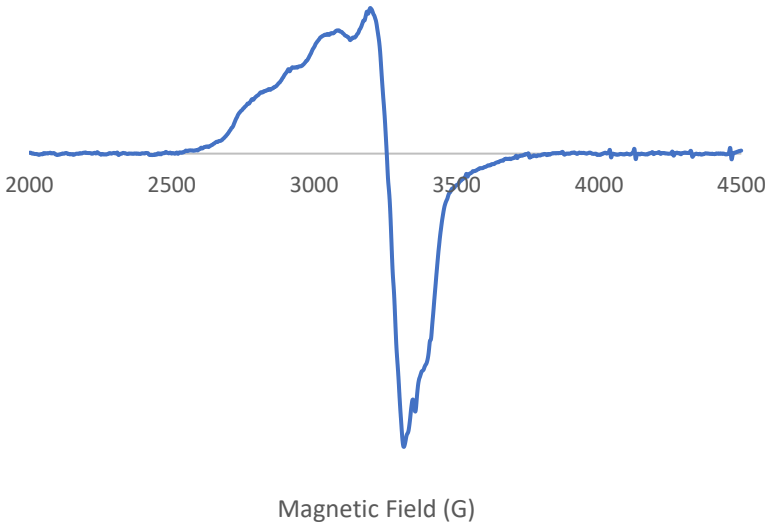

Figure 3.6 EPR spectrum of the solid catalyst at room temperature [gx, gy=g⊥= 2.061, gz=g‖= 2.324, A(Cu) = 101.7G].

3.5 Conclusion

In summary, this study has shed light on the remarkable bifunctional activity of the SNS ligand system, pioneered by the Baker group. Over the past decade, their investigations into the catalytic and mechanistic aspects of these ligands have showcased their efficacy in activation of E-H bonds during hydroboration and hydrosilylation reactions involving aldehydes, ketones, and nitriles. Building on this foundation, we have further extended the catalytic capabilities of SNS complexes in the context of valuable click reactions.

Our investigation focused on two tetranuclear copper(I) complexes, one featuring amido ligands and the other incorporating thiolate ligands. These complexes were examined as catalysts for the CuAAC reaction. In contrast to the amido complex, which exhibited high amido-N basicity leading to ligand protonation and dissociation, the thiolate complex displayed exceptional reactivity in a base-free, aqueous CuAAC environment.

The unique attributes of the thiolate ligand, characterized by its moderate basicity, enabled it to potentially serve as a proton-shuttle during the alkyne-to-alkynyl conversion. Furthermore, the insolubility of the thiolate catalyst allowed for its reuse with consistent results. However, the detection of the Cu(II) bis(thiolate) complex during the reaction indicated structural rearrangement accompanied by copper oxidation, suggesting potential long-term stability challenges for this catalyst.

This work not only underscores the diverse applications of SNS ligands but also highlights the pivotal role of ligand choice in governing the outcome of catalytic reactions. The SNS ligand system's ability to facilitate E-H bond activation, as demonstrated in previous studies, extends to the efficient synthesis of valuable triazole products through CuAAC. Moreover, the ability to perform these transformations in a base-free, aqueous environment represents a significant advancement in green chemistry practices, allowing for the rapid and sustainable production of triazole compounds.

In conclusion, our research provides valuable insights into the bifunctional activity of the SNS ligand system and its role in catalysis. While the thiolate complex demonstrates promising catalytic performance in CuAAC reactions, the challenge of long-term stability remains a subject for further investigation. This study opens new avenues for the development of SNS-ligated catalysts and green synthetic methodologies, contributing to the broader field of organic chemistry and catalysis.

3.6 Appendix

3.6.1 Spectroscopic data

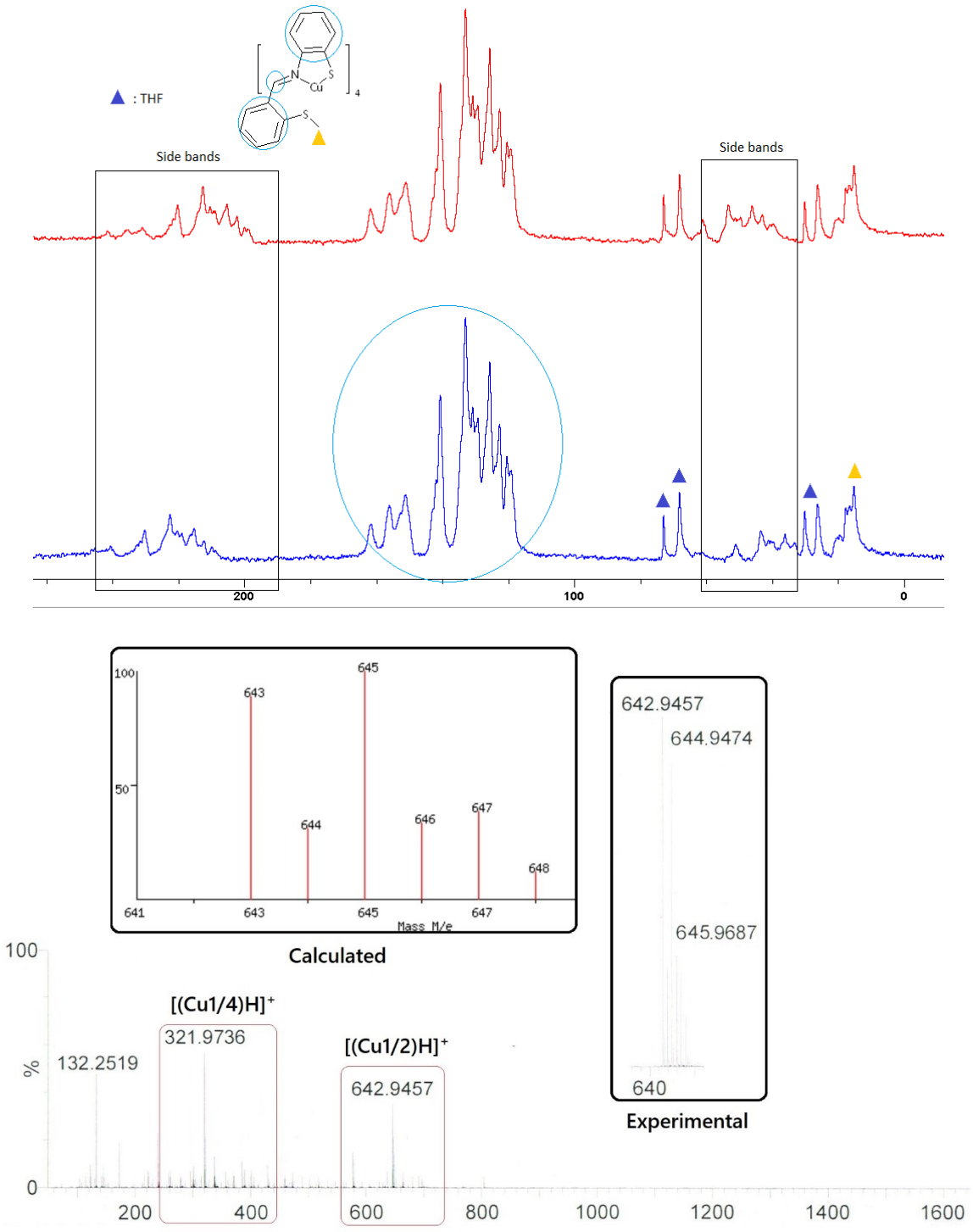

Figure A3.1 $^{13}C\{^{1}H\}$ MAS NMR spectrum (50MHz, solid) of complex **3.1** (top)[34]. ESI-mass spectrum of **3.1** (bottom) showing monomer $[(Cu\mathbf{L1})H]^+$ (Calcd 321.98, found 321.9736) and dimer $[(Cu\mathbf{L1})_2H]^+$ (Calcd 642.95, found 642.9492).

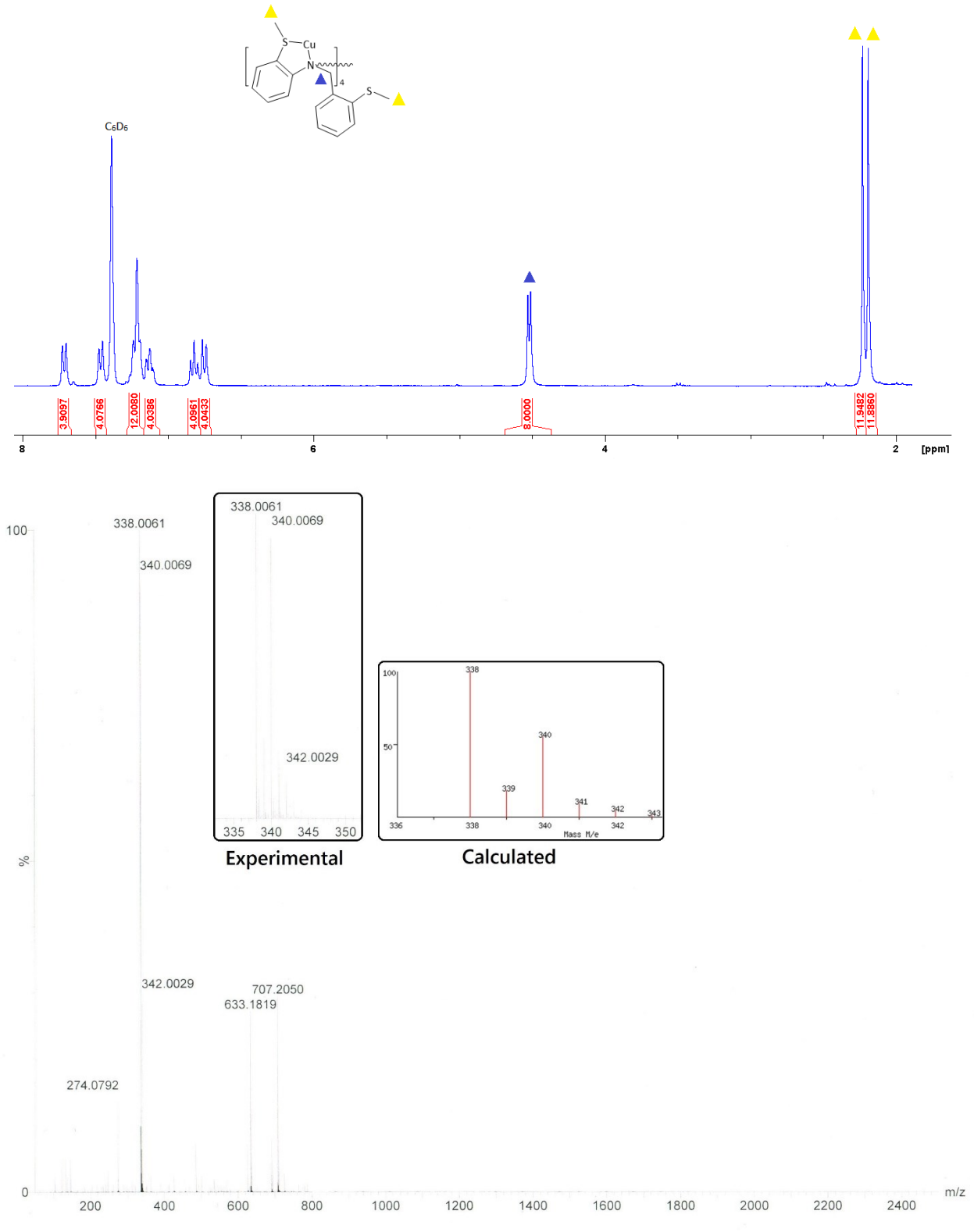

Figure A3.2 ^{1}H NMR spectrum of **3.2** (top). ESI-mass spectrum of **3.2** (bottom) showing monomer [Cu**L2**]$^{+}$ (Calcd 338.0098, found 338.0061).

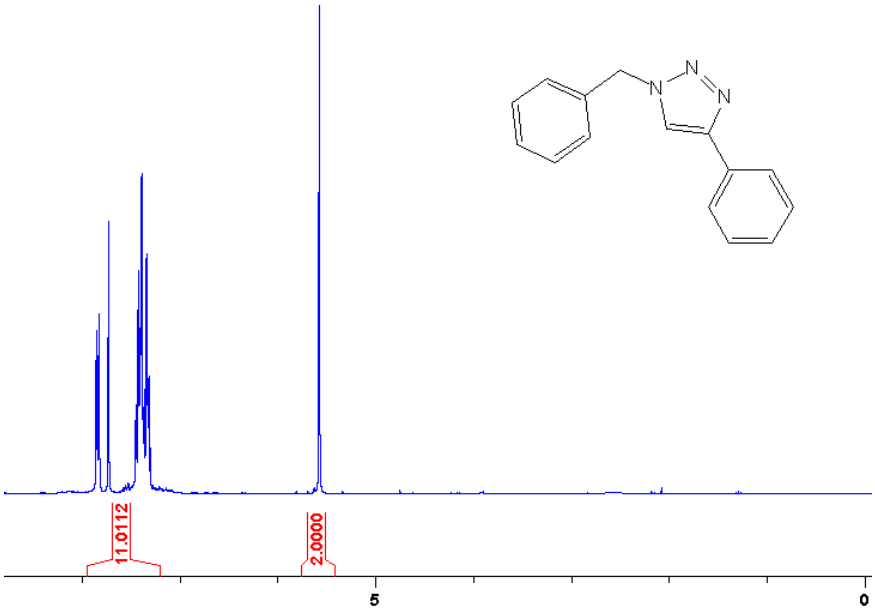

Figure A3.3 ^{1}H NMR spectrum of triazole product **3.3** from the catalytic reaction in $CDCl_3$.

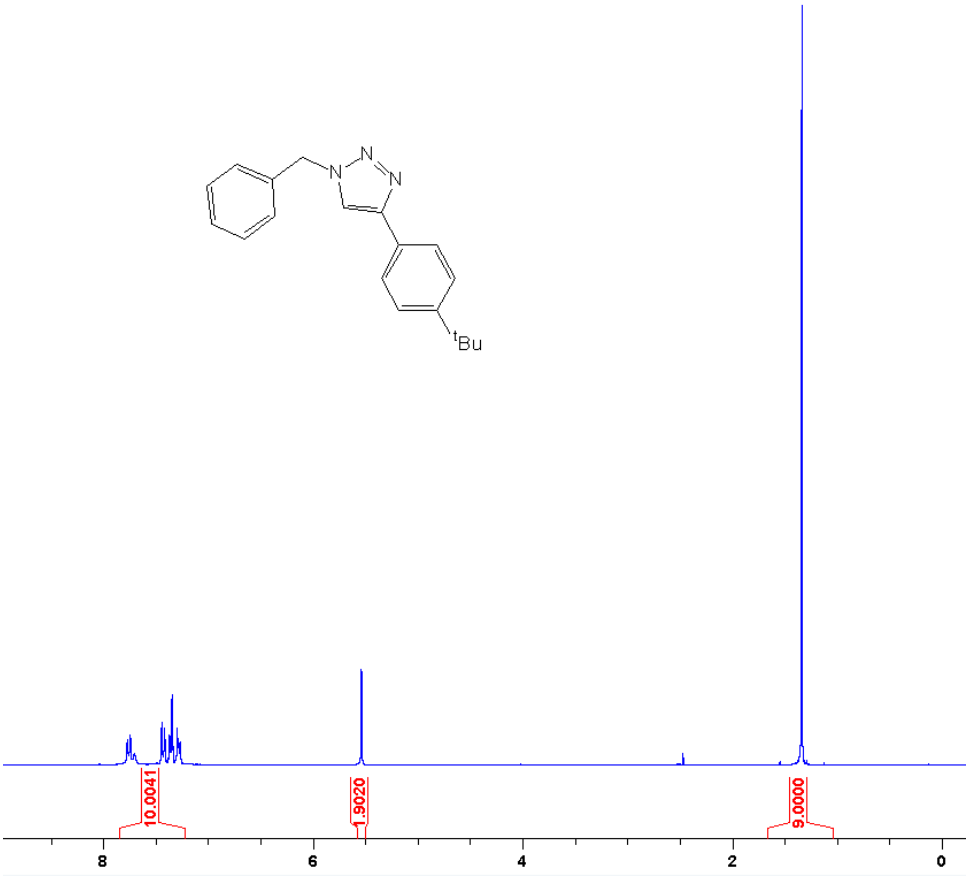

Figure A3.4 ^{1}H NMR spectrum of triazole product **3.4** from the catalytic reaction in $CDCl_3$.

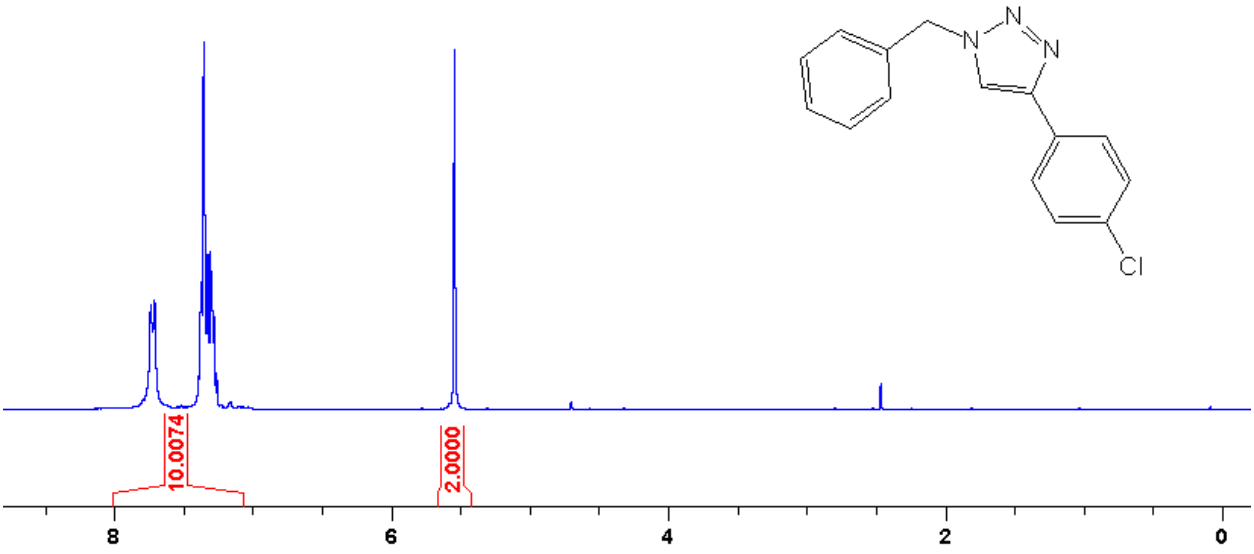

Figure A3.5 ^{1}H NMR spectrum of triazole product **3.5** from the catalytic reaction in $CDCl_3$.

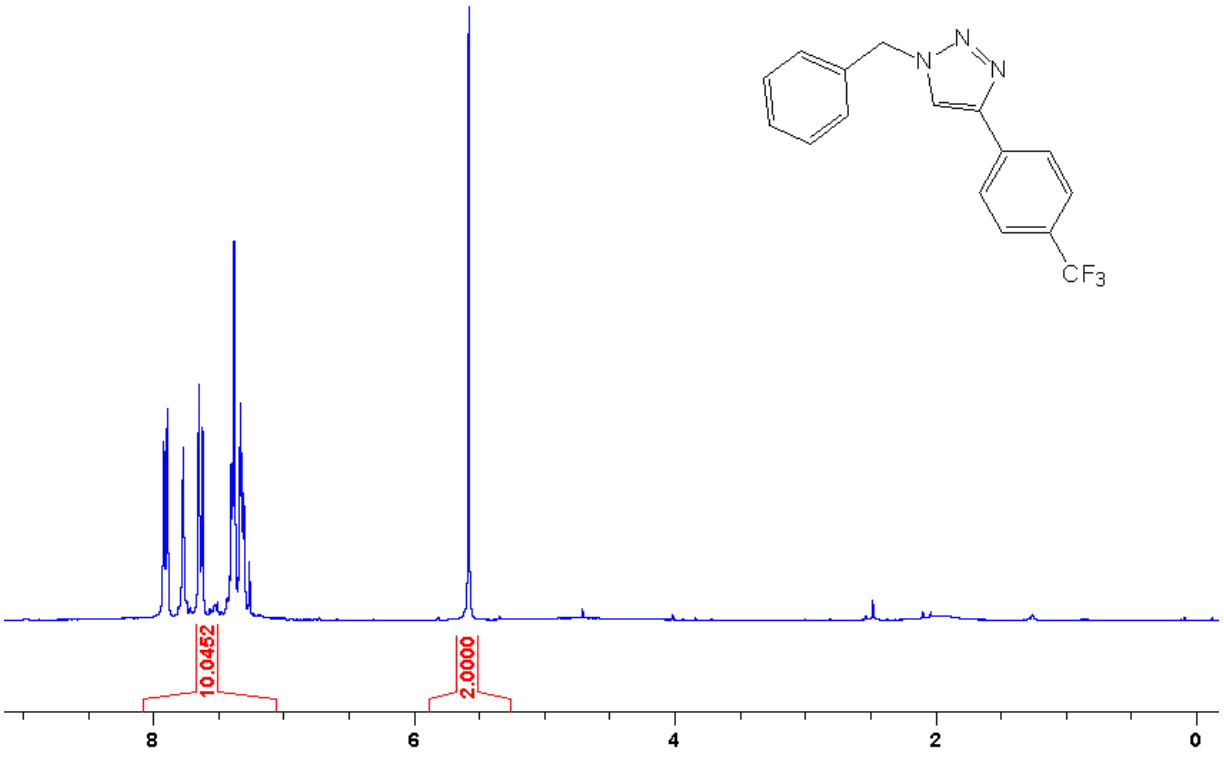

Figure A3.6 ^{1}H NMR spectrum of triazole product **3.6** from the catalytic reaction in $CDCl_3$.

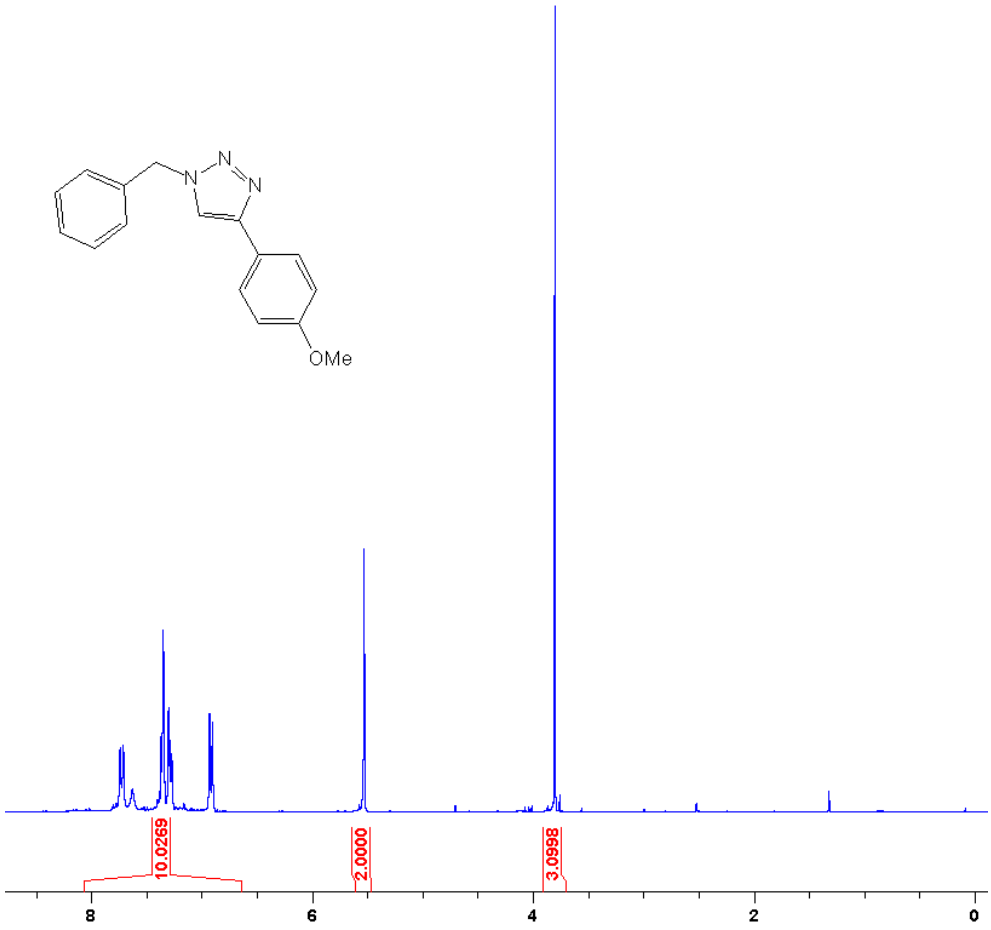

Figure A3.7 ^{1}H NMR spectrum of triazole product **3.7** from the catalytic reaction in $CDCl_3$.

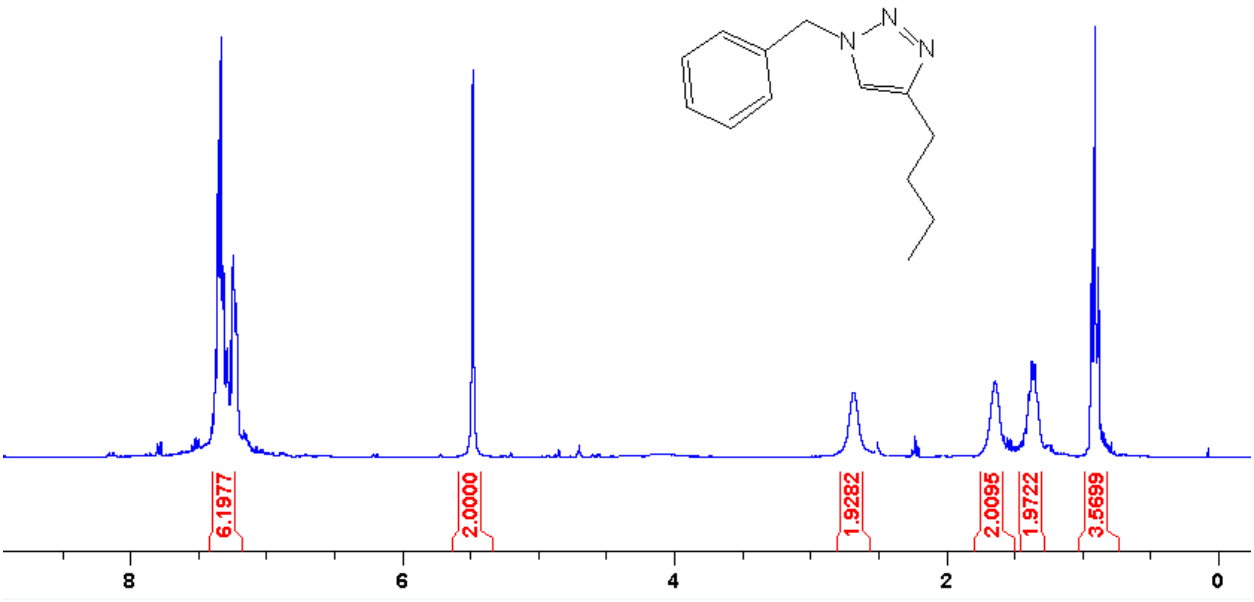

Figure A3.8 ^{1}H NMR spectrum of triazole product **3.8** from the catalytic reaction in $CDCl_3$.

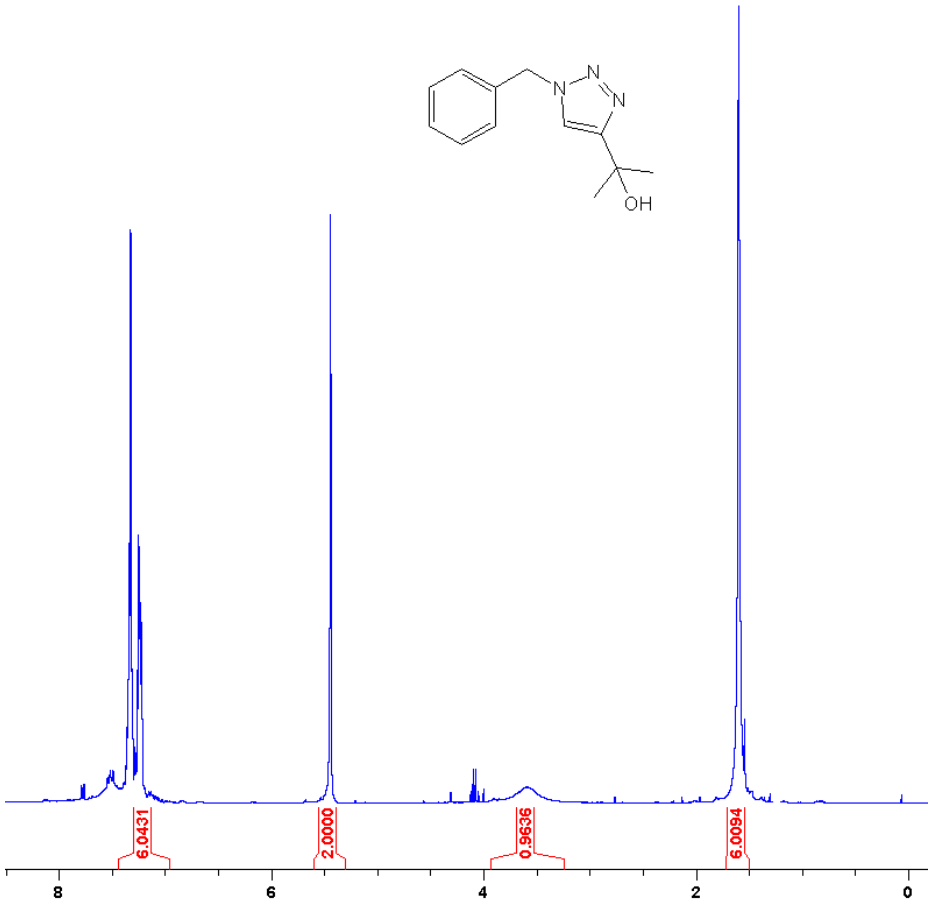

Figure A3.9 ^{1}H NMR spectrum of triazole product **3.9** from the catalytic reaction in $CDCl_3$.

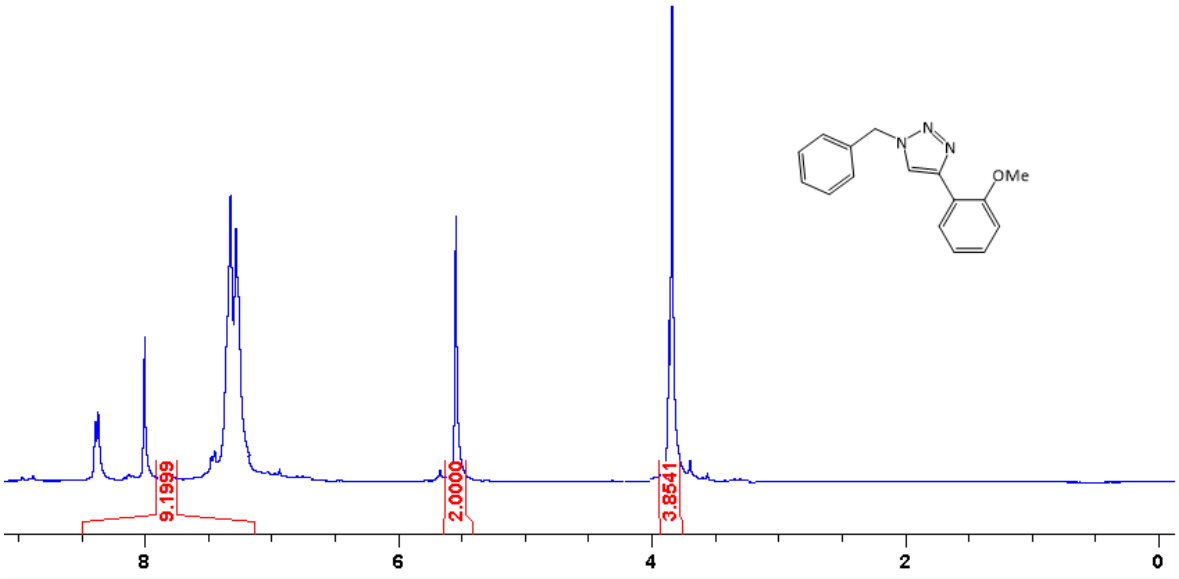

Figure A3.10 ^{1}H NMR spectrum of triazole product **3.10** from the catalytic reaction in $CDCl_3$.

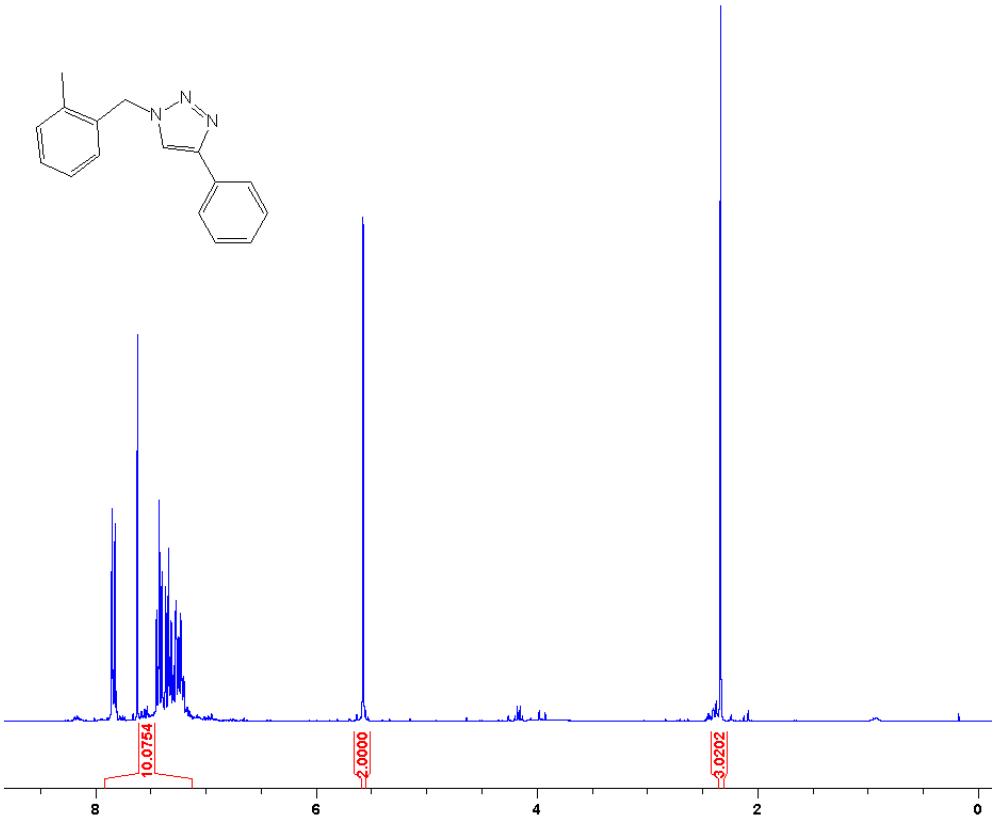

Figure A3.11 ^{1}H NMR spectrum of triazole product **3.11** from the catalytic reaction in $CDCl_3$.

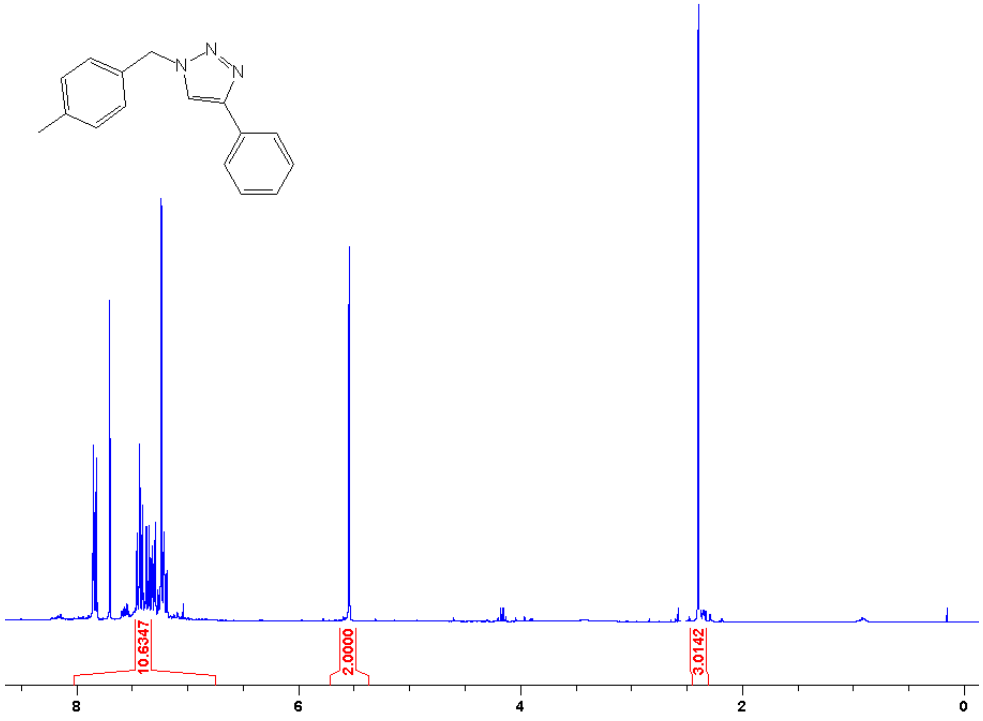

Figure A3.12 ^{1}H NMR spectrum of triazole product **3.12** from the catalytic reaction in $CDCl_3$.

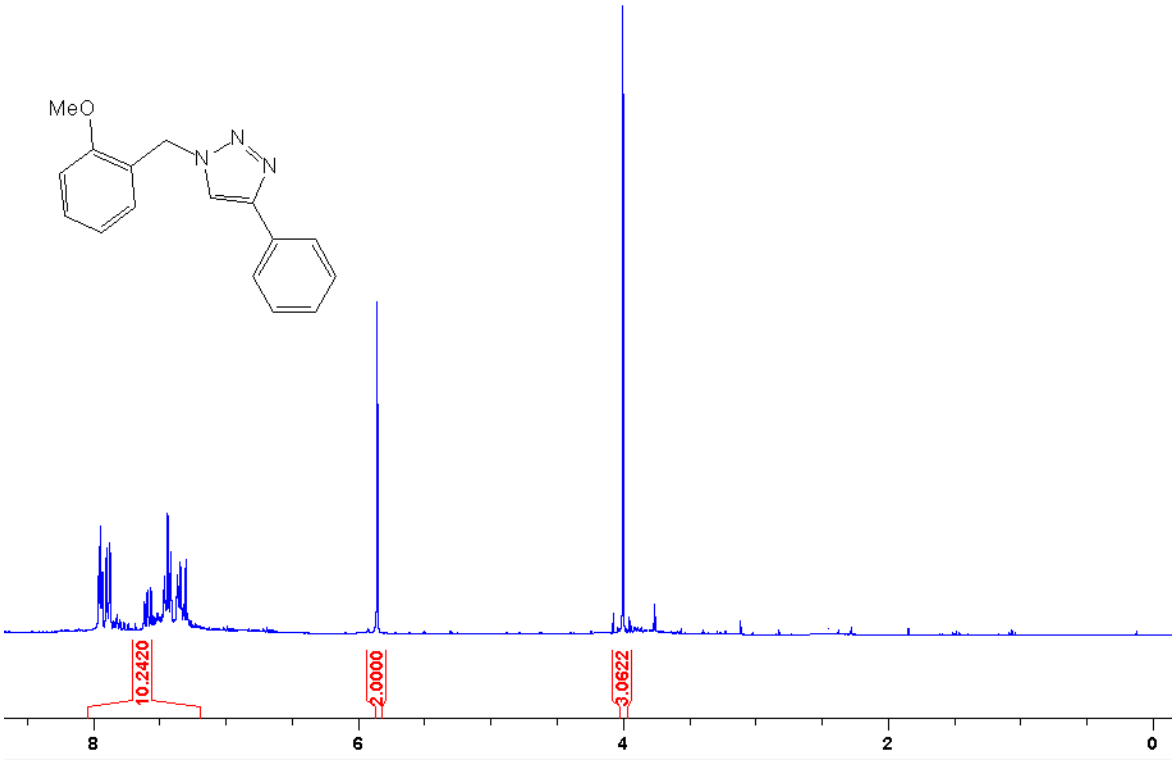

Figure A3.13 ^{1}H NMR spectrum of triazole product **3.13** from the catalytic reaction in $CDCl_3$.

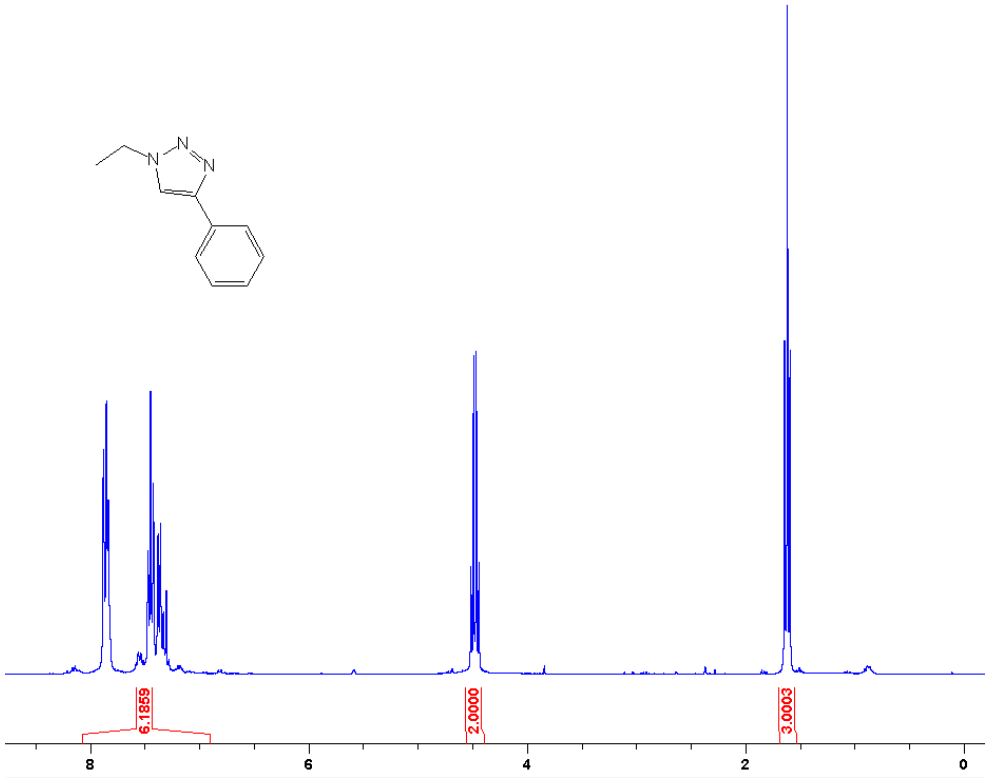

Figure A3.14 ^{1}H NMR spectrum of triazole product **3.14** from the catalytic reaction in $CDCl_3$.

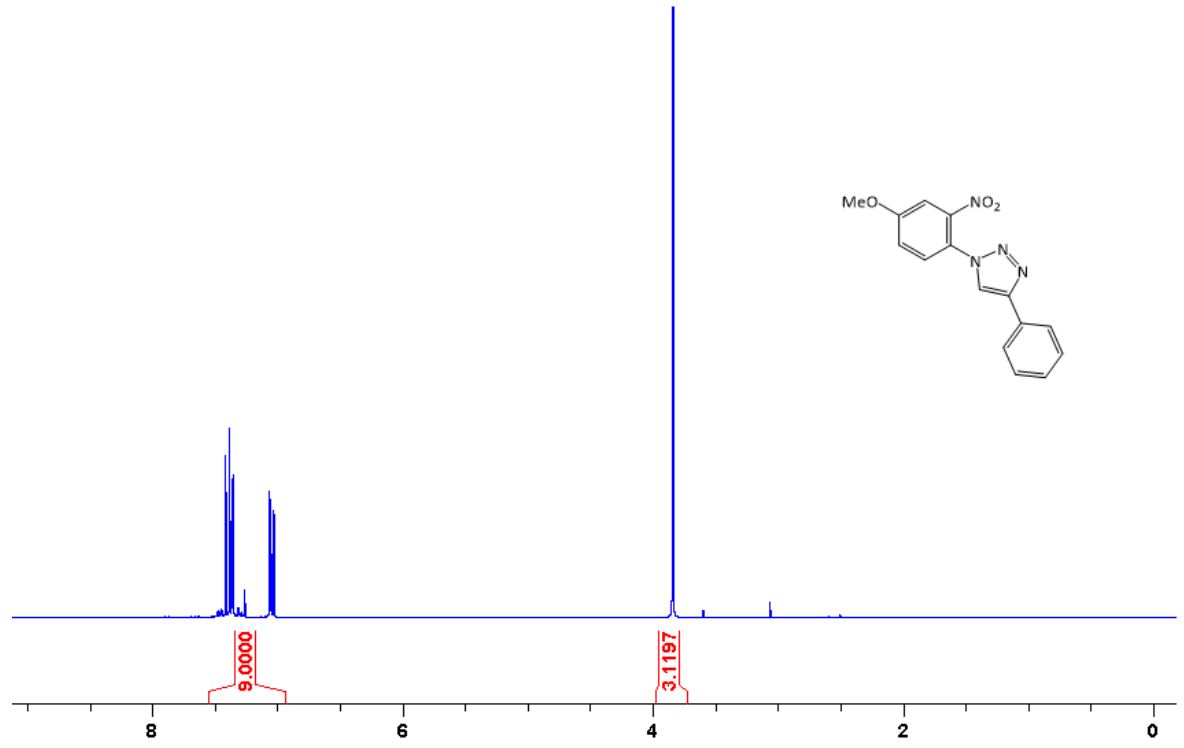

Figure A3.15 ^{1}H NMR spectrum of triazole product **3.15** from the catalytic reaction in $CDCl_3$.

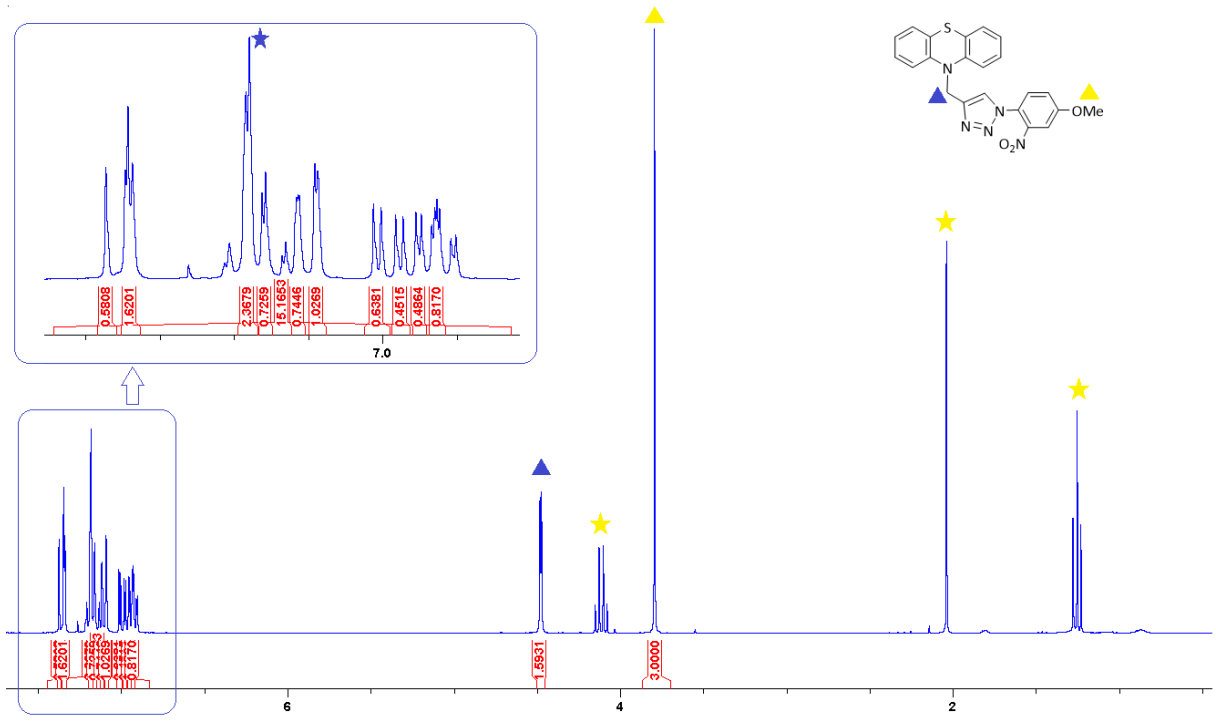

Figure A3.16 ^{1}H NMR spectrum of triazole product **3.16** from the catalytic reaction in $CDCl_3$. The ^{1}H NMR of the compound **3.16** in DMSO is available in literature.[35] Peaks with yellow star are due to ethyl acetate and peak with blue star is protic impurity in CDCl3.

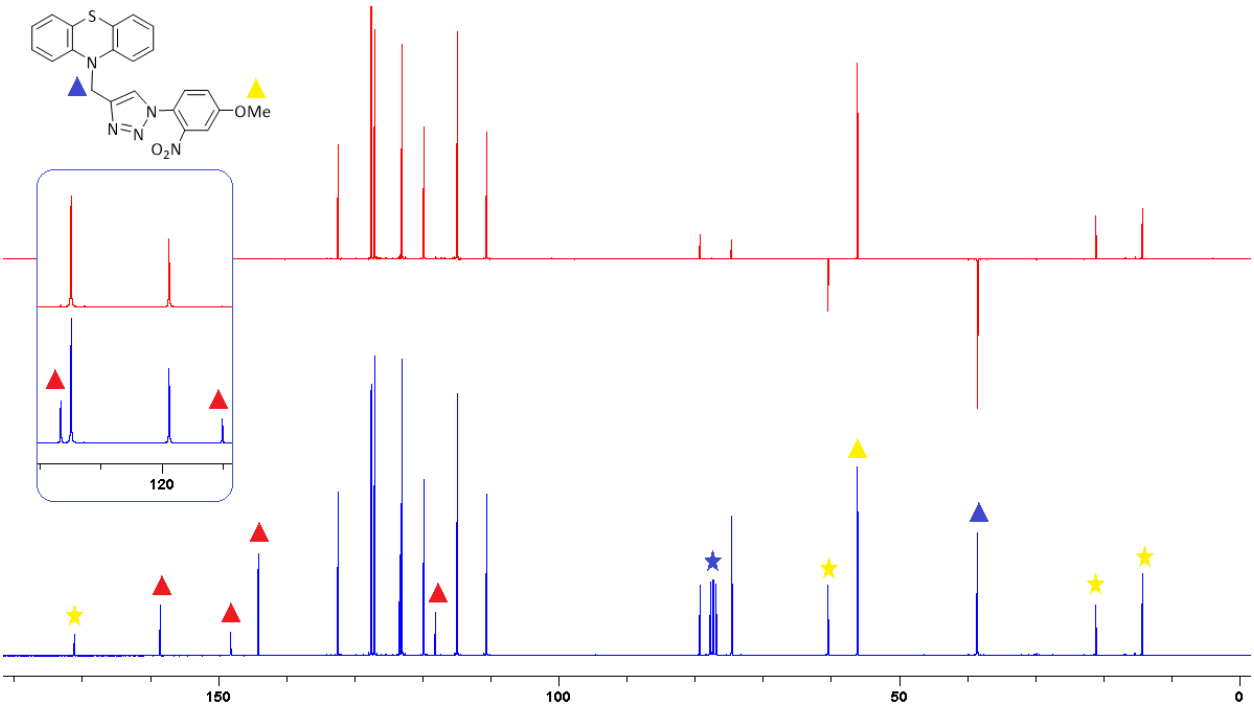

Figure A3.17 $^{13}C\{^{1}H\}$ NMR spectrum (blue on the bottom) and DEPT 135 spectrum (red on top) of triazole product **3.16** from the catalytic reaction in $CDCl_3$. The peaks with yellow stars are ethyl acetate and the triplet assigned with blue star is $CDCl_3$. The peaks labeled with red triangles are belong to carbons with no hydrogen atoms.

3.6.2 Crystallographic details

Crystallographic data were collected from single crystals mounted on MiTeGen dual thickness MicroMounts using Parabar oil. Data were collected on a Bruker Smart (**3.1**) or Kappa (**3.2**) ApexII single crystal diffractometer equipped with a graphite monochromator. The instrument was equipped with a sealed tube Mo Kα source (λ= 0.71073 Å), an ApexII CCD detector and a dry compressed air-cooling system. The samples were cooled to 203 K. Raw data collection and processing were performed with the Apex3 software package from Bruker.[36] Initial unit cell parameters were determined from 36 data frames from select ω scans. Semi-empirical absorption corrections based on equivalent reflections were applied.[37] Systematic absences in the diffraction data-set and unit-cell parameters were consistent with the assigned space group. The initial structural solutions were determined using ShelxT direct methods[38], and refined with full-matrix least-squares procedures based on F^2 using ShelXL or ShelXle.[39] Hydrogen atoms were placed geometrically and refined using a riding model. Deposition Numbers: 2232759-2232760.

Table A3.1 Data collection and refinement metrics for **3.1** and **3.2.**

	3.1 (K0590)	**3.2** (S0726)
empirical formula	$C_{56}H_{48}Cu_4N_4S_8$	$C_{60}H_{64}Cu_4N_4S_8$
formula weight ($g \cdot mol^{-1}$)	1287.62	1351.79
crystal system	Tetragonal	Tetragonal
space group	*P*-42$_1$*c*	*I* 4$_1$/*acd*
a (A)	24.1902(11)	14.4406(12)
b (A)	24.1902(11)	14.4406(12)
c (A)	22.8468(12)	14.0771(12)
α (deg)	90	90
β (deg)	90	90
γ (deg)	90	90
V (A^3)	13369.2(14)	2935.5(5)
Z	8	2
T (K)	203(2)	203(2)
ρ_{calcd} ($g \cdot cm^{-3}$)	1.279	1.529
μ (mm^{-1})	1.540	1.757
$2\theta_{max}$ (deg)	50.162	61.042
total/unique reflections	8977/3088	12226/4484
Reflections [$I_o \geq 2\sigma(I_o)$]	2317	3550
R_1, wR_2 [$I_o \geq 2\sigma(I_o)$]	0.2109, 0.0724	0.0373, 0.0942
goodness of fit	1.134	1.039
CCDC number	2232759	2232760

Table A3.2 Bond lengths (Å) for complex **3.1**

Atom1	**Atom2**	**Length Å**
Cu1	S1	2.247(5)
Cu1	N1	2.08(1)
Cu1	S1	2.181(5)
S1	C1	1.77(1)
S1	Cu1	2.181(5)
S2	C13	1.71(2)
S2	C14A	1.83(6)
N1	C6	1.41(2)
N1	C7	1.30(2)
C1	C2	1.34(3)
C1	C6	1.45(2)
C2	H2	0.94
C2	C3	1.41(3)
C3	H3	0.94
C3	C4	1.38(3)
C4	H4	0.94
C4	C5	1.40(2)
C5	H5	0.94

C5	C6	1.40(2)
C7	H7	0.94
C7	C8	1.46(2)
C8	C9	1.40(3)
C8	C13	1.44(2)
C9	H9	0.94
C9	C10	1.37(3)
C10	H10	0.94
C10	C11	1.43(3)
C11	H11	0.94
C11	C12	1.32(3)
C12	H12	0.94
C12	C13	1.41(3)
C14A	H14A	1
C14A	H14B	0.98
C14A	H14C	1
Cu1	S1	2.247(5)
Cu1	N1	2.08(1)
Cu1	S1	2.181(5)
S1	C1	1.77(1)
S2	C13	1.71(2)
S2	C14A	1.83(6)
N1	C6	1.41(2)
N1	C7	1.30(2)
C1	C2	1.34(3)
C1	C6	1.45(2)
C2	H2	0.94
C2	C3	1.41(3)
C3	H3	0.94
C3	C4	1.38(3)
C4	H4	0.94
C4	C5	1.40(2)
C5	H5	0.94
C5	C6	1.40(2)
C7	H7	0.94
C7	C8	1.46(2)
C8	C9	1.40(3)
C8	C13	1.44(2)
C9	H9	0.94
C9	C10	1.37(3)
C10	H10	0.94
C10	C11	1.43(3)
C11	H11	0.94

C11	C12	1.32(3)
C12	H12	0.94
C12	C13	1.41(3)
C14A	H14A	1
C14A	H14B	0.98
C14A	H14C	1
Cu1	S1	2.247(5)
Cu1	N1	2.08(1)
S1	C1	1.77(1)
S1	Cu1	2.181(5)
S2	C13	1.71(2)
S2	C14A	1.83(6)
N1	C6	1.41(2)
N1	C7	1.30(2)
C1	C2	1.34(3)
C1	C6	1.45(2)
C2	H2	0.94
C2	C3	1.41(3)
C3	H3	0.94
C3	C4	1.38(3)
C4	H4	0.94
C4	C5	1.40(2)
C5	H5	0.94
C5	C6	1.40(2)
C7	H7	0.94
C7	C8	1.46(2)
C8	C9	1.40(3)
C8	C13	1.44(2)
C9	H9	0.94
C9	C10	1.37(3)
C10	H10	0.94
C10	C11	1.43(3)
C11	H11	0.94
C11	C12	1.32(3)
C12	H12	0.94
C12	C13	1.41(3)
C14A	H14A	1
C14A	H14B	0.98
C14A	H14C	1
Cu1	S1	2.247(5)
Cu1	N1	2.08(1)
S1	C1	1.77(1)
S2	C13	1.71(2)

S2	C14A	1.83(6)
N1	C6	1.41(2)
N1	C7	1.30(2)
C1	C2	1.34(3)
C1	C6	1.45(2)
C2	H2	0.94
C2	C3	1.41(3)
C3	H3	0.94
C3	C4	1.38(3)
C4	H4	0.94
C4	C5	1.40(2)
C5	H5	0.94
C5	C6	1.40(2)
C7	H7	0.94
C7	C8	1.46(2)
C8	C9	1.40(3)
C8	C13	1.44(2)
C9	H9	0.94
C9	C10	1.37(3)
C10	H10	0.94
C10	C11	1.43(3)
C11	H11	0.94
C11	C12	1.32(3)
C12	H12	0.94
C12	C13	1.41(3)
C14A	H14A	1
C14A	H14B	0.98
C14A	H14C	1

Table A3.3 All angles (°) for complex **3.1**

Atom1	**Atom2**	**Atom3**	**Angle**
S1	Cu1	N1	88.3(3)
S1	Cu1	S1	140.1(2)
N1	Cu1	S1	128.9(4)
Cu1	S1	C1	96.3(5)
Cu1	S1	Cu1	82.6(2)
C1	S1	Cu1	104.3(5)
C13	S2	C14A	132(3)
Cu1	N1	C6	112.1(9)
Cu1	N1	C7	126(1)
C6	N1	C7	115(1)
S1	C1	C2	122(1)

S1	C1	C6	119(1)
C2	C1	C6	119(1)
C1	C2	H2	119
C1	C2	C3	122(2)
H2	C2	C3	119
C2	C3	H3	119
C2	C3	C4	121(2)
H3	C3	C4	119
C3	C4	H4	122
C3	C4	C5	117(2)
H4	C4	C5	122
C4	C5	H5	118
C4	C5	C6	123(1)
H5	C5	C6	118
N1	C6	C1	119(1)
N1	C6	C5	123(1)
C1	C6	C5	117(1)
N1	C7	H7	118
N1	C7	C8	125(1)
H7	C7	C8	118
C7	C8	C9	122(1)
C7	C8	C13	118(1)
C9	C8	C13	119(2)
C8	C9	H9	119
C8	C9	C10	122(2)
H9	C9	C10	119
C9	C10	H10	121
C9	C10	C11	117(2)
H10	C10	C11	122
C10	C11	H11	119
C10	C11	C12	122(2)
H11	C11	C12	119
C11	C12	H12	119
C11	C12	C13	122(2)
H12	C12	C13	119
S2	C13	C8	121(1)
S2	C13	C12	123(1)
C8	C13	C12	117(2)
S2	C14A	H14A	110
S2	C14A	H14B	110
S2	C14A	H14C	110
H14A	C14A	H14B	109
H14A	C14A	H14C	110

H14B	C14A	H14C	109
S1	Cu1	N1	88.3(3)
S1	Cu1	S1	140.1(2)
N1	Cu1	S1	128.9(4)
Cu1	S1	Cu1	82.6(2)
Cu1	S1	C1	104.3(5)
Cu1	S1	C1	96.3(5)
C13	S2	C14A	132(3)
Cu1	N1	C6	112.1(9)
Cu1	N1	C7	126(1)
C6	N1	C7	115(1)
S1	C1	C2	122(1)
S1	C1	C6	119(1)
C2	C1	C6	119(1)
C1	C2	H2	119
C1	C2	C3	122(2)
H2	C2	C3	119
C2	C3	H3	119
C2	C3	C4	121(2)
H3	C3	C4	119
C3	C4	H4	122
C3	C4	C5	117(2)
H4	C4	C5	122
C4	C5	H5	118
C4	C5	C6	123(1)
H5	C5	C6	118
N1	C6	C1	119(1)
N1	C6	C5	123(1)
C1	C6	C5	117(1)
N1	C7	H7	118
N1	C7	C8	125(1)
H7	C7	C8	118
C7	C8	C9	122(1)
C7	C8	C13	118(1)
C9	C8	C13	119(2)
C8	C9	H9	119
C8	C9	C10	122(2)
H9	C9	C10	119
C9	C10	H10	121
C9	C10	C11	117(2)
H10	C10	C11	122
C10	C11	H11	119
C10	C11	C12	122(2)

H11	C11	C12	119
C11	C12	H12	119
C11	C12	C13	122(2)
H12	C12	C13	119
S2	C13	C8	121(1)
S2	C13	C12	123(1)
C8	C13	C12	117(2)
S2	C14A	H14A	110
S2	C14A	H14B	110
S2	C14A	H14C	110
H14A	C14A	H14B	109
H14A	C14A	H14C	110
H14B	C14A	H14C	109
S1	Cu1	S1	140.1(2)
S1	Cu1	N1	128.9(4)
S1	Cu1	N1	88.3(3)
Cu1	S1	C1	96.3(5)
Cu1	S1	Cu1	82.6(2)
C1	S1	Cu1	104.3(5)
C13	S2	C14A	132(3)
Cu1	N1	C6	112.1(9)
Cu1	N1	C7	126(1)
C6	N1	C7	115(1)
S1	C1	C2	122(1)
S1	C1	C6	119(1)
C2	C1	C6	119(1)
C1	C2	H2	119
C1	C2	C3	122(2)
H2	C2	C3	119
C2	C3	H3	119
C2	C3	C4	121(2)
H3	C3	C4	119
C3	C4	H4	122
C3	C4	C5	117(2)
H4	C4	C5	122
C4	C5	H5	118
C4	C5	C6	123(1)
H5	C5	C6	118
N1	C6	C1	119(1)
N1	C6	C5	123(1)
C1	C6	C5	117(1)
N1	C7	H7	118
N1	C7	C8	125(1)

H7	C7	C8	118
C7	C8	C9	122(1)
C7	C8	C13	118(1)
C9	C8	C13	119(2)
C8	C9	H9	119
C8	C9	C10	122(2)
H9	C9	C10	119
C9	C10	H10	121
C9	C10	C11	117(2)
H10	C10	C11	122
C10	C11	H11	119
C10	C11	C12	122(2)
H11	C11	C12	119
C11	C12	H12	119
C11	C12	C13	122(2)
H12	C12	C13	119
S2	C13	C8	121(1)
S2	C13	C12	123(1)
C8	C13	C12	117(2)
S2	C14A	H14A	110
S2	C14A	H14B	110
S2	C14A	H14C	110
H14A	C14A	H14B	109
H14A	C14A	H14C	110
H14B	C14A	H14C	109
S1	Cu1	S1	140.1(2)
S1	Cu1	N1	128.9(4)
S1	Cu1	N1	88.3(3)
Cu1	S1	Cu1	82.6(2)
Cu1	S1	C1	104.3(5)
Cu1	S1	C1	96.3(5)
C13	S2	C14A	132(3)
Cu1	N1	C6	112.1(9)
Cu1	N1	C7	126(1)
C6	N1	C7	115(1)
S1	C1	C2	122(1)
S1	C1	C6	119(1)
C2	C1	C6	119(1)
C1	C2	H2	119
C1	C2	C3	122(2)
H2	C2	C3	119
C2	C3	H3	119
C2	C3	C4	121(2)

H3	C3	C4	119
C3	C4	H4	122
C3	C4	C5	117(2)
H4	C4	C5	122
C4	C5	H5	118
C4	C5	C6	123(1)
H5	C5	C6	118
N1	C6	C1	119(1)
N1	C6	C5	123(1)
C1	C6	C5	117(1)
N1	C7	H7	118
N1	C7	C8	125(1)
H7	C7	C8	118
C7	C8	C9	122(1)
C7	C8	C13	118(1)
C9	C8	C13	119(2)
C8	C9	H9	119
C8	C9	C10	122(2)
H9	C9	C10	119
C9	C10	H10	121
C9	C10	C11	117(2)
H10	C10	C11	122
C10	C11	H11	119
C10	C11	C12	122(2)
H11	C11	C12	119
C11	C12	H12	119
C11	C12	C13	122(2)
H12	C12	C13	119
S2	C13	C8	121(1)
S2	C13	C12	123(1)
C8	C13	C12	117(2)
S2	C14A	H14A	110
S2	C14A	H14B	110
S2	C14A	H14C	110
H14A	C14A	H14B	109
H14A	C14A	H14C	110
H14B	C14A	H14C	109

Table A3.4 Bond lengths (Å) for complex **3.2**

Atom1	**Atom2**	**Length**
Cu1	S1	2.535(1)

Cu1	N1	1.934(3)
Cu1	Cu1	2.5666(6)
Cu1	Cu1	2.5666(6)
Cu1	N1	1.953(3)
S1	C1	1.785(5)
S1	C2	1.763(4)
S2	C14	1.753(6)
S2	C15	1.808(6)
N1	C7	1.417(5)
N1	C8	1.474(5)
N1	Cu1	1.953(3)
C1	H1A	0.97
C1	H1B	0.97
C1	H1C	0.97
C2	C3	1.391(7)
C2	C7	1.421(6)
C3	H3	0.941
C3	C4	1.380(9)
C4	H4	0.94
C4	C5	1.36(1)
C5	H5	0.94
C5	C6	1.387(7)
C6	H6	0.941
C6	C7	1.393(6)
C8	H8A	0.98
C8	H8AB	0.98
C8	C9	1.522(6)
C9	C10	1.371(6)
C9	C14	1.413(6)
C10	H10	0.939
C10	C11	1.402(8)
C11	H11	0.94
C11	C12	1.37(1)
C12	H12	0.94
C12	C13	1.365(9)
C13	H13	0.94
C13	C14	1.400(8)
C15	H15A	0.97
C15	H15B	0.971
C15	H15C	0.97
Cu1	S1	2.535(1)
Cu1	N1	1.934(3)
Cu1	Cu1	2.5666(6)

S1	C1	1.785(5)
S1	C2	1.763(4)
S2	C14	1.753(6)
S2	C15	1.808(6)
N1	C7	1.417(5)
N1	C8	1.474(5)
N1	Cu1	1.953(3)
C1	H1A	0.97
C1	H1B	0.97
C1	H1C	0.97
C2	C3	1.391(7)
C2	C7	1.421(6)
C3	H3	0.941
C3	C4	1.380(9)
C4	H4	0.94
C4	C5	1.36(1)
C5	H5	0.94
C5	C6	1.387(7)
C6	H6	0.941
C6	C7	1.393(6)
C8	H8A	0.98
C8	H8AB	0.98
C8	C9	1.522(6)
C9	C10	1.371(6)
C9	C14	1.413(6)
C10	H10	0.939
C10	C11	1.402(8)
C11	H11	0.94
C11	C12	1.37(1)
C12	H12	0.94
C12	C13	1.365(9)
C13	H13	0.94
C13	C14	1.400(8)
C15	H15A	0.97
C15	H15B	0.971
C15	H15C	0.97
Cu1	S1	2.535(1)
Cu1	N1	1.934(3)
Cu1	Cu1	2.5666(6)
Cu1	N1	1.953(3)
S1	C1	1.785(5)
S1	C2	1.763(4)
S2	C14	1.753(6)

S2	C15	1.808(6)
N1	C7	1.417(5)
N1	C8	1.474(5)
C1	H1A	0.97
C1	H1B	0.97
C1	H1C	0.97
C2	C3	1.391(7)
C2	C7	1.421(6)
C3	H3	0.941
C3	C4	1.380(9)
C4	H4	0.94
C4	C5	1.36(1)
C5	H5	0.94
C5	C6	1.387(7)
C6	H6	0.941
C6	C7	1.393(6)
C8	H8A	0.98
C8	H8AB	0.98
C8	C9	1.522(6)
C9	C10	1.371(6)
C9	C14	1.413(6)
C10	H10	0.939
C10	C11	1.402(8)
C11	H11	0.94
C11	C12	1.37(1)
C12	H12	0.94
C12	C13	1.365(9)
C13	H13	0.94
C13	C14	1.400(8)
C15	H15A	0.97
C15	H15B	0.971
C15	H15C	0.97
Cu1	S1	2.535(1)
Cu1	N1	1.934(3)
S1	C1	1.785(5)
S1	C2	1.763(4)
S2	C14	1.753(6)
S2	C15	1.808(6)
N1	C7	1.417(5)
N1	C8	1.474(5)
C1	H1A	0.97
C1	H1B	0.97
C1	H1C	0.97

C2	C3	1.391(7)
C2	C7	1.421(6)
C3	H3	0.941
C3	C4	1.380(9)
C4	H4	0.94
C4	C5	1.36(1)
C5	H5	0.94
C5	C6	1.387(7)
C6	H6	0.941
C6	C7	1.393(6)
C8	H8A	0.98
C8	H8AB	0.98
C8	C9	1.522(6)
C9	C10	1.371(6)
C9	C14	1.413(6)
C10	H10	0.939
C10	C11	1.402(8)
C11	H11	0.94
C11	C12	1.37(1)
C12	H12	0.94
C12	C13	1.365(9)
C13	H13	0.94
C13	C14	1.400(8)
C15	H15A	0.97
C15	H15B	0.971
C15	H15C	0.97

Table A3.5 All angles (°) for complex **3.2.**

Atom1	**Atom2**	**Atom3**	**Angle**
S1	Cu1	N1	79.58(9)
S1	Cu1	Cu1	73.87(3)
S1	Cu1	Cu1	130.89(3)
S1	Cu1	N1	110.71(9)
N1	Cu1	Cu1	49.00(9)
N1	Cu1	Cu1	122.71(9)
N1	Cu1	N1	169.3(1)
Cu1	Cu1	Cu1	89.28(2)
Cu1	Cu1	N1	129.43(9)
Cu1	Cu1	N1	48.35(9)
Cu1	S1	C1	157.1(2)
Cu1	S1	C2	95.3(1)
C1	S1	C2	103.9(3)

C14	S2	C15	103.4(3)
Cu1	N1	C7	122.1(2)
Cu1	N1	C8	112.9(2)
Cu1	N1	Cu1	82.7(1)
C7	N1	C8	115.0(3)
C7	N1	Cu1	107.4(2)
C8	N1	Cu1	111.5(2)
S1	C1	H1A	109.5
S1	C1	H1B	109.5
S1	C1	H1C	109.4
H1A	C1	H1B	109.5
H1A	C1	H1C	109.5
H1B	C1	H1C	109.5
S1	C2	C3	123.7(4)
S1	C2	C7	116.3(3)
C3	C2	C7	120.0(4)
C2	C3	H3	120
C2	C3	C4	120.1(5)
H3	C3	C4	119.9
C3	C4	H4	119.6
C3	C4	C5	120.7(6)
H4	C4	C5	119.7
C4	C5	H5	119.9
C4	C5	C6	120.2(6)
H5	C5	C6	120
C5	C6	H6	119.4
C5	C6	C7	121.2(5)
H6	C6	C7	119.4
N1	C7	C2	118.4(4)
N1	C7	C6	123.9(4)
C2	C7	C6	117.7(4)
N1	C8	H8A	108.3
N1	C8	H8AB	108.3
N1	C8	C9	115.8(3)
H8A	C8	H8AB	107.4
H8A	C8	C9	108.4
H8AB	C8	C9	108.4
C8	C9	C10	122.3(4)
C8	C9	C14	118.4(4)
C10	C9	C14	119.2(4)
C9	C10	H10	119.5
C9	C10	C11	121.0(5)
H10	C10	C11	119.5

C10	C11	H11	120.7
C10	C11	C12	118.7(6)
H11	C11	C12	120.6
C11	C12	H12	118.8
C11	C12	C13	122.3(6)
H12	C12	C13	118.9
C12	C13	H13	120.3
C12	C13	C14	119.3(6)
H13	C13	C14	120.4
S2	C14	C9	118.0(4)
S2	C14	C13	122.5(4)
C9	C14	C13	119.5(5)
S2	C15	H15A	109.5
S2	C15	H15B	109.5
S2	C15	H15C	109.5
H15A	C15	H15B	109.4
H15A	C15	H15C	109.5
H15B	C15	H15C	109.4
Cu1	Cu1	N1	48.35(9)
Cu1	Cu1	S1	130.89(3)
Cu1	Cu1	N1	122.71(9)
Cu1	Cu1	Cu1	89.28(2)
N1	Cu1	S1	110.71(9)
N1	Cu1	N1	169.3(1)
N1	Cu1	Cu1	129.43(9)
S1	Cu1	N1	79.58(9)
S1	Cu1	Cu1	73.87(3)
N1	Cu1	Cu1	49.00(9)
Cu1	S1	C1	157.1(2)
Cu1	S1	C2	95.3(1)
C1	S1	C2	103.9(3)
C14	S2	C15	103.4(3)
Cu1	N1	C7	122.1(2)
Cu1	N1	C8	112.9(2)
Cu1	N1	Cu1	82.7(1)
C7	N1	C8	115.0(3)
C7	N1	Cu1	107.4(2)
C8	N1	Cu1	111.5(2)
S1	C1	H1A	109.5
S1	C1	H1B	109.5
S1	C1	H1C	109.4
H1A	C1	H1B	109.5
H1A	C1	H1C	109.5

H1B	C1	H1C	109.5
S1	C2	C3	123.7(4)
S1	C2	C7	116.3(3)
C3	C2	C7	120.0(4)
C2	C3	H3	120
C2	C3	C4	120.1(5)
H3	C3	C4	119.9
C3	C4	H4	119.6
C3	C4	C5	120.7(6)
H4	C4	C5	119.7
C4	C5	H5	119.9
C4	C5	C6	120.2(6)
H5	C5	C6	120
C5	C6	H6	119.4
C5	C6	C7	121.2(5)
H6	C6	C7	119.4
N1	C7	C2	118.4(4)
N1	C7	C6	123.9(4)
C2	C7	C6	117.7(4)
N1	C8	H8A	108.3
N1	C8	H8AB	108.3
N1	C8	C9	115.8(3)
H8A	C8	H8AB	107.4
H8A	C8	C9	108.4
H8AB	C8	C9	108.4
C8	C9	C10	122.3(4)
C8	C9	C14	118.4(4)
C10	C9	C14	119.2(4)
C9	C10	H10	119.5
C9	C10	C11	121.0(5)
H10	C10	C11	119.5
C10	C11	H11	120.7
C10	C11	C12	118.7(6)
H11	C11	C12	120.6
C11	C12	H12	118.8
C11	C12	C13	122.3(6)
H12	C12	C13	118.9
C12	C13	H13	120.3
C12	C13	C14	119.3(6)
H13	C13	C14	120.4
S2	C14	C9	118.0(4)
S2	C14	C13	122.5(4)
C9	C14	C13	119.5(5)

S2	C15	H15A	109.5
S2	C15	H15B	109.5
S2	C15	H15C	109.5
H15A	C15	H15B	109.4
H15A	C15	H15C	109.5
H15B	C15	H15C	109.4
Cu1	Cu1	S1	73.87(3)
Cu1	Cu1	N1	49.00(9)
Cu1	Cu1	Cu1	89.28(2)
Cu1	Cu1	N1	129.43(9)
S1	Cu1	N1	79.58(9)
S1	Cu1	Cu1	130.89(3)
S1	Cu1	N1	110.71(9)
N1	Cu1	Cu1	122.71(9)
N1	Cu1	N1	169.3(1)
Cu1	Cu1	N1	48.35(9)
Cu1	S1	C1	157.1(2)
Cu1	S1	C2	95.3(1)
C1	S1	C2	103.9(3)
C14	S2	C15	103.4(3)
Cu1	N1	Cu1	82.7(1)
Cu1	N1	C7	107.4(2)
Cu1	N1	C8	111.5(2)
Cu1	N1	C7	122.1(2)
Cu1	N1	C8	112.9(2)
C7	N1	C8	115.0(3)
S1	C1	H1A	109.5
S1	C1	H1B	109.5
S1	C1	H1C	109.4
H1A	C1	H1B	109.5
H1A	C1	H1C	109.5
H1B	C1	H1C	109.5
S1	C2	C3	123.7(4)
S1	C2	C7	116.3(3)
C3	C2	C7	120.0(4)
C2	C3	H3	120
C2	C3	C4	120.1(5)
H3	C3	C4	119.9
C3	C4	H4	119.6
C3	C4	C5	120.7(6)
H4	C4	C5	119.7
C4	C5	H5	119.9
C4	C5	C6	120.2(6)

H5	C5	C6	120
C5	C6	H6	119.4
C5	C6	C7	121.2(5)
H6	C6	C7	119.4
N1	C7	C2	118.4(4)
N1	C7	C6	123.9(4)
C2	C7	C6	117.7(4)
N1	C8	H8A	108.3
N1	C8	H8AB	108.3
N1	C8	C9	115.8(3)
H8A	C8	H8AB	107.4
H8A	C8	C9	108.4
H8AB	C8	C9	108.4
C8	C9	C10	122.3(4)
C8	C9	C14	118.4(4)
C10	C9	C14	119.2(4)
C9	C10	H10	119.5
C9	C10	C11	121.0(5)
H10	C10	C11	119.5
C10	C11	H11	120.7
C10	C11	C12	118.7(6)
H11	C11	C12	120.6
C11	C12	H12	118.8
C11	C12	C13	122.3(6)
H12	C12	C13	118.9
C12	C13	H13	120.3
C12	C13	C14	119.3(6)
H13	C13	C14	120.4
S2	C14	C9	118.0(4)
S2	C14	C13	122.5(4)
C9	C14	C13	119.5(5)
S2	C15	H15A	109.5
S2	C15	H15B	109.5
S2	C15	H15C	109.5
H15A	C15	H15B	109.4
H15A	C15	H15C	109.5
H15B	C15	H15C	109.4
Cu1	Cu1	N1	48.35(9)
Cu1	Cu1	Cu1	89.28(2)
Cu1	Cu1	S1	130.89(3)
Cu1	Cu1	N1	122.71(9)
N1	Cu1	Cu1	129.43(9)
N1	Cu1	S1	110.71(9)

N1	Cu1	N1	169.3(1)
Cu1	Cu1	S1	73.87(3)
Cu1	Cu1	N1	49.00(9)
S1	Cu1	N1	79.58(9)
Cu1	S1	C1	157.1(2)
Cu1	S1	C2	95.3(1)
C1	S1	C2	103.9(3)
C14	S2	C15	103.4(3)
Cu1	N1	Cu1	82.7(1)
Cu1	N1	C7	107.4(2)
Cu1	N1	C8	111.5(2)
Cu1	N1	C7	122.1(2)
Cu1	N1	C8	112.9(2)
C7	N1	C8	115.0(3)
S1	C1	H1A	109.5
S1	C1	H1B	109.5
S1	C1	H1C	109.4
H1A	C1	H1B	109.5
H1A	C1	H1C	109.5
H1B	C1	H1C	109.5
S1	C2	C3	123.7(4)
S1	C2	C7	116.3(3)
C3	C2	C7	120.0(4)
C2	C3	H3	120
C2	C3	C4	120.1(5)
H3	C3	C4	119.9
C3	C4	H4	119.6
C3	C4	C5	120.7(6)
H4	C4	C5	119.7
C4	C5	H5	119.9
C4	C5	C6	120.2(6)
H5	C5	C6	120
C5	C6	H6	119.4
C5	C6	C7	121.2(5)
H6	C6	C7	119.4
N1	C7	C2	118.4(4)
N1	C7	C6	123.9(4)
C2	C7	C6	117.7(4)
N1	C8	H8A	108.3
N1	C8	H8AB	108.3
N1	C8	C9	115.8(3)
H8A	C8	H8AB	107.4
H8A	C8	C9	108.4

H8AB	C8	C9	108.4
C8	C9	C10	122.3(4)
C8	C9	C14	118.4(4)
C10	C9	C14	119.2(4)
C9	C10	H10	119.5
C9	C10	C11	121.0(5)
H10	C10	C11	119.5
C10	C11	H11	120.7
C10	C11	C12	118.7(6)
H11	C11	C12	120.6
C11	C12	H12	118.8
C11	C12	C13	122.3(6)
H12	C12	C13	118.9
C12	C13	H13	120.3
C12	C13	C14	119.3(6)
H13	C13	C14	120.4
S2	C14	C9	118.0(4)
S2	C14	C13	122.5(4)
C9	C14	C13	119.5(5)
S2	C15	H15A	109.5
S2	C15	H15B	109.5
S2	C15	H15C	109.5
H15A	C15	H15B	109.4
H15A	C15	H15C	109.5
H15B	C15	H15C	109.4

3.6.3 Details of DFT analysis

General information

All DFT calculations were performed using Gaussian 16 on Grex server from Westgrid (provided by Compute Canada/Calcul Canada). Geometry optimizations were carried out using the mixed basis set 6-31g** for all light atoms (C, H, O, S, N) and def2TZVP for copper atoms. The M06L functional was exploited in aqueous solvent using the CPCM model. Local minima were assessed by convergence and the absence of imaginary frequencies in the frequency calculation. The mechanism of the first step of the catalytic reaction was inspected by considering the different possible formation pathways of the copper alkynyl intermediate in order to investigate the bifunctional ability of the thiolate ligand in complex **3.1**. The electronic energy, thermal enthalpy and free Gibbs energy were calculated for each intermediate and the other molecules in the equation regarding each pathway.

Path 1. Deprotonation by the S group and formation of copper alkynyl monomer (SMe group in trans position):

Complex **3.1** (Tetramer)

Cu	-0.88736800	-0.44783400	-1.25121700
S	-0.82256900	1.79049700	-1.83844900
S	-5.52669300	-2.10159300	-4.16835300
N	-3.02090700	-0.20840100	-1.30365200
C	-2.45990100	2.15746300	-1.23937100
C	-2.85838000	3.48256100	-1.04094100
H	-2.12889400	4.27404000	-1.19220200
C	-4.15231900	3.79225900	-0.63336400
H	-4.42818500	4.82848800	-0.45942600
C	-5.07577100	2.77144500	-0.41821900
H	-6.07925700	2.99917800	-0.07087400
C	-4.70612600	1.44963300	-0.64188100
H	-5.41873900	0.64621000	-0.47082900
C	-3.40860200	1.12774800	-1.06461300
C	-3.89173200	-0.97483000	-1.88739100
H	-4.82439800	-0.52624000	-2.25544600
C	-3.74054600	-2.39796500	-2.09951700
C	-2.89194000	-3.14968700	-1.27509300
H	-2.35111600	-2.62806500	-0.48805800
C	-2.77939200	-4.52322100	-1.41238700
H	-2.12710600	-5.08339200	-0.74868900
C	-3.52815800	-5.17141800	-2.39345600
H	-3.45598400	-6.24841400	-2.51446600
C	-4.37877600	-4.45290000	-3.22869100
H	-4.94174000	-4.98357800	-3.98769900
C	-4.50062000	-3.06587600	-3.09784100
Cu	0.65916600	-1.75167900	0.40644500
S	0.22149600	-2.37882300	-1.77108400
S	6.21580800	-3.57308000	1.53390000
N	2.71773600	-1.73417700	-0.13156600
C	1.81237100	-1.87847100	-2.39374300
C	2.01603400	-1.81189600	-3.77682800
H	1.18685700	-2.05654900	-4.43560600
C	3.24035600	-1.42238000	-4.30828600
H	3.36580700	-1.36054900	-5.38540600
C	4.28352200	-1.06797600	-3.45456200
H	5.22872900	-0.71399300	-3.85471400
C	4.10597400	-1.15162700	-2.07969400
H	4.91009300	-0.85182900	-1.41227000
C	2.89188200	-1.58925500	-1.52825800
C	3.75999100	-2.10336300	0.55242200
H	4.67475100	-2.35346600	0.00194900
C	3.83692500	-2.25063500	1.98858900
C	2.84699400	-1.71988800	2.82719400
H	2.04537200	-1.14518500	2.36973100

C	2.89986500	-1.86320900	4.20345800
H	2.11905900	-1.43352300	4.82442900
C	3.98008000	-2.53384300	4.77261600
H	4.04451300	-2.65573400	5.85002500
C	4.99720800	-3.04679500	3.97204600
H	5.82714600	-3.55793200	4.44537900
C	4.94737800	-2.91738100	2.58071800
C	7.45978100	-4.14487700	2.70586800
H	8.29274700	-4.49624400	2.09675700
H	7.80779300	-3.33218700	3.34610700
H	7.09315600	-4.97549200	3.31169400
Cu	0.70638000	1.36716700	-0.20058100
S	1.08228500	1.88952800	2.03586700
S	4.49405900	4.77100800	-2.70466500
N	2.82232800	1.61633600	-0.41149300
C	2.81158600	1.47388100	2.01886900
C	3.51574900	1.31678500	3.21636600
H	2.97036300	1.38442200	4.15404300
C	4.88197400	1.05341300	3.21938900
H	5.39992400	0.90832400	4.16319900
C	5.57047600	0.94228400	2.01325500
H	6.63021800	0.70509800	2.00241600
C	4.89262000	1.12839400	0.81349400
H	5.42147600	1.03786900	-0.13236400
C	3.51909000	1.40978100	0.79944300
C	3.43965300	2.29289600	-1.33248400
H	4.40493300	2.75646200	-1.08772900
C	2.96102400	2.49067200	-2.68353000
C	2.08189500	1.56599800	-3.26388400
H	1.76323400	0.71662000	-2.66246800
C	1.66795800	1.68917400	-4.57993500
H	0.99968400	0.94873800	-5.00989200
C	2.13613900	2.75819000	-5.34228300
H	1.82542800	2.86961600	-6.37708000
C	3.00674700	3.69533600	-4.79330500
H	3.34544900	4.52129400	-5.40791500
C	3.43263700	3.57917500	-3.46644200
C	5.04235200	5.77630900	-4.09716700
H	5.78257200	6.46480800	-3.68933100
H	5.51438300	5.16303500	-4.86693000
H	4.22234600	6.35632100	-4.52433900
Cu	-0.38017300	0.13821100	1.81227200
S	-0.37770800	-2.10404800	2.42001400
S	-5.32951300	2.40793700	4.20283400
N	-2.50281300	0.04187400	2.01315600
C	-2.10470400	-2.36637100	2.09487100

C	-2.61225700	-3.67042800	2.07179300
H	-1.92698500	-4.49707200	2.24012300
C	-3.95710700	-3.91659200	1.81966200
H	-4.32192400	-4.93917800	1.78868500
C	-4.81836500	-2.85167800	1.56108200
H	-5.86003600	-3.03151200	1.31318200
C	-4.33589300	-1.55009200	1.60399300
H	-5.00132000	-0.72055000	1.37811200
C	-2.99163800	-1.28205000	1.90544500
C	-3.32866800	0.93177500	2.47830200
H	-4.30875200	0.59069300	2.83233100
C	-3.07988200	2.35002200	2.60643500
C	-2.00387900	2.95939500	1.94707900
H	-1.38952900	2.34317400	1.29450900
C	-1.74815200	4.31527700	2.06230900
H	-0.90880800	4.75606000	1.53216300
C	-2.59819500	5.10007900	2.83824400
H	-2.41937200	6.16651200	2.94098900
C	-3.69395200	4.53307500	3.48357900
H	-4.33925600	5.17142500	4.07525300
C	-3.95472400	3.16317000	3.38196900
C	-6.22650000	3.81665300	4.88078100
H	-7.12414000	3.39790900	5.33599900
H	-6.52102500	4.51650900	4.09654400
H	-5.64933700	4.33052100	5.65160900
C	-6.47405000	-3.35135700	-5.05740600
H	-7.19853200	-2.79989100	-5.65678400
H	-5.84147800	-3.93876900	-5.72542100
H	-7.00951200	-4.00699800	-4.36827300
$E_{electronic}$ (Ha) =	-12129.3573378		
H (Ha)=	-12128.383622		
G (Ha) =	-12128.572745		

Phenyl Acetylene			
C	3.23004200	0.00001300	-0.00001700
H	4.29617700	0.00005200	-0.00005100
C	2.01625200	-0.00004200	0.00002000
C	0.59324200	-0.00002900	0.00001200
C	-0.11975400	1.21186400	0.00000500
C	-0.11980100	-1.21188500	0.00000600
C	-1.50922900	1.20663500	-0.00000300
H	0.42758000	2.14970800	0.00000700
C	-1.50928300	-1.20660100	-0.00000400
H	0.42748100	-2.14975900	0.00000800
C	-2.20792100	0.00002800	-0.00000800

H	-2.04931700	2.14876000	-0.00000700
H	-2.04939500	-2.14871200	-0.00000800
H	-3.29381500	0.00005900	-0.00001600

$E_{electronic}$ (Ha) =	-308.360964774
H (Ha)=	-308.244079
G (Ha) =	-308.281916

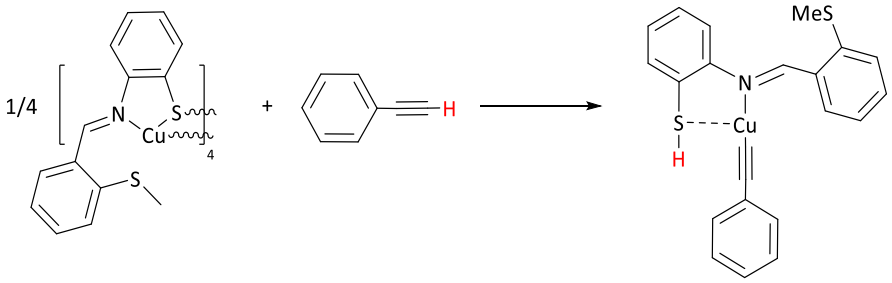

Complex **3.1**

Int **A**

Int **A**			
Cu	0.57073900	0.43609800	-0.05560800
S	-0.25517800	2.53320300	1.86497600
S	-4.63974800	-1.60927800	0.75610500
N	-1.33692400	0.79014900	-0.26425900
C	-1.17746400	3.11225100	0.46728100
C	-1.47876100	4.46195700	0.27141200
H	-1.10724300	5.20129700	0.97480300
C	-2.25571800	4.86053500	-0.81117100
H	-2.46785800	5.91541200	-0.95400900
C	-2.75850200	3.91502900	-1.70318000
H	-3.36184900	4.22385900	-2.55042700
C	-2.46970500	2.56954600	-1.51398300
H	-2.82055000	1.82084500	-2.21884400
C	-1.67559400	2.15832000	-0.43886900
C	-2.30434100	-0.07663000	-0.35246300
H	-3.32914900	0.30569100	-0.42029400
C	-2.13981400	-1.51230200	-0.37295900
C	-0.96686800	-2.09843700	-0.87977600
H	-0.17979600	-1.44703800	-1.25682300
C	-0.82340600	-3.47302700	-0.96018300
H	0.08381900	-3.90463900	-1.36916000
C	-1.86928300	-4.29203300	-0.53287600
H	-1.77533700	-5.37217500	-0.59344600
C	-3.04280100	-3.74271900	-0.02964600
H	-3.83361000	-4.40447000	0.30378700
C	-3.19967600	-2.35525900	0.05882100
C	-5.80818400	-2.98018800	0.83789800

H	-6.75708800	-2.53947300	1.14369800
H	-5.51007300	-3.72030600	1.58240800
H	-5.93329900	-3.45079300	-0.13881400
H	0.21226900	3.73895600	2.22511000
C	2.38418100	0.05389400	-0.03001300
C	3.59448700	-0.19818400	-0.01618100
C	4.98783000	-0.48185200	0.00200600
C	5.72849900	-0.55272300	-1.19505600
C	5.66854800	-0.69856500	1.21709900
C	7.09056100	-0.82749000	-1.17395400
H	5.21778500	-0.38824100	-2.13991300
C	7.03073100	-0.97345200	1.23030400
H	5.11134900	-0.64730700	2.14851900
C	7.74947000	-1.03939200	0.03689900
H	7.64199700	-0.87682200	-2.10898800
H	7.53530500	-1.13712100	2.17870000
H	8.81403700	-1.25404900	0.05036700
$E_{electronic}$ (Ha) =	-3340.65165842		
H (Ha)=	-3340.292291		
G (Ha) =	-3340.379605		
ΔG (Path 1)	0.181989 Ha = 28.6 kcal/mol		

Path 2. Deprotonation by the S group and formation of copper alkynyl monomer (SMe group in cis position):

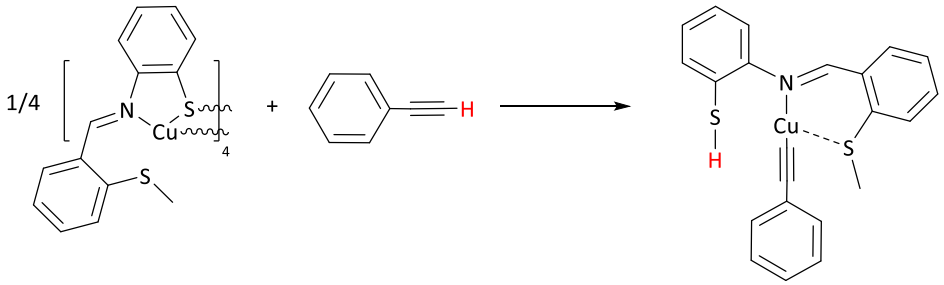

Complex **3.1** Int **B**

Int **B**			
Cu	0.01979600	-0.09605800	0.49088000
S	0.77126900	2.14836200	2.13204000
S	1.79348000	-1.37306900	1.57820900
N	1.71682800	0.90131100	-0.28741300
C	0.91042900	2.99502600	0.57863800
C	0.57166500	4.33898000	0.41277400
H	0.18811100	4.90655200	1.25532900
C	0.72107700	4.94725500	-0.82906300
H	0.43923200	5.98852000	-0.94982700

C	1.21938600	4.22396600	-1.91270600
H	1.32042600	4.69468100	-2.88525000
C	1.56952100	2.89002100	-1.75269700
H	1.91899800	2.30945700	-2.60161100
C	1.42488700	2.26316600	-0.50917700
C	2.69705600	0.34820800	-0.93098800
H	3.29807300	0.95201600	-1.62192300
C	3.07589300	-1.04543100	-0.85334400
C	3.90165400	-1.51043600	-1.89323100
H	4.22184200	-0.79626100	-2.64769400
C	4.28140900	-2.83898300	-1.98879700
H	4.90762200	-3.17228400	-2.80918900
C	3.84636300	-3.73583600	-1.01621200
H	4.12787700	-4.78295100	-1.06989600
C	3.06336200	-3.30035200	0.04931400
H	2.76871300	-4.01704200	0.80629700
C	2.67480200	-1.96307400	0.15560300
C	1.30697100	-2.88900100	2.42606000
H	0.66541500	-2.56590800	3.24589700
H	2.17230400	-3.40939100	2.83880900
H	0.73961400	-3.54542400	1.76434600
C	-1.79578400	-0.33381400	0.15149100
C	-3.00331200	-0.51835600	-0.05531800
H	-0.06585000	3.03430000	2.69371800
C	-4.38936000	-0.72721300	-0.28905200
C	-4.83499300	-1.49773600	-1.38317700
C	-5.36334100	-0.17091700	0.56616800
C	-6.19121200	-1.70033600	-1.60791900
H	-4.09865600	-1.93410900	-2.05274900
C	-6.71778600	-0.37803700	0.33518000
H	-5.03834400	0.42574600	1.41430600
C	-7.14099000	-1.14302500	-0.75176500
H	-6.50981700	-2.29809400	-2.45782100
H	-7.44922700	0.06083000	1.00863900
H	-8.20035300	-1.30327400	-0.92972900
$E_{electronic}$ (Ha) =	-3340.65333949		
H (Ha)=	-3340.294076		
G (Ha) =	-3340.380696		
ΔG (Path 2)	0.177625 Ha = 27.86 kcal/mol		

Path 3. Deprotonation by water and formation of copper alkynyl in tetranuclear complex:

H_2O			
O	0.00000000	0.00000000	0.11970300
H	0.00000000	0.75156000	-0.47881200

H	0.00000000	-0.75156000	-0.47881200
$E_{electronic}$ (Ha) =	-76.4174212		
H (Ha)=	-76.391862		
G (Ha) =	-76.413288		

H_3O^+			
H	0.24252300	-0.88916900	0.23457800
H	-0.89153400	0.23473900	0.23472300
H	0.64940900	0.65432100	0.23457900
O	-0.00005000	0.00001400	-0.08798500
$E_{electronic}$ (Ha) =	-76.81969281		
H (Ha)=	-76.780433		
G (Ha) =	-76.803371		

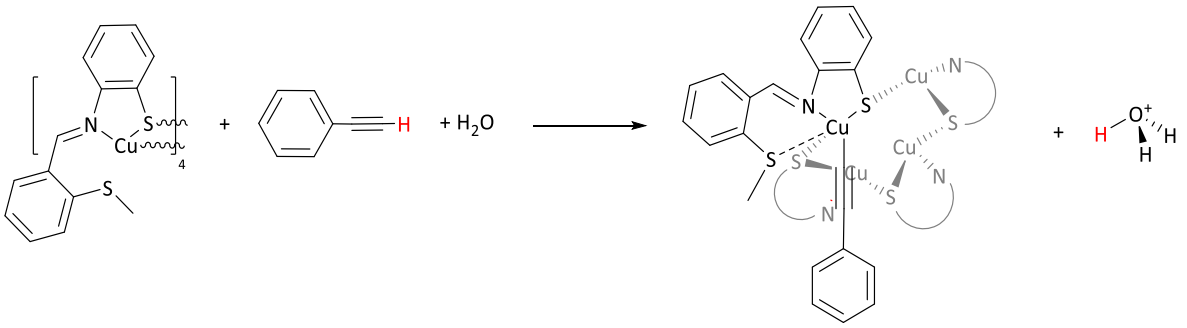

Complex **3.1**

Int **C**

Int **C**			
Cu	-2.09206000	1.75176300	1.03782800
S	-0.99781300	1.12145900	2.92620900
S	-6.47380100	-0.33783200	-0.90612000
N	-2.64698500	-0.50503100	0.95694200
C	-1.76749200	-0.44457700	3.21066200
C	-1.66066800	-1.03757900	4.47827900
H	-1.06369400	-0.53570300	5.23613400
C	-2.31180600	-2.22720300	4.78062200
H	-2.20916200	-2.66100700	5.77162600
C	-3.06083700	-2.87960300	3.79969400
H	-3.54088100	-3.83034700	4.01349900
C	-3.16258000	-2.32273600	2.53296400
H	-3.71256400	-2.84752300	1.75521000
C	-2.54848600	-1.09710300	2.22005700
C	-3.66863700	-0.74891800	0.19516700
H	-4.53445700	-1.31045400	0.57631300
C	-3.74070200	-0.24116400	-1.15886100

C	-2.55723500	0.08626800	-1.83197200
H	-1.61431400	-0.11147100	-1.32509600
C	-2.57241200	0.61697200	-3.11308900
H	-1.63568600	0.85058900	-3.61291600
C	-3.79464000	0.82475000	-3.74676900
H	-3.83077500	1.23305800	-4.75342700
C	-4.98977600	0.51698300	-3.09781800
H	-5.92766900	0.71194800	-3.60587900
C	-4.98112500	-0.00928000	-1.80402400
Cu	1.12991200	-0.09525800	-1.42528000
S	0.18090400	1.93088900	-1.00606800
S	4.73945900	0.00380300	-5.66716300
N	2.92587400	0.98570600	-1.94010400
C	1.64853200	2.91261700	-1.18019300
C	1.59895200	4.28261700	-0.89822000
H	0.65366300	4.71155500	-0.57671200
C	2.73273000	5.08250900	-0.98860300
H	2.67021000	6.13618700	-0.72864200
C	3.94926900	4.52102600	-1.37573800
H	4.84981300	5.12675700	-1.41494500
C	4.00878600	3.17224800	-1.70444500
H	4.96091800	2.72258200	-1.97496200
C	2.86761200	2.35751400	-1.63374500
C	3.75517300	0.60237000	-2.86363300
H	4.25875200	1.35626700	-3.48443200
C	4.10697000	-0.77964600	-3.11476300
C	3.99154400	-1.72408600	-2.08362900
H	3.58684400	-1.38876900	-1.13119500
C	4.41322300	-3.03258000	-2.25028500
H	4.32553400	-3.74102900	-1.43136400
C	4.95825500	-3.42031800	-3.47421400
H	5.29755100	-4.44131800	-3.62353100
C	5.07521500	-2.50932600	-4.51999000
H	5.49105700	-2.84235200	-5.46405000
C	4.65779000	-1.18377900	-4.35928200
C	5.72343400	-0.83975800	-6.92065600
H	5.88779000	-0.10607500	-7.70996500
H	6.68961300	-1.15319600	-6.52078900
H	5.19269900	-1.69513300	-7.34270900
Cu	0.58930500	0.68260600	1.04624700
S	1.84495300	-1.12922100	2.03728500
S	4.31123100	5.34461800	3.32659300
N	2.64014700	1.76737900	1.60624100
C	3.43133800	-0.53399400	1.49201700
C	4.48207000	-1.43337500	1.27874400
H	4.28692000	-2.49606600	1.40207800

C	5.74230600	-0.99487300	0.88521500
H	6.53082100	-1.71855900	0.69795900
C	5.97322700	0.36716100	0.69925200
H	6.94193200	0.72150500	0.35902100
C	4.95216800	1.27756800	0.94229200
H	5.11764700	2.33786700	0.76821200
C	3.68044400	0.85147400	1.35885700
C	2.97095700	2.89478100	2.14819900
H	4.01546600	3.04280000	2.45439400
C	2.07695600	4.00501200	2.41259300
C	0.71386400	3.93070900	2.09187400
H	0.34730500	3.02743100	1.60733900
C	-0.15488200	4.97969000	2.34177600
H	-1.20593400	4.88749100	2.08081300
C	0.34148700	6.14981400	2.91418900
H	-0.32064200	6.98661200	3.11742900
C	1.69326200	6.26610200	3.22321300
H	2.05166300	7.19285200	3.65536100
C	2.57721000	5.20878800	2.98114900
C	4.46592800	7.00387300	4.01355100
H	5.52442100	7.12384500	4.24520100
H	4.17513200	7.76840600	3.29060600
H	3.88962300	7.11385400	4.93409100
Cu	0.76389400	-1.97005300	0.26863000
S	0.80928900	-2.25711200	-2.06145400
S	-0.33354400	-7.46521700	1.35055900
N	-0.78193600	-3.42636700	0.18980600
C	-0.91108600	-2.72213100	-2.12995900
C	-1.63993700	-2.62100200	-3.31762300
H	-1.16017300	-2.18263800	-4.18896600
C	-2.96217600	-3.05046300	-3.38835300
H	-3.51572700	-2.93612400	-4.31623900
C	-3.57901700	-3.59571100	-2.26442600
H	-4.61913800	-3.90664000	-2.30230700
C	-2.85982500	-3.73111700	-1.08145000
H	-3.33284800	-4.14593100	-0.19404600
C	-1.52859600	-3.30356700	-1.00297700
C	-0.89625300	-4.54452100	0.83910600
H	-1.48288100	-5.35552900	0.38638200
C	-0.28488400	-4.82724100	2.12101400
C	0.00012500	-3.78721100	3.01620900
H	-0.27779900	-2.77609400	2.72965000
C	0.55184400	-4.03898800	4.26280000
H	0.74418600	-3.21652600	4.94559200
C	0.82567900	-5.35381800	4.63356500
H	1.25528600	-5.56980200	5.60762300

C	0.54772000	-6.40878800	3.76792400
H	0.77632900	-7.42106300	4.08095000
C	-0.00928100	-6.16626200	2.50913800
C	-0.08220500	-8.95617100	2.33232800
H	-0.36458000	-9.78639900	1.68475400
H	-0.72294300	-8.96198800	3.21611000
H	0.96310700	-9.07792900	2.62212200
C	-7.73852900	0.40443700	-1.95687300
H	-8.66793700	0.34938600	-1.38882600
H	-7.50457900	1.45483100	-2.15288900
H	-7.86517700	-0.14111200	-2.89426000
C	-3.45459100	2.74381100	0.18176700
C	-4.49257700	3.16316300	-0.35301100
C	-5.69931400	3.56001400	-0.98955900
C	-5.73957600	3.84322100	-2.37168000
C	-6.90732700	3.65868400	-0.26641400
C	-6.92831700	4.20332500	-2.99563400
H	-4.82139100	3.76470900	-2.94807500
C	-8.09322300	4.01819000	-0.89603600
H	-6.89925000	3.43943000	0.79837900
C	-8.11319800	4.29326800	-2.26389700
H	-6.93114800	4.41280800	-4.06234300
H	-9.01006800	4.08184800	-0.31549600
H	-9.04120100	4.57301100	-2.75411900
$E_{electronic}$ (Ha) =	-12437.24494		
H (Ha)=	-12436.16516		
G (Ha) =	-12436.37455		
ΔG (Path 3)	0.090025 Ha = 56.49 kcal/mol		

Path 4. Proton capture by S group and formation of dimer complex (proton and alkyne group located on different monomers and SMe group located in trans position):

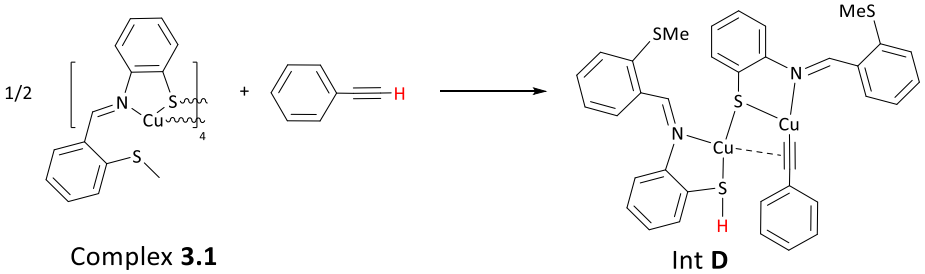

Complex **3.1** Int **D**

Int **D**			
Cu	-0.27246600	-1.99400500	0.92166800
S	1.82088600	-1.91938900	2.07853300
S	-4.15283700	1.77391600	0.64099300
N	-0.58462900	-0.15207200	1.81694700

C	1.81009200	-0.12554500	2.10751200
C	3.02095000	0.55665200	2.22757200
H	3.94829100	-0.00838300	2.26597300
C	3.04099500	1.94488600	2.29283000
H	3.98853800	2.46874500	2.36911300
C	1.84007200	2.65419100	2.27455300
H	1.84446400	3.73842500	2.33749900
C	0.63239000	1.98335200	2.15929700
H	-0.28728000	2.55861900	2.11013100
C	0.59161700	0.58537500	2.04525800
C	-1.77231700	0.36743300	1.87597200
H	-1.92235400	1.43354600	2.08630800
C	-2.94790300	-0.45610700	1.67178400
C	-2.91014400	-1.81625600	2.03046900
H	-2.01716400	-2.19631900	2.52532000
C	-4.00579900	-2.64480000	1.84285000
H	-3.95922600	-3.68804800	2.13746200
C	-5.16931200	-2.11278000	1.29168200
H	-6.03756800	-2.74642700	1.13438800
C	-5.24190800	-0.76859500	0.93986200
H	-6.15805800	-0.38909900	0.50257900
C	-4.14471500	0.07708700	1.12555900
C	-5.79354600	1.98160800	-0.07158600
H	-5.83933900	3.01675400	-0.41025400
H	-5.92772000	1.31958100	-0.93093100
H	-6.58182900	1.81456700	0.66488900
S	-0.93763000	-3.02636600	-0.95577000
S	-1.33252200	3.92502900	-0.19319100
N	-0.82984000	-0.07404900	-1.71726700
C	-2.28102400	-2.03424500	-1.56601300
C	-3.53245700	-2.62364000	-1.76810200
H	-3.66198500	-3.67178300	-1.51176600
C	-4.59835300	-1.89040600	-2.27757900
H	-5.56142900	-2.37028800	-2.42733100
C	-4.42223000	-0.54603900	-2.59967700
H	-5.23777200	0.02939500	-3.02881000
C	-3.18496200	0.05525500	-2.40357100
H	-3.03695700	1.09121000	-2.69691800
C	-2.10248600	-0.66726800	-1.87530800
C	-0.81797200	1.18484800	-1.38058500
H	-1.77166100	1.64542300	-1.08851900
C	0.33550200	2.06052700	-1.36312100
C	1.57172300	1.64759500	-1.88622600
H	1.64594000	0.64326300	-2.29105100
C	2.68049700	2.47664800	-1.87880200
H	3.62641900	2.12474700	-2.27953200

C	2.56237600	3.76611300	-1.36142500
H	3.41926400	4.43356900	-1.34840200
C	1.34538800	4.21720700	-0.86112200
H	1.28381300	5.22608800	-0.47065300
C	0.22212300	3.38446400	-0.85054000
C	-0.95788400	5.57161500	0.43717000
H	-1.88582500	5.92761300	0.88522500
H	-0.18483000	5.53721500	1.20823600
H	-0.66727800	6.25746600	-0.36073100
Cu	0.78574700	-1.53152000	-1.39506700
H	2.55921500	-2.01306500	0.93543300
C	3.86431900	-1.29560700	-0.98175300
C	2.65991800	-1.42319000	-1.25649700
C	5.23942900	-1.10973500	-0.67297500
C	6.10500900	-0.45185700	-1.57088600
C	5.77724800	-1.56806000	0.54781800
C	7.44509800	-0.26053100	-1.25686800
H	5.70805500	-0.09525300	-2.51761500
C	7.11737400	-1.36929300	0.85694600
H	5.12696800	-2.08711700	1.24898200
C	7.95908000	-0.71515000	-0.04244300
H	8.09343000	0.24899800	-1.96459400
H	7.50811500	-1.72982400	1.80459000
H	9.00644500	-0.56205400	0.20043100
$E_{electronic}$ (Ha) =	-6373.001616		
H (Ha)=	-6372.399318		
G (Ha) =	-6372.522937		
ΔG (Path 4)	0.090703 Ha = 28.45 kcal/mol		

Path 5. Proton capture by S group and formation of dimer complex (proton and alkyne group located on different monomers and SMe group located in cis position):

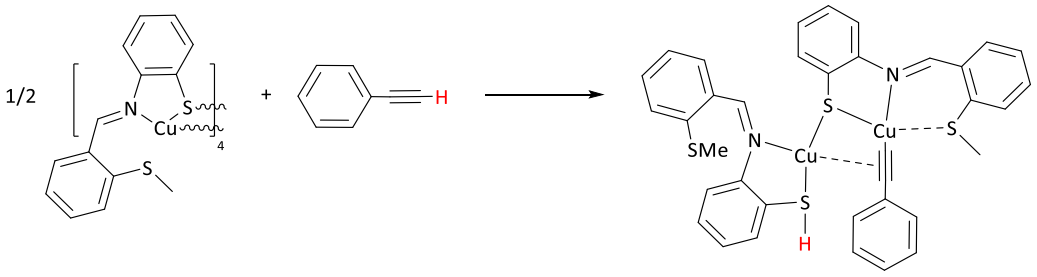

Complex **3.1** Int **E**

Int **E**			
Cu	1.33659400	-0.34083800	0.20861000
S	2.33824800	0.79323900	-1.74045200

S	0.51183400	-2.46713800	0.75040500
N	3.29926900	-1.30706400	0.02073200
C	3.91037100	0.83999600	-0.89166100
C	4.79888000	1.90498000	-1.01834400
H	4.52751200	2.76235400	-1.62773500
C	6.01772800	1.87595200	-0.34660000
H	6.69458300	2.72064300	-0.42826400
C	6.36302800	0.76902900	0.42810200
H	7.31194800	0.74645600	0.95483800
C	5.49069600	-0.30764600	0.53885600
H	5.73786700	-1.16173100	1.16331200
C	4.25338800	-0.28214800	-0.11500300
C	3.69096400	-2.53199900	-0.10360900
H	4.74771900	-2.72453700	-0.33556900
C	2.87999800	-3.73386900	-0.06537200
C	3.58435100	-4.90937400	-0.39817600
H	4.65342900	-4.82450900	-0.57622400
C	2.96234000	-6.13856200	-0.52687500
H	3.53859200	-7.01990700	-0.78660700
C	1.58674100	-6.21886600	-0.32692200
H	1.06917100	-7.16791800	-0.42676700
C	0.86147900	-5.08485300	0.02075400
H	-0.20296900	-5.18268800	0.19839600
C	1.48141100	-3.83978300	0.16877700
C	-1.17142200	-2.90224900	0.25419400
H	-1.73872100	-1.96959400	0.34253000
H	-1.18190300	-3.26070600	-0.77655400
H	-1.60051600	-3.64809100	0.92516500
S	1.36523300	1.19349300	2.01091000
S	-1.11794400	0.25020000	-1.75630300
N	-0.39967300	2.48925600	-0.09352900
C	1.66957600	2.71526300	1.14970600
C	2.85602800	3.41577400	1.38774400
H	3.58032600	2.99271900	2.07998700
C	3.12334300	4.62120800	0.74585100
H	4.05993400	5.13698400	0.93829700
C	2.20341600	5.14447500	-0.16173600
H	2.41223200	6.07282200	-0.68478200
C	1.02181900	4.45833200	-0.41878800
H	0.32357900	4.83442800	-1.16225700
C	0.73039600	3.24812000	0.23307100
C	-1.50261400	3.08845500	-0.42209500
H	-1.61676100	4.17221700	-0.26709800
C	-2.66000100	2.41437800	-0.96189100
C	-3.87953300	3.11064300	-0.88343000
H	-3.86796800	4.10665300	-0.44639600

C	-5.07075000	2.55710200	-1.32270300
H	-6.00045400	3.10961200	-1.23470700
C	-5.05039700	1.27957100	-1.87890300
H	-5.97173500	0.81322200	-2.21811400
C	-3.85503800	0.58005800	-2.00523700
H	-3.88038300	-0.40849500	-2.44845300
C	-2.64555100	1.12102300	-1.55711200
C	-1.58008800	-1.10802200	-2.85447400
H	-0.64593200	-1.63378200	-3.06341200
H	-2.27142500	-1.80653400	-2.37648200
H	-2.00492700	-0.74734200	-3.79366800
Cu	-0.76469100	0.74631300	1.42473200
H	2.02946900	2.09258900	-1.56034100
C	-3.68036900	-0.31670200	1.39279700
C	-2.51599900	0.08477000	1.52839000
C	-5.00171600	-0.76437700	1.12893600
C	-6.12387800	-0.11999200	1.68821100
C	-5.23063400	-1.84829500	0.25529800
C	-7.41330500	-0.53554900	1.37771300
H	-5.96677000	0.72068900	2.35912800
C	-6.52210700	-2.26053600	-0.04859100
H	-4.37560500	-2.35284300	-0.18961800
C	-7.62157900	-1.60644500	0.50836400
H	-8.26305500	-0.01893900	1.81631300
H	-6.67282600	-3.09573700	-0.72760000
H	-8.63054500	-1.92801600	0.26694200

$E_{electronic}$ (Ha) =	-6372.995577
H (Ha)=	-6372.393296
G (Ha) =	-6372.519458
ΔG (Path 5)	0.097661 Ha = 30.64 kcal/mol

Path 6. Proton capture by S group and formation of dimer complex (proton and alkyne group located on the same monomer and SMe group located in trans position):

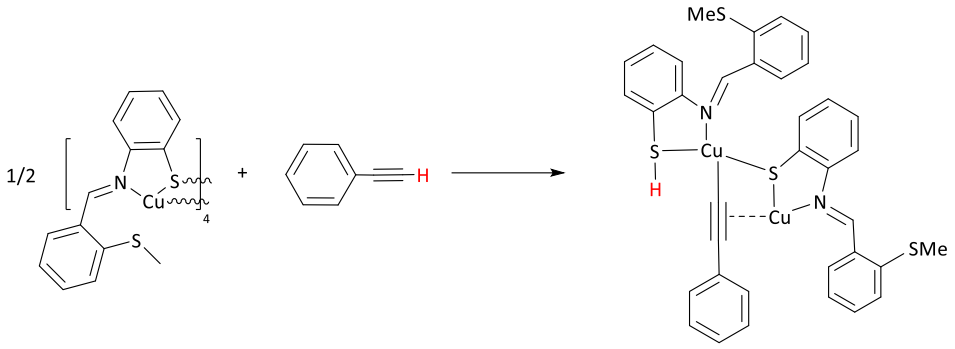

Complex **3.1** Int **F**

Int **F**			
Cu	0.32013700	-0.33167600	-1.37411100
S	0.25439800	1.75633900	-2.67166000
S	6.17737700	-0.35599400	-1.20917800
N	2.06667400	0.56277700	-0.73063100
C	0.91128700	2.61720400	-1.25140100
C	0.59899600	3.94818900	-0.97575700
H	-0.08178400	4.48788200	-1.62724100
C	1.16457400	4.57644800	0.13021000
H	0.90248800	5.60624700	0.35218900
C	2.05804100	3.88665900	0.94928500
H	2.48230800	4.36977400	1.82363800
C	2.38216300	2.56579800	0.67174300
H	3.03261100	2.00466200	1.33719600
C	1.81613700	1.91768400	-0.43320600
C	3.26877300	0.10530200	-0.55428800
H	4.06384400	0.81803900	-0.30308600
C	3.65260100	-1.28542200	-0.64909200
C	2.70722100	-2.30382000	-0.43882000
H	1.68099300	-2.01657100	-0.21474400
C	3.07174000	-3.63954300	-0.45393800
H	2.32802800	-4.40954100	-0.27507000
C	4.40539100	-3.97965300	-0.68392900
H	4.70871200	-5.02243200	-0.69881800
C	5.36307100	-2.99430700	-0.89751100
H	6.38896000	-3.28963300	-1.08458300
C	5.00863500	-1.64081600	-0.88347100
C	7.76011400	-1.21602600	-1.13044200
H	8.52080700	-0.43937900	-1.20959700
H	7.88076700	-1.73541700	-0.17812000
H	7.88331800	-1.91242000	-1.96165900
S	0.88404200	-0.89170600	2.62199500
S	-2.96031800	3.31453900	-1.60498200

N	-1.37888900	0.89827500	1.61378100
C	0.56788800	0.78304900	3.06212000
C	1.40470000	1.42070400	3.99302000
H	2.22036200	0.84902700	4.42885700
C	1.21584000	2.74742200	4.35654400
H	1.88178700	3.20691600	5.08207000
C	0.16085800	3.47851800	3.80650500
H	-0.01263900	4.50868100	4.10364400
C	-0.68233300	2.87165900	2.88798100
H	-1.53043100	3.42409400	2.49145400
C	-0.49076300	1.53698100	2.48866600
C	-2.02763000	1.59989300	0.73196200
H	-1.74224100	2.64562500	0.54521400
C	-3.15096600	1.07337500	-0.01663200
C	-3.75333000	-0.13439200	0.37511300
H	-3.34732200	-0.64338900	1.24609600
C	-4.83486600	-0.66554600	-0.30811100
H	-5.27506200	-1.60423300	0.01610000
C	-5.34618100	0.01825900	-1.40935200
H	-6.19480800	-0.38022700	-1.95754400
C	-4.78402100	1.22608800	-1.81509300
H	-5.20749800	1.74023800	-2.66989300
C	-3.69476500	1.76910400	-1.12937500
C	-3.92090000	3.80597000	-3.04881700
H	-3.48660200	4.74950300	-3.37957300
H	-3.83478100	3.07409900	-3.85397300
H	-4.96884100	3.96993100	-2.79214500
Cu	-0.59385200	-1.13002100	0.97518700
H	-0.99861400	2.27469300	-2.56919700
C	-1.73503200	-2.44105900	-0.36959100
C	-0.93865100	-1.66885400	-0.96110200
C	-2.74961300	-3.35819200	0.03395800
C	-3.08618800	-3.50585200	1.39222100
C	-3.46042400	-4.10714100	-0.92345800
C	-4.10593600	-4.36664500	1.77910200
H	-2.53582800	-2.92703800	2.13339400
C	-4.47481800	-4.96963900	-0.52726700
H	-3.21073900	-3.99713500	-1.97483100
C	-4.80486300	-5.10177400	0.82198700
H	-4.35580700	-4.46483000	2.83157200
H	-5.01552500	-5.53978700	-1.27736900
H	-5.60171600	-5.77415900	1.12535900

$E_{electronic}$ (Ha) =	-6373.001786
H (Ha)=	-6372.399746
G (Ha) =	-6372.528031

ΔG (Path 6)	0.080515 Ha = 25.26 kcal/mol

Path 7. Proton capture by S group and formation of dimer complex (proton and alkyne group located on the same monomer and SMe group located in cis position):

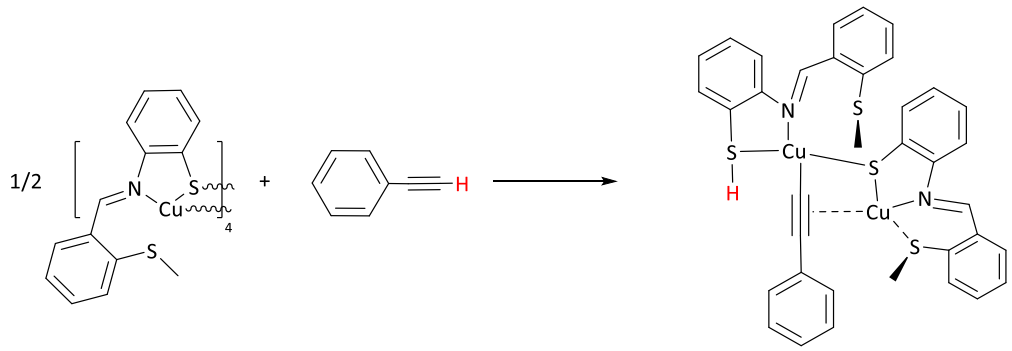

Complex **3.1** Int **G**

Int **G**			
Cu	1.17551400	0.01116400	-0.28351400
S	-0.19779100	1.48872000	2.21249100
S	2.43471300	-2.41870800	-0.89654600
N	0.51766400	-1.22650200	1.30551500
C	-1.33733800	0.13287300	2.10924600
C	-2.67931900	0.24550200	2.48213600
H	-3.06359900	1.20639300	2.81688100
C	-3.51927300	-0.86454500	2.43930700
H	-4.56439400	-0.75074300	2.71329000
C	-3.02175700	-2.10465000	2.04835900
H	-3.67222700	-2.97329900	2.01355100
C	-1.68300500	-2.22961700	1.68856200
H	-1.27964000	-3.18178200	1.35152200
C	-0.83820900	-1.11862400	1.70048200
C	1.25640400	-2.02494700	2.00926400
H	0.81691100	-2.50583800	2.89330800
C	2.68728900	-2.23553000	1.82936100
C	3.42934400	-2.34054700	3.01756900
H	2.89070100	-2.35976100	3.96209000
C	4.81643500	-2.35650500	3.00711100
H	5.36990300	-2.41002800	3.93856100
C	5.48470900	-2.29575600	1.78552000
H	6.57034000	-2.29880600	1.75477700
C	4.77192900	-2.27022600	0.59086700
H	5.31348500	-2.27903100	-0.34899900
C	3.37371800	-2.25892700	0.59072300
C	3.57765500	-1.81191100	-2.15373700

H	2.98999100	-1.72594000	-3.06957300
H	3.93569400	-0.81824700	-1.86543700
H	4.40691600	-2.49875300	-2.33118500
S	-0.23437100	-0.23281800	-2.20824200
S	-2.82193500	2.57060700	-0.00417500
N	-2.98681700	-0.57718000	-0.94814100
C	-1.16782200	-1.74077500	-2.04725200
C	-0.62545800	-2.93681600	-2.53511700
H	0.36087500	-2.91353300	-2.99113500
C	-1.32173500	-4.13635200	-2.44529800
H	-0.86925000	-5.05035900	-2.81880300
C	-2.58983800	-4.16461100	-1.86280900
H	-3.13055400	-5.10087900	-1.76483800
C	-3.15312500	-2.98917900	-1.38758700
H	-4.12038300	-3.01619700	-0.89304600
C	-2.46519000	-1.76946600	-1.48033700
C	-4.26545100	-0.39459900	-0.90205000
H	-4.93120000	-1.14920600	-1.34116300
C	-4.98584100	0.70391300	-0.27568000
C	-6.35739800	0.43463000	-0.07823400
H	-6.73930900	-0.52361000	-0.42157100
C	-7.21270400	1.32625600	0.54623700
H	-8.25743500	1.06881700	0.68556100
C	-6.71705000	2.54831400	0.99325700
H	-7.36543100	3.26255000	1.49031700
C	-5.37471700	2.85301300	0.80112400
H	-4.98544300	3.80397900	1.15436700
C	-4.50648300	1.96325800	0.16305100
C	-3.08443100	3.94400000	-1.16857400
H	-2.11023200	4.40883700	-1.32076900
H	-3.47016600	3.57107600	-2.11697100
H	-3.77077500	4.67165700	-0.73386100
Cu	-1.58679200	0.95862500	-0.91483500
H	-1.12956800	2.39793900	2.54559300
C	3.77799600	1.76347500	-0.40089800
C	2.69752300	1.15738400	-0.32669600
C	5.02354300	2.44266600	-0.48059400
C	6.23182700	1.72759900	-0.62535200
C	5.09811900	3.85026200	-0.41795900
C	7.45067600	2.39019700	-0.70411900
H	6.19478900	0.64151700	-0.67346900
C	6.32060800	4.50643100	-0.49670800
H	4.17896900	4.41954700	-0.30643400
C	7.50454200	3.78296100	-0.64058000
H	8.36662500	1.81563000	-0.81580200
H	6.35008300	5.59185200	-0.44596000

H	8.45858600 4.29840200 -0.70229800
$E_{electronic}$ (Ha) =	-6372.981012
H (Ha)=	-6372.378685
G (Ha) =	-6372.506296
ΔG (Path 7)	0.123985 Ha = 38.9 kcal/mol

Calculations demonstrate Int **F** with the lowest ΔG (25.2 kcal/mol) as the most thermodynamically favorable copper alkynyl intermediate. In this pathway the acidic proton in the terminal alkyne is captured by the basic S arm which results in formation of the dimeric copper complex with the alkynyl coordinated to the copper on the same monomer while the SMe group is located in the trans position. This finding suggests a bifunctional role for the thiolate ligand in the catalyst.

3.7 References

1 Das, U. K.; Higman, C. S.; Gabidullin, B.; Hein J. E.; Baker, R. T., Efficient and selective iron-complex-catalyzed hydroboration of aldehydes, *ACS. Catal.*, 2018, **8**, 1076.

2 Elsby, M. R.; Son, M.; Oh, C.; Martin, J.; Baik M. H.; Baker, R. T., Mechanistic study of metal-ligand cooperativity in Mn(II)-catalyzed hydroboration: Hemilabile SNS ligand enables metal hydride-free reaction pathway, *ACS. Catal.*, 2021, **11**, 9043.

3 Ataie, S.; Hogeterp, S.; Ovens, J. S.; Baker, R. T., SNS ligand-assisted catalyst activation in Zn-catalysed carbonyl hydroboration, *Chem. Commun.*, 2022, **58**, 3795.

4 Ataie, S.; Lohoar, M. I.; Mangin, L. P.; Baker, R. T., Coinage metal amido and thiolate SNS complexes: Consequences of catalyst speciation in Cu(I)-catalysed carbonyl hydroboration, *Chem. Commun.,* 2023, **59**, 4044.

5 Ataie, S.; Dudra, S. L.; Johnson, E. R.; Baker, R. T., Selective cobalt(II)-SNS dithiolate complex-catalyzed bifunctional hydroboration of aldehydes: Kinetic and mechanistic studies, *ACS Catal.*, 2023, **13**, 10076.

6 Elsby, M. R.; Baker, R. T., Cu(I)-SNS complexes for outer-sphere hydroboration and hydrosilylation of carbonyls, *Chem. Commun.*, 2019, **55**, 13574.

7 Ataie, S.; Ovens, J. S.; Baker, R. T., Solvent-free Zn (NSNO) complex-catalysed dihydroboration of nitriles, *Chem. Commun.,* 2022, **58***,* 8266.

8 Ataie, S.; Baker, R. T., Comparing B-H bond activation in $Ni^{II}X$(NNN)-catalyzed nitrile dihydroboration (X = anionic N-, C-, O-, S-, or P- donor), *Inorg. Chem.,* 2022, **61**, 19998.

9 Ataie, S.; Baker, R. T., Bifunctional activation of NHC-zinc pre-catalyst for effective hydroboration of quinolines and nitriles, *ChemCatChem*, 2023, e202300649.

10 Das, U. K.; Daifuku, S. L.; Iannuzzi, T. E.; Gorelsky, S. I.; Korobkov, I.; Gabidullin, B.; Neidig, M. L.; Baker, R. T., Iron(II) complexes of a hemilabile SNS amido ligand: Synthesis, characterization and reactivity, *Inorg. Chem.*, 2017, **56**, 13766.

11 Das, U. K.; Daifuku, S. L.; Gorelsky, S. I.; Korobkov, I.; Neidig, M. L.; Roy, J. J. L.; Murugesu M.; Baker, R. T., Mononuclear, dinuclear, and trinuclear iron complexes featuring a new monoanionic SNS thiolate ligand, *Inorg. Chem.*, 2016, **55**, 987.

12 (a) Kolb, H. C.; Finn, M. G.; Sharpless, K. B.; Click chemistry: diverse chemical function from a few good reactions, *Angew. Chem., Int. Ed. Engl.,* 2001, **40**, 2004. (b) Tornøe, C. W.; Christensen, C.; Meldal, M.; Peptidotriazoles on solid phase: [1,2,3]-Triazoles by regiospecific copper(I)-catalyzed 1,3-dipolar cycloaddition of terminal alkynes to azides, *J. Org. Chem*., 2002, **67**, 3057. (c) Agard, N. J.; Prescher, J. A.; Bertozzi, C. R., A strain-promoted [3+2] azide-alkyne cycloaddition for covalent modification of biomolecules in living system, *J. Am. Chem. Soc.,* 2004, **126**, 15046.

13 Kolb, H. C.; Sharpless, K. B., The growing impact of click chemistry on drug discovery, *Drug Discov. Today Rev.,* 2003, **8**, 1128.

14 Paul, R.; Dutta, D.; Dash, J., Target-directed azide-alkyne cycloaddition for assembling HIV-1 TAR RNA binding ligands, *Angew. Chem., Int. Ed.*, 2020, **59**, 12407.

15 Wu, P.; Feldman, A. K.; Nugent, A. K.; Hawker, C. J.; Scheel, A.; Voit, B.; Pyun, J.; Frechet, J. M. J.; Sharpless, K. B.; Fokin, V. V., Efficiency and fidelity in a click-chemistry route to triazole dendrimers by the copper(I)-catalyzed ligation of azides and alkynes, *Angew. Chem., Int. Ed. Engl.*, 2004, **43**, 3928.
16 Rostovtsev, V.; Green, L. G.; Fokin, V. V.; Sharpless, K. B., A stepwise Huisgen cycloaddition process: Copper(I)-catalyzed regioselective ligation of azides and terminal alkynes, *Angew. Chem., Int. Ed.*, 2002, **41**, 2596.
17 Mandoli, A., Azide-alkyne cycloaddition reaction (CuAAC), *Molecules,* 2016, **21**, 1174.
18 Alonso, F.; Moglie Y.; Radivoy, G., Copper nanoparticles in click chemistry, *Acc. Chem. Res*., 2015, **48**, 2516.
19 Molteni, G.; Bianchi, C. L.; Marinoni, G.; Santo, N.; Ponti, A., Cu/Cu-oxide nanoparticles as catalyst in the click azide-alkyne cycloaddition, *New. J. Chem*., 2006, **30**, 1137-1139.
20 Hein, J. E.; Fokin, V. V., Copper-catalyzed azide-alkyne cycloaddition (CuAAC) and beyond: New reactivity of copper(I) acetylides, *Chem. Soc. Rev*., 2010, **39**, 1302-1315.
21 Appukkuttan, P.; Dehaen, W.; Fokin, V. V.; van der Eycken, E., A microwave-assisted click chemistry synthesis of 1,4-disubstituted 1,2,3-triazoles via a copper(I)-catalyzed three-component reaction, *Org. Lett.*, 2004, **6**, 4223-4225.
22 Wang, F.; Fu, H.; Jiang, Y. Y.; Zhao, Y. F., Quick and highly efficient copper-catalyzed cycloaddition of aliphatic and aryl azides with terminal alkynes on water, *Green Chem.*, 2008, **10**, 452.
23 Bagherzadeh, M.; Mahmoudi, H.; Ataie, S.; Hafezi-Kahnamouei, M.; Shahrokhian, S.; Bellachioma, G.; Vaccaro, L., Synthesis, characterization and comparison of two copper(II) complexes containing Schiff-base and diazo ligands as new catalysts in CuAAC reaction, *Inorg. Chim. Acta*., 2019, **492**, 213.
24 Ahlquist, M.; Fokin, V. V., Enhanced reactivity of dinuclear copper(I) acetylides in dipolar cycloadditions, *Organometallics,* 2007, **26**, 4389.
25 Worrell, B. T.; Malik, J. A.; Fokin, V. V., Direct evidence of a dinuclear copper intermediate in Cu(I)-catalyzed azide-alkyne cycloaddition, *Science*, 2013, **340**, 457-460.
26 Gonzalez-Lainez, M.; Gallego, M.; Munarriz, J.; Azpiroz, R.; Passarelli, V.; Jimenez, M. V.; Perez-Torrente, J. J., Copper-catalyzed azide-alkyne cycloaddition (CuAAC) by functionalized NHC-based polynuclear catalyst: Scope and mechanistic insight, *Organometallics*, 2022, **41**, 2154-2169.
27 Xu, Z.; Zhao, S. J.; Liu, Y., 1,2,3-triazole-containing hybrids as potential anticancer agents: Current developments, action mechanisms and structure-activity relationships, *Eur. J. Med. Chem.,* 2019, **183**, 111700.
28 Kalvet, I.; Tammiku-Taul, J.; Maeorg, U.; Tamm, K.; Burk P.; Sikk, L., NMR and DFT study of the copper(I)-catalyzed cycloaddition reaction: H/D Scrambling of alkynes and variable reaction order of the catalyst, *ChemCatChem*, 2016, **8**, 1804-1808.

29 Lazreg, F.; Slawin, A. M. Z.; Cazin, C. S. J., Heteroleptic bis(N-heterocyclic carbene)copper(I) complexes: highly efficient systems for the [3+2] cycloaddition of azides and alkynes, *Organometallics*, 2012, **31**, 7969-7975.
30 Zhu, L.; Bassard, C. J.; Zhang, X.; Guha, P. M.; Clark, R. J., On the mechanism of copper(I)-catalyzed azide-alkyne cycloaddition, *Chem. Rec.,* 2016, **16**, 1501-1517.
31 Jin, L.; Tolentino, D. R.; Melaimi, M.; Bertrand, G., Isolation of bis(copper) key intermediates in Cu-catalyzed azide-alkyne click reaction, *Sci. Adv.,* 2015, **1**, No. e1500304.
32 Lal, S.; Rzepa, H. S.; Diez-Gonzalez, S., Catalytic and computational studies of N-heterocyclic carbene or phosphine-containing copper(I) complexes for the synthesis of 5-iodo-1,2,3-triazoles, *ACS. Catal.,* 2014, **4**, 2274.
33 All structures were optimized using the M06-L functional in conjunction with the implicit CPCM solvation model. A combination of 6-31g and def2tzvp basis sets was used; the latter for the copper atoms.
34 Albkuri, Y. M.; Oven, J. S.; Martin, J.; Baker, R. T., Nickel(II)-SNS thiolate complexes: Reactivity and solution dynamics, *Inorg. Chem*., 2021, **60**, 10934-10942.
35 Liu, N.; Jin, Z.; Zhang, H.; Jin, J., Antitumor evaluation of novel phenothiazine derivatives that inhibit migration and tubulin polymerization against gastric cancer MGC-803 cells, *Invest. New Drug*, 2019, **37**, 188.
36 APEX software suite v 2010 Bruker AXS Inc. Madison Wisconsin USA, 2010.
37 Blessing, R. H., An empirical correction for absorption anisotropy, *Acta Crystallogr*., 1995, **A51**, 33-38.
38 Sheldrick, G. M., A short history of SHELXL, *Acta Crystallogr*., 2008, **A64**, 112-122.
39 Hubschle, C. B.; Sheldrick G. M.; Dittrich, B., ShelXle: A Qt graphical user interface for SHELXL, *J. Appl. Cryst*., 2011, **44**, 1281-1284.

Chapter Four: Palladium Thiolate-SNS Complexes as Catalysts for Heck Cross-Coupling

4.1 Contribution to Knowledge

Palladium Thiolate-SNS complexes as Catalysts for Heck Cross-Coupling, Atousa Khanzadeh, Saeed Ataie, Maxwell I. Lohoar, R. Tom Baker, manuscript in preparation.

Author Contributions

Atousa did the catalysis and catalyst speciation studies. Maxwell did some preliminary synthesis and catalysis experiments and Saeed did some synthesis and all X-ray diffraction studies. Atousa and Prof. Baker are writing the manuscript.

Abstract: Phosphine-free catalysts for the Heck cross-coupling reaction offer potential advantages in terms of air- and water stability. Using a potentially tridentate thiolate-imine-thioether SNS pincer ligand, we synthesized two palladium(II) complexes, PdI(κ^3-SNS^{Me}) (**4.1**) and Pd(κ^2-SNS^{Me})$_2$ (**4.2**) and compared their catalytic activity for the Heck cross-coupling reaction. In the presence of triethylamine, complex **4.1** exhibited good reactivity with low catalyst loading, yielding the olefin product efficiently across various substrates over 5 h. In contrast, complex **4.2** failed to produce the desired product, primarily due to its isomerization to a Pd(II)-N_2S_2 complex via imine C-C bond formation at elevated temperatures. The latter cannot access enough coordination sites for both oxidative addition and alkene coordination.

4.2 Introduction

In Chapter 2, I demonstrated the potential of amido-SNS ligands for activation of B-H bonds and subsequent catalytic hydroboration of carbonyl compounds using cobalt complexes. We followed this up by a comparison of copper amido- and thiolate-SNS complexes as catalysts for azide-alkyne cycloaddition, showing the advantage of the thiolate complex under aqueous reaction conditions, thus opening up new possibilities for harnessing the potential of the thiolate SNS ligand. Continuing our journey to expand the application of these complexes across a wide spectrum of catalytic reactions, in this chapter we explore the reactivity of palladium thiolate complexes as catalysts for C-C bond formation, with a specific focus on the Heck reaction.

Over the past half-century, transition metal-catalyzed coupling reactions, such as the Heck,[17] Suzuki,[18] Sonogashira,[19] Stille[20] and many others, have revolutionized synthetic organic chemistry. These reactions have emerged as indispensable tools for the construction of carbon-carbon bonds, offering access to a diverse array of complex and sophisticated molecules with applications spanning agrochemicals, pharmaceuticals, and chemical manufacturing industries.[21,22] Among these transformative methodologies, the Heck reaction and its related chemistry hold a distinctive position, providing a gateway to a rich reservoir of intricate molecules. The Heck reaction, which was independently discovered by Mizoroki[23] and Heck[24] in the 1970s, represents a cornerstone in this field. It typically involves the transformation of monosubstituted alkenes through their coupling with electrophiles, such as organohalides or -triflates[25], facilitated by a palladium catalyst and a base. This elegant reaction yields more highly substituted alkenes with exceptional regio- and stereocontrol. Beyond halides, leaving groups including sulfonyl chlorides,[26] diazonium salts,[27] and carboxylic acids[28] have also found utility in the Heck reaction. Furthermore, both electron-rich[29] and electron-poor alkenes[30] have been employed over time to

furnish an impressive array of alkene products. Different kinetic and theoretical studies have investigated the mechanism of this reaction and suggest a catalytic cycle including the following steps: **1.** Pre-activation of the catalyst, **2.** Oxidative addition of the electrophile-X substrate, **3.** Alkene coordination and insertion, **4.** β-hydride elimination-dissociation and **5.** Termination (**Scheme 4.4**).[31]

Palladium catalysis is an indispensable and potent tool for coupling reactions, demonstrating remarkable versatility in the gentle reduction and oxidation of various organic functional groups.[32] Palladium's unique capabilities stem from several key attributes, notably its ability to effortlessly switch between two stable oxidation states, 0 and +2, and its abundant sources of palladium-containing species, characterized by both vacant and occupied nonbonding orbitals.[33] These attributes underpin the diverse and extensive chemistry exhibited by palladium compounds. Specifically, palladium readily participates in a spectrum of reactions, including reductive elimination, carbometalation, migratory insertion, and nucleophilic substitution. These reactions culminate in the formation of carbon-carbon bonds, exemplified by cross-coupling reactions.[34-36] As a result of these remarkable properties, there has been a substantial and ongoing effort to discover efficient Pd-catalysts for the Heck reaction.

The selection of an appropriate ligand for a metal-catalyzed homogeneous reaction holds immense significance, rivaling the importance of the metal choice itself.[37] Ligand design, akin to fine art, often demands a personalized and intuitive approach tailored to each catalytic system. The right ligand decision can profoundly impact various aspects, including the solubility of active species, catalyst shielding and steric properties, electron density around the metal atom, reactivity throughout the catalytic cycle, catalyst longevity and turnover numbers (TON), and, in the case of chiral ligands, enantioselectivity.[38] While the role of metal catalysts in Heck coupling reactions is indisputable, conventional homogeneous palladium-phosphine systems have historically dominated the field as widely adopted and efficient catalysts for carbon-carbon coupling.[39] However, these phosphine-based ligands come with inherent limitations. They can be costly, sensitive to air, and occasionally pose toxicity concerns, prompting questions regarding their practicality and sustainability in large-scale applications.[40] In response, alternative ligands such as palladacycles,[41] N-heterocyclic[42] and carbocyclic carbene ligands,[43] as well as various N-, O-, and S-donor ligands,[44-46] have emerged as phosphine-free options. Many of these phosphine-free ligands offer stability, reduced toxicity, and cost-effectiveness when compared to their phosphine counterparts, leading to their widespread adoption in the realm of organometallic chemistry.

In this context, the focus of our work shifts toward the development of more sustainable and environmentally benign catalytic systems. Our catalyst design features Pd coordinated to thiolate SNS ligands. This innovative ligand architecture presents several distinct advantages. The thiolate ligand is nontoxic, easily synthesized from inexpensive and readily available starting materials, and remarkably air-stable,[47] overcoming some of the inherent drawbacks associated with phosphine ligands. Furthermore, the thiolate arm within our SNS ligand framework demonstrates intriguing potential. It can serve as a bridging element, forming dinuclear compounds that act as stable precatalysts in the catalyst cocktail.[47,48] Additionally, the thioether donor exhibits the potential to play a hemilabile role in the catalytic cycle, assisting in the formation of the active catalyst species.[48]

In 1992, Kawamoto and Kushi illustrated the thermal transformation of nickel and cobalt bis(thiolate) complexes, $M(NS)_2$, into their $M(N_2S_2)$ counterparts by imine C-C bond formation (**Scheme 1.12**).[49] They acknowledged that the resulting N_2S_2 ligand possessed characteristics of redox non-innocence, suggesting it likely functioned as a dianionic ligand with two electrons integrated within its

ligand structure. The thiolate SNS ligand (**L1**) within M(**L1**)$_2$ complexes has also exhibited the capacity to undergo thermal isomerization, resulting in the formation of a non-innocent N_2S_2 ligand.[50] This intriguing capability can be harnessed as a significant asset in catalytic reactions that demand the stabilization of a specific oxidation state within the central metal. In such scenarios, the redox-active ligand can effectively serve as an electron reservoir, maintaining the metal's oxidation state.[51]

In this study, we delve into the development and exploration of Pd-catalyzed Heck reactions using the thiolate-SNS ligand system. We showcase not only the synthetic utility of this catalytic system but also its potential to offer more sustainable and practical solutions in the realm of carbon-carbon bond formation.

4.3 Results and Discussion

4.3.1 Preparation of Pd thiolate-SNS complexes

Four-coordinate complexes PdI(κ^3-SNS^{Me}) (**4.1**) and Pd(κ^2-SNS^{Me})$_2$ (**4.2**) were synthesized from readily available palladium (II) salts with respectively one and two equiv. of the deprotonated thiolate ligand (**L1**) (**Scheme 4.1**). Complex **4.1** shows a slightly distorted square planar geometry (τ'_4 = 0.07) while the

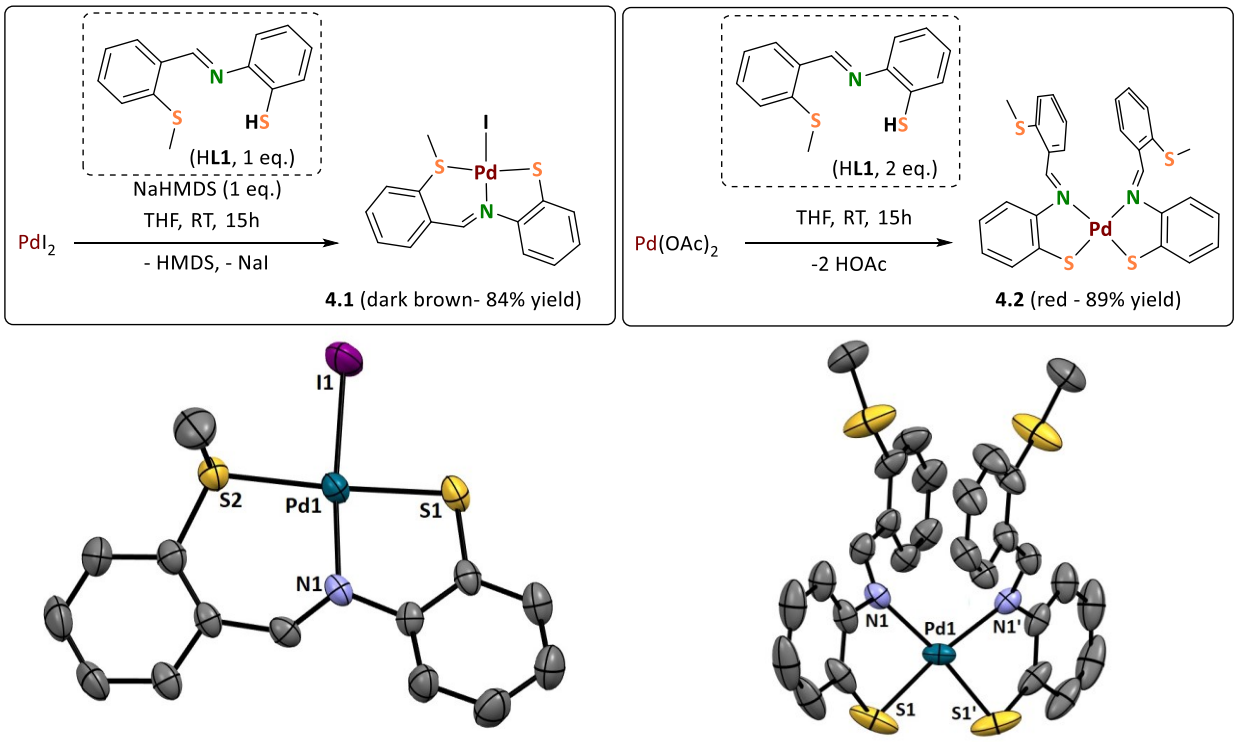

Scheme 4.1 Synthesis and molecular structures of **4.1** and **4.2.** Selected bond distances (Å) and angles (°) for **4.1**: Pd-S1 = 2.252(1), Pd-S2 = 2.293(1), Pd-N = 2.047(3), Pd-I = 2.5834(6), N-Pd-I = 174.58(9), S1-Pd-S2 = 175.38(4), N-Pd-S1 = 87.43(9), N-Pd-S2 = 97.01(9), S1-Pd-I = 87.17(3), S2-Pd-I = 88.40(3), and for **4.2**: Pd-N1 = Pd-N1' = 2.090(0), Pd-S1 = Pd-S1' = 2.266(0), N1-Pd-S1 = N1'-Pd-S1' = 83.39(0), N1-Pd-N1' = 102.25(0), S1-Pd-S1' = 91.62(0), N1-Pd-S1' = N1'-Pd-S1 = 171.94(0).

geometry of **4.2** shows a bigger distortion (T'_4 = 0.11) presumably because of the steric hindrance between the thioether moieties. The bond length between Pd and S1 is very close in **4.1** and **4.2** (2.252(1) vs.

2.266(0) Å), while the Pd1-N1 bond distance in **4.1** (2.047(3) Å) is significantly smaller than that of **4.2** (2.090(0) Å). The strain in the 5-membered thiolate metallocycle in **4.1** is less than that of **4.2** (N1-Pd1-S1 = 87.43(9) and 83.39(0) for **4.1** and **4.2** respectively), leading **4.1** to be closer to an ideal square planar geometry.

4.3.2 Heck reaction catalyzed by complex 4.1

Starting with the reaction of styrene with 1.2 equiv of iodobenzene, we first found that neither PdI_2 nor complex **4.2** at 5 mol% loading gave any of the coupling product in DMF solvent after 24 h at 120 °C.

Table 4.3 Optimization table for PdI(SNS^{Me})-catalyzed Heck reaction. NR = no reaction.

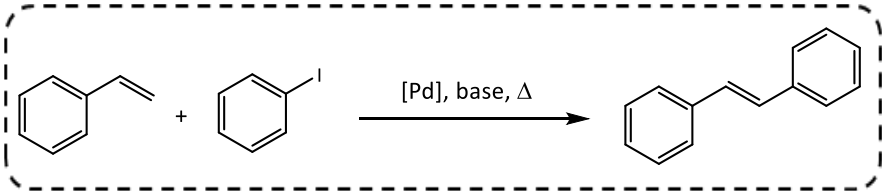

Entry	Complex	Cat. (mol%)	Base (2 eq.)	Solvent	Time (h)	Temperature (°C)	Yield (%)
1	PdI_2	5	NEt_3	DMF	24	120	NR
2	**4.2**	3	NEt_3	DMF	24	120	NR
3	**4.2**	5	NEt_3	DMF	24	130	NR
4	**4.1**	3	NEt_3	DMF	24	120	100
5	**4.1**	1.5	NEt_3	DMF	24	120	100
6	**4.1**	1	NEt_3	DMF	24	120	84
7	**4.1**	0.5	NEt_3	DMF	24	120	78
8	**4.1**	1.5	NEt_3	H_2O	24	115	48
9	**4.1**	1.5	NEt_3	EtOH	24	115	NR
10	**4.1**	1.5	NEt_3	Tol	24	115	38
11	**4.1**	1.5	NEt_3	Dioxane	24	115	85
12	**4.1**	1.5	KO^tBu	DMF	24	120	NR
13	**4.1**	1.5	Na_2CO_3	DMF	24	120	90
14	**4.1**	1.5	NEt_3 1.5 eq.	DMF	24	120	85
15	**4.1**	1.5	NEt_3	DMF	24	115	100
16	**4.1**	1.5	NEt_3	DMF	24	105	100
17	**4.1**	1.5	NEt_3	DMF	24	95	87
18	**4.1**	1.5	NEt_3	DMF	24	60	NR
19	**4.1**	1.5	NEt_3	DMF	10	105	100
20	**4.1**	1.5	NEt_3	DMF	5	105	100
21	**4.1**	1.5	NEt_3	DMF	4	105	88

Table 4.4 Substrate scope table for the PdI(SNS^{Me})-catalyzed Heck reaction under optimized conditions

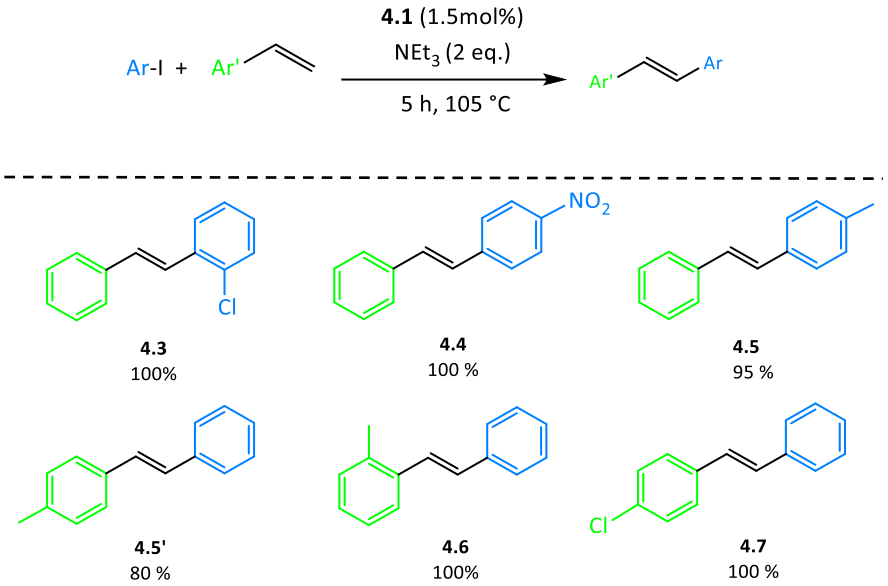

(**Table 4.1;** entries 1-3). In contrast, complex **4.1** exhibited excellent reactivity and selectivity at 1.5 mol% loading.

With the optimized conditions in place, we proceeded to explore the substrate scope of the reaction, examining various aryl groups with different electron-donating or electron-withdrawing substituents at different positions (**Table 4.2**). Notably, when chlorobenzene was introduced into the reaction mixture, the catalyst failed to generate the desired coupling product.

To assess catalyst **4.1**'s potential for reusability, following the completion of the initial Heck reaction, a second batch of starting materials was introduced into the reaction vial under standard laboratory conditions. Notably, the results of this subsequent run demonstrated a remarkable 100% conversion rate, underscoring the catalyst's impressive reusability. Furthermore, this outcome reaffirms the catalyst's robust stability in the presence of environmental factors such as air and moisture. This characteristic aligns with findings from analogous studies in the field, where catalysts exhibiting high reusability and stability have proven to be invaluable assets in sustainable and cost-effective synthetic processes. Additionally, following filtration of the reaction mixture through Celite, there was no black solid observed, providing compelling evidence for a homogeneous catalytic reaction. This finding was further confirmed by examining the GC-MS spectra of the filtrate which displayed no indication of free protonated thiolate ligands. These observations underscore the fundamental role played by our thiolate ligand in stabilizing the palladium coordination sphere.

4.3.3 Probable Heck reaction pathways using Pd thiolate-SNS complexes

To account for the lack of catalytic activity of complex **4.2**, we turn to existing knowledge in the field of NS ligands. As noted in Chapter 1, thermolysis of the nickel analog gave a Ni(N_2S_2) complex via an imine coupling reaction.[50] Based on this background we anticipate the formation of Pd(N_2S_2) at elevated temperature (**Scheme 4.2**). In the generally accepted mechanism for the Heck reaction, the Pd^0 active catalyst requires two *cis* vacant sites in order to oxidatively add the iodobenzene and a third to bind the alkene. Even if complex **4.2** could undergo reduction to Pd^0 by the triethylamine base (*vide supra*), the

rigidity of its tetradentate ligand and consequent lack of two *cis* vacant sites would prevent it from performing the oxidative addition reaction.

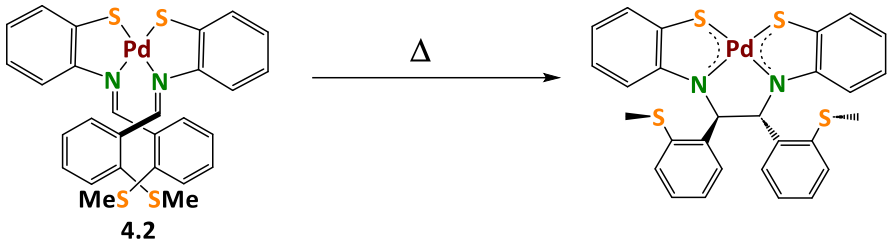

4.2

Scheme 4.2 Isomerization of **4.2** to the Pd(N_2S_2) complex.

For complex **4.1** the catalyst activation step is likely reduction to Pd^0 by the triethylamine base (**Scheme 4.3**) accompanied by loss of iodide. The resulting zerovalent $(Pd(SNS))^-$ anion (possibly stabilized by the DMF solvent) then undergoes oxidative addition of iodobenzene followed by alkene coordination and insertion into the Pd-Ph bond. Finally, reductive elimination affords the Pd-H which is then deprotonated to regenerate the active catalyst (**Scheme 4.4**). Our ongoing research endeavors are dedicated to providing conclusive evidence to support this reaction pathway. This connection between our observations and the broader context of NS ligands underscores the significance of our findings and their potential impact on the development of new cross-coupling catalyst systems.

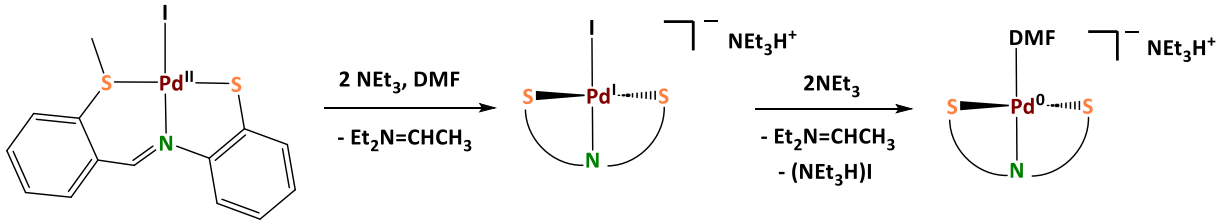

Scheme 4.3 Proposed reduction of **4.1** to Pd^0 by triethylamine base.

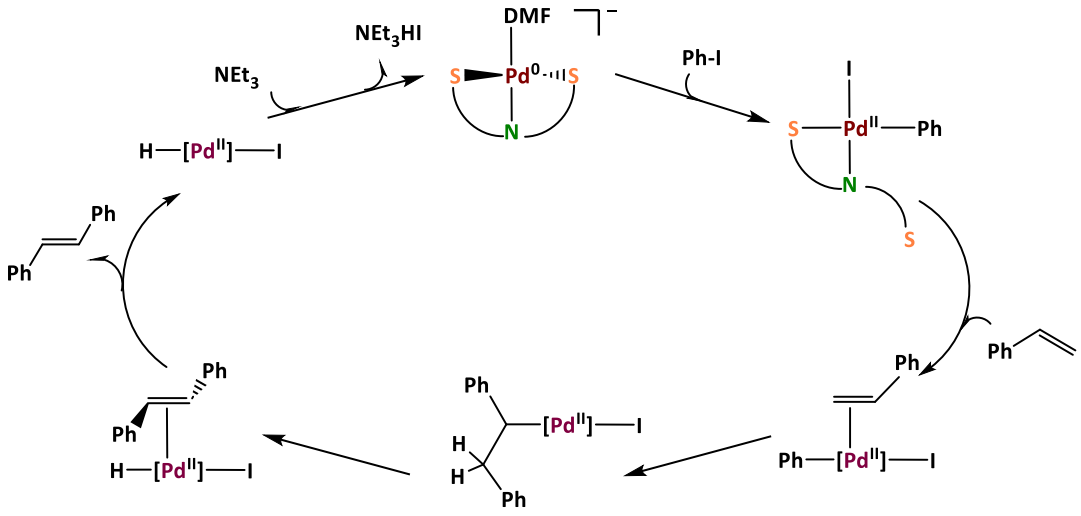

Scheme 4.4 Proposed reaction pathway for Heck reaction catalyzed by **4.1.**

4.4 Experimental Section

4.4.1 General considerations

Synthesis of complexes **4.1** and **4.2** were carried out under dinitrogen, using an MBraun glovebox and stored in the glovebox. THF, DCM, DMF and hexane were dried on columns of activated alumina using a J. C. Meyer (formerly Glass Contour) solvent purification system. Anhydrous $CDCl_3$ and DMSO were dried with activated alumina (ca. 10 wt %) overnight, followed by filtration. SNS ligands were synthesized based on previous publications from the Baker group.[47] All substrates were purchased from commercial suppliers. ^1H and $^{13}C\{^1H\}$ NMR spectra were recorded on a 300 MHz Bruker Avance or Avance II instrument. ^1H NMR spectra were referenced to solvent residual protons (DMSO-d_6, δ 3.55; $CDCl_3$, δ 7.26) and all NMR spectra were recorded at room temperature (21−25 °C). Mass spectra were recorded on an AB Sciex Q1MS mass spectrometer with electrospray ionization in positive mode (ion spray voltage, 5000.0 V; TEM, 400 °C; declustering potential, 11.00 V; focusing potential, 300.0 V) with samples prepared to ca. 0.05 mg/mL in acetonitrile. X-ray diffraction data were collected on a Bruker Smart or Kappa diffractometer equipped with an ApexII CCD detector and a sealed-tube Mo K source (λ= 0.71073 Å).

4.4.2 Synthesis of 4.1

A vial was charged with 215 mg H**L1** (0.83 mmol) and 165 mg of KHMDS (0.83 mmol) in 10 mL of THF and the mixture was stirred for 15 min. In a second vial 300 mg of PdI_2 (0.83 mmol) was dissolved in 5 mL of THF and the mixture from the first vial was added dropwise with stirring. After stirring the resulting mixture for 24 h at room temperature, the solvent was removed under vacuum and the residue washed with hexanes. The complex was then dissolved in DCM and filtered to remove the salt. Evaporation of the filtrate under vacuum gave complex **4.1** as a dark brown powder (343 mg, 84% yield). ^1H NMR (300 MHz, DMSO): δ 9.02 (s, 1H, imine H), 8.29 (d, 1H, aromatic), 8.14 (d, 1H, aromatic), 7.90 (d, 1H, aromatic), 7.81 (m, 2H, aromatic), 7.32 (d, 1H, aromatic), 7.16 (t, 1H, aromatic), 7.00 (t, 1H, aromatic), 3.04 (s, 3H, S-CH_3); $^{13}C\{^1H\}$ NMR (75.5 MHz, DMSO-d_6): δ 159.92 (s, 1C, aromatic), 150.44 (s, 1C, aromatic), 148.11 (s, 1C, aromatic), 141.19 (s, 1C, aromatic), 135.82 (s, 1C, aromatic), 134.21 (s, 1C, aromatic), 133.72 (s, 1C, aromatic), 131.46 (s, 1C, aromatic), 130.54 (s, 1C, aromatic), 128.64 (s, 1C, aromatic), 124.80 (s, 1C, aromatic), 122.93 (s, 1C, aromatic), 120.13 (s, 1C, aromatic), 28.63 (s, 1C, S-CH_3), ESI-MS: $[PdI(SNS^{Me})H]^+$ 490.8495, calculated 490.85.

4.4.3 Synthesis of 4.2

A vial was charged with 85 mg H**L1** (0.33 mmol), 75 mg of $Pd(OAC)_2$ (0.33 mmol) and 10 mL of THF. After stirring the resulting mixture for 24 h at room temperature, the solvent dried under vacuum. Hexane added to the residual and the complex collected on frits and dried under vacuum and collected as a red powder in 89% yield (554 mg). ^1H NMR (300 MHz, $CDCl_3$): δ 9.00 (d, 2H, imine H), 8.26 (s, 2H, aromatic), 7.44 (t, 4H, aromatic), 7.30 (m, 2H, aromatic), 7.03 (t, 2H, aromatic), 6.93 (t, 2H, aromatic), 6.84 (t, 2H, aromatic), 6.69 (t, 2H, aromatic), 4.46 (s, 6H, S-CH_3); $^{13}C\{^1H\}$ NMR (75.5 MHz, $CDCl_3$) 151.42 (s, 2C, aromatic), 132.13 (s, 2C, aromatic), 131.83 (s, 2C, aromatic), 130.93 (s, 2C, aromatic), 129.59 (s, 2C, aromatic), 128.79 (s, 2C, aromatic), 128.56 (s, 2C, aromatic), 127.43 (s, 2C, aromatic), 125.86 (s, 2C, aromatic), 125.31 (s, 2C, aromatic), 122.33 (s, 2C, aromatic), 120.84 (s, 2C, aromatic), 118.87 (s, 2C, aromatic), 17.50 (s, 2C, S-CH_3), ESI-MS: $[Pd(SNS^{Me})_2]Na$ 646.9964 , calculated 644.98.

4.4.4 Catalytic Heck reaction procedure

Based on the optimization conditions established, the following procedure was employed for conducting substrate scope reactions. A vial was charged with complex **4.1** (7 mg, 1.5 mol%), alkene substrate (1 mmol), organohalide substrate (1.2 mmol), triethylamine (2 mmol), and DMF (2 mL). The vial was stirred for 5 h at 105 °C. Subsequently, product isolation was carried out under standard laboratory conditions as follows: Water and ethyl acetate were introduced into the vial, and the product was separated into the organic solvent through a liquid-liquid extraction process. The solvent was then removed under vacuum, and the resulting product was isolated in hexane and further dried under vacuum. The product yield was determined based on the final weight of the collected product.

4.4.5 Catalyst speciation studies

To more comprehensively investigate the activation step and assess catalyst stability under the reaction conditions, we performed some stoichiometric NMR experiments. Specifically, we dissolved complex **4.1** in DMSO-d_6, with and without triethylamine, transferred the solutions into NMR tubes, and heated them at 120 °C for 24 h. The colour of both solutions turned from green to red. The ^{1}H and ^{13}C NMR spectra were then compared with those of **4.1**.

The ^{1}H NMR analysis, as illustrated in **Figure A4.6**, provided valuable insights. Notably, it revealed the presence of imine protons, indicating that the thiolate ligand remained coordinated to the metal. This observation substantiates the notion that the ligand effectively stabilizes the metal complex even under the reaction conditions. Furthermore, a closer examination of the ^{1}H NMR spectrum revealed that approximately half of the triethylamine remained unreacted. However, the remainder of the triethylamine had undergone reaction, leading to the formation of various byproducts within the reaction mixture. The data collected for the ^{1}H and ^{13}C with ^{1}H decoupling for the product of reacting **4.1** with triethylamine in DMF at elevated temperature recorded as follows: ^{1}H NMR (300 MHz, DMSO-d_6): δ 9.18 (s, 1H, imine H), 8.21 (d, 1H, aromatic), 8.00 (d of t, 2H, aromatic), 7.71 (d, 1H, aromatic), 7.56 (m, 2H, aromatic), 7.41(t of d, 1H, aromatic), 7.12 (t of d, 1H, aromatic), 4.52 (t, 1H, NEt_3-byproduct), 3.56 (m, 1H, NEt_3-byproduct), 3.38 (d, 1H, NEt_3-byproduct), 3.34 (d, 1H, NEt_3-byproduct), 3.00 (s, 1H, NEt_3-byproduct), 2.99 (s, 3H, S-CH_3), 2.85 (s, 1H, NEt_3-byproduct), 2.69 (s, 1H, NEt_3-byproduct), 1.72 (q, 1.5H, CH_2-NEt_3), 1.19 (broad, 2.5H, NEt_3-byproduct), 1.05 (t, 1.7H, CH_3-NEt_3). $^{13}C\{^{1}H\}$ NMR (75.5 MHz, DMSO-d_6): δ 161.91 (s, 1C, aromatic), 154.16 (s, 1C, aromatic), 145.87 (s, 1C, aromatic), 140.50 (s, 1C, aromatic), 133.97 (s, 1C, aromatic), 133.65 (s, 1C, aromatic), 132.05 (s, 1C, aromatic), 130.64 (s, 1C, aromatic), 129.84 (s, 1C, aromatic), 129.29 (s, 1C, aromatic), 128.75 (s, 1C, aromatic), 122.61 (s, 1C, aromatic), 120.88 (s, 1C, aromatic), 72.66 (s, NEt_3-byproduct), 67.43 (s, NEt_3-byproduct), 65.39 (s, NEt_3-byproduct), 60.74 (s, NEt_3-byproduct), 27.87 (s, 1C, S-CH_3), 25.52 (s, 1C, CH_2-NEt_3), 15.55 (s, 1C, CH_3-NEt_3).

In summary, our experimental findings underscore the effectiveness of the ligand in stabilizing the metal complex during the activation step and provide insights into the reactivity of triethylamine under the specified reaction conditions.

4.5 Conclusion

In conclusion, this study has made valuable contributions to the broader exploration of SNS-thiolate complexes in the realm of Pd-catalyzed phosphine-free Heck reactions. Our primary aim in this research was to not only assess the catalyst's performance but also to expand the scope of applications for these complexes within the context of this important reaction.

While complex **4.2** did not exhibit reactivity in the Heck reaction, it likely undergoes the same isomerization process observed for Co and Ni NS complexes.[50] This discovery underscores the versatile nature of the redox-active N_2S_2 ligand and hints at its potential in various other chemical transformations and redox processes.

One notable highlight from our investigations is the catalytic performance of air-stable complex **4.1**. While it is not the absolute best catalyst yet reported,[52] it did exhibit commendable catalytic activity, even in aqueous solution. Importantly, it facilitated the catalytic cycle effectively, allowing for the Heck coupling reactions to proceed with a relatively low catalyst loading over a reasonable reaction time. This indicates its potential as a promising catalyst, particularly within the domain of sustainable catalysis.

Crucially, this work builds upon the foundation laid by prior research within the Baker group, which predominantly focused on harnessing SNS-thiolate complexes for catalytic processes involving E-H bond activation, such as hydroboration and hydrosilylation of unsaturated bonds.[5,6,53] In the previous chapter we expanded these applications in the form of the CuAAC catalyst (Cu**L1**)$_4$ and suggested a proton shuttle role for the thiolate donor.[54] In this chapter we disclose the first application of the thiolate SNS-donor in cross-coupling catalysis. Although we have not yet identified a unique role for metal-ligand cooperativity in the Heck reaction, the thioether donor hemilability creates additional coordination sites and the thiolate donor is able to stabilize multiple Pd oxidation states, allowing for effective catalysis. Our study thus significantly broadens the horizons for the SNS-thiolate ligand by introducing novel applications for complexes bearing this unique motif. By expanding the applications of these complexes, we advance the field of organometallic chemistry and sustainable catalysis, opening up new possibilities for their use in a range of reactions.

4.6 Appendix

4.6.1 Spectroscopic data

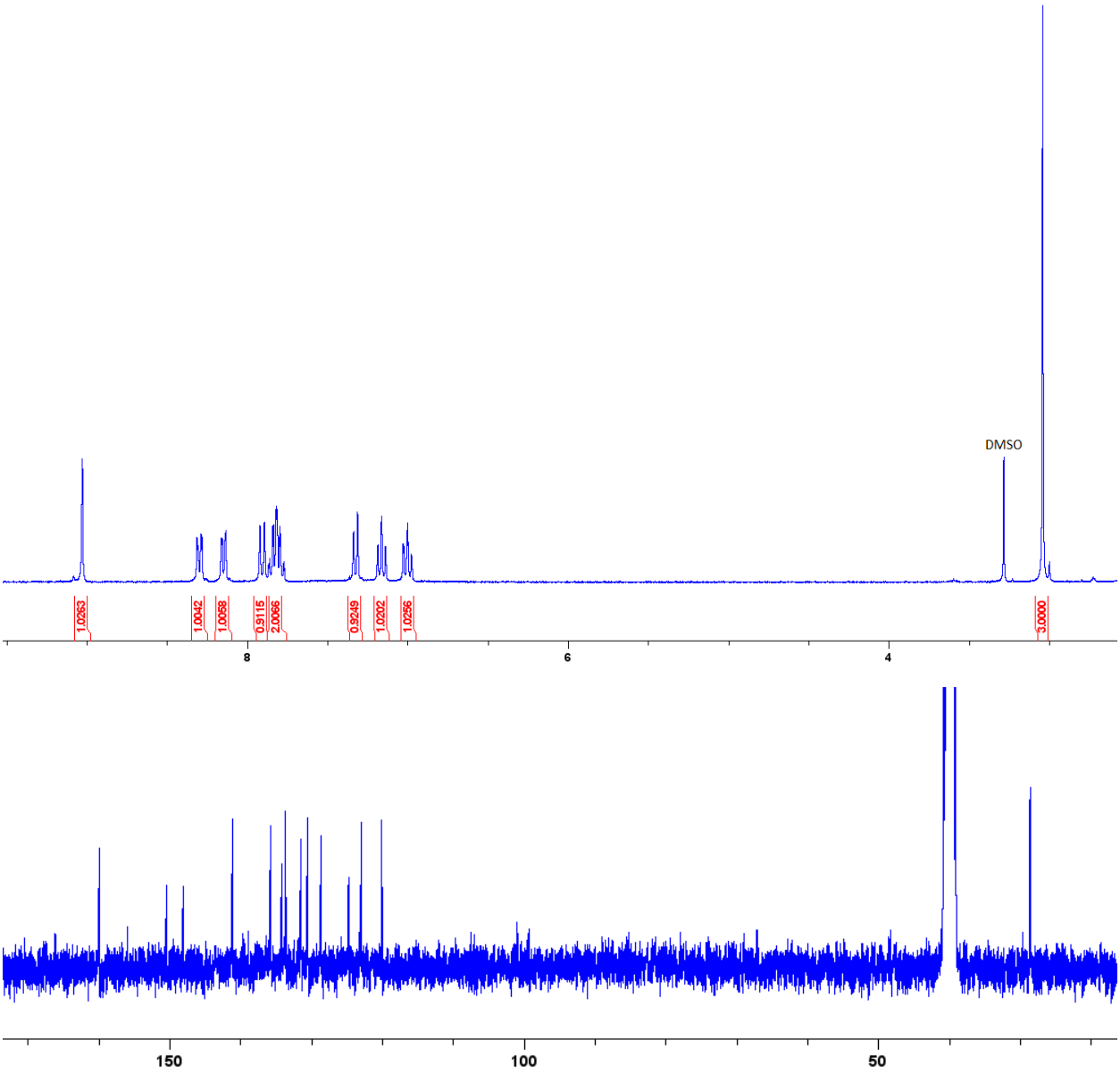

Figure A4.1 ^{1}H NMR (top) and ^{13}C{^{1}H} NMR (bottom) spectrum of **4.1** in DMSO.

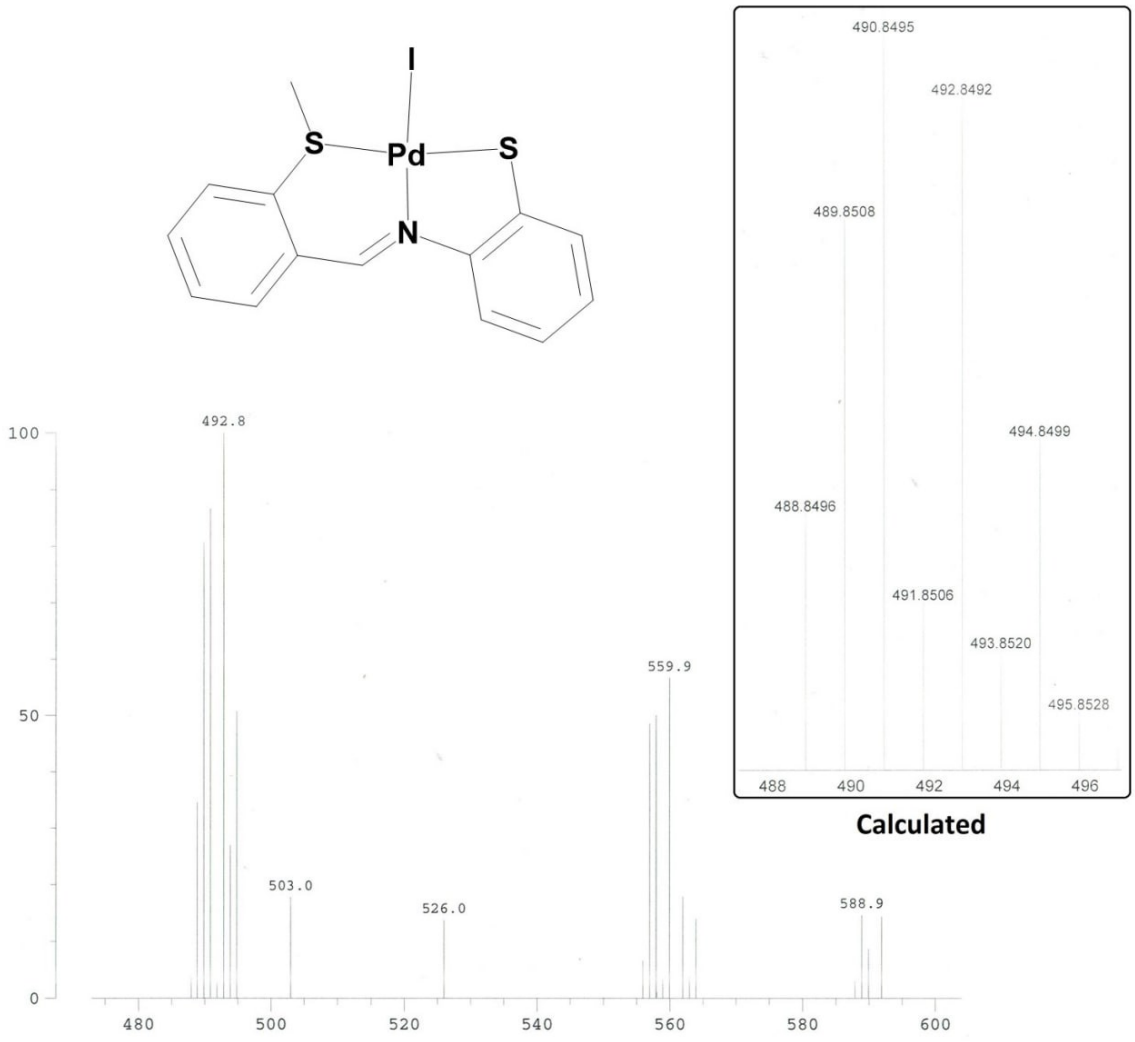

Figure A4.2 ESI-mass spectrum of **4.1**. $[PdI(SNS^{Me})H]^+$: calcd. 490.85, found 490.8495.

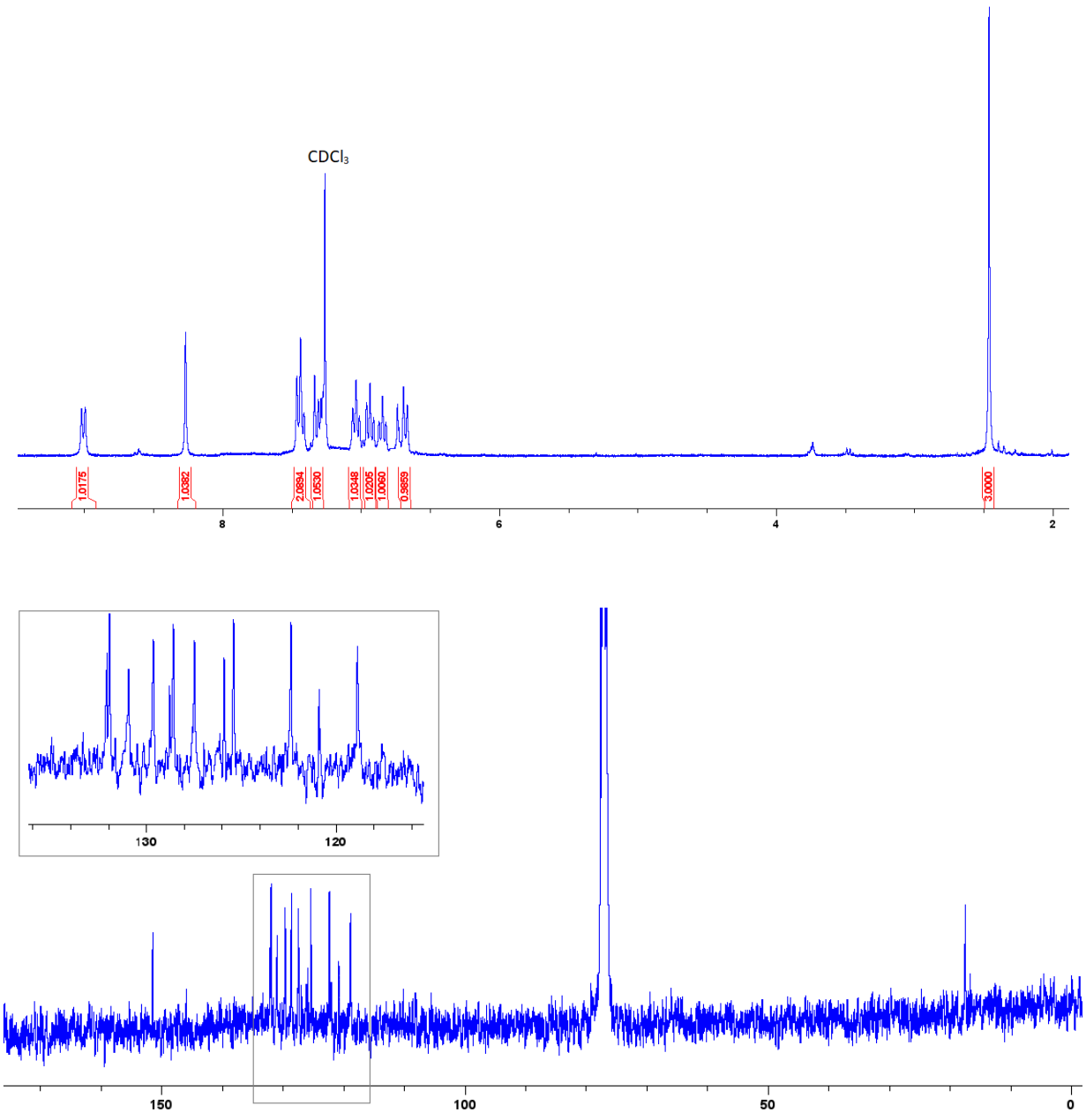

Figure A4.3 ^{1}H NMR (top) and ^{13}C{^{1}H} NMR (bottom) spectrum of **4.2** in $CDCl_3$.

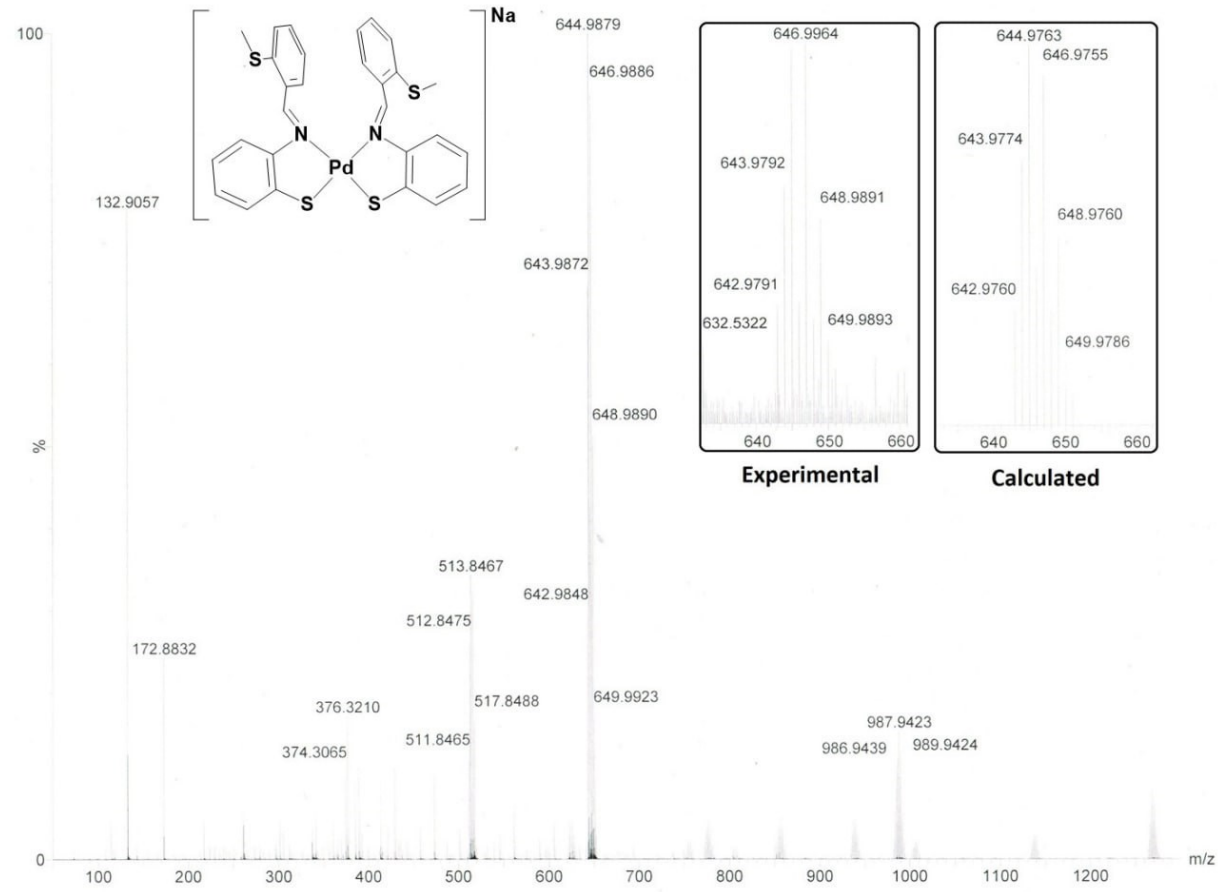

Figure A4.4 ESI-mass spectrum of **4.2**. $[Pd(SNS^{Me})_2]Na$: calcd. 644.98, found 646.9964.

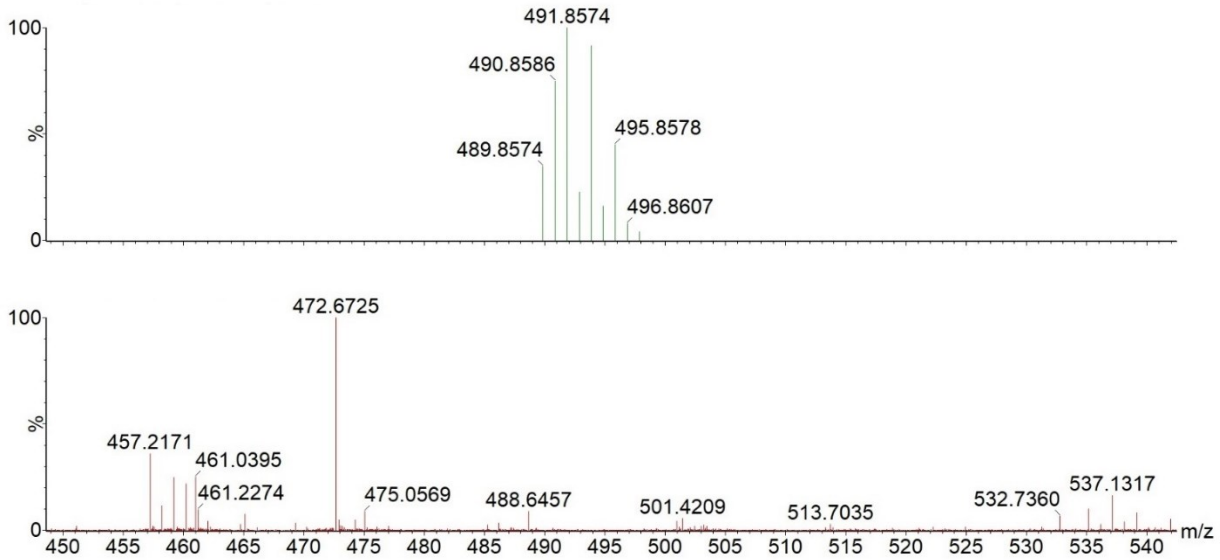

Figure A4.5 ESI-mass spectrum of isolated catalyst **4.1** after running the Heck reaction.

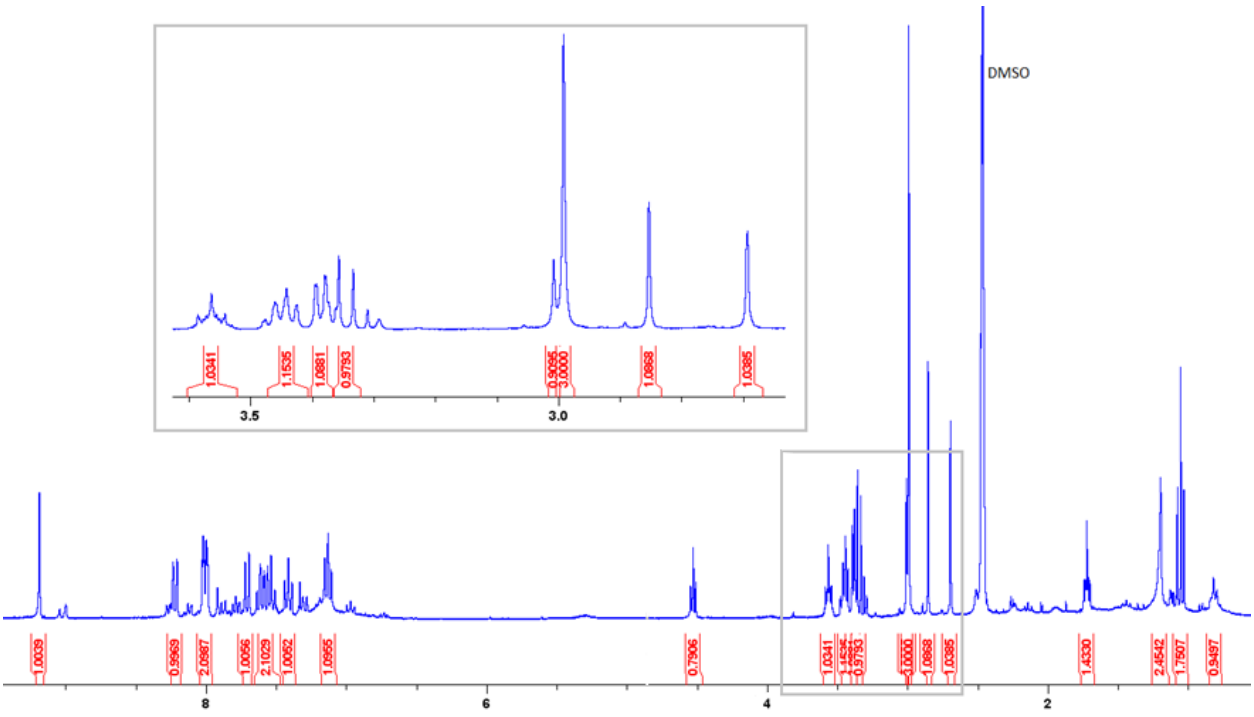

Figure A4.6 ^{1}H NMR spectrum for catalyst **4.1** speciation study.

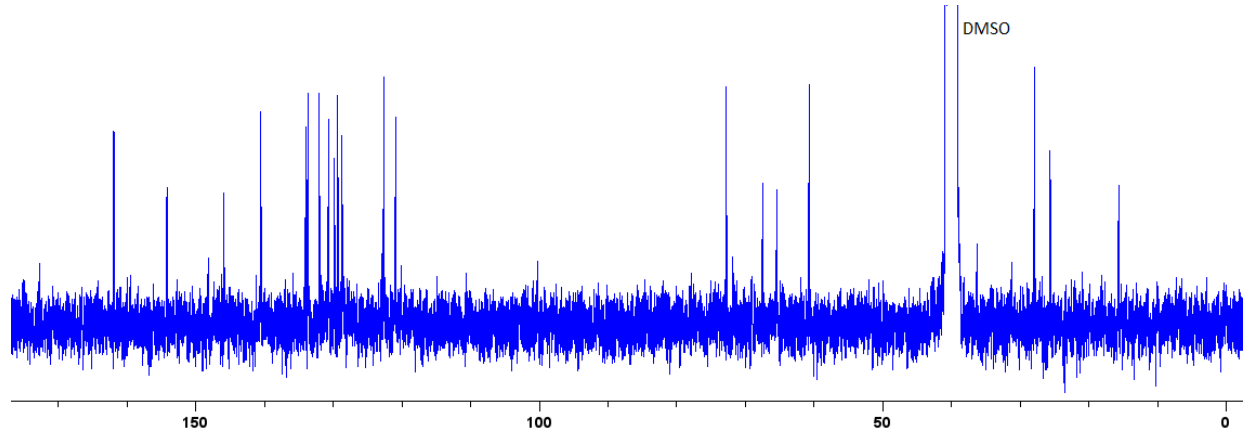

Figure A4.7 ^{13}C{^{1}H} NMR for catalyst **4.1** speciation study.

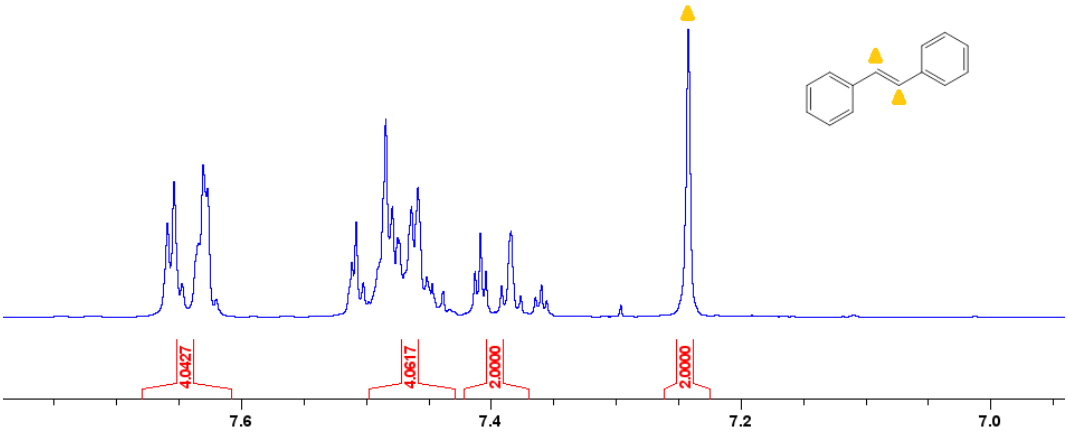

Figure A4.8 ^{1}H NMR spectrum of stilbene in acetone-d_6.

^{1}H NMR data (d-acetone, 300 MHz) for products 4.3-4.7:

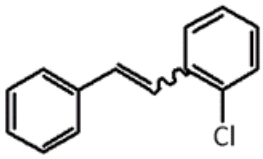

4.3
(E) : (Z) = 80 : 1

***(E)*-2-chlorostilbene:** δ 7.42, 7.23 (d, $^3J_{HH}$= 16.2 Hz, 2H), 7.27-7.82 ppm (m, 9H)

***(Z)*-2-chlorostilbene:** δ 6.68, 6.77 (d, $3J_{HH}$= 12.2 Hz, 2H), 6.90-7.82 ppm(m, 9H)

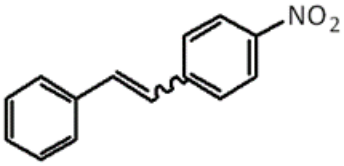

4.4
(E) : (Z) = 6 : 1

***(E)*-4-nitrostilbene:** δ 7.34, 7.42 (d, $^3J_{HH}$=9.7 Hz, 2H), 7.24-8.29 ppm (m, 9H)

***(Z)*-4-nitrostilbene:** δ 6.78, 6.90 (d, $^3J_{HH}$=12.3 Hz, 2H), 7.24-8.29 ppm (m, 9H)

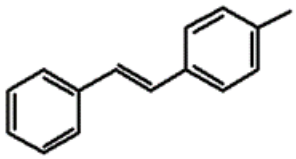

4.5

***(E)*-4-methylstilbene:** δ 2.29 (s, CH_3, 3H), 7.14, 7.20(d, $^3J_{HH}$=16.5 Hz, 2H), 7.23-7.59 ppm (m, 9H)

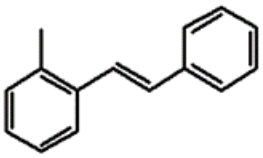

4.6
(E) : (Z) = 75 : 1

***(E)*-2-methylstilbene:** δ 2.41 (s, CH_3, 3H), 7.08, 7.44 (d, $^3J_{HH}$= 16.2 Hz, 2H), 7.13-7.68 ppm (m, 9H)

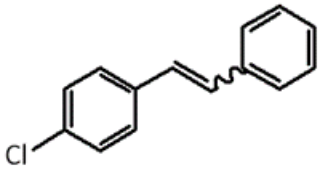

4.7
(E) : (Z) = 35 : 1

***(E)*-2-chlorostilbene:** δ 7.19, 7.25 (d, $^3J_{HH}$= 16.2 Hz, 2H), 7.24-7.63 ppm (m, 9H)

***(Z)*-2-chlorostilbene:** δ 6.68, 6.74 (d, $3J_{HH}$= 12 Hz, 2H), 7.24-7.63 ppm (m, 9H)

4.6.2 Crystallographic data

Crystallographic data were collected from single crystals mounted on MiTeGen dual thickness MicroMounts using Parabar oil. Data were collected on a Bruker Smart ApexII single crystal diffractometer equipped with a graphite monochromator. The instrument was equipped with a sealed tube Mo K$\boldsymbol{\alpha}$ source ($\boldsymbol{\lambda} = 0.71073$ Å), an ApexII CCD detector and a dry compressed air-cooling system. The samples were cooled to 273 K. Raw data collection and processing were performed with the Apex3 software package from Bruker.[55] Initial unit cell parameters were determined from 36 data frames from select $\boldsymbol{\omega}$ scans. Semi-empirical absorption corrections based on equivalent reflections were applied.[56] Systematic absences in the diffraction data-set and unit-cell parameters were consistent with the assigned space group. The initial structural solutions were determined using ShelxT direct methods,[57] and refined with full-matrix least-squares procedures based on $\boldsymbol{F^2}$ using ShelXL or ShelXle.[58] Hydrogen atoms were placed geometrically and refined using a riding model. Deposition Numbers: 2292482-2292483.

Table A4.1 Data collection and refinement metrics for **4.1** and **4.2**.

	4.1 (S1143)	**4.2** (S1141)
empirical formula	C_{14} H_{12} I N Pd S_2	C_{28} H_{24} N_2 Pd S_4
formula weight (g·mol^{-1})	491.67	623.13
crystal system	Monoclinic	Monoclinic
space group	*P* $2_1/c$	*C* 2/*c*
a (A)	11.4163(6)	12.0855(7)
b (A)	12.5682(7)	15.9618(8)
c (A)	21.6954(13)	14.5880(7)
α (deg)	90	90
β (deg)	96.603(2)	111.774(2)
γ (deg)	90	90
V (A^3)	3092.3(3)	2613.3(2)
Z	8	4
T (K)	273(2)	273(2)
ρ_{calcd} (g·cm^{-3})	2.112	1.584
μ (mm^{-1})	3.452	1.051
$2\theta_{max}$ (deg)	50.046	52.728
total/unique reflections	16086/5453	7693/2678
Reflections [$I_o \geq 2\sigma(I_o)$]	4105	2313
R_1, wR_2 [$I_o \geq 2\sigma(I_o)$]	0.0297, 0.0615	0.0319, 0.0319
goodness of fit	1.022	1.057
CCDC number	2292482	2292483

Table A4.2 Bond lengths (Å) for **4.1.**

Atom1	**Atom2**	**Length (Å)**
I1	Pd1	2.5834(6)
Pd1	S1	2.252(1)
Pd1	S2	2.293(1)
Pd1	N1	2.047(3)

S1	C14	1.738(4)
S2	C1	1.808(5)
S2	C2	1.775(4)
N1	C8	1.286(4)
N1	C9	1.451(4)
C1	H1A	0.96
C1	H1B	0.96
C1	H1C	0.959
C2	C3	1.397(6)
C2	C7	1.395(6)
C3	H3	0.93
C3	C4	1.385(7)
C4	H4	0.93
C4	C5	1.370(6)
C5	H5	0.93
C5	C6	1.377(6)
C6	H6	0.931
C6	C7	1.394(5)
C7	C8	1.461(5)
C8	H8	0.93
C9	C10	1.384(6)
C9	C14	1.400(5)
C10	H10	0.93
C10	C11	1.371(6)
C11	H11	0.931
C11	C12	1.396(7)
C12	H12	0.93
C12	C13	1.360(6)
C13	H13	0.93
C13	C14	1.402(6)
I2	Pd2	2.5885(6)
Pd2	S3	2.250(1)
Pd2	S4	2.298(1)
Pd2	N2	2.054(3)
S3	C28	1.735(4)
S4	C15	1.810(5)
S4	C16	1.778(4)
N2	C22	1.278(5)
N2	C23	1.455(5)
C15	H15A	0.96
C15	H15B	0.96
C15	H15C	0.96
C16	C17	1.399(6)
C16	C21	1.387(6)
C17	H17	0.93

C17	C18	1.369(7)
C18	H18	0.931
C18	C19	1.368(9)
C19	H19	0.93
C19	C20	1.378(6)
C20	H20	0.93
C20	C21	1.397(5)
C21	C22	1.463(5)
C22	H22	0.93
C23	C24	1.382(6)
C23	C28	1.408(5)
C24	H24	0.93
C24	C25	1.373(6)
C25	H25	0.93
C25	C26	1.394(7)
C26	H26	0.93
C26	C27	1.373(6)
C27	H27	0.93
C27	C28	1.393(5)

Table A4.3 Bond angles (°) for **4.1.**

Atom1	**Atom2**	**Atom3**	**Angle (deg)**
I1	Pd1	S1	87.17(3)
I1	Pd1	S2	88.40(3)
I1	Pd1	N1	174.58(9)
S1	Pd1	S2	175.38(4)
S1	Pd1	N1	87.43(9)
S2	Pd1	N1	97.01(9)
Pd1	S1	C14	97.9(1)
Pd1	S2	C1	106.3(2)
Pd1	S2	C2	110.1(1)
C1	S2	C2	99.9(2)
Pd1	N1	C8	126.5(3)
Pd1	N1	C9	115.6(2)
C8	N1	C9	117.7(3)
S2	C1	H1A	109.5
S2	C1	H1B	109.5
S2	C1	H1C	109.5
H1A	C1	H1B	109.4
H1A	C1	H1C	109.5
H1B	C1	H1C	109.5
S2	C2	C3	114.6(3)
S2	C2	C7	124.9(3)

C3	C2	C7	120.5(4)
C2	C3	H3	119.9
C2	C3	C4	120.3(4)
H3	C3	C4	119.8
C3	C4	H4	120.1
C3	C4	C5	119.9(4)
H4	C4	C5	120
C4	C5	H5	120.2
C4	C5	C6	119.5(4)
H5	C5	C6	120.2
C5	C6	H6	118.7
C5	C6	C7	122.6(4)
H6	C6	C7	118.7
C2	C7	C6	117.1(3)
C2	C7	C8	129.0(3)
C6	C7	C8	113.9(3)
N1	C8	C7	131.3(4)
N1	C8	H8	114.3
C7	C8	H8	114.3
N1	C9	C10	124.3(3)
N1	C9	C14	116.5(3)
C10	C9	C14	119.2(4)
C9	C10	H10	119.4
C9	C10	C11	121.2(4)
H10	C10	C11	119.4
C10	C11	H11	120.2
C10	C11	C12	119.7(4)
H11	C11	C12	120.1
C11	C12	H12	120.1
C11	C12	C13	119.9(4)
H12	C12	C13	120
C12	C13	H13	119.5
C12	C13	C14	121.0(4)
H13	C13	C14	119.5
S1	C14	C9	122.0(3)
S1	C14	C13	119.0(3)
C9	C14	C13	119.0(4)
I2	Pd2	S3	87.63(3)
I2	Pd2	S4	87.94(3)
I2	Pd2	N2	175.20(9)
S3	Pd2	S4	174.31(4)
S3	Pd2	N2	87.59(9)
S4	Pd2	N2	96.86(9)
Pd2	S3	C28	98.2(1)
Pd2	S4	C15	101.3(2)

Pd2	S4	C16	109.8(1)
C15	S4	C16	99.4(2)
Pd2	N2	C22	126.3(3)
Pd2	N2	C23	115.6(2)
C22	N2	C23	118.0(3)
S4	C15	H15A	109.4
S4	C15	H15B	109.4
S4	C15	H15C	109.4
H15A	C15	H15B	109.5
H15A	C15	H15C	109.5
H15B	C15	H15C	109.5
S4	C16	C17	115.1(3)
S4	C16	C21	124.7(3)
C17	C16	C21	120.2(4)
C16	C17	H17	119.5
C16	C17	C18	120.9(4)
H17	C17	C18	119.6
C17	C18	H18	120.1
C17	C18	C19	119.6(5)
H18	C18	C19	120.2
C18	C19	H19	120
C18	C19	C20	119.9(5)
H19	C19	C20	120
C19	C20	H20	119
C19	C20	C21	122.0(4)
H20	C20	C21	119
C16	C21	C20	117.3(4)
C16	C21	C22	129.0(4)
C20	C21	C22	113.6(3)
N2	C22	C21	131.7(4)
N2	C22	H22	114.2
C21	C22	H22	114.1
N2	C23	C24	124.5(3)
N2	C23	C28	116.6(3)
C24	C23	C28	119.0(4)
C23	C24	H24	119.1
C23	C24	C25	121.9(4)
H24	C24	C25	119
C24	C25	H25	120.2
C24	C25	C26	119.5(4)
H25	C25	C26	120.3
C25	C26	H26	120.4
C25	C26	C27	119.1(4)
H26	C26	C27	120.5
C26	C27	H27	119

C26	C27	C28	122.0(4)
H27	C27	C28	119
S3	C28	C23	122.0(3)
S3	C28	C27	119.7(3)
C23	C28	C27	118.4(3)

Table A4.4 Bond lengths (Å) for **4.2.**

Atom1	**Atom2**	**Length (Å)**
Pd1	S1	2.266
Pd1	N1	2.09
Pd1	S1	2.266
Pd1	N1	2.09
S1	C1	1.753(3)
S2	C13	1.762(4)
S2	C14	1.762(4)
N1	C6	1.441(4)
N1	C7	1.278(4)
C1	C2	1.396(6)
C1	C6	1.398(5)
C2	H2	0.93
C2	C3	1.367(7)
C3	H3	0.93
C3	C4	1.370(9)
C4	H4	0.931
C4	C5	1.389(5)
C5	H5	0.93
C5	C6	1.379(5)
C7	H7	0.93
C7	C8	1.461(5)
C8	C9	1.395(5)
C8	C13	1.405(4)
C9	H9	0.929
C9	C10	1.377(5)
C10	H10	0.93
C10	C11	1.374(5)
C11	H11	0.929
C11	C12	1.373(5)
C12	H12	0.929
C12	C13	1.394(6)
C14	H00A	0.96
C14	H00D	0.96
C14	H00E	0.96
S1	C1	1.753(3)

S2	C13	1.762(4)
S2	C14	1.762(4)
N1	C6	1.441(4)
N1	C7	1.278(4)
C1	C2	1.396(6)
C1	C6	1.398(5)
C2	H2	0.93
C2	C3	1.367(7)
C3	H3	0.93
C3	C4	1.370(9)
C4	H4	0.931
C4	C5	1.389(5)
C5	H5	0.93
C5	C6	1.379(5)
C7	H7	0.93
C7	C8	1.461(5)
C8	C9	1.395(5)
C8	C13	1.405(4)
C9	H9	0.929
C9	C10	1.377(5)
C10	H10	0.93
C10	C11	1.374(5)
C11	H11	0.929
C11	C12	1.373(5)
C12	H12	0.929
C12	C13	1.394(6)
C14	H00A	0.96
C14	H00D	0.96
C14	H00E	0.96

Table A4.5 Bond angles (°) for **4.2.**

Atom1	**Atom2**	**Atom3**	**Angle (deg)**
S1	Pd1	N1	83.39
S1	Pd1	S1	91.62
S1	Pd1	N1	171.94
N1	Pd1	S1	171.94
N1	Pd1	N1	102.25
S1	Pd1	N1	83.39
Pd1	S1	C1	96.3
C13	S2	C14	103.5(2)
Pd1	N1	C6	112.6
Pd1	N1	C7	128.6
C6	N1	C7	118.5(3)

S1	C1	C2	122.2(3)
S1	C1	C6	120.0(2)
C2	C1	C6	117.8(3)
C1	C2	H2	119.4
C1	C2	C3	121.1(4)
H2	C2	C3	119.5
C2	C3	H3	119.7
C2	C3	C4	120.5(4)
H3	C3	C4	119.8
C3	C4	H4	119.9
C3	C4	C5	120.2(4)
H4	C4	C5	119.9
C4	C5	H5	120.3
C4	C5	C6	119.4(3)
H5	C5	C6	120.2
N1	C6	C1	115.3(3)
N1	C6	C5	123.6(3)
C1	C6	C5	121.1(3)
N1	C7	H7	117.4
N1	C7	C8	125.3(3)
H7	C7	C8	117.3
C7	C8	C9	120.5(3)
C7	C8	C13	120.3(3)
C9	C8	C13	119.0(3)
C8	C9	H9	119.5
C8	C9	C10	121.0(3)
H9	C9	C10	119.5
C9	C10	H10	120.1
C9	C10	C11	119.7(3)
H10	C10	C11	120.2
C10	C11	H11	119.7
C10	C11	C12	120.6(3)
H11	C11	C12	119.7
C11	C12	H12	119.6
C11	C12	C13	120.7(3)
H12	C12	C13	119.6
S2	C13	C8	117.9(2)
S2	C13	C12	123.1(3)
C8	C13	C12	119.0(3)
S2	C14	H00A	109.5
S2	C14	H00D	109.4
S2	C14	H00E	109.5
H00A	C14	H00D	109.5
H00A	C14	H00E	109.5
H00D	C14	H00E	109.5

Pd1	S1	C1	96.3
C13	S2	C14	103.5(2)
Pd1	N1	C6	112.6
Pd1	N1	C7	128.6
C6	N1	C7	118.5(3)
S1	C1	C2	122.2(3)
S1	C1	C6	120.0(2)
C2	C1	C6	117.8(3)
C1	C2	H2	119.4
C1	C2	C3	121.1(4)
H2	C2	C3	119.5
C2	C3	H3	119.7
C2	C3	C4	120.5(4)
H3	C3	C4	119.8
C3	C4	H4	119.9
C3	C4	C5	120.2(4)
H4	C4	C5	119.9
C4	C5	H5	120.3
C4	C5	C6	119.4(3)
H5	C5	C6	120.2
N1	C6	C1	115.3(3)
N1	C6	C5	123.6(3)
C1	C6	C5	121.1(3)
N1	C7	H7	117.4
N1	C7	C8	125.3(3)
H7	C7	C8	117.3
C7	C8	C9	120.5(3)
C7	C8	C13	120.3(3)
C9	C8	C13	119.0(3)
C8	C9	H9	119.5
C8	C9	C10	121.0(3)
H9	C9	C10	119.5
C9	C10	H10	120.1
C9	C10	C11	119.7(3)
H10	C10	C11	120.2
C10	C11	H11	119.7
C10	C11	C12	120.6(3)
H11	C11	C12	119.7
C11	C12	H12	119.6
C11	C12	C13	120.7(3)
H12	C12	C13	119.6
S2	C13	C8	117.9(2)
S2	C13	C12	123.1(3)
C8	C13	C12	119.0(3)
S2	C14	H00A	109.5

S2	C14	H00D	109.4
S2	C14	H00E	109.5
H00A	C14	H00D	109.5
H00A	C14	H00E	109.5
H00D	C14	H00E	109.5

4.7 References

1. Das, U. K.; Higman, C. S.; Gabidullin, B.; Hein J. E.; Baker, R. T., Efficient and selective iron-complex-catalyzed hydroboration of aldehydes, *ACS. Catal.*, 2018, **8**, 1076.
2. Elsby, M. R.; Son, M.; Oh, C.; Martin, J.; Baik M. H.; Baker, R. T., Mechanistic study of metal-ligand cooperativity in Mn(II)-catalyzed hydroboration: hemilabile SNS ligand enables metal hydride-free reaction pathway, *ACS. Catal.*, 2021, **11**, 9043.
3. Ataie, S.; Hogeterp, S.; Ovens, J. S.; Baker, R. T., SNS ligand-assisted catalyst activation in Zn-catalysed carbonyl hydroboration, *Chem. Commun.*, 2022, **58**, 3795.
4. Ataie, S.; Lohoar, M. I.; Mangin, L. P.; Baker, R. T., Coinage metal amido and thiolate SNS complexes: consequences of catalyst speciation in Cu(I)-catalysed carbonyl hydroboration, *Chem. Commun.,* 2023, **59**, 4044.
5. Ataie, S.; Dudra, S. L.; Johnson, E. R.; Baker, R. T., Selective cobalt(II)-SNS dithiolate complex-catalyzed bifunctional hydroboration of aldehydes: kinetic and mechanistic studies, *ACS Catal.*, 2023, **13**, 10076.
6. Elsby, M. R.; Baker, R. T., Cu(I)-SNS complexes for outer-sphere hydroboration and hydrosilylation of carbonyls, *Chem. Commun.*, 2019, **55**, 13574.
7. Ataie, S.; Ovens, J. S.; Baker, R. T., Solvent-free Zn (NSNO) complex-catalysed dihydroboration of nitriles, *Chem. Commun.,* 2022, **58***,* 8266.
8. Ataie, S.; Baker, R. T., Comparing B-H bond activation in $Ni^{II}X$(NNN)-catalyzed nitrile dihydroboration (X = anionic N-, C-, O-, S-, or P- donor), *Inorg. Chem.,* 2022, **61**, 19998.
9. Ataie, S.; Baker, R. T., Bifunctional activation of NHC-zinc pre-catalyst for effective hydroboration of quinolines and nitriles, *ChemCatChem*, 2023, e202300649.
10. Rostovtsev, V.; Green, L. G.; Fokin, V. V.; Sharpless, K. B., A stepwise Huisgen cycloaddition process: copper(I)-catalyzed regioselective ligation of azides and terminal alkynes, *Angew. Chem., Int. Ed.*, 2002, **41**, 2596.
11. Mandoli, A., Azide-alkyne cycloaddition reaction (CuAAC), *Molecules,* 2016, **21**, 1174.
12. Alonso, F.; Moglie Y.; Radivoy, G., Copper nanoparticles in click chemistry, *Acc. Chem. Res*., 2015, **48**, 2516.
13. (a) Kolb, H. C.; Finn, M. G.; Sharpless, K. B.; Click chemistry: diverse chemical function from a few good reactions, *Angew. Chem., Int. Ed. Engl.,* 2001, **40**, 2004. (b) Tornøe, C. W.; Christensen, C.; Meldal, M.; Peptidotriazoles on solid phase: [1,2,3]-Triazoles by regiospecific copper(I)-catalyzed 1,3-dipolar cycloaddition of terminal alkynes to azides, *J. Org. Chem*., 2002, **67**, 3057. (c) Agard, N. J.; Prescher, J. A.; Bertozzi, C. R., A strain-promoted [3+2] azide-alkyne cycloaddition for covalent modification of biomolecules in living system, *J. Am. Chem. Soc.,* 2004, **126**, 15046.
14. Kolb, H. C.; Sharpless, K. B., The growing impact of click chemistry on drug discovery, *Drug Discov. Today Rev.,* 2003, **8**, 1128.
15. Paul, R.; Dutta, D.; Dash, J., Target-directed azide-alkyne cycloaddition for assembling HIV-1 TAR RNA binding ligands, *Angew. Chem., Int. Ed.*, 2020, **59**, 12407.
16. Molteni, G.; Bianchi, C. L.; Marinoni, G.; Santo, N.; Ponti, A., Cu/Cu-oxide nanoparticles as catalyst in the click azide-alkyne cycloaddition, *New. J. Chem*., 2006, **30**, 1137-1139.

17. Heck, F., Acylation, methylation, and carboxyalkylation of olefins by group VIII metal derivatives, *J. Am. Chem. Soc.,* 1968, **90**, 5518-5526.
18. Miyaura, K.; Suzuki Yamada, A., A new stereospecific cross-coupling by the palladium-catalyzed reaction of 1-alkenylboranes with 1-alkenyl or 1-alkenyl halides, *Tet. Lett.,* 1979, **20**, 3437-3440.
19. Sonogashira, K.; Tohda, Y.; Hagihara, N., A convenient synthesis of acetylenes: catalytic substitutions of acetylenic hydrogen with bromoalkenes, iodoarenes and bromopyridines, *Tet. Lett*., 1975, **16**, 4467-4470.
20. Milstein, D.; Stille, J. K., A general, selective, and facile method for ketone synthesis from acid chlorides and organotin compounds catalyzed by palladium, *J. Am. Chem. Soc.,* 1978, **100**, 3636-3638.
21. Dounay, B.; Overman, L. E., The asymmetric intramolecular Heck reaction in natural product total synthesis, *Chem. Rev.,* 2003, **103**, 2945-2964.
22. Beletskaya, I. P.; Cheprakov, A. V., The Heck reaction as a sharpening stone of palladium catalysis, *Chem. Rev*., 2000, **100**, 3009-3066.
23. Tsutomu, M.; Kunio, M.; Atsumu, O., Arylation of olefin with aryl iodide catalyzed by palladium, *Bull. Chem. Soc. Jpn.,* 1971, **44**, 581.
24. Heck, F.; Nolley, J. P., Palladium-catalyzed vinylic hydrogen substitution reactions with aryl, benzyl, and styryl hallides, *J. Am. Chem. Soc*., 1972, **37**, 2320-2322.
25. Cacchi, S.; Morera, E.; Ortar, G., Palladium-catalysed vinylation of enol triflates, *Tet. Lett*., 1984, **25**, 2271-2274.
26. Dubbaka, S. R.; Vogel, P., Palladium-catalyzed desulfitative Mizoroki-Heck coupling of sulfonyl chlorides with mono- and disubstituted olefins: rhodium-catalyzed desulfitative Heck-type reactions under phosphine- and base-free conditions, *Chem. Eur. J.,* 2005, **11**, 2633-2641.
27. Felphin, F. X.; Miqueu, K.; Sotiropoulos, J. M.; Fouquet, E.; Ibraguren, O.; Laudien, J., Room-temperature ligand and base free Heck reaction of aryl diazonium salts at low palladium loading: sustainable preparation of substituted stilbene derivatives, *Chem. Eur. J*., 2010, **16**, 5191-5204.
28. Koy, M.; Sandfort, F.; Tlahuex-Aca, A.; Quach, L.; Daniliuc, C. G.; Glorius, F., Palladium-catalyzed decarboxylative Heck-type couplong of activated aliphatic carboxylic acids enabled by visible light, *Chem. Eur. J*., 2018, **24**, 4552-4555.
29. Amatore, C.; Godin, B.; Jutand, A.; Lemaitre, F., Rate and mechanism of the Heck reactions of arylpalladium complexes ligated by a bidentate P,P ligand with and electron-rich alkene (isobutyl vinyl ether), *Organometallics*, 2007, **26**, 1757-1761.
30. Yang, C.; Lee, M. H.; Nolan, S. P., Highly efficient reactions of aryl bromides with n-butyl acrylate mediated by a palladium/phosphine-imidazolium salt system, *Org. Lett.,* 2001, **3**, 1511-1514.
31. Jagtap, S., Heck reaction-state of the art, *Catalysts*, 2017, **7**, 267-320.
32. Tsuji, J., *Palladium reagents and catalysts: Innovations in organic synthesis*, Wiley, 1995.
33. Eaborn, C., Organometallics in synthesis: A manual, *J. Organomet. Chem.,* 1995, **490**,C38.
34. Schore, N. in *Comprehensive organometallic chemistry II*, Hegedus, L. S,, Ed., 1995.
35. Jenner, G., Applied homogeneous catalysis with organometallic compounds, *Appl. Catal*., 1997, **153**, 254.
36. Tsuji, J., *Transition metal reagents and catalysts*, Wiley, 2002.
37. Astruc, D., *Organometallic chemistry and catalysis*, Springer, 2007.

38. Mannepalli, L. K.; Gadipelly, C.; Deshmukh, G.; Likhar, P.; Pottabathula, S., Advances in C-C coupling reactions catalyzed by homogeneous phosphine free palladium catalysts, *Bull. Chem. Soc. Jpn*., 2020, **93**, 355-372.
39. Roy, D.; Uozumi, Y., Recent advances in palladium-catalyzed cross-coupling reactions at ppm to ppb molar catalyst loading, *Adv. Synth. Catal*., 2018, **360**, 602-625.
40. Alisha, M.; Philip, R. M.; Anilkumar, G., An overview of rhodium-catalysed Heck type reactions, *J. Organomet. Chem.,* 2022, **959**, 12207.
41. Herrmann, W. A.; Bohm, V. W.; Reisinger, C. P., Application of palladacycles in Heck type reactions, *J. Organomet. Chem*., 1999, **576**, 23-41.
42. Fortman, G. C.; Nolan, S. P., N-heterocyclic carbene (NHC) ligands and palladium in homogeneous cross-coupling catalysis: a perfect union, *Chem. Soc. Rev*., 2011, **40**, 5151-5169.
43. Yao, Q.; Zabawa, M.; Woo, J.; Zheng, C., Carboxylic carbene ligands derived from aromatic nitrones: formation and catalytic activity of their Pd(II) complexes, *J. Am. Chem. Soc*., 2007, **129**, 3088-3089.
44. Cui, X.; Li, Z.; Tao, C. Z.; Xu, Y.; Li, J.; Liu, L.; Guo, Q. X., N,N-dimethyl-β-aniline as an inexpensive and efficient ligand for palladium-catalyzed heck reaction, *Org. Lett.,* 2006, **8**, 2467-2470.
45. Bergbreiter, D. E.; Osburn, P. L.; Liu, Y. S., Tridentate SCS palladium(II) complexes: new, highly stable, recyclable catalysts for the Heck reaction, *J. Am. Chem. Soc*., 1999, **121** (41), 9531-9538.
46. Cui, X.; Li, J.; Liu, L.; Gou, Q. X., 1,3-dicarbonyl compounds as phosphine-free ligands for Pd-catalyzed Heck and Suzuki reactions, *Chin. Chem. Lett*., 2007, **18**, 625-628.
47. Das, U. K.; Daifuku, S. L.; Gorelsky, S. I.; Korobkov, I.; Neidig, M. L.; Le Roy, J. J.; Murugesu, M.; Baker, R. T., Mononuclear, dinuclear and trinuclear iron complexes featuring a new monoanionic SNS thiolate ligand, *Inorg. Chem*., 2016, **55**, 987-997.
48. Alkburi, Y. M.; Oven, J. S.; Martin, J.; Baker. R. T., Nickel (II)-SNS thiolate complexes: Reactivity and solution dynamics, *Inorg. Chem.,* 2021, **60**, 10934-10942.
49. Tatsuya, K.; Hiro, K.; Yoshihiko, K., Valence isomerization, synthesis and characterization of cobalt and nickel complexes with non-innocent N_2S_2 ligand, *Bull. Chem. Soc. Jpn.,* 1997, **70**, 1599-1606.
50. Albkuri, Y. M. University of Ottawa PhD thesis, 2021.
51. Luca, O. R.; Crabtree, R. H., Redox-active ligands in catalysis, *Chem. Soc. Rev*., 2013, **42**, 1440-1459.
52. Yu, S.; Zhou, L.; Ye, S.; Tong, X., Domino sequences involving stereoselective hydrazone-type Heck reaction and denitrogenative [1,5]-sigmatropic rearrangement, *J. Am. Chem. Soc*., 2023, **145**, 7621-7627.
53. Elsby, M. R.; Oh, C.; Son, M.; Kim, S. Y. H.; Baik, M. H.; Baker, R. T., Spin-state crossover in photo-catalyzed nitrile dihydroboration via Mn-thiolate cooperation, *Chem. Sci*., 2022, **13**, 12550-12559.
54. Khanzadeh, A.; Ataie, S.; Baker, R. T., Tetracopper(I) thiolate- and amido-(SNS) complexes and copper-catalyzed azide-alkyne cycloaddition in water, *Dalton Trans*., 2023, **52**, 11768-11772.
55. APEX Softward Suite v 2010 Bruker AXS Inc. *Madison Wisconsin USA*, 2010.
56. Blessing, R. H., An empirical correction for absorption anisotropy**,** *Acta Crystallogr.,* 1995, **A51**, 33–38.
57. Sheldrick, G. M., A Short History of SHELX, *Acta Crystallogr.,* 2008, **A64**, 112–122.
58. Hübschle, C. B.; Sheldrick, G. M.; Dittrich, B., *ShelXle*: A Qt graphical user interface for *SHELXL, J. Appl. Crystallogr.,* 2011, **44**, 128 1–1284.

Chapter Five: Conclusions and Future Work

5.1 Key Findings

Catalysis is essential in modern synthetic chemistry, with about 90% of commercial chemicals relying on catalytic processes. The global catalyst market has grown steadily over the years and, although the history of catalyst development goes back centuries, catalysis research is still vibrant. Synthetic chemists face the challenge of producing compounds with high efficiency, selectivity, and sustainability. Homogeneous transition metal catalysis has a longstanding history of facilitating challenging chemical transformations to produce valuable products.[1] The most effective and selective organometallic catalysts often rely on second and third-row so-called 'precious metals' like Pd, Pt, Rh, Ru, and Ir. These heavy transition metal complexes exhibit a more predictable tendency to undergo 2-electron elementary steps in various reaction pathways,[2] enabling important reactions such as C–C and C–N coupling, C–H bond functionalization, olefin metathesis, and H–X additions.[3] However, these metals are typically toxic, costly, and in limited supply. Therefore, skillful ligand design is crucial for coordination chemists to harness the full potential of these metals. When these metal complexes are intended for use in biological contexts,[4] the ligand motif plays a critical role in determining their distribution, localization, and behavior within dynamic systems.[5]

The ligand environment surrounding the metal also plays a crucial role in optimizing catalytic efficiency.[6] Traditionally, phosphine-based ligands have been widely used, but they pose challenges due to their toxicity, sensitivity to air and moisture, and high cost. To transition towards more sustainable, biocompatible, and environmentally friendly catalytic systems, there has been a shift towards exploring phosphine-free base-metal complexes. In this context, the Baker research group has focused on developing non-toxic, eco-friendly, and stable SNS ligands. These ligands can be easily synthesized from readily available starting materials.[7,8] As summarized in Chapter 1, the Baker group has specifically investigated thiolate and amido SNS ligand complexes, aiming to compare the soft S-donor and hard N-donor properties while broadening the applications of these compounds in functionalizing unsaturated E-H bonds through metal-ligand cooperation.[9]

In the second chapter of our exploration, we embarked on a journey through our attempts to mono-protonate the amido pincer ligand within the *mer*-cobalt bis(amido) complex (**2.1**). Our objective was to displace one of the SNS ligands with a more stabilizing ancillary ligand, aiming to create a sustainable and active hydroboration catalyst. Instead, even with a single equiv. of acid, a second protonation occurred, affording the *fac*-isomer of the cobalt bis(amine) dication (**2.2**). In an alternate strategy, we treated **2.1** with one equivalent of an imidazolium chloride salt (IAd•HCl) to yield a divalent chlorocobalt amido complex (**2.3**) containing an abnormally-coordinated NHC ligand (*a*-IAd). Intriguingly, (**2.3**) exhibited remarkable catalytic potential, facilitating the hydroboration of a wide range of carbonyl compounds with high yields over a short timeframe with low catalyst loading. After demonstrating that pinacolborane reacts with both amido and chloride ligands of **2.3** to generate 'CoH_2(*a*-IAd)' *in situ*, we contrasted its catalytic performance with $[CoCl_2(IAd)]_2$ (**2.4)** which contains a normally coordinated IAd ligand. Assuming that **2.4** forms the analogous 'CoH_2(IAd)' catalyst *in situ,* our results suggest that the more basic *a*-IAd ligand supports a more active Co hydroboration catalyst than IAd. Moreover, the increased catalyst lifetime of **2.3** (vs. **2.4**) suggests a potential role for borylated **L2** in stabilizing the Co

catalyst. The bifunctional catalyst activation strategy employed by catalyst **2.3** thus resembles that reported previously by the Baker group using a Zn bis(pyrrolylamine) NHC precatalyst.[10]

In the third chapter of our research journey, our objective was to broaden the applications of SNS ligands and first row metals with a different chemical reaction, namely copper-catalyzed azide-alkyne cycloaddition (CuAAC).[11] In the absence of an ancillary NHC ligand,[12] copper(I) reactions with the SNS ligands afforded tetranuclear complexes, one featuring thiolate ligands (**3.1**) and the other amido ligands (**3.2**). Although complex **3.2** suffered from amido ligand protonation by the coordinated alkyne C-H bond, leading to ligand dissociation and poor catalytic activity, complex **3.1** demonstrated impressive reactivity, successfully yielding triazole products in excellent yields, within a base-free aqueous environment, in just two hours. This catalytic system exhibited noteworthy substrate tolerance, accommodating electron-donating and -withdrawing groups in various positions. Furthermore, our catalyst facilitated the synthesis of bioactive compound **3.16**, with potential applications in anti-cancer and anti-fungal drug development.[13] This achievement marked a significant expansion of the utility of the stable and biocompatible thiolate-SNS ligand. Our mechanistic insights, derived from DFT calculations, unveiled a potential bifunctional role for the thiolate donor during the initial step of the catalytic cycle, in which it may play a critical role in forming the copper-alkynyl intermediate by reversibly capturing the acidic proton from the Cu-coordinated terminal alkyne.

In our subsequent chapter, we sought to apply the thiolate SNS ligand to an important C-C cross-coupling reaction. In this endeavor, we introduced two new palladium(II) thiolate complexes: **4.1**, featuring a single iodide and a (κ^3-**L1**) ligand coordinated to the central palladium, and **4.2**, a palladium bis-thiolate (κ^2-**L1**) complex. These two complexes were rigorously tested for their catalytic capabilities in mediating the Heck reaction, a cornerstone of cross-coupling chemistry. The outcomes of these investigations proved to be quite intriguing. Complex **4.1** emerged as an efficient catalyst, displaying catalytic activity in facilitating the Heck reaction under relatively mild reaction conditions. Impressively, with 1.5 mol% loading of catalyst **4.1**, we achieved complete conversion of the starting materials within 5 hours with electron-donating or -withdrawing groups on each substrate. Despite not being the very best catalyst system reported for the Heck reaction, this investigation serves as a valuable case study in the comparative assessment of catalyst activity among similar coordination complexes. In stark contrast, the performance of complex **4.2** presented a perplexing challenge due to its striking lack of catalytic activity. To unravel this mystery, we delved into the annals of bis-NS complexes and their propensity to undergo isomerization when exposed to elevated temperatures. This transformation led to the formation of a distinctive Pd(N_2S_2) complex adorned with a redox-active ligand. The active palladium(0) catalyst species necessitates vacant coordination sites to enable the oxidative addition of the organohalide and subsequent coordination of the alkene substrate. Consequently, the tightly bound tetradentate N_2S_2 ligand acts as a hindrance, precluding the formation of the active catalyst species by occupying crucial coordination sites around the metal. This elucidation not only sheds light on the inactivity of **4.2** but also underscores the pivotal role of ligand structure in dictating the catalytic behavior of these complexes, thus expanding our understanding of this fascinating field.

5.2 Future Outlook

The work presented in this thesis significantly advances the applications of SNS ligands both with other first row metals like cobalt and for other chemical reactions such as copper-catalyzed azide-alkyne cycloaddition and Pd-catalyzed Mizoroki-Heck cross-coupling. Previous work in the Baker group showed that a Co imine bis(thiolate) bearing a small NHC ligand effected the selective hydroboration of aldehydes (vs ketones) via a non-hydride inner-sphere bifunctional mechanism.[14] In Chapter 2 we showed that use of the amido-SNS ligand generated a more active NHC cobalt dihydride catalyst that was capable of hydroborating aldehydes and ketones but not more challenging substrates such as amides, esters, alkenes or alkynes. To further advance the hydroboration activity of SNS complexes, we could investigate the reduction of our active $Co^{II}Cl$(*a*-IAd) catalyst to its Co(I) analog and investigate its capacity for alkene hydroboration as demonstrated by Geetharani's $Co^{I}Cl$(IPr) precatalyst, proposed to oxidatively add HBpin to a Co^{III} boryl hydride intermediate.[15]

Over the past decade, there have been significant strides in the development of highly potent chemical tools designed to control, detect, and visualize intricate biological processes occurring within living organisms.[16] The realm of intracellular metal catalysts has witnessed considerable growth in recent decades, finding applications in diverse areas such as cell-surface modifications,[17] bioimaging techniques,[18] *in situ* drug synthesis,[19] and pro-drug activation.[20] Furthermore, these catalysts have displayed the remarkable ability to catalytically transform harmful chemical toxins into non-hazardous substances.[21] However, designing effective intracellular catalysts presents certain challenges. Many coordination complexes used in this context are inherently incompatible with the essential elements of life—air and water.[22] Additionally, these complexes must exhibit non-toxic properties, maintain activity under physiological conditions, and be tolerant of the various biological nucleophiles present within living systems.

An early milestone in this journey was achieved in 1985 when Vigh and colleagues successfully merged soluble inorganic catalysts with living cells.[23] In their groundbreaking work, they demonstrated that a ruthenium triarylphosphine chloride complex could hydrogenate C-C double bonds in unsaturated fatty acids using hydrogen gas. Nonetheless, it was noted that prolonged exposure to the ruthenium catalyst and hydrogen resulted in extensive cell damage.

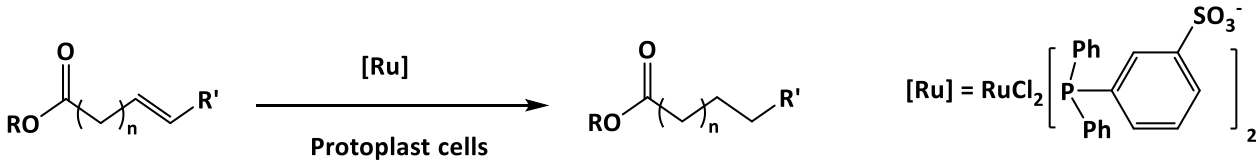

Scheme 5.1 Intracellular hydrogenation by Vigh.

In another example, Lin and co-workers harnessed palladium aminopyrimidine complexes to facilitate Sonogashira C-C bond cross-coupling reactions within *E. coli.*[24]

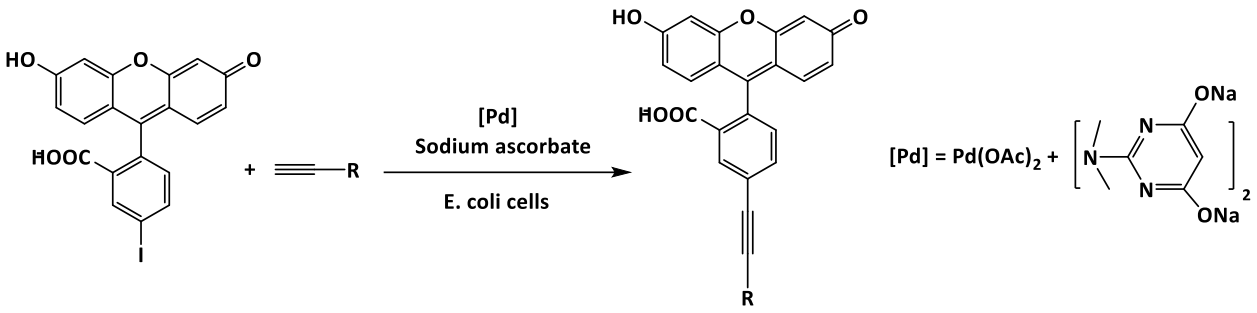

Scheme 5.2 Intracellular Sonogashira cross-coupling by Lin group.

The copper-catalyzed azide-alkyne cycloaddition (CuAAC) reaction, discovered in 2002,[11] swiftly made a profound impact across numerous scientific domains, including chemical synthesis, drug development, and materials science.[25] CuAAC's versatility in chemical biology became evident early on. Within a year of its discovery, CuAAC was effectively employed to label the surfaces of intact bacterial cells.[26] By 2005, these reactions had even been executed within living cells. For instance, Tirrell and colleagues were able to monitor the synthesis of a model protein, barstar, containing unnatural alkynyl amino acids in auxotrophic *E. coli* by tagging it with coumarin azides using the CuAAC ligation method.[27]

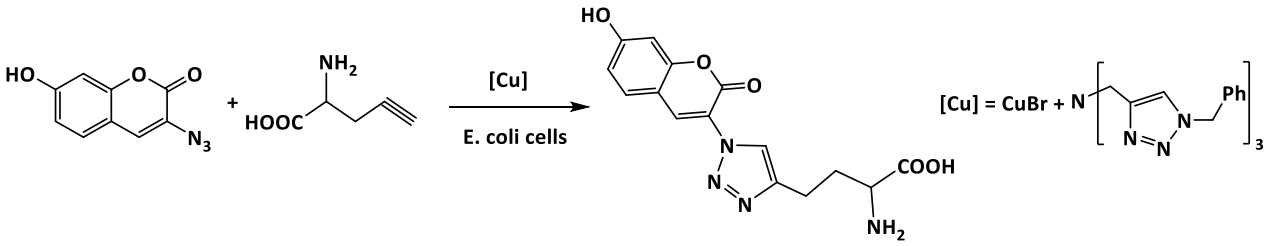

Scheme 5.3 Intracellular CuAAC by Tirrell group.

The SNS ligands, known for their non-toxicity and biocompatibility, offer a promising avenue for intracellular catalysis. Notably, thiolate (**L1**) complexes have demonstrated robust stability even in the presence of air and moisture, rendering them well-suited for potential intracellular applications.

As elucidated in Chapter Three, the copper(I) thiolate complex exhibited remarkable catalytic activity in facilitating azide-alkyne cycloaddition reactions in aqueous environments. This catalytic system displayed a high level of reactivity, yielding bioactive compound **3.16** with potential applications as an anti-cancer drug. With slight modifications aimed at enabling catalyst activity at lower temperatures, this system may serve as an *in situ* drug synthesis catalyst or as a catalyst for converting triazole compounds within living cells. Furthermore, it is imperative to conduct additional investigations to closely monitor the generation of copper(II) species and ascertain the possibility of reducing these oxidized entities in subsequent catalytic cycles through the introduction of azide reagents. In the event that copper(II) species prove to be non-reactive, our future research endeavors may necessitate the modification of the SNS ligand. One promising avenue could involve the incorporation of chlorine groups onto the aromatic ring of the SNS ligand, a strategic alteration aimed at diminishing the oxidizing potential at the central copper atom, potentially revitalizing the catalytic activity.

Finally, the promising catalytic activity demonstrated by the palladium(II) complex introduced in Chapter four, paves the way for exciting future prospects. In upcoming research endeavors, the potential of this catalyst could be systematically explored in various cross-coupling reactions, including Sonogashira and Suzuki couplings, conducted under biologically relevant conditions. If this catalyst proves to be effective at facilitating these reactions at mild temperature and in aqueous environments, it could hold the key to a transformative breakthrough. If this catalyst proves to be effective at facilitating these reactions at mild temperature and in aqueous environments, the promising palladium(II) complex introduced in Chapter four may become a valuable tool for conducting intracellular cross-coupling reactions, offering the ability to modify biomolecules within living cells with precision (**Scheme 5.2**).This avenue of investigation not only expands the scope of chemical biology but also holds great promise for innovative applications in drug development, cellular engineering, and beyond.

5.3 References

1. (a) van Leeuwen, P. W. N. M., *Homogeneous catalysis: Understanding the art*, Springer Sci. Busi. Med., 2006, (b) Chiusoli, G. P; Maitlis, P. M, Eds.; *Metal-catalysis in industrial organic processes*; *Royal Society of Chemistry*, 2019.
2. Elschenbroich, C., *Organometallics*, J. Wiley and Sons, 2016.
3. (a) Hartwig, J. F, Evolution of C-H bond functionalization from methane to methodology*, J. Am. Chem. Soc*., 2016, **138**, 2-24. (b) Grubbs, R. H., Olefin-metathesis catalysts for the preparation of molecules and materials, *Angew. Chem*. *Int. Ed.,* 2006, **45**, 3760-3765. (c) Suzuki, A., Cross-coupling reactions of organoboranes: An easy way to construct C-C bonds, *Angew. Chem., Int. Ed.,* 2011, **50**, 6722-6737.
4. Monneret, C., Platinum anticancer drugs, from serendipity to rational design, *Ann. Pharm Fr.*, 2011, **69**, 286-295.
5. (a) Riccardi, L.; Genna, V.; De Vivo, M., Metal-ligand interaction in drug design, *Nat. Rev. Chem*., 2018, **2**, 100-112. (b) Mjos, K. D.; Orvig, C., Metallodrugs in medicinal inorganic chemistry, *Chem. Rev.,* 2014, **8**, 4540-4563.
6. Astruc, D., *Organometallic chemistry and catalysis*, Springer, 2007.
7. Das, U. K.; Daifuku, S. L.; Gorelsky, S. I.; Korobkov, I.; Neidig, M. L.; Le Roy, J. J.; Murugesu, M.; Baker, R. T., Mononuclear, dinuclear and trinuclear iron complexes featuring a new monoanionic SNS thiolate ligand, *Inorg. Chem.,* 2016, **55**, 987-997.
8. Das, U. K.; Daifuku, S. L.; Iannuzzi, T. E.; Gorelsky, S. I.; Korobkov, I.; Gabidullin, B.; Neidig, M. L.; Baker, R. T., Iron (II) complexes of a hemilabile SNS amido ligand: Synthesis, characterization, and reactivity, *Inorg. Chem*., 2017, **56**, 13766−13776.
9. Elsby, M. R.; Baker, R. T., Through the looking glass: Using the lens of [SNS]-pincer ligands to examine first-row metal bifunctional catalysts, *Acc. Chem. Res*., 2023, **56**, 798-809.
10. Ataie, S.; Baker, R. T., Bifunctional activation of NHC-zinc pre-catalyst for effective hydroboration of quinolines and nitriles, *ChemCatChem,* 2023, e202300649.
11. (a) Kolb, H. C.; Finn, M. G.; Sharpless, K. B.; Click chemistry: diverse chemical function from a few good reactions, *Angew. Chem., Int. Ed. Engl.,* 2001, **40**, 2004. (b) Tornøe, C. W.; Christensen, C.; Meldal, M.; Peptidotriazoles on solid phase: [1,2,3]-triazoles by regiospecific copper(I)-catalyzed 1,3-dipolar cycloaddition of terminal alkynes to azides, *J. Org. Chem*., 2002, **67**, 3057. (c) Agard, N. J.; Prescher, J. A.; Bertozzi, C. R., A strain-promoted [3+2] azide-alkyne cycloaddition for covalent modification of biomolecules in living system, *J. Am. Chem. Soc.,* 2004, **126**, 15046.
12. Elsby, M. R.; Baker, R. T., Cu(I)-SNS complexes for outer-sphere hydroboration and hydrosilylation of carbonyls, *Chem. Commun*., 2019, **55**, 13574-13577.
13. Xu, Z.; Zhao, S. J.; Liu, Y., 1,2,3-triazole-containing hybrids as potential anticancer agents: Current developments, action mechanisms and structure-activity relationships, *Eur. J. Med. Chem.,* 2019, **183**, 111700.
14. Ataie. S.; Dudra, S. L.; Johnson, E. R.; Baker, R. T. Selective cobalt(II)-SNS dithiolate complex-catalyzed bifunctional hydroboration of aldehydes: Kinetics and mechanistic studies, *ACS Catal.,* 2023, **15**, 10076–10084.

15. Verma, P. K.; A. Sethulekshmi, S.; Geetharani, K., Markovnikov-selective Co(I)-catalyzed hydroboration of vinylarenes and carbonyl compounds, *Org. Lett.*, 2018, **20**, 7840-7845.
16. (a) Prescher, J. A.; Bertozzi, C. R., Chemistry in living systems, *Nature Chem. Bio.,* 2005, **1**, 13-21. (b) Schreiber, S. L., Small molecules: The missing link in the central dogma, *Nature Chem. Bio*., 2005, **1**, 64-66. (c) Giephen, B. N. G.; Adams, S. R.; Ellisman, M. H.; Tsien, R. Y., The fluorescent toolbox for assessing protein location and function, *Science*, 2006, **312**, 217-224.
17. Hong, V.; Steinmetz, N. F.; Manchester, M.; Finn. M. G., Labeling live cells by copper-catalyzed azide-alkyne click chemistry, *Bioconjugate Chem*., 2010, **21**, 1912-1916.
18. Bose, S.; Ngo, A. H.; Do, L. H., Intracellular transfer hydrogenation mediated by unprotected organoiridium catalysts, *J. Am. Chem. Soc*., 2017, **139**, 8792-8795.
19. Clavadestscher, J.; Hoffmann, S.; Lilienkampf, A.; Mackay, L.; Yusop, R. M.; Rider, S. A.; Mullins, J. J.; Bradley, M., Copper catalysis in living system and *in situ* drug synthesis, *Angew. Chem., Int. Ed.,* 2016, **55**, 15662-15666.
20. Du, B.; Li, D.; Wang, J.; Wang, E., Designing metal-contained enzyme mimics for prodrug activation, *Adv. Drug Delivery Rev.,* 2017, **118**, 78-93.
21. Iu, Y.; Zhai, S.; Jiang, X.; Liu, Y.; Wang, K.; Wang, C.; Zhang, M.; Liu, X.; Bu, W., Intracellular mutual promotion of redox homeostasis regulation and iron metabolism disruption for enduring chemodynamic therapy, *Adv. Funct. Mater*., 2021, **31**, 2010390-2010399.
22. Hartwig, J. F., *Organotransition metal chemistry*, University Science, 2010.
23. Vigh, L.; Joo, F.; Cseplo, A., Modulation of membrane fluidity in living protoplasts of *nicotiana plumbaginifolia* by catalytic hydrogenation, *Eur. J. Biochem*., 1985, **146**, 241-244.
24. Li, N.; Lim, R. K. V.; Edwardraja, S.; Lin, Q., Copper-free Sonogashira cross-coupling for functionalization of alkyne-encoded proteins in aqueous medium and in bacterial cells, *J. Am. Chem. Soc*., 2011, **133**, 15316-15319.
25. Medal, M.; Tornqe, C. W., Cu-catalyzed azide-alkyne cycloaddition, *Chem. Rev.,* 2008, **108**, 2952-3015.
26. Link, A. J.; Tirrell, D. A., Cell surface labeling of *Escherichia coli* via copper(I)-catalyzed [3+2] cycloaddition, *J. Am. Chem. Soc.,* 2003, **125**, 11164-11165.
27. Beatty, K. E.; Xie, F.; Wang, Q.; Tirrell, D. A., Selective dye-labeling of newly synthesized proteins in bacterial cells, *J. Am. Chem. Soc*., 2005, **127**, 14150-14151.